# ROLE OF THE SIXTH TRANSMEMBRANE DOMAIN IN THE CALCIUM-DEPENDENT GATING OF THE INTERMEDIATE CONDUCTANCE CALCIUM-ACTIVATED POTASSIUM CHANNEL, KCa3.1.

by

**Mark Andrew Bailey**

B.S., Gannon University, 2002

Submitted to the Graduate Faculty of

The Department of Cell Biology and Molecular Physiology in partial fulfillment

of the requirements for the degree of

Doctor of Philosophy

University of Pittsburgh

2010

UNIVERSITY OF PITTSBURGH

SCHOOL OF MEDICINE

This dissertation was presented

by

Mark Andrew Bailey

It was defended on

23 September 2010

and approved by

Peter Drain, Ph.D., Associate Professor, Cell Biology and Physiology

Michael Grabe, Ph.D., Assistant Professor, Department of Biological Sciences

Thomas Kleyman, M.D., Professor, Department of Medicine, Renal-Electrolyte Division

Committee Chair: Raymond Frizzell, Ph.D., Professor, Cell Biology and Physiology

Dissertation Advisor: Daniel Devor, Ph.D., Associate Professor, Cell Biology and Physiology

**ROLE OF THE SIXTH TRANSMEMBRANE DOMAIN IN THE CALCIUM-DEPENDENT GATING OF THE INTERMEDIATE CONDUCTANCE CALCIUM-ACTIVATED POTASSIUM CHANNEL, KCa3.1.**

Mark Andrew Bailey, Ph.D

University of Pittsburgh, 2010

Ion channels are the molecular units that underlie electrical signaling in cells. Many physiological processes are dependent upon this signaling mechanism, as dysregulation often leads to severe pathophysiological consequences. The intermediate conductance calcium-activated potassium channel (KCa3.1) functions as heteromeric complexes with calmodulin (CaM), which is constitutively bound to the calmodulin-binding domain (CaMBD) of KCa3.1 located in the C-terminus, just distal to the sixth transmembrane domain (S6). This arrangement enables CaM to function as an intracellular $Ca^{2+}$-sensor, coupling changes in the intracellular $Ca^{2+}$ concentration to the regulation of channel activity. Understanding how channels gate or transition from the closed to the open conformation is a fundamental question in the field of ion channel biophysics. A chemomechanical gating model was proposed to explain how $Ca^{2+}$-binding causes the channel to transition from a non-conducting to a conducting configuration. However, this model lacks a specific mechanism explaining how the conformational change in the CaMBD is coupled to the activation gate. Therefore, the goal of this dissertation was to investigate the role of S6 in the activation mechanism of KCa3.1. Specifically, I tested the hypothesis that the non-luminal residues in the C-terminal portion of S6 function as an interacting surface to couple CaM to the activation gate. Biochemical perturbation and site directed mutagenesis targeting predicted non-luminal residues in S6 act to shift the gating

equilibrium toward the open state by increasing the apparent $Ca^{2+}$ affinity and dramatically slowing the deactivation process. Kinetic modeling using a 6-state gating scheme showed these perturbations act to slow the transition between the open state back to the closed state. The modification in the steady-state and kinetic behavior of the channel in combination with the kinetic analysis indicate the shift in gating equilibrium is caused by slowing the closing transition, suggesting the non-luminal surface of S6 is allosterically coupled to the activation gate. Therefore, in addition to being a structural component of the pore; S6 is also a dynamic component of the activation mechanism. Continuing to identify regions of the channel participating in the activation mechanism is critical to understand how $Ca^{2+}$ binding leads to channel opening.

## TABLE OF CONTENTS


**PREFACE** ..... **XIII**

**1.0 INTRODUCTION** ..... **1**

**1.1 OVERVIEW** ..... **1**

**1.2 LIGAND AND BINDING-SITE INTERACTION** ..... **2**

**1.2.1 Ion Channels as Allosteric Proteins** ..... **5**

**1.3 EARLY BIOPHYSICAL APPROACH TO INVESTIGATING ION CHANNEL GATING** ..... **6**

**1.3.1 Elucidating the Components of Membrane Current** ..... **6**

**1.3.2 Single versus Separate Channel Hypothesis** ..... **9**

**1.3.3 Ionic Pores versus Carrier Proteins** ..... **12**

**1.3.4 Gating Currents** ..... **15**

**1.3.4.1 Dissolved ions and molecules as gates or sensors** ..... **15**

**1.4 MOLECULAR APPROACH FOR INVESTIGATING ION CHANNEL GATING** ..... **17**

**1.4.1 Cloning of the $K^+$ Channel** ..... **20**

**1.4.2 The Cloned $K^+$ Channel** ..... **21**

**1.5 STRUCTURE-FUNCTION APPROACH FOR INVESTIGATING ION CHANNEL GATING** ..... **24**

**1.5.1 The Pore ..... 25**

**1.5.2 The Gate ..... 26**

**1.6 SUBSTITUTED CYSTEINE ACCESSIBILITY METHOD ..... 29**

**1.6.1 SCAM and Ion Channels ..... 29**

**1.6.1.1 Experimental Assumptions ..... 30**

**1.7 CURRENT VIEW OF ION CHANNEL GATING AND THE STRUCTURE OF THE PROTEIN ..... 31**

**1.8 STRUCTURAL APPROACH FOR INVESTIGATING ION CHANNEL GATING ..... 36**

**1.8.1 Permeation Pathway and Selectivity Filter: KcsA X-Ray Structure ..... 36**

**1.8.2 Gate: KirBac 1.1 Crystal Structure ..... 39**

**1.8.3 Sensor Domain: MthK X-Ray Structure ..... 41**

**1.8.4 The Coupling Mechanism ..... 43**

**1.8.4.1 Potential method to assess coupling ..... 43**

**1.8.5 Potential Gating Mechanism ..... 44**

**1.9 THE INTERMEDIATE CONDUCTANCE CALCIUM ACTIVATED POTASSIUM CHANNEL – KCa3.1 ..... 46**

**1.9.1 KCa3.1 in Physiology ..... 46**

**1.9.2 Regulation of Vascular Tone through Activation of the EDHF Response 47**

**1.9.3 Contribution of KCa3.1 to the EDHF Response ..... 50**

**1.9.4 Structure of KCa3.1 ..... 51**

**1.9.5 $Ca^{2+}$-dependent Regulation of KCa3.1 ..... 52**

**1.9.6 Chemomechanical Gating Model ..... 53**

**1.9.7 The Current State of KCa3.1 ..... 54**

**1.10 STATEMENT OF THE PROBLEM ..... 56**

**1.10.1 Goals of this Dissertation ..... 57**

**2.0 CHARACTERIZATION OF THE PCMBS-DEPENDENT MODIFICATION OF KCa3.1 CHANNEL GATING ..... 59**

**2.1 ABSTRACT ..... 59**

**2.2 INTRODUCTION ..... 60**

**2.3 MATERIALS AND METHODS ..... 62**

**2.4 RESULTS ..... 69**

**2.4.1 PCMBS can be used as a Probe to Modulate KCa3.1 Gating ..... 69**

**2.4.2 Characterization of Potentiation by PCMBS ..... 71**

**2.4.3 Cysteine 276 Confers PCMBS-sensitivity to KCa3.1 Potentiation ..... 79**

**2.4.4 Gating of KCa3.1 can be described with a 4-State Model ..... 87**

**2.4.5 PCMBS slows the $k_{53}$ Transition ..... 92**

**2.4.6 L281W replicates the PCMBS phenotype ..... 96**

**2.5 DISCUSSION ..... 103**

**2.5.1 Differences in Chemistries of the Compounds may explain discrepancy regarding the effect on the WT-Channel ..... 103**

**2.5.2 PCMBS potentiates Channel Activation by shifting the Gating Equilibrium toward the Open Conformation ..... 104**

**2.5.3 Modeling the $Ca^{2+}$-dependent Gating of KCa3.1 ..... 106**

**2.5.4 Potential Mechanism of PCMBS ..... 108**

**2.6 ACKNOWLEDGEMENTS ..... 112**

**3.0 DISCUSSION AND FUTURE DIRECTIONS ..... 113**

**3.1 MERCURIAL BASED SULFHYDRYL REAGENTS AS PROBES FOR NON-LUMINAL CYSTEINE RESIDUES ..... 116**

**3.2 S6 IS A DYNAMIC COMPONENT OF THE GATING MECHANISM ..... 118**

**3.3 KCa3.1 VERSUS KCa2.3 ..... 120**

**3.4 CYSTEINE 276 AS AN IMPORTANT SITE FOR THE COUPLING OF $Ca^{2+}$ BINDING TO CHANNEL GATING ..... 122**

**3.5 POTENTIAL COUPLING MECHANISM ..... 123**

**3.6 CONCLUSION/FUTURE DIRECTIONS ..... 125**

**4.0 APPENDIX ..... 130**

**4.1 INTRODUCTION: STRUCTURE-FUNCTION INVESTIGATIONS OF S6 IN KCa3.1 AND KCa2.3 ..... 130**

**4.2 RESULTS ..... 132**

**4.2.1 Results Table 1 ..... 132**

**4.2.2 Results Table 2 ..... 133**

**4.2.3 Results Table 3 ..... 134**

**4.2.4 Results Table 4 ..... 135**

**4.2.5 Results Table 5 ..... 136**

**4.2.6 Results Table 6 ..... 137**

**4.3 DISCUSSION/CONCLUSIONS ..... 138**

**4.4 APPENDIX FIGURES ..... 140**

**4.5 APPENDIX TABLES ..... 160**

**BIBLIOGRAPHY ..... 183**

## LIST OF TABLES

Table 1. Exponential fits comparing the activation and deactivation kinetics of KCa3.1..... 77

Table 2. Summary of the 6-State model used to describe the kinetic behavior of KCa3.1±PCMBS..... 90

Table A.1 Sequence alignment between KCa3.1 and KCa2.3 .....160

Table A.2 KCa3.1 $Ca^{2+}$ concentration experiments..... 161

Table A.3 KCa2.3 $Ca^{2+}$ concentration experiments..... 162

Table A.4 KCa3.1 activation and deactivation rates..... 163

Table A.5 KCa2.3 activation and deactivation rates..... 165

Table A.6 Primers ..... 168

Table A.7 Sensitivity analysis..... 172

Table A.8 Sequence alignment ..... 182

## LIST OF FIGURES

Figure 1. Allosteric models. 4

Figure 2. Components of membrane current 8

Figure 3. Single versus separate channel hypothesis 11

Figure 4. Early ion channel model. 14

Figure 5. 1970's model of a voltage-gated ion channel 19

Figure 6. Ramification of $K^+$ channels in higher animals 23

Figure 7. 1990's model of a voltage-gated ion channel 33

Figure 8. Premonitions of ion channel gating 34

Figure 9. X-ray structure of KcsA illustrating the selectivity filter 38

Figure 10. Crystal structure of KirBac1.1 illustrating the location of the potetial activation gate $Phe^{146}$ 40

Figure 11. Gating mechanism of a $Ca^{2+}$-dependent $K^+$ channel, MthK 42

Figure 12. PCMBS increases KCa3.1 steady-state current 70

Figure 13. PCMBS increases steady-state $P_{o(max)}$ 72

Figure 14. PCMBS shifts apparent Ca2+-affinity 74

Figure 15. PCMBS modulates channel kinetics 76

Figure 16. Homology model of the pore region for the open state of KCa3.1 using the rKv1.2 structure..... 80

Figure 17. PCMBS increases channel activation for KCa3.1 C277A ..... 81

**F**igure 18. C276A prevents the PCMBS-mediated increase in channel activation ..... 83

Figure 19. PCMBS modulates C277A channel kinetics in a manner similar to the WT-channel ..... 85

Figure 20. C276A prevents the PCMBS-mediated modulation in channel kinetics..... 86

Figure 21. A 4-state model can be used to fit the activation and deactivation kinetics for KCa3.1.. ..... 89

Figure 22. PCMBS slows transition $k_{53}$, as determined through the constrained version of the model..... 95

Figure 23. $Trp^{281}$ and $Trp^{282}$ recapitulate the PCMBS-mediated shift in apparent $Ca^{2+}$ affinity ..... 98

Figure 24. $Trp^{281}$ recapitulates the PCMBS-mediated modulation in deactivation kinetics..... 100

Figure 25. A 4-state model can be used to fit the activation and deactivation kinetics for KCa3.1 L281W ..... 102

Figure 26. Homology model of the pore region for the open and closed state of KCa3.1 ..... 111

Figure A.1. Thimerosal shifts the apparent $Ca^{2+}$ affinity in KCa3.1 ..... 141

Figure A.2. C276A prevents the thimerosal-dependent increase in apparent $Ca^{2+}$ affinity ..... 142

Figure A.3. PCMBS does not increase the steady-state current in (A) KCa2.3 or (B) KCa2.3 G534C. ..... 144

Figure A.4. KCa3.1 $Ca^{2+}$ concentration response experiments ..... 148

Figure A.5. KCa2.3 $Ca^{2+}$ concentration response experiments ..... 152

Figure A.6. KCa3.1 activation and deactivation rates ..... 155

Figure A.7. KCa2.3 activation and deactivation rates ..... 158

Figure A.8. Estimate of KCa2.3 $P_{o(max)}$ ..... 159

# PREFACE

This work would not have been possible without the support and guidance from my dissertation advisor, Dr. Daniel Devor. Dan allowed me to be independent and develop a dissertation project around my interests and abilities. This approach worked out well because I will continue to investigate the biophysical properties of these channels as a postdoc. Additionally, I really appreciate being able to see the project through to the end, rather than being pushed out the door once I fulfilled the minimal requirements for a degree. Thanks for your support and maybe I will help out with the F194 project someday. I would also like to thank the members of my dissertation committee: Dr. Peter Drain, Dr. Ray Frizzell, Dr. Michael Grabe, and Dr. Tom Kleyman for all their helpful suggestions and support during my graduate work. I would like to acknowledge Dr. Michael Grabe, who introduced me to kinetic and structural modeling. Thanks for all of your help; this collaboration was a key component of my dissertation. I would also like to acknowledge Dr. Peter Drain, who in addition to talking sports, spent a lot of time discussing all things related to ion channel gating. Thanks for your time; I really enjoyed all of our discussions.

I would also like to thank my parents, who were always supportive throughout my education. Most importantly, they let me move back home (temporarily) to write my dissertation when I was not able to renew my apartment lease in Pittsburgh.

# 1.0 INTRODUCTION

## 1.1 OVERVIEW

Ion channels are allosteric proteins with at least two conformational states: the open state and the closed state. The act of transitioning between these conformational states is a process termed gating. One of the most fundamental questions in the field of ion channel biophysics tries to understand how ion channels transition between various conformational states. The intermediate conductance calcium-activated potassium channel (KCa3.1) is a ligand-gated ion channel that is solely activated by the binding of intracellular $Ca^{2+}$. This channel can be modeled as having three separate domains that work in concert to transfer the chemical energy of $Ca^{2+}$ binding into a mechanical force to open the pore. These domains are: the pore-forming domain, the $Ca^{2+}$-binding domain, and the coupling domain. As detailed in the introduction, the pore-forming domain and the $Ca^{2+}$-binding domain are well characterized. However, the location and mechanism of the coupling domain are poorly understood. The purpose of this dissertation was to characterize the role of the sixth transmembrane domain (S6) in the activation mechanism of KCa3.1. Specifically, I focused on the non-luminal surface of the C-terminal portion of S6 and asked whether this region participates in the activation of KCa3.1. I demonstrate that altering this

region influences the steady-state and kinetic behavior of the channel. These data, in addition to our kinetic analysis indicate this region is important for the closing transition, suggesting the non-luminal surface of the C-terminal portion of S6 is allosterically coupled to the activation gate. Therefore, in addition to being a structural component of the pore, S6 is dynamically associated with the activation mechanism.

## 1.2 LIGAND AND BINDING-SITE INTERACTION

Proteins are inherently dynamic structures whose function is dictated by interactions with other molecules called ligands [1]. The interaction between a ligand and its binding site is relatively simple in the case of a single ligand binding to a single site on a protein. However, this interaction becomes increasingly more complex when multiple ligands bind to multiple sites. For instance, there may be no interaction between binding sites, so that the binding of the initial ligand has no affect on the affinity at the other binding sites. On the other hand, there can also be cooperativity, so that the binding of the initial ligand increases or decreases the affinity at the other binding sites. Cooperativity between binding sites is recognized as a key regulatory function of most proteins. Since much effort has been expended to understand how protein-ligand interactions affect the binding properties of downstream binding sites the term allostery was introduced to describe this aspect of protein function [2].

Two models were proposed to address cooperativity in allosteric proteins: the Koshland-Nemethy-Filmer model (KNF) [3] and the Monod-Wyman-Changeux model (MWC) [4]. The KNF model is also known as the sequential model, because conformational, and thus affinity changes, occur in sequence from one subunit to the next in response to successive ligand binding

[3]. This model proposes that the inherent flexibility of proteins allows ligand binding at an individual subunit to affect the tertiary conformation of the adjacent subunit, and with that increases the affinity for the next ligand to bind. This process continues in sequence until the last subunit is bound by ligand (Fig. 1. A). Therefore, the transformation from a ligand free state to a fully-ligand bound state is the accumulation of successive conformational changes within the subunits. At the opposite extreme is the MWC model, also known as the concerted model (Fig. 1. B). Unlike the KNF model, this model proposes that there are two symmetric quaternary conformations of the protein structure and ligand binding at one site does not alter the affinities of the other sites, but alters the conformational equilibrium between the two quaternary conformations of the protein [4].

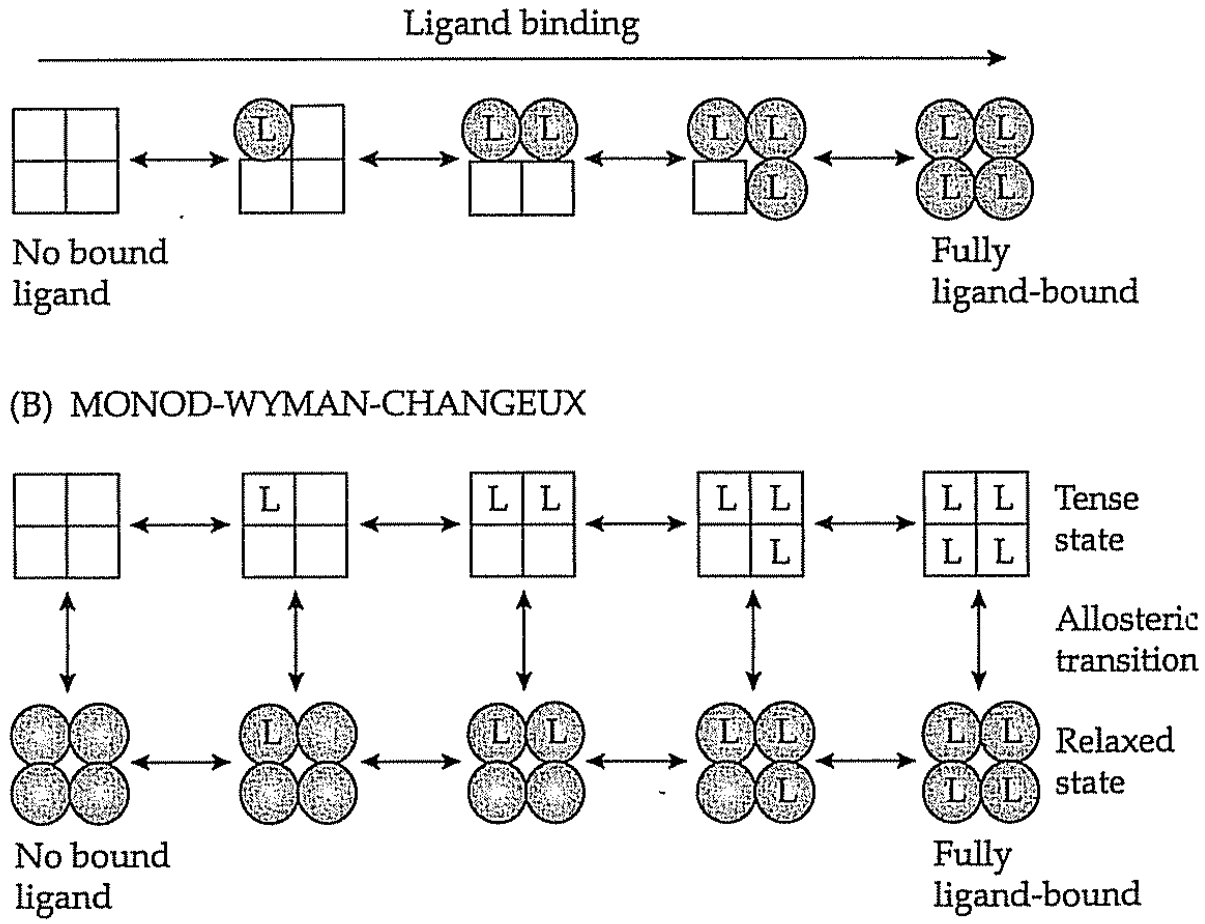


**Figure 1. Allosteric models.** Illustration of the Koshland-Nemethy-Filmer and Monod-Wyman-Changeux models for positive allosteric cooperativity of ligand binding using a hypothetical tetrameric protein. (A) The Koshland-Nemethy-Filmer (KNF) model proposes that binding of each ligand induces a conformational change in the subunit to which it is bound and in the adjacent subunits increasing their affinity for binding of the next ligand. (B) In the Monod-Wyman-Changeux (MWC) model there are only two conformational states, tense and relaxed, each having intrinsic ligand affinities that are not altered by ligand binding to other subunits. Rather, ligand binding shifts the conformation equilibrium from the tense to relaxed state.

### 1.2.1 Ion Channels as Allosteric Proteins

Ion channels are a class of allosteric proteins that have been extensively studied in an effort to understand how these proteins transition from one conformational state to another. Ion channels are ion permeable pathways through the plasma membrane that have at least two well defined conformational states: open and closed [5]. In the open state, the channel acts as a conduit through which selected ions flow passively down their electrochemical gradient. The electrochemical gradient is defined as the driving force that determines the passive transport of ions through a channel. This gradient includes a contribution from the concentration gradient of the solute and a second contribution from the electrical potential of charged solutes that exist between the inside and outside of the cell [6]. In the second state, the closed state, the ion-conducting pathway is closed, preventing the flow of ions, regardless of the electrochemical gradient. Gating is the process through which the pore transitions between the closed and open states. The conformational changes enabling the pore to transition from a non-conducting to a conducting state are allosterically coupled to other parts in the protein. Therefore, the allosteric property of ion channels allows the free energy of channel opening to be dictated by changes in membrane voltage, mechanical force, or ligand binding.

## 1.3 EARLY BIOPHYSICAL APPROACH TO INVESTIGATING ION CHANNEL GATING

The observation that ion channels gate was a monumental achievement that lead to the field of ion channel biophysics. The foundation for this field can be traced to the initial work of Hodgkin and Huxley, who characterized membrane current in squid giant axons [7-11]. Their initial work helped to elicit curiosity in ion channel research. Many discoveries since Hodgkin's and Huxley's initial work have helped to form our current understanding of gating. Therefore, I would like to introduce what I consider to be the most significant of these discoveries since the initial contributions of Hodgkin and Huxley. However, no list would be complete without first introducing Hodgkin's and Huxley's contribution toward the understanding of membrane current.

### 1.3.1 Elucidating the Components of Membrane Current

Axon physiology gained momentum with the development of the voltage clamp technique by Kenneth Cole [12]. The voltage clamp is an electrical technique for measuring the flow of ions across membranes. Unlike conventional methods, where current is applied and the subsequent change in membrane potential is measured, the voltage clamp technique holds the membrane potential constant while the membrane current is measured [5]. The development of the voltage clamp allowed Hodgkin and Huxley to directly measure ion movement across excitable membranes. Using the voltage clamp technique, Hodgkin and Huxley set out to characterize membrane current and the underlying permeability mechanisms [7-11]. Their experimental design relied upon two assumptions: 1) ions tend to move passively down their electrochemical

gradient. Therefore, the direction of ion flow could be predicted at a given concentration gradient and membrane potential. 2) Permeability changes are insensitive to the concentration of the major ions: $Na^+$, $K^+$, and $Cl^-$. Therefore, the movement of one ion can be stopped by replacing that ion by an impermeable species with little consequence on the movement of the other ions [5]. Incorporating these assumptions into their experimental design, Hodgkin and Huxley determined that the membrane current measured from a voltage-clamped squid axon (depolarized to 0 mV from the normal resting potential) is composed of four components (Fig. 2) [9]. These components can be divided into two major categories: ionic current, which is carried by the movement of ions, and the capacitive current, which is a quick transient spike of current that is over before the voltage step is completed. The ionic portion of the membrane current constitutes the action potential and is made up of two major components: the sodium current ($I_{Na}$) and the potassium current ($I_K$) and a minor component termed the leakage current ($I_{leak}$). $I_{Na}$ is the transient inward flow of $Na^+$ ions, $I_K$ is the outward flow of $K^+$ ions, and $I_{leak}$ is the small, relatively voltage-independent background conductance (Fig. 2).

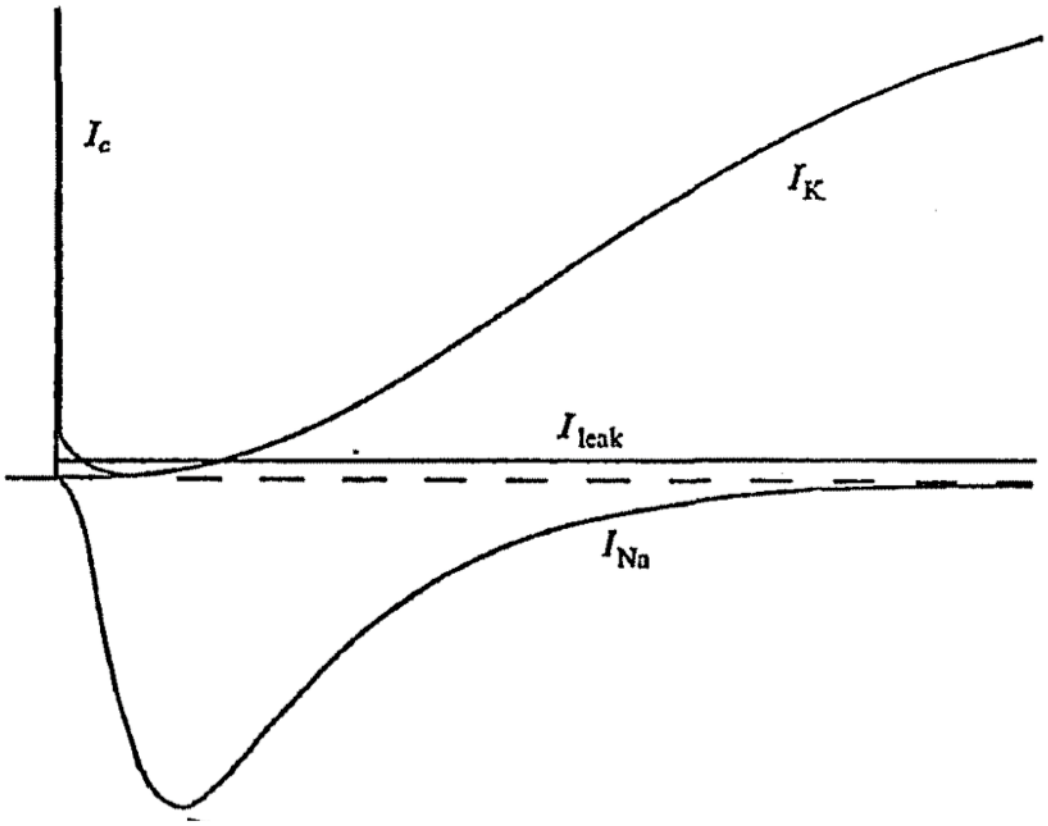


**Figure 2. Components of membrane current.** Membrane current is composed of ionic current and capacitive current ($I_c$). The ionic portion of the current is primarily composed of $Na^+$ current ($I_{Na}$) and $K^+$ current ($I_K$), and a minor component from the leakage current ($I_{leak}$). [Reprinted with permission from Armstrong C.M., *Quarterly Review of Biophysics*, vol. 7, issue 2, pg. 182. Copyright 1974 by the Cambridge University Press.]

While investigating the components of membrane current, Hodgkin and Huxley made the first observation that the onset of membrane current is dependent upon membrane potential [7]. Thus, the changes in $Na^+$ and $K^+$ conductance, ($g_{Na}$) and ($g_K$) respectively, are dependent upon how the membrane electric field affects the orientation of charged molecules associated with these conductances. Therefore, $g_{Na}$ and $g_K$ are dependent upon the orientation of these charged particles, and only when these particles are in a particular position will membrane current be observed [7]. The observation that membrane current is composed of multiple conductances, and the activation of these conductances are dependent upon membrane potential directly lead to investigations regarding the nature of the charged particles associated with current activation, and whether these conductances are separate or share a common pathway.

### 1.3.2 Single versus Separate Channel Hypothesis

The observation that total membrane current consists of multiple conductances directly lead to investigations as to whether the $Na^+$ and $K^+$ components of membrane current are combined or separate systems. This problem later became know as the single versus separate channel hypothesis (Fig. 3) [13, 14]. The experiments that are credited with providing the most insight into this problem used a pharmacological approach to specifically target and dissect the components of membrane current [15, 16]. The initial evidence suggested that $g_{Na}$ and $g_K$ utilize separate pathways based upon the specificity of TEA (tetraethylammonium ion) and TTX (tetrodotoxin) [15]. When TTX is applied to the outside of an axon it blocks $Na^+$ current without affecting the time course or magnitude of the $K^+$ current [17]. Therefore, from this observation it was assumed that TTX blocks the $Na^+$ channels leaving the $K^+$ channels unblocked. The corollary is that TEA blocks $K^+$ current leaving the $Na^+$ channels unaffected [18-20]. Therefore,

the use of TTX and TEA provided strong evidence that $g_{Na}$ and $g_K$ are separate systems. However, the single channel hypothesis, argued by L. Mullins, states that the channel first conducts $Na^+$ ions after which it inactivates, and only then will it conduct $K^+$ ions [21]. Mullins argued that TTX simply blocks the $Na^+$ component and TEA the $K^+$ component [13, 14, 21]. However, Clay Armstrong and colleagues conducted a series of experiments in support of the dual channel mechanism using the proteolytic enzyme pronase [22, 23]. Pronase is rather selective for it does not alter $K^+$ or $Na^+$ activation rather it eliminates $Na^+$ inactivation. These experiments illustrated that the onset of $K^+$ activation was not affected by eliminating $Na^+$ inactivation. Because $K^+$ activation is intact after eliminating $Na^+$ inactivation, this result suggested that $g_{Na}$ and $g_K$ are separate systems. Thus, Armstrong's experiments provided the strongest evidence in support of the dual channel hypothesis.

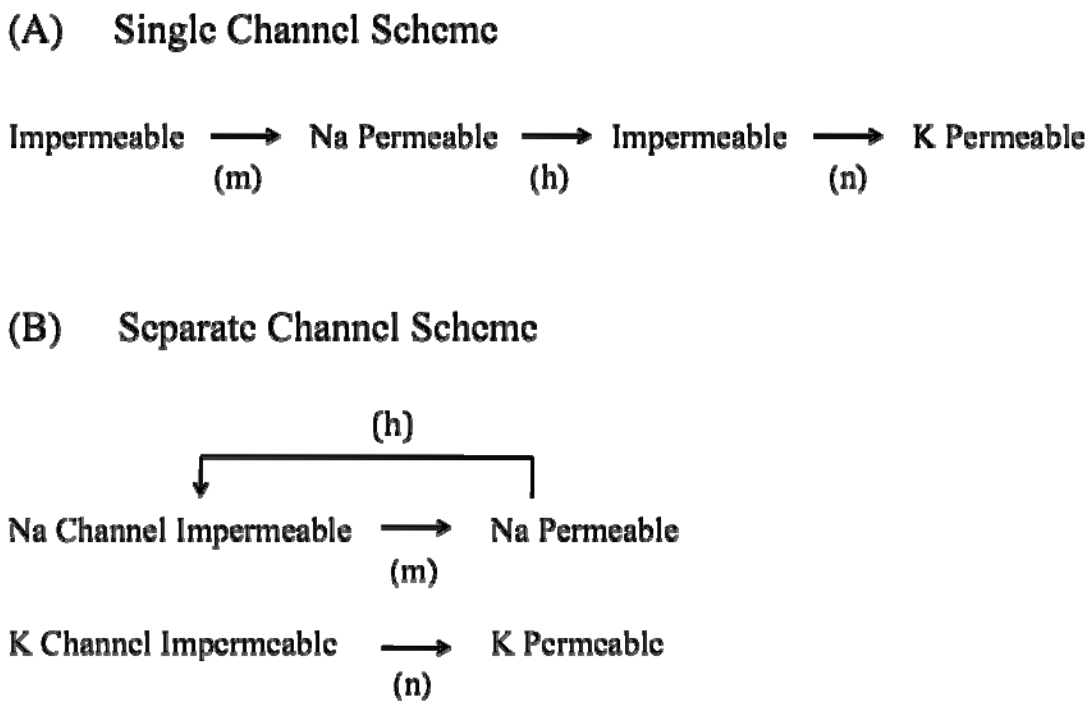


**Figure 3. Single versus separate channel hypothesis.** (A) Single channel scheme assumes that a single voltage-dependent time constant controls the change of the membrane from impermeable to $K^+$ permeable. The $Na^+$ permeable phase is governed by two time constants, and any lengthening of these time constants, especially (h) will prevent the appearance of the $K^+$ permeable state. (B) The separate channel scheme has a $Na^+$ permeable state that can be turned on by the (m) process and turned off either by (h) or by a voltage change reversing (m). The $K^+$ process is independent from the $Na^+$ channel and is turned on or off by the (n) process. [Adapted from Mullins L.J., 1968. A single channel or a dual channel mechanism for nerve excitation. *Journal of General Physiology*. vol 52, pg. 550.]

### 1.3.3 Ionic Pores versus Carrier Proteins

Implicit in the work from Hodgkin and Huxley is whether ions use pores or carrier proteins to pass through the cell membrane. There is strong evidence that the passive transport of $K^+$ and $Na^+$ ions through the membrane occurs through pores. Part of this evidence comes from Armstrong's lab, which postulated a pore mechanism from their characterization of the interaction between quaternary ammonium (QA) compounds and $K^+$ channels [16, 18, 24, 25]. Specifically, their experiments tested for a pore model and not a carrier model for ion transport. The TEA derivative, nonyltriehtylammonium ion ($C_9$), is an effective blocker of $K^+$ channels. When $C_9$ is applied to the inside of an axon, $K^+$ current ($I_K$) does not reach a steady-state level during the voltage step, but inactivates in a manner similar to $Na^+$ current ($I_{Na}$). The mechanism of $C_9$ inactivation can only be explained by a model $K^+$ pore. The model has four states when $C_9$ is present (Fig. 4. A). (1) At the resting potential the activation gate is closed preventing $C_9$ from entering the mouth of the pore. (2) After the depolarization step, the gate is open permitting the $K^+$ ion to move through the pore (3) $C_9$ is capable of entering the pore through the inner mouth, inactivating the channel. (4) Repolarizing to the resting potential causes the channel to transition from the inactivated state to the closed state, trapping the $C_9$ ion in the channel. There are two methods to speed recovery that give strong evidence to the ionic pathway being a pore rather than a carrier [16, 22]. The first method is to increase external $K^+$ concentration, and the second method is to make the membrane potential more negative. Only the pore model can explain the mechanism behind each of these results. As illustrated in Fig. 4 (B), the hydrophobic binding of $C_9$ prevents the molecule from spontaneously leaving the pore. The presence of a $K^+$ ion at point X pushes $C_9$ out of the pore through electrostatic repulsion. Therefore, increasing external $K^+$ concentration and making the membrane potential more negative increases the probability of

finding a $K^+$ ion at point X. These effects with $C_9$ would be difficult to reconcile using a carrier model indicating that ions transverse the cell membrane using pores.

A.

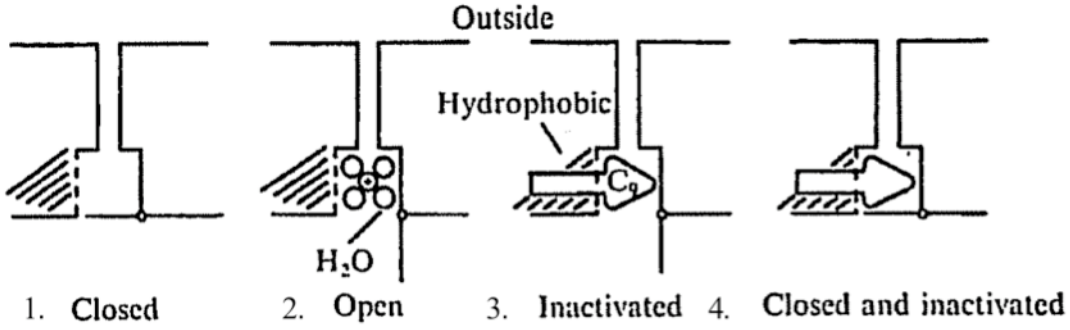


B.

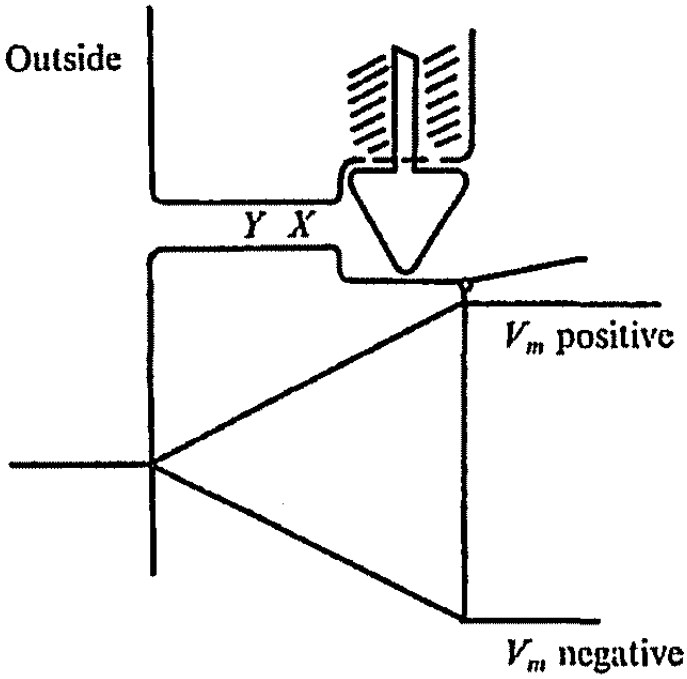


**Figure 4. Early ion channel model.** Models from Clay Armstrong's C9 experiments illustrating that ions transverse the membrane through ion channels rather than carrier proteins. (A) Model illustrating the four hypothetical states of a pore when C9 is in the cytoplasm. (B) Model to explain the accelerated removal of C9 from the pore when extracellular $[K^+]$ is high or when $V_m$ is negative. [Reprinted with permission from Armstrong C.M., *Quarterly Review of Biophysics*, vol. 7, issue 2, pgs. (A) 186 and (B) 189. Copyright 1974 by the Cambridge University Press.]

### 1.3.4 Gating Currents

"…it seems difficult to escape the conclusion that the changes in ionic permeability depend on the movement of some component of the membrane which behaves as though it had a large charge or dipole moment." A.L. Hodgkin and A.F. Huxley 1952 [7].

Channel gating, as it was originally predicted by Hodgkin and Huxley in 1952, is the voltage-dependent opening and closing of pores [7]. Their seminal work characterizing the components of membrane current formed the foundation for the field of ion channel biophysics. Hodgkin and Huxley made the first prediction that charged particles in the membrane are responsible for manipulating the permeability changes that accompany the activation of $Na^+$ and $K^+$ channels [7]. Their original hypothesis was responsible for initiating much of the work attempting to identify these charged particles, and determining whether they are associated with the membrane or exclusively with the channels. In the next section, I will briefly summarize some of the original ideas concerning these charged particles and how they are associated with channel gating.

#### 1.3.4.1 Dissolved ions and molecules as gates or sensors

Originally, it was thought that dissolved ions and molecules functioned as both the voltage sensor and the gate for $Na^+$ and $K^+$ channels [26, 27]. The most studied of these ions was $Ca^{2+}$. It was well known that increasing the concentration of free $Ca^{2+}$ surrounding nerve or muscle increased the depolarization level required to reach firing threshold [28]. Gordon and Welsh first theorized that $Ca^{2+}$ ions plug the pores acting as both the voltage sensor and the gate [27]. However, many observations from the field did not support this model. For example, 1) $Ca^{2+}$ can pass through an open $Na^+$ channel, 2) excitability is maintained for a prolonged period of time in the presence of $Ca^{2+}$ chelating agents, and 3) $Ca^{2+}$-free solutions did not alter the voltage-

dependence of $Na^+$ channel activation [29-32]. In addition to $Ca^{2+}$, non-physiological ions block channels in a voltage-dependent manner, therefore they were also considered to function as the voltage sensor and the gate [16]. However, perfusing axons with non-physiological ions does not affect the time course of channel opening or closing [33-35]. These results indicated that dissolved or non-physiological ions cannot function as the voltage sensor machinery or gate [26]. Furthermore, it is unlikely that simply perfusing an axon washes out the components necessary for voltage sensing, suggesting the charged particles are an inherent component of the membrane [26]. Because these gating particles were now considered to be part of the membrane, it could be proposed that the gating process is dependent upon these particles undergoing a conformational change within the membrane.

> "Thermodynamically there is no way for channels to continue to open and close millions of times without direct input of energy into the sensing-gating process on every cycle. Arguments have already been presented against direct contributions from conventional metabolic sources or from the ion gradient. The only remaining source of energy is the electric field. The field must do electric work on the sensor-gate by moving some charges through the intramembrane field. Hence, while work is being done a small membrane current reflecting these internal rearrangements will flow." Bertil Hille 1976 [26].

The existence of carrier currents, or as they are most often referred, gating currents were predicted to exist by Hodgkin and Huxley in 1952 [7]. However, both Hodgkin and Huxley, and later Chandler and Meves were unsuccessful in trying to observe gating currents [7, 33]. In both cases, the relatively low channel density was to blame for their inability to measure these currents. Additionally, as discussed by Hodgkin and Huxley, the magnitude of these currents were unknown, but were expected to be a fraction of the maximum current [7]. Therefore, Chandler and Meves attempted to reduce the interference of ionic currents by replacement with non-permeable cations, although they still failed to resolve gating currents [33]. It wasn't until Armstrong and Francisco Bezanilla first recorded the small transient currents in 1973 [36] that

they were shown to exist 21 years after they were first predicted by Hodgkin and Huxley. Like Chandler and Meves, Armstrong and Bezanilla reduced ionic currents through ionic replacement [36]. In their experiments, they replaced $Na^+$ on the outside with Tris+tris(hydroxymethyl) methyl ammonium ion and they replaced $K^+$ with $Cs^+$ on the inside. They also used TTX, which does not affect gating currents, to eliminate the remaining current through $Na^+$ channels. The problem Chandler and Meves had with the signal to noise, Armstrong and Bezanila rectified with signal averaging techniques to increase the signal to noise ratio. There is considerable evidence to suggest that gating currents are associated with the activation of $Na^+$ channels [37, 38]. First, the time course between $I_{Na}$ and the associated gating current is nearly identical. Second, the addition of internal $Zn^{2+}$ eliminates both ionic and gating current, and these currents recover together after wash-out of the cation. Third, prolonged depolarization eliminates both $I_{Na}$ and the gating current, which recovers together when the holding potential is restored. Finally, inactivation of the channel temporarily eliminates the gating currents. When the channel is in the inactivated state, it prevents the activation gate from closing, and therefore inhibits the gating charge from returning to the off position.

## 1.4 MOLECULAR APPROACH FOR INVESTIGATING ION CHANNEL GATING

Up until the early 1970's, most of our understanding regarding the structures involved in gating was derived from the voltage clamp technique (Fig. 5). This method was so effective that it biased our approach toward the study of ion channels; no one thought to consider the chemical nature of the channel. However, a new era in the study of channel structure began in 1973 when the nicotinic acetylcholine receptor (nAChR) and the $Na^+$ channel were first identified as

proteins [23, 39]. Since ion channels are proteins, much effort was expended for the development and refinement of techniques for solubilizing and purifying membrane proteins without destroying their function [5]. For instance, nAChR was isolated from the electric organ plasma membranes of the electric ray, *Torpedo*. Membrane proteins were solubilized with detergents to form micelles containing a protein molecule surrounded by detergents and a few lipid molecules. Affinity columns bound with α-neurotoxins, such as α-bungarotoxin, were used to separate the micelles containing nAChR, which were eluted with a high concentration of cholinergic ligand [40-45]. The complete amino acid sequence was determined by a combination of protein chemistry and molecular genetics [46-48]. To ensure the sequences were sufficient to express the protein in a fully functional form, complementary DNAs (cDNAs) were expressed in heterologous expression systems, such as *Xenopus* oocytes [49, 50]. Heterologously expressed channels enabled the functional characteristics of the cloned protein to be compared with the endogenous channel [51]. Therefore, the study of ion channels took on an interdisciplinary approach in the 1980's, as methods in molecular biology and protein chemistry enabled us to investigate the chemical structure of ion channels.

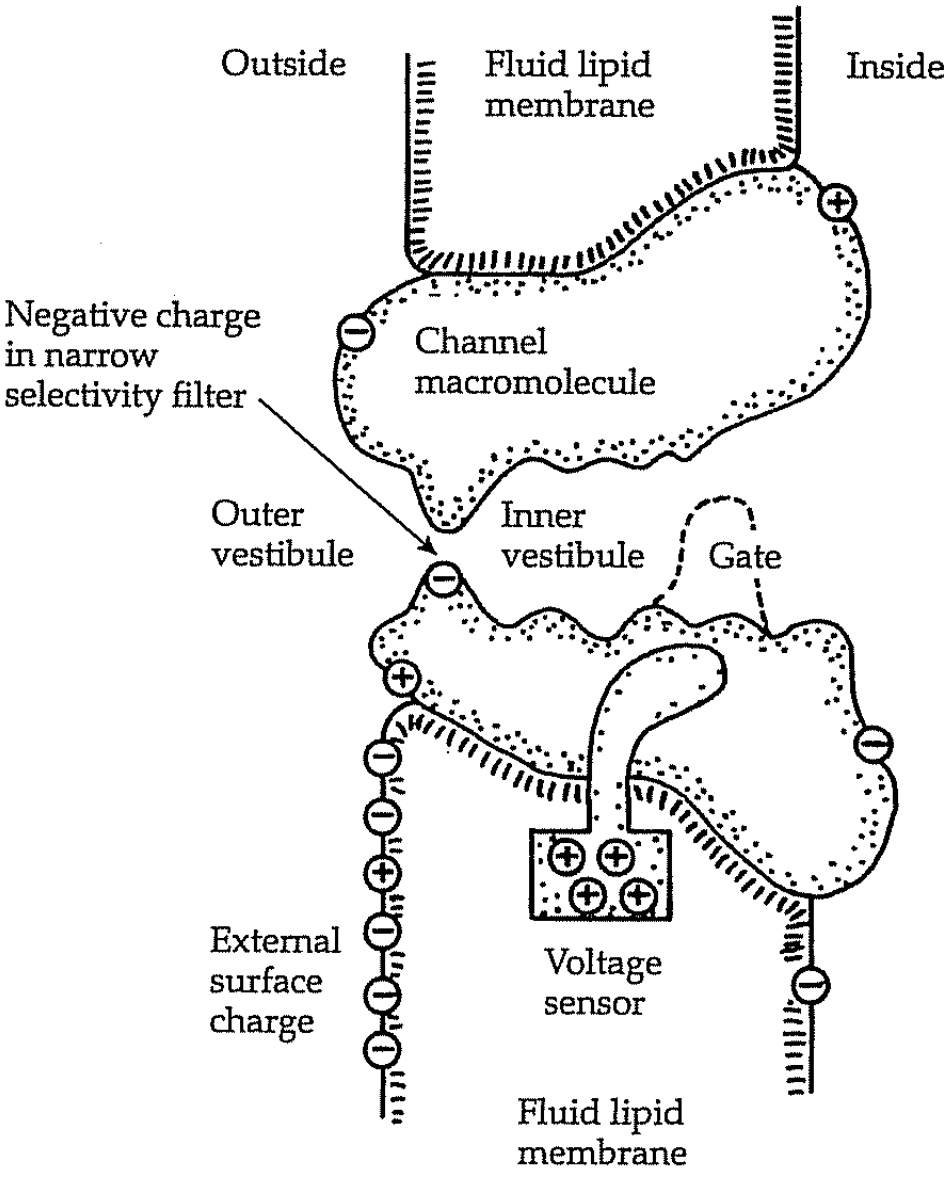


**Figure 5. 1970's model of a voltage-gated ion channel**. The channel is drawn as a transmembrane protein with a lumen down the center. The components are labeled with terms used in 1975. [Figure is based upon Hille B., *Progress in Biophysics and Molecular Biology*, vol. 21, pgs. 1-32, 1970. Reprinted in Hille Handbook of Physiology. The Nervous System, vol. 1, pt. 1, 1977. Reprinted with permission from the American Physiological Society, copyright 1977.]

### 1.4.1 Cloning of the $K^+$ Channel

Initial attempts in $K^+$ channel protein chemistry proved to be difficult [5, 52-54]. Unlike the nAChR, $Na^+$ and $Ca^{2+}$ channels, high affinity ligands were not available for $K^+$ channels during this time period [5]. Therefore, the biochemical approach used to determine the primary sequence of nAChR and $Na^+$ channels could not be utilized. Another approach needed to be taken, and this approach benefitted from a behavioral mutant, Shaker, from *Drosophila melanogaster* [53]. This mutation caused ether-anesthetized flies to shake uncontrollably [5]. The abnormalities causing this behavior were traced to a disruption in action potential firing, suggesting that a gene within the Shaker locus encoded for a $K^+$ channel [55, 56]. This mutation enabled the sequence to be obtained by positional cloning [5]. The goal in positional cloning is to identify fragments of chromosomal DNA from the coding region of the gene rather than to look for derived RNA messages. One starts by locating the position of the chromosomal mutation. Next, the gene is identified through a process known as chromosome walking by using a clone of an already known piece of genomic DNA located as near as possible to the suspected gene [5]. Subsequent investigations determined that the Shaker gene encodes for an α-subunit, which corresponds to a single copy of the six transmembrane (6 TM) domain that is repeated four times in voltage-gated $Na^+$ and $Ca^{2+}$ channels [57-61]. This makes sense in evolutionary terms because voltage-gated $Na^+$ and $Ca^{2+}$ channels are thought to have evolved from $K^+$ channels. It is likely that the precursor channel that gave rise to $Na^+$ and $Ca^{2+}$ channels arose from a single-domain channel through two rounds of gene duplication. The first round consisted of converting the single-domain channel into a two-domain channel, which was duplicated again to form the four-domain precursor channel [62]. Therefore, $K^+$ channels are evolutionary older than $Na^+$ and $Ca^{2+}$ channel, and as suggested by the structure of these channels, the fully assembled $K^+$ channel is

expected to be a complex of four subunits assembled into a tetramer around a centrally located pore. Roderick Mackinnon later provided the first experimental confirmation that the subunits of the Shaker $K^+$ channel assemble as a tetramer [63].

### 1.4.2 The Cloned $K^+$ Channel

The cloning of the Shaker $K^+$ channel provided the means for discovering a diverse family of $K^+$ channels [63-66]. Cloning projects have revealed over 80 related mammalian genes for α-subunits of $K^+$ channels that come in many different architectural forms [5]. $K^+$ channels can be recognized by the $K^+$ channel signature sequence, (-TXXTXGYGD-), contained in the pore-lining P-loops [67]. $K^+$ channel architecture varies from the simplest 2TM channels such as $K_{ir}$ and KcsA, to the 4TM 2-pore channels such as TWIK, to the 6TM architecture of the voltage-gated $K^+$ channels (Kv), to the largest 7TM architecture of large conductance $Ca^{2+}$-activated $K^+$ (BK) channels (KCa1.x), see Fig. (6). Also included in the 6TM family of ion channels is the SK subfamily, which includes the small (KCa2.1, KCa2.2, and KCa2.3) and intermediate conductance (KCa3.1) $Ca^{2+}$-activated $K^+$ channels, which are the subject of this dissertation. These channels share little sequence similarity with the BK channels; rather these channels are more closely related to the Kv family of $K^+$ channels. This can be explained through the hypothetical phylogeny of voltage-gated ion channels [62]. The earliest known structures are the 1-domain 2TM channels, and through the subsequent addition of 4TMs gave rise to the 1-domain 6TM channels, which encompasses the voltage-gated $K^+$ channels and the ligand gated ions channels [62]. This would explain why KCa3.1 and KCa2.x are more closely related to the Kv channels than the BK channels. Furthermore, through two rounds of gene duplication, the 1-domain 6TM channels gave rise to the 4-domain 6TM of the voltage-gated $Na^+$ and $Ca^{2+}$

channels.

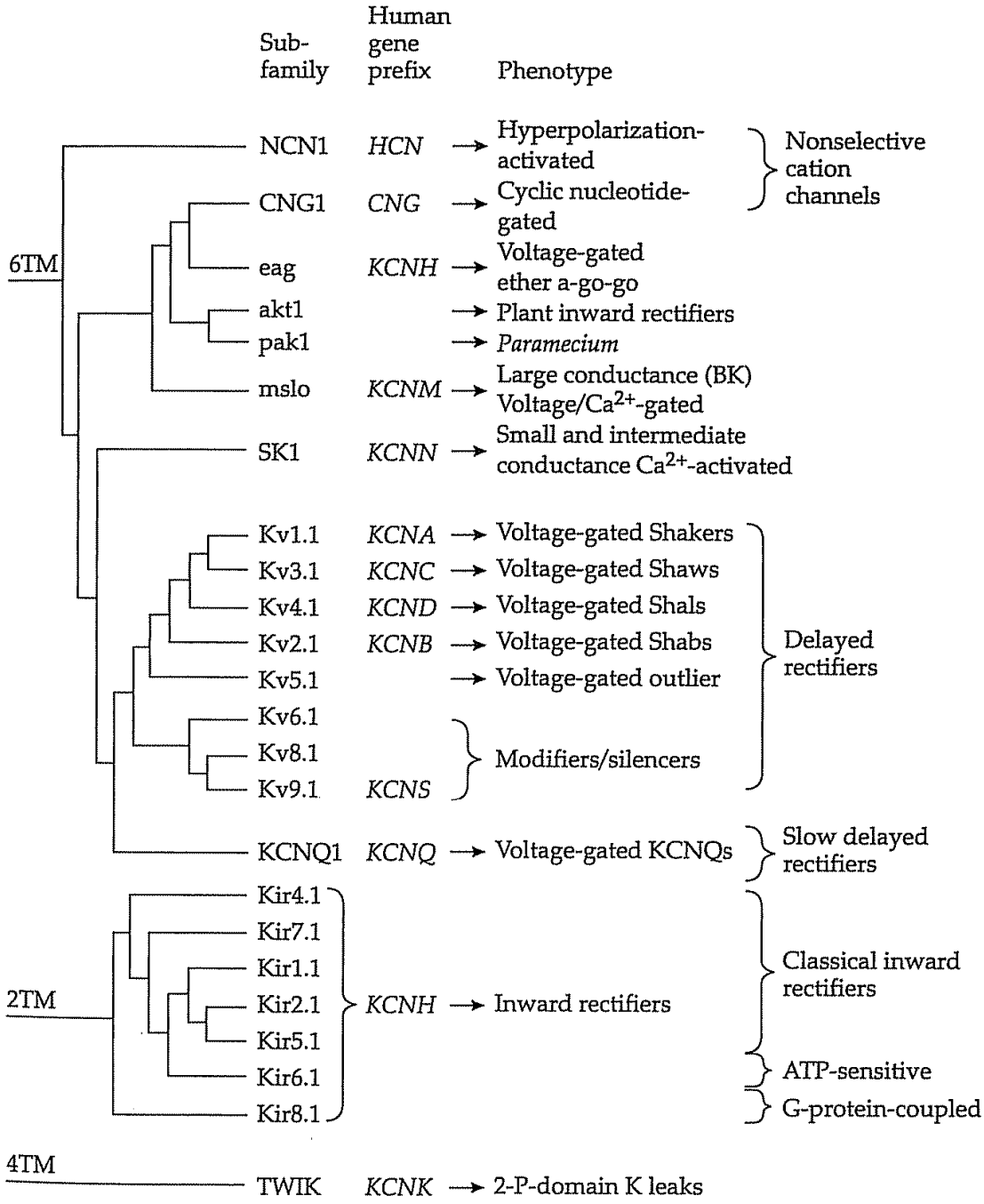
Sub-family
Human gene prefix
Phenotype
NCN1
HCN
Hyperpolarization-activated
Nonselective cation channels
CNG1
CNG
Cyclic nucleotide-gated
6TM
eag
KCNH
Voltage-gated ether a-go-go
akt1
Plant inward rectifiers
pak1
Paramecium
mslo
KCNM
Large conductance (BK) Voltage/Ca2+-gated
SK1
KCNN
Small and intermediate conductance Ca2+-activated
Kv1.1
KCNA
Voltage-gated Shakers
Kv3.1
KCNC
Voltage-gated Shaws
Kv4.1
KCND
Voltage-gated Shals
Kv2.1
KCNB
Voltage-gated Shabs
Kv5.1
Voltage-gated outlier
Delayed rectifiers
Kv6.1
Kv8.1
Kv9.1
KCNS
Modifiers/silencers
KCNQ1
KCNQ
Voltage-gated KCNQs
Slow delayed rectifiers
Kir4.1
Kir7.1
Kir1.1
Kir2.1
Kir5.1
Kir6.1
Kir8.1
2TM
KCNH
Inward rectifiers
Classical inward rectifiers
ATP-sensitive
G-protein-coupled
4TM
TWIK
KCNK
2-P-domain K leaks

**Figure 6. Ramification of $K^+$ channels in higher animals.** Known K-channel genes are sorted by similarity of amino acid sequence. The coarsest grouping separates them by membrane topology (2TM, 4TM, 6TM). This diagram was made by aligning 89 channel sequences, mostly from mammals, using just 47-49 amino acids including their P-regions and extending into the subsequent hydrophobic domain. A dendrogram was made with the Clustal algorithm and then converted into a cladogram using the MacClade program. Finally, the full tree was simplified by retaining only one representative member of each subfamily and discarding the other small branches. Branch lengths do not represent time, but the branching is expected to preserve evolutionary relationships. The HCN channels are relatives that also pass $Na^+$ ions; the akt and pak channels are from plants and *Paramecium*, respectively. [The figure was prepared by W.J. Joiner and A.M. Quin. Reprinted with permission from W.J. Joiner.]

## 1.5 STRUCTURE-FUNCTION APPROACH FOR INVESTIGATING ION CHANNEL GATING

Heterologous expression of $K^+$ channels combined with site-directed mutagenesis elicited the development of hypotheses regarding the regions of the channel responsible for permeation and gating [5]. The mutated channels were expressed in *Xenopus* oocytes or other heterologous expression systems (e.g., HEK (human embryonic kidney), CHO (Chinese hamster ovary) or COS (monkey kidney) cells) and channel function was examined and compared to the WT-channel [49, 50]. This experimental approach used structure-function logic to indirectly investigate channel structure. When interpreting these results it is typically assumed that the mutated region of the channel is associated directly with the structure that corresponds to the manipulated function. For instance, a mutation in a region that alters permeation or single channel conductance, is thought to be associated with the permeation pathway. Therefore, in an ideal situation, the structural perturbations caused by the mutation are local, enabling a direct link with channel function. However, mutations can disrupt channel structure indirectly at a second site or globally, complicating the interpretation of how a mutated region is associated with channel function. Therefore, when interpreting experiments from mutagenesis it is helpful to have converging lines of evidence obtained from multiple experimental approaches. Mutagenesis is often combined with chemical modification or some form of structural determination to ensure that the effects are specific for one function, rather than disturbing multiple functions of the channel [5]. One such method is the substituted cysteine accessibility method (SCAM) [68-70]. SCAM will be defined and discussed later as this method was used extensively to understand the architecture of S6 in KCa3.1.

As mentioned previously, the cloning of Shaker, and subsequent $K^+$ channels enabled the indirect examination of channel architecture through structure-function studies. Furthermore, much of our current understanding regarding pore structure is the culmination of many investigations from the early 80's through the middle to late 90's. I would like to briefly highlight the methodologies used in several investigations, which were credited for defining the regions of the channel that are associated with the pore and the gate.

### 1.5.1 The Pore

Investigations into the $K^+$ channel pore used several experimental approaches to isolate regions of the channel associated with the pore. One of the methods involved swapping regions between $K^+$ channels with known functional differences associated with permeation and block, as a means to isolate the sequence involved in formation of the pore [71-74]. If the transplanted region is associated with the pore, then the chimeric channel should adopt the biophysical properties of the donor channel. Hartmen et al., [71] used this technique to investigate whether the P-loop is associated with the pore. The 21 amino acid segment linking S5 to S6 was transplanted from the voltage-activated NGK2 $K^+$ channel to DRK1, a $K^+$ channel differing in single channel conductance and sensitivity to both external and internal TEA. Supporting their hypothesis, the chimera exhibited characteristic, such as single channel conductance and block by external and internal TEA, similar to the donor NGK2 channel. This result suggests that the 21 amino acid segment linking S5 to S6 controls many of the essential biophysical properties of the pore in addition to forming part of the permeation pathway. Utilizing the same approach Lopez et al., [74] transplanted S6 of NGK2 into the Shaker $K^+$ channel as a means to investigate whether S6 is associated with the pore. The chimeric channel adopted the single channel conductance and

sensitivity to internal TEA and barium of the donor channel, suggesting that in addition to the P-loop, S6 is associated with the pore. The second method utilized structure-function studies of pore blockers such as TEA and CTX [75-81]. The basis for many of these structure-function studies came from the initial observation that CTX blocks the BK channel by binding to the external surface of the mouth of the pore [77]. By analogy, it was assumed that CTX also blocks the Shaker $K^+$ channel in a similar manner [79]. Many of these investigations came from the lab of Roderick Mackinnon, whose lab used site-directed mutagenesis to isolate the residues required for CTX block, thereby indirectly mapping the external surface of the pore [79, 81, 82]. The results from a series of investigations determined that the lateral segment of the P-loop, between S5 and S6, forms the external mouth of the pore [60, 61]. It was also observed that the P-loop residues required for CTX block also function as the binding site for externally applied TEA [80]. Therefore, in a separate investigation, Yool et al., [73] determined the residues in the middle of the P-loop that are important for internal TEA block. Furthermore, mutation of these residues also altered the permeation properties to $K^+$, $Rb^+$, and $NH_4$, suggesting these residues contribute to both the internal TEA binding site as well as forming part of the permeation pathway.

### 1.5.2 The Gate

Structure-function studies were also instrumental in providing insight into the regions of the channel forming the gate [5, 83]. The gate was thought to be a structure that physically blocks the pore to prevent ion diffusion [84]. The gate is in the open configuration when the channel is activated, enabling ions to flow down their electrochemical gradient. Upon dissociation of ligand or reversal in membrane potential, the channel transitions directly to the closed state. Ion

diffusion is blocked as the gate returns to the original position. This type of mechanism is referred to as activation-deactivation gating. However, in the continued presence of ligand or depolarizing membrane potentials, some channels block ion diffusion by entering into an intermediate inactive state. In this state, the channel is open, but ion diffusion is blocked through either collapse of the selectivity filter, termed C-type inactivation [85-90] or an auto-inhibitory part of the channel protein, termed N-type inactivation [91-96]. This mechanism is referred to as activation-inactivation gating; the channel must transition from the inactivate state to the open state before entering into the closed state. Thus, gating involves large conformational changes in protein structure, which have been difficult to understand without direct knowledge of channel structure. A clue for the location of the gate came from experiments showing that fast inactivation [84, 97] of $Na^+$ and $K^+$ channels may result from a cytoplasmic gate such as the amino terminal peptide of the Shaker B $K^+$ (ShB) channel blocking the permeation pathway [93, 96]. Isacoff et al. [83] reported that the intracellular loop between transmembrane segments S4 and S5 most likely forms part of the receptor for the inactivation gate. Their results indicated that the glutamate at position 395 might be the counter-charge for the positively charges residues of the inactivation ball. Their investigation showed that mutation of position 395 affected the stability of the inactivated state as well as single channel conductance. However, mutations at other positions in the S4-S5 linker also produced alterations in the rates of the N-type inactivation [98]. Furthermore, the activation gating of the Shaker channel is also very sensitive to mutations in this region [99], and it is known that binding of the inactivation ball and other blockers is dependent on the activation state of the channel. Therefore, mutations in this region might change the apparent affinity for the ball by a direct change in the binding site, or indirectly by changing gating [100]. Holmgren et al. [98] used the method of cysteine substitution and

subsequent chemical modification to help distinguish direct and indirect effects, with the goal of identifying residues that directly interact with the inactivation gate. Their investigation showed a particularly strong effect of charge modification at position 391, consistent with a direct electrostatic interaction. At this position, chemical modification altered the kinetics of ball peptide binding without altering other biophysical properties of the channel. Results with reagents that attach different charged groups at 391C suggest that there are both electrostatic and steric interactions between this site and the ball peptide. These findings identify this site to be in or near the receptor site for the inactivation ball. Four lines of evidence support this idea. First, inactivation only occurs after the voltage-dependent gate opens, suggesting the open conformation of the pore exposes a receptor for the gate [96]. Second, inactivation is produced by the binding of only one gate to a single pore opening [101, 102]. Third, high concentrations of extracellular $K^+$ reduce inactivation, most likely by pushing the gate from its intracellular side [92]. Fourth, inactivation mimics the action of quaternary amines, which are thought to be pore blockers [25, 91]. In a subsequent investigation, Zhou et al., [103] showed that the central cavity and inner pore of the $K^+$ channel form the receptor site for both the inactivation gate and small-molecule inhibitors. They propose that inactivation occurs by a sequential reaction in which the gate binds initially to the cytoplasmic channel surface and then enters the pore as an extended peptide. Therefore, combining mutagenesis with permeation and block structure-function studies provided insight into the regions of the $K^+$ channel that form the pore and the gate.

## 1.6 SUBSTITUTED CYSTEINE ACCESSIBILITY METHOD

As previously mentioned, combining chemical modification with site-directed mutagenesis is an effective way to determine whether the observed phenotype caused by a mutation is the result of a local or global change in channel structure [5]. Chemical modification using membrane impermeant reagents applied to the extracellular or intracellular aspect of transmembrane proteins has been useful in determining residues that are accessible from the outside and inside of the membrane, respectively [104]. However, structural mapping greatly improved with the development of site directed mutagenesis, and the cloning of ion channels. SCAM or substituted cysteine accessibility method combines site-directed mutagenesis and chemical modification with thiol specific regents to assess the accessibility of introduced cysteines [68-70, 105, 106]. Typically, as a test of cysteine accessibility, a biochemical test is used to measure the extent to which the thiol reagent is incorporated into the protein [104]. The development of reagents that react quickly under physiological conditions has allowed this technique to be applied to the study of ion channel structure [106-108].

### 1.6.1 SCAM and Ion Channels

Ion channels provide a distinct advantage over other proteins when trying to assess the extent of chemical modification and hence cysteine accessibility. Channel function is easily measured through patch clamping, allowing for real-time functional measurements to take the place of conventional biochemical tests. If the modified cysteine is located in a gating sensitive region, modification of this residue will alter channel gating, which can be assessed through patch clamping [104]. Cysteine residues are classified as either exposed or buried based upon the

extent of modification. SCAM neglects fluctuation in protein structure. Therefore, no cysteine is considered unreactive due to the possibility that the buried cysteines may react slowly. To gauge the extent of modification, it is useful to determine the time course, modification rate, and state dependence of the modified cysteine. However, reactivity is not simply based upon accessibility to the reagent, as reactivity can also be affected by acid dissociation of the Cys-SH, steric constraints on the formation of an activated complex, and for charged reagents, the electric field along the path to the residue. Although adding to the difficulty in interpreting the results, these factors can be dissected out by comparing the reaction rates for reagents that differ in charge or size [69]. The most common approach is to compare accessibility between the different methanethiosulfonate (MTS) reagents. Arthur Karlin and colleagues designed a set of water-soluble reagents based on the MTS moiety [106, 107]. The MTS reagents readily transfer a hydrophilic moiety to the target sulfhydryl by forming an -SS- bridge [5]. The regents [2-(trimethylammonium) ethyl] methanethiosulfonate bromide (MTSET) and sodium (2-sulfanoethyl) methanethiosulfonate (MTSES) are the same size (10 Å x 5.8 Å) but differ in their charge, with MTSET being positively and MTSES being negatively charged [5, 109]. The third commonly used MTS reagent, 2-aminoethyl methanethiosulfonate hydrobromide (MTSEA) is the smallest (diameter of 4.6 Å) but is charged only at acidic pH and crosses membranes slowly [5, 109]. Therefore, extra caution is required when using this compound.

#### 1.6.1.1 Experimental Assumptions

SCAM has been credited in helping to identify residues that line the channel, determining the size of the channel, differences in the channel structure during different functional states, location of the selectivity filter, and mapping the electrostatic potential profile of the channel [45, 110-113]. As with any method, certain experimental assumptions are taken when interpreting the

data. 1) When studying membrane-embedded channel proteins, the first objective is to ensure that the WT-channel is not irreversibly altered by the addition of the MTS reagent. 2) While substituting cysteines along the channel it is assumed that no previously buried WT-cysteines are exposed through mutation. 3) The sulfhydryl group of natural or engineered cysteines is in one of three environments: water accessible, lipid accessible, or in the protein interior [69]. 4) The channel lining is considered to be part of the water accessible surface, and hydrophilic charged reagents react faster with sulfhydryls in a water accessible surface than in a lipid accessible surface [69]. 5) An irreversible change in channel function is assumed to mean modification of a substituted cysteine and that this cysteine is exposed to the water filled lumen. 6) The position of the substituted cysteine side-chain is nearly the same as that of the WT-side-chain. Therefore, SCAM is used to indirectly determine the orientation of the WT side-chain [69]. Although this method is useful for understanding protein structure, the interpretation of negative results can be difficult. A negative result could mean that the cysteine is inaccessible to the reagent, or the cysteine reacts with the reagent but modification has no effect on protein function [69]. In the section on KCa3.1, I will discuss how this method was used to probe the architecture of S6.

## 1.7 CURRENT VIEW OF ION CHANNEL GATING AND THE STRUCTURE OF THE PROTEIN

The initial characterization of membrane current, and the related investigations that followed helped to fuel the next 40 years of ion channel research. During this time period it became accepted that ion channels enable ions to move down their electrochemical gradient due to the formation of an ion conducting pathway, a selectivity filter, and a gate. The movement of ions is

regulated by the opening and closing of the ion conduction pathway, a process referred to as gating. Gating is controlled by sensor domains that when activated increase the pore's probability to be in the open conformation. Ion channels that open in response to changes in membrane potential are called voltage-gated ion channels and those that open in response to ligand binding are called ligand-gated ion channels. The basic function of these sensing domains is to perform mechanical work on the ion conduction pore to alter its conformation between a non-conducting and a conducting conformation. Therefore, a voltage-sensor converts electrical energy into a mechanical force whereas a ligand-binding domain converts chemical energy into mechanical force to open the pore. Thus, ion channel gating is the result of electromechanical or chemomechanical coupling between a sensor domain and the pore, enabling the channel to transition from the closed to the open conformation. Although much progress has been made toward understanding the mechanism of ion channel gating, the fundamental goal still remains to obtain a structure to complement the vast amounts of biophysical data.

Prior to 1998, the majority of our understanding about structure came through a combination of techniques based in the areas of electrophysiology and molecular biology. Although these techniques provided invaluable insight on the gating mechanism, these approaches are only capable of indirectly gathering information about channel structure (Fig. 7). Therefore, another approach was needed to launch ion channel research to the next level. This breakthrough came in 1998 when the laboratory of Rod MacKinnon developed the first crystal structure of a bacterial $K^+$ channel homolog, KcsA [67]. The x-ray structure opened new avenues of investigation, while at the same time grounding 40 years of ion channel biophysics within a structural framework (Fig. 8).

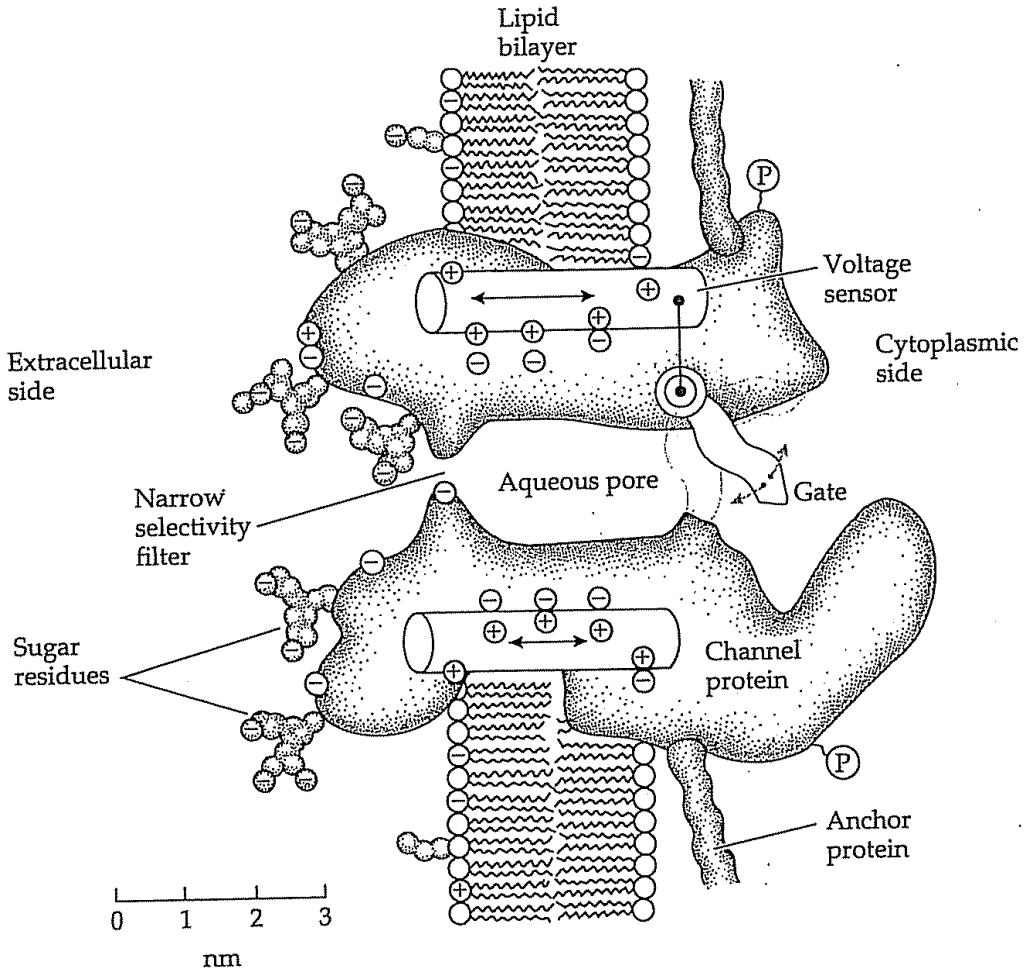


**Figure 7. 1990 's model of a voltage-gated ion channel.** Comparing this model to Fig. 5 shows the progression from a simple macromolecule with a rudimentary gate, voltage sensors, and selectivity filter to a more detailed model. During the period after the drawing of Fig. 5, the field learned that the channel is composed of four α-helical segments with positively charged residues functioning as voltage sensors; channels are heavily glycosylated and tied to other intracellular proteins. [Reprinted with permission from *Ion Channel of Excitable Membranes*, 3rd edition, pg. 86. Copyright 2001 by Sinauer Associates.]

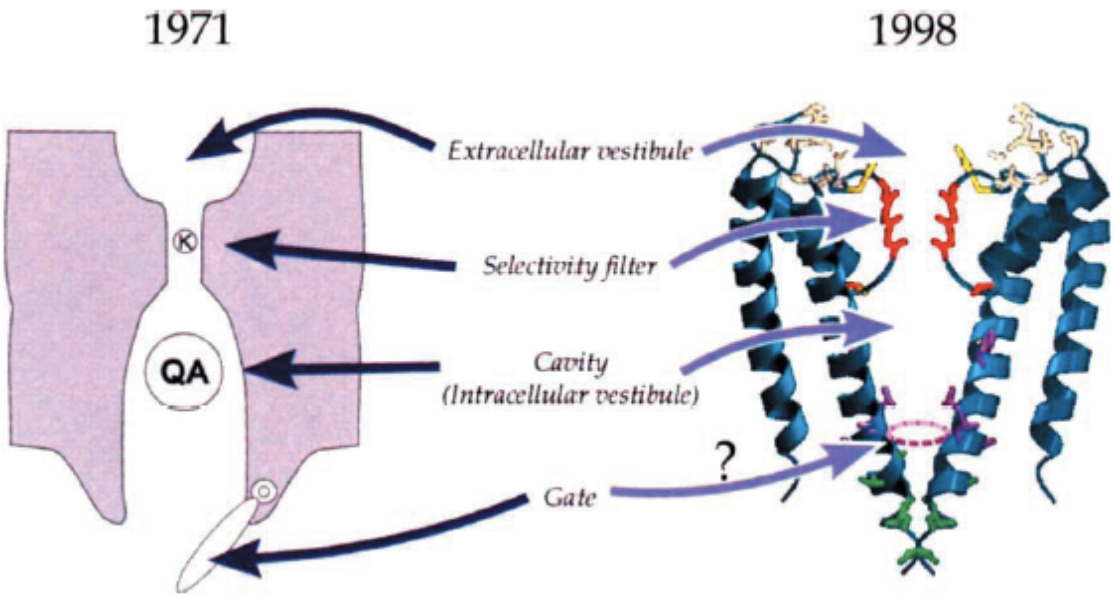


**Figure 8. Premonitions of ion channel gating.** The 1998 publication of the KcsA crystal structure grounded the preceding 30 years of biophysical experimentation into a structural framework. Thanks to the contributions of many investigators, the key ion channel land marks were predicted as early as the 1970's; without the aid of any real structural data. As shown by the 1971 Armstrong gating model, it was accepted that channels consist of a pore, which transverses the membrane enabling a high rates of ion transport while maintaining a high degree of selectivity with a selectivity filter. The selectivity filter is sandwiched by non-selective vestibules, into which molecules can enter and inhibit permeation by blocking the pore. Pore blocker such as quaternary ammonium (QA) were essential in predicting the location of the activation gate, and illustrated that gating involved a change in the access to the intracellular mouth of the pore. Although the $K^+$ channel crystal structure simply confirmed what was already known about the basic $K^+$ channel architecture, it was essential for providing structural detail not attainable by combining techniques in molecular biology and electrophysiology. Furthermore, the structure helped to eliminate the guess-work involved in structure-function studies necessary for further refining the regions involved in the gating mechanism.
[Reprinted with permission from Yellen G., *Nature Structural Biology*, vol. 5, number 6, pg. 421. Copyright 1998 by the Nature Publishing Group.]

Therefore, much of our understanding related to ion channel structure can be credited to the solved crystal structures. Structures have been obtained for channels having different types of sensing domains, in addition to obtaining structures in different conformational states. Making comparisons between the different channel types have helped to reinforce our understanding of the pore and the structures involved in gating. For instance, from the x-ray structure of the ligand-gated ion channel, MthK, we know the pore domain is separate from the $Ca^{2+}$-binding domain [114, 115]. Two separate domains means the conformational change occurring in the $Ca^{2+}$-binding domain must be coupled via a physical linkage or coupling domain to the activation gate enabling the pore to transition from the closed to open conformation. The idea that the sensing domain is separate from pore domain holds true for every structure solved to date, and is likely true for all ion channels. Since this dissertation is about the ligand-gated ion channel, KCa3.1, we will consider how ligand-gated ion channels are modeled in terms of their domains and how they function in concert to allosterically couple ligand binding to channel gating. Ligand-gated ion channels are structurally modeled as having three domains: the pore-forming domain, the ligand-binding domain, and the coupling domain [116]. The pore-forming domain, as alluded to previously, contains the permeation pathway and activation gate, which is responsible for controlling the flow of ions down their electrochemical gradient. The ligand-binding domain contains the ligand binding sites, and the coupling domain links the ligand-binding domain to the activation gate.

The next section will summarize the structural and mechanistic insight gained by examining the KcsA, KirBac1.1, and MthK atomic structures. These channels will be discussed in terms of the structural features that comprise the ion selective permeation pathway, the activation gate, and where it applies, the ligand-binding domain. Comparing channel structures

in two different conformational states is useful for developing hypotheses regarding the gating mechanism. Therefore, I will present a possible mechanism to explain how ion channels transition from the closed to the open conformation by comparing the closed conformation of KcsA to the open conformation of MthK.

## 1.8 STRUCTURAL APPROACH FOR INVESTIGATING ION CHANNEL GATING

### 1.8.1 Permeation Pathway and Selectivity Filter: KcsA X-Ray Structure [67]

The $K^+$ channel from *Streptomyces lividans* is an integral membrane protein with sequence similarity to all known $K^+$ channels, particularly within the pore region [67, 117]. The channel is a tetramer composed of four identical subunits, each having two membrane spanning transmembrane domains (TM1 and TM2). The subunit is oriented so that the inner helix (TM2) faces the central pore and the outer helix (TM1) faces the lipid membrane (Fig 9). The pore takes the shape of an inverted tee-pee with the selectivity filter being at the base of the inverted tee-pee facing the extracellular side of the membrane [67]. The structure of the selectivity filter provides a mechanism for how $K^+$ channels obtain a high degree of selectivity while maintaining a high throughput rate.

The selectivity filter maintains high throughput and selectivity by incorporating structural features that serve to ensure $K^+$ ions move small distances from one binding site to the next; all the while maintaining proper pore diameter [67]. Ensuring that $K^+$ ions diffuse small distances from one binding site to the next in the selectivity filter allows for electrostatic repulsion between two $K^+$ ions, creating the high throughput rates, up to $10^8$ ions per second, observed in

ion channels [67]. Creating, and maintaining proper pore diameter ensures selectivity [5, 16, 67]. When an ion enters the selectivity filter it dehydrates, and to compensate for the energetic cost of dehydration the carbonyl oxygen atoms from the channel protein take the place of the water [5, 16, 67]. The specific diameter of a $K^+$ channel pore allows only $K^+$ ions to pass through, preventing the movement of ions with different diameters. Ions larger than $K^+$ ions (2.66 Å) are sterically excluded from the pore, whereas ions smaller than $K^+$, such as $Na^+$ (1.9 Å), are excluded because they do not interact favorably with the rigid oxygen atoms of the pore wall [5, 16, 67]. The inability of $Na^+$ to interact with the carbonyl oxygen atoms results in the potential energy of the atom being higher in the pore compared to water such that entry of the $Na^+$ atom into a $K^+$ channel pore is an event of low probability [5, 16, 67].

In addition to providing insight into the structure of the selectivity filter, KcsA also provided investigators with insight into the gate, as the bundle crossing, at the cytoplasmic ends of the inner helices, is proposed to function as the activation gate [67]. However, the structure of KirBac1.1 gives a better representation for the location and function of the activation gate as discussed below.

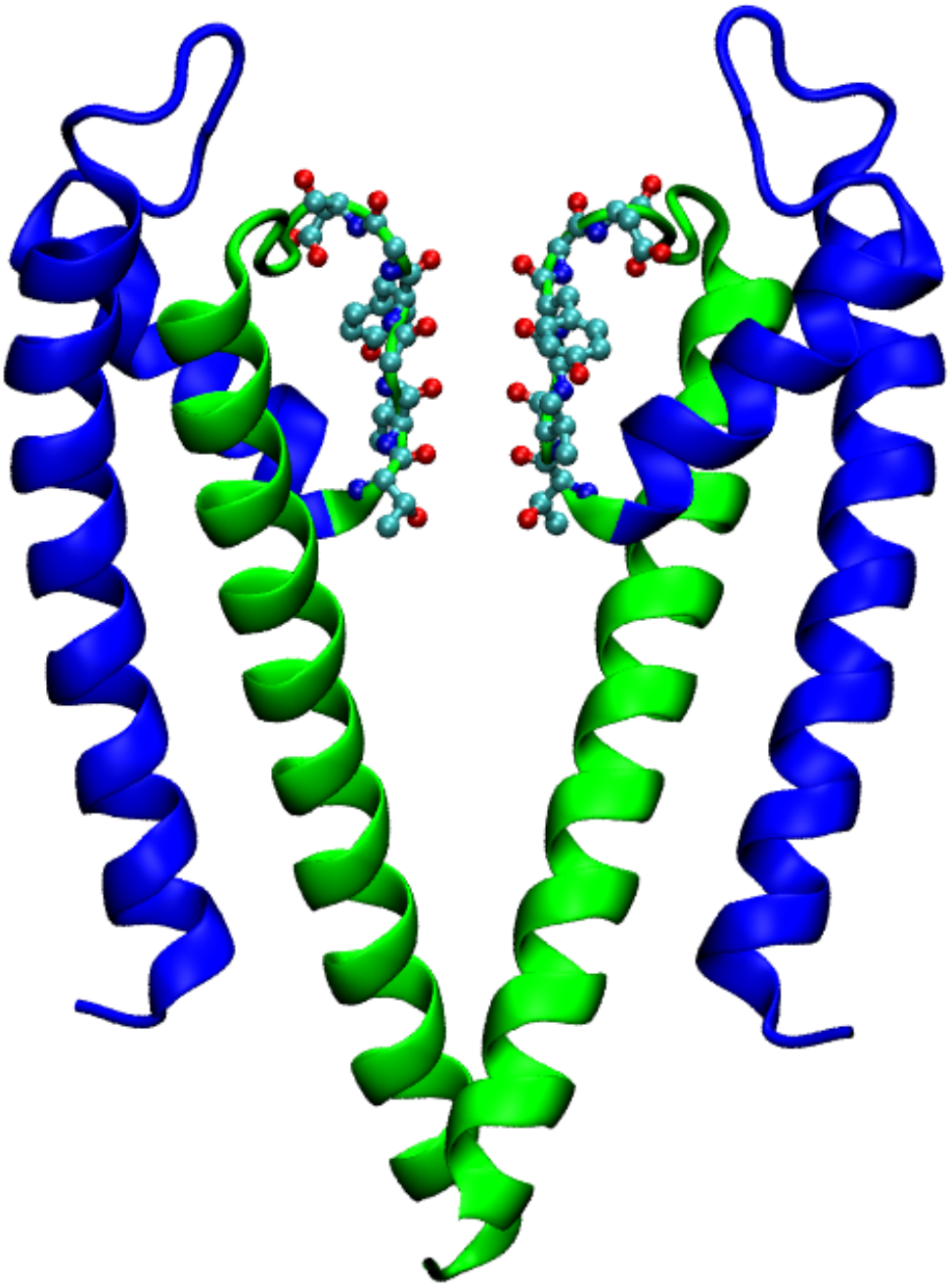

**Figure 9. X-ray structure of KcsA illustrating the selectivity filter.** Two of the four subunits are shown for clarity. The outer helix (TM1), equivalent to S5 in 6TM $K^+$ channels, and the P-helix are shown in blue. The inner helix (TM2), equivalent to S6 and the selectivity filter, are shown in green. The residues along the selectivity filter are illustrated in CPK format. The oxygen atoms are colored red, the carbon atoms are cyan, and the nitrogen atoms are blue. As illustrated in the figure, the oxygen atoms are aligned toward the lumen of the pore forming a rigid filter that surrounds the extracellular entrance to the pore. The specific diameter of the filter permits favorable interactions with dehydrated $K^+$ ions allowing for movement through the pore (PDB 1BL8).

### 1.8.2 Gate: KirBac 1.1 Crystal Structure [118]

The KirBac1.1 channel belongs to the inward-rectifier family of $K^+$ channels [5]. The channel is a homotetramer with four identical subunits, each containing two transmembrane domains (Fig. 10). The structure is believed to be in the closed state, providing a model for the location of the activation gate and the structural elements involved in gating [118]. The closed state of a channel is characterized as the inability of ions to move through the ion conduction pathway. The gate is proposed to sterically block the movement of ions [5, 16, 83, 119-121]. The structure of KirBac1.1 provides evidence that the four hydrophobic side-chains of $Phe^{146}$, located at the cytoplasmic portion of the pore, completely block the ion conduction pathway [118]. Therefore, as the channel transitions into the closed conformation it is thought that the side-chains from these residues rotate into the center of the ion-conduction pathway to sterically blocking ion flow [118]. The fact that hydrophobic residues are used as an activation gate implies that controlling the flow of water indirectly regulates ion movement [122, 123]. Therefore, if water is blocked, this immobilizes any ions that are in the water filled cavity. This idea was tested using molecular dynamics simulations looking at the movement of water in a model channel [124]. Consistent with the hypothesis, blocking the flow of water indirectly blocked the movement of ions [125].

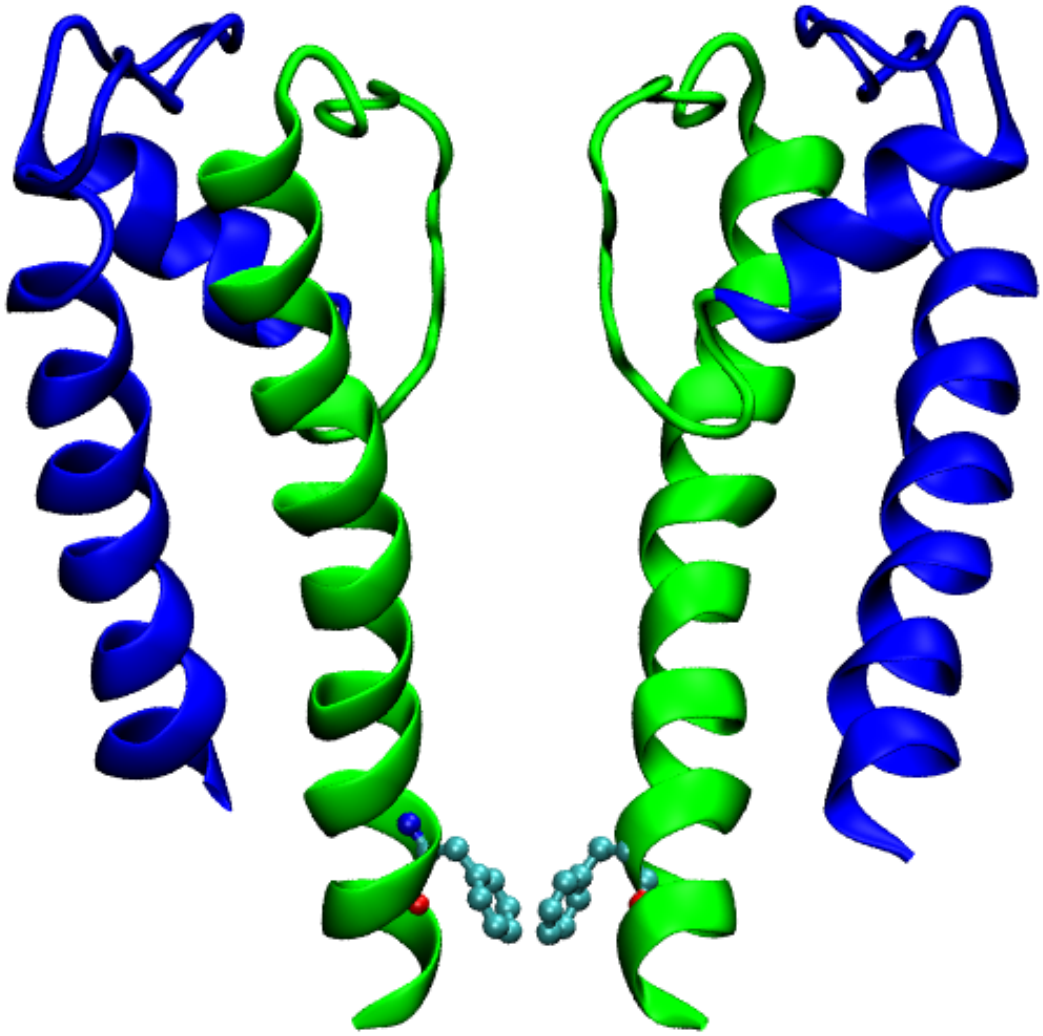

**Figure 10. Crystal structure of KirBac1.1 illustrating the location of the potential activation gate Phe$^{146}$.** Two of the four subunits are shown for clarity. The outer helix (TM1), equivalent to S5 in 6TM $K^+$ channels, and the P-helix are shown in blue. The inner helix (TM2), equivalent to S6, and the selectivity filter are shown in green. Phe$^{146}$ is represented in CPK format, and the oxygen atoms are colored red, the carbon atoms are cyan, and the nitrogen atoms are blue. As illustrated by this figure, the side-chain of Phe$^{146}$ is oriented toward the pore lumen in the closed conformation. This orientation would suggest that as the channel transitions from the open to the closed conformation, Phe$^{146}$ rotates into the ion conduction pathway blocking ion diffusion (PDB 1P7B).

### 1.8.3 Sensor Domain: MthK X-Ray Structure

As mentioned previously, controlling the conformation of the gate is critical for the operational state of the channel and hence, controlling downstream signaling processes. Although not as extensively studied as voltage-gated ion channels, the sensor mechanism in ligand-gated ion channels is better understood due to both its inherent simplicity and an x-ray structure of the MthK channel. MthK, a bacterial channel from *Methanobacterium thermoautotrophicum*, is a tetrameric two transmembrane channel that is activated by the binding of intracellular $Ca^{2+}$ to a C-terminal ligand-binding domain [114, 115, 126]. The ligand-binding domain in this channel is termed a regulator of $K^+$ conductance (RCK) domain. MthK is composed of eight RCK domains, one from each of the four pore forming subunits and four from the intracellular solution; possibly arising from a separate gene encoding for an RCK domain [126]. A tight and static dimer interface connects each channel domain to the corresponding soluble domains. These four dimers form a gating ring at the most intracellular portion of the channel. A second flexible interface forms between adjacent dimers, and this interface constitutes the $Ca^{2+}$ binding cleft. In order for the channel to open, the gating ring must convert the chemical energy of $Ca^{2+}$ binding into a mechanical force to open the pore [114]. The structure of the gating ring provides a possible mechanism to account for $Ca^{2+}$-dependent activation (Fig. 11). $Ca^{2+}$-binding reshapes the cleft resulting in the flexible interface undergoing a conformational change that causes the rigid units at the fixed interface to tilt, thereby expanding the diameter of the gating ring pulling open the pore's inner helices [126]. This conformational change allows the pore to transition from a non-conducting to a conducting configuration. Even though the crystal structure of MthK provided insight into the $Ca^{2+}$-dependent activation mechanism, very little is understood about how the chemical energy of $Ca^{2+}$ binding is transduced into a mechanical force to gate the channel.

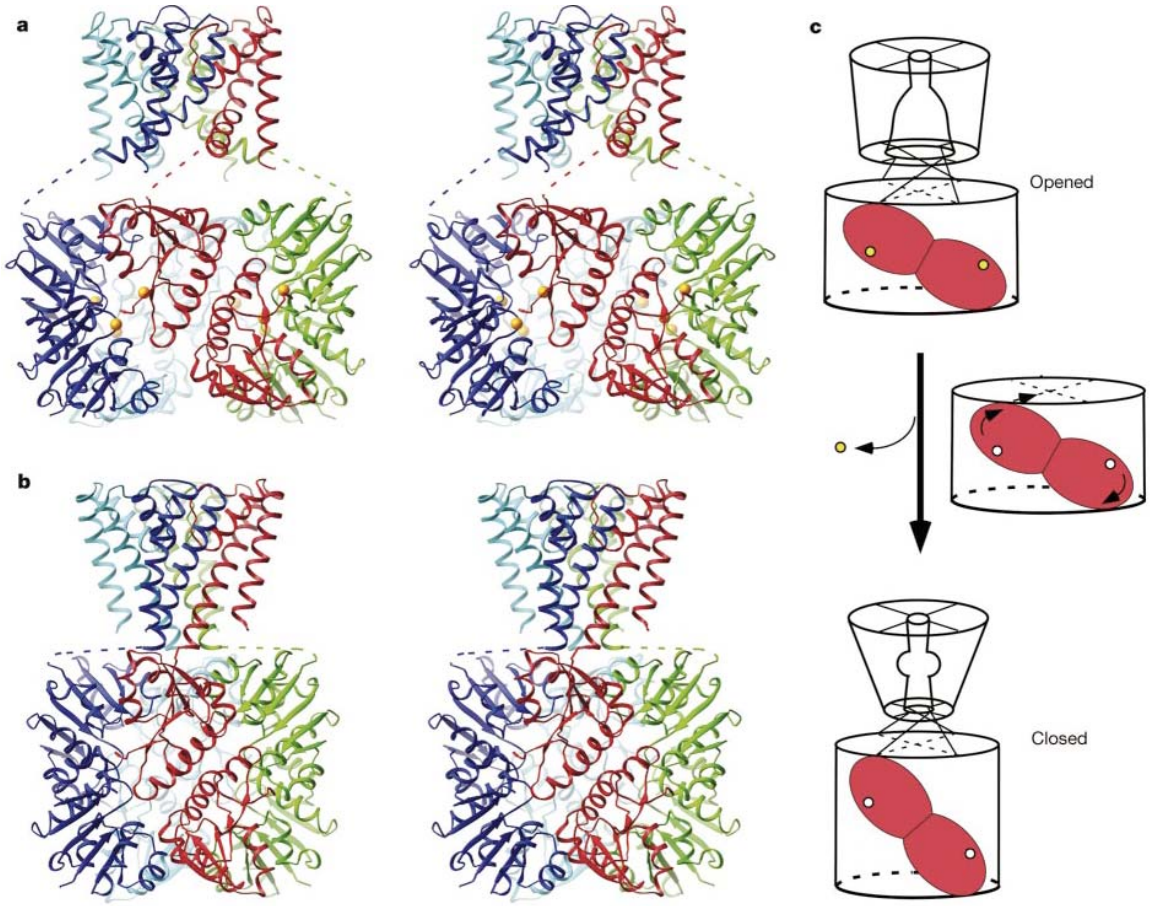


**Figure 11. Gating mechanism of a $Ca^{2+}$-dependent $K^+$ channel, MthK.** (A) Crystal structure of the MthK channel in the open conformation. RCK domains forming a fixed interface are the same color. The flexible interface contains the $Ca^{2+}$ binding cleft, which is located between the main lobes of two adjacent RCK domains; shown here with $Ca^{2+}$ ions as yellow spheres. (B) Hypothetical model of MthK in the closed conformation. (C) Model of the conformational changes associated with gating. A single dimer is shown in red. The release of $Ca^{2+}$ results in a large conformational change in the RCK domain, causing the pore to transition from the open to the closed conformation. [Reprinted with permission from Jiang Y., *Nature*, vol. 417, pg. 520. Copyright 2002 by the Nature Publishing Group.]

### 1.8.4 The Coupling Mechanism

Unlike the previous domains, the location and mechanism of the coupling domain cannot be definitively determined from static crystal structures. The coupling mechanism can be a direct linker between the sensing domain and the activation gate. However, the mechanism can also be indirect, making it difficult to locate a specific region of the protein responsible for this function. Several hypotheses have been proposed to explain the coupling mechanism. The first hypothesis states that the linker between transmembrane domains functions to couple the movement of the sensing domain to the pore [127, 128]. The region of the C-terminus between the cytoplasmic end of S6 and the $Ca^{2+}$-binding domain in BK [129] and the cyclic nucleotide-binding domain in CNG channels [130-133] has been implicated as a region that couples the energy of ligand binding to channel opening. The second hypothesis states that coupling occurs at the interaction surface between transmembrane domains [127, 128]. Thus, the movement of one domain would influence the movement of an adjacent domain. The S5-S6 interaction has been implicated as an important interaction surface mediating the transition between the closed and open states of the channel [127, 134, 135].

#### 1.8.4.1 Potential method to assess coupling

As previously mentioned, our understanding of the structures associated with the coupling mechanism are lacking compared to our knowledge of the channel regions associated with the pore and the sensing domain. However, recent progress has been made utilizing an experimental approach that immobilizes moving parts of the channel to isolate the critical regions involved in the coupling mechanism. This technique, introduced by Horn et al., [136] involves using a bifunctional cysteine reagent (benzophenone-4-carboxamidocysteine methanethiosulfonate) to

covalently bind introduced cysteines. Exposing the reagent to ultraviolet light causes the ketone group on the benzophenone to insert into adjacent C-H bonds, as a way to inhibit the relative movement between secondary structural regions of the channel. If the relative movement between these domains is critical to the function of the channel, then immobilizing these structures will have an observable effect on the biophysical properties of the channel. Systematically immobilizing different regions of the channel may potentially provide a method to map the regions of the channel involved in the coupling mechanism. However, in the words of Richard Horn, "The ultimate scientific fantasy in the minds of many channelologists is to have a detailed motion picture (in Technicolor, of course!) of channels exposed to their favorite stimuli and opening and closing in response to them [127]."

### 1.8.5 Potential Gating Mechanism

Solving the crystal structure of $K^+$ channels has provided structural and mechanistic insight not possible using methods based in electrophysiology and molecular biology. Nevertheless, one of the main questions in the area of ion channel biophysics remains understanding how the channel transitions from the closed to the open conformation. Since crystal structures are static representations of inherently dynamic molecules, the mechanism of conformational change is incompletely understood. Solving channel structures in different conformations has allowed for the development of hypotheses to further understand the gating mechanism. Comparing KcsA ("closed state") and MthK ("open state") has allowed for the question of conformational change to be addressed. These structures together provided valuable insight into the conformational changes that accompany channel gating. Comparing the pore structure of KcsA to that of MthK shows that there are large structural differences along the inner helices. In KcsA the inner helix

is straight, whereas in MthK the inner helices are bent and splayed open. Further examination of the MthK inner helix reveals that the bend occurs at a hinge point located at the level of a glycine residue, located just below the selectivity filter. Glycine, because of its small side-chain permits freedom of rotation about the $\phi$ and $\psi$ dihedral angles, which enables backbone conformations to be adopted that are not sterically tolerated by other amino acids [2]. Therefore, glycines confer flexibility to protein structure and make an ideal candidate for a hinge point or gating hinge. The location and function of the glycine residue explains the different conformations apparent between the inner helices of KcsA and MthK. Therefore, a possible mechanism to explain the conformational change occurring as the channel transitions from the closed to the open conformation would involve the ligand-binding domains exerting an outward lateral force on the C-terminal portion of the inner helices [114]. This force creates a torque at the gating hinge causing the inner helices to go from a straight conformation to a splayed open conformation, which is predicted to represent the open conformation of the pore [126]. This model represents one of a number of gating hypotheses to explain the conformational changes in the pore as the channel transitions from the closed to the open conformation. For instance, the conserved glycine in Kv channels is not predicted to function as a gating hinge. Rather, a PVP motif located in the C-terminal portion of the transmembrane domain is predicted to function in a similar capacity [137]. Thus, even within the family of $K^+$ channels multiple mechanisms might exist to transfer the activation energy from the sensor domain to the activation gate.

## 1.9 THE INTERMEDIATE CONDUCTANCE CALCIUM ACTIVATED POTASSIUM CHANNEL – KCa3.1

The intermediate conductance $Ca^{2+}$-activated $K^+$ channel (KCa3.1) is a $Ca^{2+}$ dependent $K^+$ channel, which shares 40% homology with the small conductance family of $K^+$ channels (KCa2.1, KCa2.2, and KCa2.3). KCa3.1, originally cloned in 1997 from human pancreas [138] and placenta [139], is a tetramer composed of four identical subunits, each having six transmembrane domains (S1-S6) with the pore composed of S5, the P-helix, and S6. Macroscopic and single channel recordings display inward rectification in symmetric $K^+$ with a chord conductance of 39 pS in the inward direction and 10 pS in the outward direction [138, 139]. KCa3.1 currents are reversibly blocked by charybdotoxin (CTX) ($K_i$ = 2.5 nM) and clotrimazole (CLT) ($K_i$ = 24.8 nM) [138], and activated by DC-EBIO ($K_{0.5}$ = 84 uM) [140, 141].

### 1.9.1 KCa3.1 in Physiology

KCa3.1 is expressed in the cells of non-excitable tissues, such as cells of the hematopoetic system where it is utilized to mediate volume regulation in lymphocytes and erythrocytes [138, 139, 142-144]. Furthermore, KCa3.1 is expressed in low levels in resting T lymphocytes, but is up regulated during activation by mitogens [145]. Activation of this channel causes hyperpolarization of the membrane potential, which functions to maintain the intracellular $Ca^{2+}$ concentration required for mitogen activation [146, 147]. KCa3.1 is also expressed in organs involved in salt and fluid transport including the colon, lung, placenta, and salivary glands [138, 139, 142-144, 148]. In the colon, KCa3.1 is important in $Ca^{2+}$-mediated transepithelial $Cl^-$ secretion. That is, $Ca^{2+}$-mediated $Cl^-$ secretion is dependent upon the opening of a CTX-sensitive,

$Ca^{2+}$-activated basolateral membrane $K^+$ conductance in the absence of any change in apical membrane $Cl^-$ conductance [149]. Therefore, activation of a $K^+$ conductance hyperpolarizes the apical and basolateral membrane potentials, increasing the electrochemical driving force for $Cl^-$ exit through constitutively active apical membrane $Cl^-$ channels [150-154]. Examination of the single channel properties of these KCa channels from T84 cells indicates they are of intermediate conductance, and display all of the biophysical and pharmacological properties of the cloned KCa3.1 channel [155]. Finally, these channels are also expressed in endothelial cells, reflecting their role in the regulation of smooth muscle vascular tone [156, 157].

### 1.9.2 Regulation of Vascular Tone through Activation of the EDHF Response

Regulating smooth muscle tone in arterioles is an important mechanism for adjusting the perfusion pressure of a particular tissue or capillary bed [6]. Smooth muscle tone can be regulated systemically or through local factors such as mechanical stimuli, and the release of chemical and humoral factors [158]. The endothelium is an important source of local chemical factors released in response to the binding of substances in the blood that activate specific receptors in the endothelium [159-164].

The endothelium is a simple squamous epithelial layer that covers the luminal surface of all blood vessels, and helps to regulate the balance between vasoconstriction and vasorelaxation. The inability of the endothelium to adapt to changes in blood flow is referred to as endothelial dysfunction and is often associated with many cardiovascular diseases such as hypertension, atherosclerosis and heart failure [159, 165-167]. The endothelial dependent regulation of vascular tone is generally attributed to the release of nitric oxide and prostacyclin through the activation of nitric oxide synthase and cyclooxygenase pathways, respectively. These pathways

function to produce relaxation in vascular smooth muscle cells (VSMCs) by causing VSMCs hyperpolarization and subsequent relaxation [160, 161, 164, 168, 169]. However, several studies have presented evidence for the existence of a third pathway that is independent of both cyclooxygenase and NO synthase and is also associated with the hyperpolarization of VSMCs [162, 169-172]. This third pathway is mediated through the release of a diffusible substance or the spread of an electrical signal that is generated by the endothelium, resulting in hyperpolarization of the adjacent VSMCs and subsequent relaxation [162, 169]. Therefore, this pathway is referred to as the endothelial derived hyperpolarizing factor (EDHF).

The EDHF pathway is most prominent in resistance-sized arteries [160, 161, 164, 173]. Therefore, the contribution of this pathway to the regulation of vascular tone increases as vessel size decreases. EDHF is activated through agonist stimulating G protein-coupled receptors as well the calcium ionophore A 23187, thapsigargin, and cyclopiazonic acid [169]. These compounds function to increase endothelial $[Ca^{2+}]_i$ resulting in hyperpolarization of the endothelial cells, and in some blood vessels eliciting endothelium dependent hyperpolarization of VSMCs. EDHF is also characterized as being insensitive to block by specific blockers of BK channels, but being sensitive to the block of KCa3.1 and KCa2.3 channels [174]. Furthermore, the addition of DC-EBIO, which activates both KCa3.1 and KCa2.3, causes endothelial cell hyperpolarization and subsequent hyperpolarization of VSMCs [165, 166]. KCa3.1 and KCa2.3 are expressed in the endothelium of freshly isolated arteries but are not found in the associated VSMCs [175-178]. The addition of substance-P and bradykinin, both of which initiate the EDHF mediated response in the porcine coronary arteries, activate an outward current sensitive to the block of either KCa3.1 or KCa2.3 [179, 180]. Therefore, these results suggest that KCa3.1 and KCa2.3 are associated with the activation of the EDHF pathway.

Although the factors associated with this pathway are still unresolved, it is thought that an agonist induced increase in $[Ca^{2+}]_i$ activates KCa3.1 and KCa2.3 and the activation of these channels results in endothelial hyperpolarization, and the initiation of the EDHF response [172]. Although, activation of KCa3.1 and KCa2.2 are required for initiation of the EDHF response, the mechanism for the spread of hyperpolarization from the endothelial cells to the VSMCs is still unknown. However, two possible mechanisms have been proposed. The first mechanism, states that endothelial hyperpolarization spreads directly to the VSMCs through gap junctions [171]. Gap junctions link VSMCs with other VSMCs and endothelial cells with other endothelial cells, and as indicated below, endothelial cells with smooth muscle cells. The gap junction proteins, Cx 37, 40, and 43, are the predominant forms expressed in the vascular wall, and in the rodent Cx 37 and Cx 40 are involved in myoendothelial gap-junction communication [181-183]. In rat mesenteric arteries, antibodies directed against Cx 40 block the EDHF-mediated response when loaded in endothelial cells [182]. In the second mechanism, activation of KCa3.1 and KCa2.3 results in the accumulation of $K^+$ ions in the intracellular cleft [171]. The increase in $[K^+]$ ion hyperpolarizes the VSMCs by activating either the inward rectifying $K^+$ channels or the $Na^+/K^+$ pump expressed in these cells [184, 185]. The hyperpolarization caused by an increase in extracellular $K^+$ is counterintuitive because the Nerst equation would predict depolarization and subsequent contraction [171]. However, the activation of inward rectifying $K^+$ channels and the $Na^+/K^+$ pump would offset any depolarization resulting from an increase in extracellular $K^+$ ions [186]. Whether the hyperpolarization spreads through gap junctions or is the result of activating Kir and $Na^+/K^+$ pump the net result of each of these pathways is smooth muscle hyperpolarization causing the voltage-dependent $Ca^{2+}$ channel in the VSMCs to close, decreasing intracellular $[Ca^{2+}]_i$ and subsequent smooth muscle relaxation.

### 1.9.3 Contribution of KCa3.1 to the EDHF Response

Although KCa3.1 and KCa2.3 have been implicated as being important for the initiation of the EDHF pathway, their precise contribution to this pathway is unknown. The role of these channels toward the initiation of this pathway has been proposed mainly on the basis of isolated vessels and pharmacological methods to illustrate that these channels are associated with this response [165]. Several investigations have reported the contribution of a single channel to blood pressure regulation mediated through the EDHF signaling mechanism. For instance, it has been reported that KCa3.1 deficient mice ($IK1^{-/-}$) exhibited a partial defect in EDHF signaling and moderately elevated blood pressure [166].

Genetic manipulation of KCa2.3 has also been shown to alter blood pressure [167]. However, unlike the mice deficient in KCa3.1, the levels of KCa2.3 are manipulated by site-specific insertion of a tetracycline-based genetic switch ($KCa2.3^{T/T}$) [187]. Thus, dietary doxycycline treatments decrease KCa2.3 expression, whereas in untreated mice the channel is over expressed 3-fold. Although these investigations provided valuable insight into the EDHF signaling mechanism, it is unknown whether the phenotype observed in the $KCa3.1^{-/-}$ or $KCa2.3^{T/T}$ mice was due to modulating the EDHF signaling mechanism. A recent study investigated the contribution of both KCa3.1 and KCa2.3 to the acetylcholine-induced EDHF-mediated smooth muscle hyperpolarization by generating mice deficient for both channels ($KCa3.1^{-/-}$ and $KCa2.3^{T/T}$) [165]. This approach also enabled the rescuing effects of KCa2.3 over expression and pharmacological manipulation of KCa3.1 to be examined on mice lacking the other channel. This study illustrates that, as expected, both channels contribute equally to the generation of endothelial $K_{Ca}$ currents. However, KCa3.1 is more important to the acetylcholine-induced EDHF-mediated smooth muscle hyperpolarization. The absence of KCa3.1 impairs

smooth muscle hyperpolarization more than the loss of KCa2.3 alone. Over expression of KCa2.3 in KCa3.1$^{-/-}$/KCa2.3$^{T/T}$ mice restored the acetylcholine induced smooth muscle hyperpolarization to near WT-levels. However, potentiation of KCa3.1, by the channel activator SKA-31, strongly enhanced hyperpolarization in KCa3.1 expressing and KCa2.3 deficient mice to above WT-levels. Therefore, converging lines of evidence suggest that KCa3.1 makes a larger contribution to the acetylcholine induced smooth muscle hyperpolarization. The different roles for KCa3.1 and KCa2.3 in the EDHF signaling mechanism also became apparent when examining the EDHF dilator response. The loss of KCa3.1 alone resulted in a large effect at intermediate acetylcholine concentrations, which is in direct contrast to the suppression of KCa2.3 alone, which had no effect. Furthermore, over expression of KCa2.3 in KCa3.1 deficient mice enhanced dilation but not to WT-levels. As expected, potentiation of KCa3.1 in KCa2.3 deficient mice enhanced the EDHF response, suggesting that KCa2.3 is only important for the EDHF dilator response in the absence of KCa3.1. Therefore, this study illustrates that KCa3.1 plays a key role in mediating acetylcholine-induced smooth muscle hyperpolarization and the EDHF dilation in response to acetylcholine.

### 1.9.4 Structure of KCa3.1

Activation of the EDHF pathway and subsequent regulation of vascular tone is dependent upon the ability of KCa3.1 to sense and respond to changes in intracellular $Ca^{2+}$ concentration. This mechanism is mediated through calmodulin (CaM), which, as explained below, allows the channel to function as an intracellular $Ca^{2+}$-sensor, enabling channel activity to correspond to changes in intracellular $Ca^{2+}$ concentration. KCa3.1 contains positively charged residues along S4, similar to the Kv channels, but the channel is entirely voltage independent and gated solely

by the binding of intracellular $Ca^{2+}$. Channel activation is mediated through a $Ca^{2+}$-dependent gating mechanism, which is dependent upon the co-assembly of channel α-subunit with CaM. KCa3.1 functions as a heteromeric complex with CaM, a $Ca^{2+}$-binding protein, that is constitutively bound to the channel's calmodulin-binding domain (CaMBD) located in the C-terminus, just distal to S6 [138, 188, 189]. Additionally, CaM has been shown to constitutively bind to the channel even in the absence of $Ca^{2+}$, an important point to keep in mind for the discussion below [188, 190, 191]. Upon binding of $Ca^{2+}$ to CaM, the CaM/CaMBD undergoes a conformational change, which is coupled to the pore, enabling the channel to transition from a non-conducting to a conducting configuration [189, 192, 193]. This association allows CaM to behave as an intracellular $Ca^{2+}$-sensor, coupling changes in intracellular $Ca^{2+}$ concentration $[Ca^{2+}]_i$ to the regulation of channel activity.

### 1.9.5 $Ca^{2+}$-dependent Regulation of KCa3.1

CaM, is expressed in all eukaryotic cells, and mediates many $Ca^{2+}$-dependent signaling processes. Structurally, CaM contains N- and C-terminal globular domains, each possessing two high affinity $Ca^{2+}$ binding E-F hand motifs; E-F 1 and 2 in the N-terminus and E-F 3 and 4 in the C-terminus [194]. The interaction between CaM and the channel α-subunit has been extensively studied in KCa2.2 [188-193, 195, 196]. Since there is a high degree of homology in the CaM/CaMBD between KCa3.1 and KCa2.2, the mechanism proposed for the interaction between CaM/CaMBD and KCa2.2 is also expected to apply for KCa3.1. The original investigation proposed a modular design for the interaction between CaM and KCa2.2. Keen et al., [188] proposed that the N-terminal E-F hands are responsible for the $Ca^{2+}$-dependent interactions, whereas the C-terminal E-F hands dictate the $Ca^{2+}$-independent interactions. This

hypothesis was investigated through amino acid substitutions that systematically reduce or eliminate $Ca^{2+}$ binding to E-F hands 1-4. The results from their investigation indicated that E-F hands 3 and 4 do not affect $Ca^{2+}$-dependent gating, but mutations to E-F hands 1 or 2 result in shifts in apparent $Ca^{2+}$ affinity, suggesting that E-F hands 1 and 2 are necessary and sufficient for $Ca^{2+}$ gating. However, a more recent investigation calls into question the modular design hypothesis [190]. Rather than suggesting that a single functional E-F hand 1 or 2 is sufficient to gate the channel, albeit with a lower apparent $Ca^{2+}$ affinity, this investigation illustrates that when one N-lobe E-F hand loses its $Ca^{2+}$ binding capacity, CaM can no longer associate with the channel [190]. Therefore, the modular design hypothesis needs to be revised to express that the E-F hands in the N-lobe, in addition to their role in $Ca^{2+}$-dependent interactions, are also involved in the $Ca^{2+}$-independent interaction between CaM and the channel α-subunit.

### 1.9.6 Chemomechanical Gating Model

A chemomechanical gating model has been proposed to describe the gating of the closely related channel KCa2.2 [192, 193]. This model is based on the premise that the CaMBD of KCa2.2 is associated with the C-terminal region of S6 through the C-terminal linker, so that the conformational changes occurring in the CaM/CaMBD are directly transmitted to the pore to elicit gating. Furthermore, since $Ca^{2+}$ binding to CaM/CaMBD drives channel opening, there must be a large conformational change in the CaMBD to elicit opening of the activation gate. Crystal structures of the KCa2.2 apoCaM/CaMBD and $Ca^{2+}$/CaM/CaMBD were solved and utilized to develop a mechanism to explain $Ca^{2+}$-dependent activation subsequent to $Ca^{2+}$ binding [192, 193]. Comparison of the apoCaM/CaMBD structure to the Ca/CaM/CaMBD structure allows a mechanism to be proposed in which $Ca^{2+}$ binding to each CaM N-lobe would expose a

hydrophobic patch, thereby allowing the N-lobe to interact with an adjacent CaMBD monomer. As each N-lobe grabs the C-terminal region of the corresponding CaMBD, the events associated with this reorientation cause a >90 degree rotation in CaM/CaMBD. Since the CaMBD is directly attached to the C-terminal portion of S6, the large conformational change is directly transmitted to S6 through a yet unknown mechanism, enabling the pore to transition from a non-conducting to a conducting configuration. Therefore, in this model two CaMBD dimers serve as levers to drive opening of the pore.

### 1.9.7 The Current State of KCa3.1

Although little is understood regarding the coupling mechanism in KCa3.1, the C-terminal portion of S6 is thought to transform the activation energy from the CaM/CaMBD into a mechanical force to alter the conformational state of the pore. The first investigation examining the pore architecture of KCa3.1 used SCAM to identify two regions ($Val^{275}$-$Val^{282}$ and $Ala^{283}$-$Ala^{286}$) along S6 that display functional differences to [2-(trimethylammonium)ethyl] methanethiosulfonate bromide (MTSET) binding [113]. The addition of MTSET caused inhibition at positions $Val^{275}$, $Thr^{278}$, and $Val^{282}$, and activation at positions $Ala^{283}$ and $Ala^{286}$. Understanding the structural differences between these regions is key for understanding how S6 contributes to the activation process. Within the $Val^{275}$-$Val^{282}$ region, only residues $Val^{275}$, $Thr^{278}$, and $Val^{282}$ were accessible to MTSET, implying these residues line the lumen of the pore. This was later confirmed when it was observed with single channel recordings that MTSET causes inhibition by reducing channel conductance [113]. A homology model of the closed state of KCa3.1 based on the x-ray structure of KcsA predicted that $Cys^{276}$, $Cys^{277}$, and $Leu^{281}$ are oriented away from the pore. The non-luminal orientation of these residues would explain why

they are protected from MTSET modification. $Ala^{279}$ is predicted to face the lumen, but this orientation is not supported by the SCAM experiments. The L280C mutation results in a non-functional channel, therefore the contribution of $Leu^{280}$ to the structure of S6 could not be assessed. Modification of $Val^{275}$, $Thr^{278}$, and $Val^{282}$ is dependent on the open state, indicating the closed state blocks MTSET from accessing these positions. The 283-286 region is very distinctive because all residues are accessible to MTSET in the open configuration, suggesting this region is not embedded in the membrane [113]. MTSET-dependent activation is state-independent for A283 and A286 suggesting that in the closed state these residues are still accessible to hydrophilic reagents. However, in the closed conformation V284 and V285 showed a reduced MTSET accessibility, suggesting the 283-286 region undergoes important structural changes during gating. In total, the results from the scan of S6 indicates that 275-282 possess features that correspond to the inner cavity region of KcsA and 283-286 actively participate in coupling the conformational changes in CaM/CaMBD to opening of the pore.

The location of the gate, in the closed conformation of KCa3.1, cannot be accounted for by the bundle crossing formed by the C-terminal ends of S6 [111], as represented by KcsA [67]. Comparison of the modifications rates of MTSEA (diameter 4.6 Å) for a residue located in the central cavity (275C) to a residue located at the C-terminal end of S6 (286C) for the closed configuration were found to differ by less than 7-fold, whereas experiments performed with the larger MTSET reagent (diameter 5.8 Å) resulted in a modification rate $10^3$-$10^4$ faster for the cysteine located in the C-terminal end compared to the cysteine in the central cavity [111]. In addition, modification rates for 275C using Et-$Hg^+$, which is smaller than MTSET with dimensions corresponding to a sphere with a diameter of 4.1 Å, and $Ag^+$ (2.55 Å) were shown to be state independent. Finally, modification rates for MTSET were $10^3$ times faster for the open

compared to the closed state [111]. These results would argue that the closed KCa3.1 structure cannot have a restrictive barrier at the C-terminal end of S6, rather it would suggest that the closed structure is better represented by a narrow passage way centered at V282, which connects the inner cavity to the cystolic medium. As illustrated by the modification rates, this passage would not be restrictive to the diffusion of small reagents similar in size to the $K^+$ ion, suggesting that the C-terminal end of S6 does not form an obstructive barrier for the diffusion of $K^+$ ions in the closed configuration. These results are similar to investigations localizing the activation gate in KCa2.2 at or near to the selectivity filter [197, 198], suggesting that the C-terminal end of S6 cannot function as the activation gate. Therefore, these results would suggest that S6 acts as a transducer conveying the structural changes occurring in the C-terminal section of the helix to the selectivity filter, enabling the pore to transition from a non-conducting to a conducting configuration.

## 1.10 STATEMENT OF THE PROBLEM

These investigations provided insight into the architecture of S6, and specifically how the luminal residues participate in the activation mechanism. However, we still do not fully understand how ligand binding is coupled to opening of the pore. Furthermore, with the exception of the luminal residues on the C-terminal portion of S6, we do not know if additional sites function to allosterically couple the conformational changes in CaM/CaMBD to the activation gate. Therefore, to obtain a better understanding of the coupling mechanism, it is important to isolate regions of the channel that are involved in this process. KCa3.1 has four endogenous cysteines residues along S6, and of those four residues, $Cys^{269}$, $Cys^{276}$, and $Cys^{277}$

are predicted to have a non-luminal orientation [113]. The addition of parachloromercuribenze sulfonate (PCMBS) to the intracellular side of an excised membrane patch expressing KCa3.1 increases steady-state current. This compound was shown to modify the behavior of the Shaker $K^+$ channel by modifying cysteine(s) not accessible using MTS reagents [199-201]. The increased sensitivity for partially buried cysteines was explained by the unique geometry and chemistry of this compound [200]. Therefore, we hypothesized that the increase in KCa3.1 steady-state current with PCMBS is due to modification of an endogenous cysteine(s) in S6. Since these residues are predicted to have a non-luminal orientation, we characterized the functional effect of PCMBS on KCa3.1 to assess the role of these residues in the activation mechanism.

### 1.10.1 Goals of this Dissertation

The goal of this dissertation was to characterize the role of S6 in the activation mechanism of KCa3.1. S6 was investigated by characterizing the effect of PCMBS and tryptophan substitutions on the gating of KCa3.1. Specifically, I tested the hypothesis that the non-luminal residues along the C-terminal portion of S6 participate in the activation mechanism. Based on this hypothesis the following questions were addressed: 1) How does PCMBS activate the WT-channel? 2) Which cysteine is responsible for conferring PCMBS-sensitivity? 3) What is the potential molecular mechanism for the function of PCMBS?

Presently, there are no methods to directly assess the conformational changes associated with channel gating. However, characterizing the mechanism underlying the functional effect of PCMBS will give insight into the regions associated with the activation mechanism.

Furthermore, understanding how PCMBS disrupts gating will indirectly provide a mechanism for the conformational changes associated with the activation mechanism of KCa3.1.

# 2.0 CHARACTERIZATION OF THE PCMBS-DEPENDENT MODIFICATION OF KCa3.1 CHANNEL GATING



## 2.1 ABSTRACT

Intermediate conductance, calcium-activated potassium channels (KCa3.1) are gated by the binding of intracellular $Ca^{2+}$ to calmodulin (CaM), a $Ca^{2+}$ binding protein that is constitutively associated with the C-terminus of the channel. Although previous studies indicated that the pore-lining residues along the C-terminal portion of S6 contribute to the activation mechanism, little is known about whether the non-luminal face of S6 contributes to this process. Here we demonstrate that the sulfhydral reagent, parachloromercuribenze sulfonate (PCMBS), modifies an endogenous cysteine residue predicted to have a non-luminal orientation ($Cys^{276}$) along the sixth transmembrane segment (S6). Modification of $Cys^{276}$ manipulates the steady-state and kinetic behavior of the channel by shifting the gating equilibrium toward the open state, resulting in a left-shift in apparent $Ca^{2+}$-affinity and a slowing in the deactivation process. Utilizing a 6-state gating scheme, our analysis shows that PCMBS slows the transition between the open state back to the third closed state. Interpreting this result in the context of the steady-state and kinetic

data suggests that PCMBS functions to shift the gating equilibrium toward the open state by disrupting channel closing. In an attempt to understand whether the non-luminal face of S6 participates in the activation mechanism, we conducted a partial tryptophan scan of this region. Substituting a tryptophan for $Leu^{281}$ recapitulated the affect on the steady-state and kinetic behavior observed with PCMBS. Considering the predicted non-luminal orientation of $Cys^{276}$ and $Leu^{281}$, a simple physical interpretation of these results is that the non-luminal face of S6 forms a critical interaction surface mediating the transition into the closed conformation, suggesting the non-luminal C-terminal portion of S6 is allosterically coupled to the activation gate.

## 2.2 INTRODUCTION

Proteins are inherently dynamic structures. Regulating the transition between conformational states is critical for proper function and, on a larger scale, maintaining control of a multitude of physiological processes. Ion channels are one class of protein that exemplifies this connection between structure and function, since switching between open and closed states controls a whole host of physiological responses. In this study, we probe the nature of these transitions and how they are controlled by external factors in the $Ca^{2+}$-activated potassium channel, KCa3.1 [138, 139]. KCa3.1 is composed of four subunits, each having six transmembrane domains (S1-S6) with a pore domain located between S5 and S6. Channel activation is mediated through a $Ca^{2+}$-dependent gating mechanism, which is dependent upon the co-assembly of channel $\alpha$-subunit with calmodulin (CaM)[189]. CaM, a $Ca^{2+}$-binding protein, is constitutively bound to the channel's calmodulin-binding domain (CaMBD) located in the C-terminus, just distal to S6.

Upon binding of $Ca^{2+}$ to CaM, the CaM/CaMBD undergoes a conformational change, which is coupled to the pore, enabling the channel to transition from a non-conducting to a conducting configuration [188, 190]. This association allows CaM to behave as an intracellular $Ca^{2+}$-sensor, coupling changes in intracellular $Ca^{2+}$ concentration to the regulation of channel activity. The unique association with CaM allows this channel to regulate the molecular signaling mechanisms underlying the control of vascular tone [172]. In vascular endothelium, cell stimulation initiates an increase in intracellular $Ca^{2+}$ ($Ca^{2+}_i$). Increasing $Ca^{2+}_i$ activates KCa3.1, resulting in endothelial cell hyperpolarization, a requirement for the initiation of the endothelial derived hyperpolarizing factor (EDHF) response [202]. The activation of this EDHF pathway ultimately results in the hyperpolarization of adjacent vascular smooth muscle cells (VSMCs), which enables subsequent arteriolar dilation and decrease in vascular tone [168, 169].

Activation of the EDHF pathway and subsequent regulation of vascular tone is dependent upon tight regulation of KCa3.1 channel activity. Although little is understood regarding the coupling mechanism in these channels, the C-terminal portion of S6 is thought to transform the activation energy from the CaM/CaMBD into a mechanical force to alter the conformational state of the pore [110, 111, 113, 192, 193]. The first investigation examining the pore architecture of KCa3.1 used the substituted cysteine accessibility method (SCAM) to identify a region within S6 that is expected to contribute to the lumen (V275-V282) and a second region expected to participate in the activation mechanism (A283-A286) [113]. Additionally, it has been suggested that in the closed conformation, the cytoplasmic ends of S6 do not function as a barrier to the movement of $K^+$ ions [111] as it does in KcsA [67]. Rather, the activation gate is suggested to be located at or near the selectivity filter, with the C-terminal portion of S6 (V282-A286) participating in the activation mechanism [110, 111, 113]. However, in contrast to the

previous investigations, which determined the role of cysteines engineered along the luminal face of S6, we observe that the non-luminal face of S6 also participates in the activation mechanism. $Cys^{276}$ and $Leu^{281}$ are predicted to have a non-luminal orientation, and our results suggest that perturbations at these positions, using either parachloromercuribenze sulfonate (PCMBS) ($Cys^{276}$) or tryptophan substitution ($Trp^{281}$), shifts the gating equilibrium toward the open conformation. Activation and deactivation kinetics, as measured by $Ca^{2+}$-jump experiments, are markedly slowed, suggesting that perturbing these positions disrupts a transition that is allosterically coupled to the activation gate. Therefore, our results indicate the transition of KCa3.1 to the closed conformation is dependent on the interaction surface formed by the non-luminal face of S6, specifically the C-terminal portion of the helix. Results from our kinetic analysis indicate that PCMBS and L281W disrupt channel behavior through a common mechanism by manipulating the transition from the open state back to the third and final closed state. Our results, together with previous investigations, lead us conclude that the luminal and non-luminal faces of the C-terminal portion of S6 actively function to couple the conformational changes in the CaM/CaMBD to the pore, thus permitting the channel to transition from a non-conducting to a conducting conformation.

## 2.3 MATERIALS AND METHODS

*Molecular Biology.* KCa3.1 (hIK1) cDNA was kindly provided by J.P. Adelman (Vollum Institute, Oregon Health Sciences University). The cDNA was subcloned into pcDNA3.1(+) (Invitrogen, Carlsbad, CA) using the *EcoRI* and *XhoI* restriction sites. All mutations were generated using the Stratagene QuikChange™ site-directed mutagenesis strategy (Stratagene, La

Jolla, CA). The fidelity of all constructs utilized in this study, were confirmed by sequencing (ABI PRISM 377 automated sequencer, University of Pittsburgh) and subsequent sequence alignment (NCBI BLAST) using GenBank$^{TM}$ accession number AF022150.

*Cell culture.* Human embryonic kidney (HEK293) cells were obtained from the American Type Culture Collection (Manassas, VA) and cultured in Dulbecco's modified Eagle's medium (DMEM; Invitrogen) supplemented with 10% fetal bovine serum and 1% penicillin-streptomycin in a humidified 5% $CO_2$/95% $O_2$ incubator at 37 $^{o}$C. Cells were transfected using LipofectAMINE 2000 (Invitrogen) following the manufacturer's instructions. Stable cell lines were generated for all constructs by subjecting cells to antibiotic selection (1mg/ml G418). Note that clonal cell lines were not subsequently selected from this stable population in order to avoid clonal variation.

*Electrophysiology.* The effects of PCMBS on KCa3.1 were assessed with inside-out patch-clamp experiments as a functional assay. Currents were recorded using an Axopatch 200B amplifer (Axon Instruments, Inc.). During patch-clamp experiments, the bath solution contained 145 mM K-gluconate, 5 mM KCl, 1.3 mM $MgCl_2$, 10 mM HEPES, 1 mM EGTA, and 300 μM ATP (pH adjusted to 7.2 with KOH). Sufficient $CaCl_2$ was added to obtain the desired free $Ca^{2+}$ concentration (program kindly provided by Dr. Dave Dawson, Oregon Health Sciences University) and applied to the intracellular surface of the patch through a rapid solution exchanger (RSC-160; Biologic). To obtain a $Ca^{2+}$-free bath solution EGTA (1 mM) was added without $CaCl_2$ (estimated free $Ca^{2+}$ <10 nM). Electrodes were fabricated from thin-walled borosilicate glass (World Precision Instruments, Sarasota, FL), pulled on a vertical puller (Narishige, Long Island, NY), fire-polished, and had a resistance of 1-5 MΩ. The pipette solution was 140 mM K-gluconate, 5 mM KCl, 1 mM $MgCl_2$, 10 mM HEPES and 1 mM $CaCl_2$

(pH adjusted to 7.2 with KOH). All experiments were performed at room temperature. All patches were held at a holding potential of –100 mV. The voltage is referenced to the extracellular compartment, as is the standard method for membrane potentials. Inward currents are defined as the movement of positive charge from the extracellular compartment to the intracellular compartment and are presented as downward deflections from the baseline in all recordings. Ionic currents were low-pass filtered at 2 kHz by using an AxoPatch 200B amplifier and digitized at 5 kHz using a Digidata 1322A interfaced with a PC computer running pCLAMP 9.2 software (all instruments including software; Axon Instruments). Currents were analyzed using Clampfit 9.2 (Axon Instruments) and Biopatch software (version 3.3, Bio-logic).

*Variance analysis.* Macroscopic membrane patches were excised into 10 μM $Ca^{2+}$, after which a complete $Ca^{2+}$-concentration response experiment was performed (see figure for specific details). At the end of the $Ca^{2+}$-concentration response experiment, PCMBS (500 μM) was added to the 10 μM $Ca^{2+}$ concentration, and the experiment continued until the current reached a second steady-state PCMBS-mediated maximum current level. The total current record, to be used for variance analysis, was divided into 250 episodes and mean current <I> and variance ($\sigma^2$) were calculated for each episode using Channelab Software (Synaptosoft Inc., Decatur, GA, USA). The increase in channel open probability ($P_o$), mediated through PCMBS, was estimated by determining the difference between the $P_{o(max)}$ value in the presence and absence of PCMBS. Furthermore, the number of channels (N) in the patch and single channel amplitude (i) are obtained by fitting the $\sigma^2$ against <I> distribution to Equation 1:

$$\sigma^2 = iI - \frac{I^2}{N} \qquad (1)$$

The $P_{o(max)}$ can then be calculated using Equation 2:

$$Po_{\max} = \frac{I_{\max}}{iN} \quad (2)$$

Where, $I_{max}$ is the maximum current observed and i and N are the mean values for single channel amplitude and number of channels calculated from Equation 1. The product of i and N would give the theoretical current at $P_o = 1$, hence, channel $P_o$ can be calculated at any given current as a proportion of $P_{o(max)}$ [203].

*$Ca^{2+}$ jump experiments.* Macroscopic membrane patches expressing KCa3.1 were excised from HEK293 cells and intracellular solution was quickly switched using a rapid solution exchanger (RSC-160; Biologic). In order to estimate the kinetics of activation and deactivation, the protocol requires that the internal solution be alternated between a $Ca^{2+}$-free solution for 3 seconds and a series of $Ca^{2+}$-containing solutions (concentrations reported in the results section) for 1.5 seconds with a 5 ms interval between switches. Activation and deactivation currents were recorded, superimposed, and averaged using Clampfit 9.2 (Axon Instruments) software. Time constants describing channel activation and deactivation kinetics were determined by fitting the activation and deactivation current records with a standard single exponential function. The deactivation kinetics were well described using a single exponential. However, the activation kinetics were sigmodial in shape, due to the delay in channel activation, and not well described with a single exponential function. This delayed response in channel activation can be explained through two factors. The first factor is based upon the volume of solution that must be exchanged between the surface of the patch and the tip of the patch pipette. The larger the volume, the longer it takes for a complete solution exchange, thus increasing the duration of the delay in channel activation.

Because this factor is dictated by the size and positioning of the membrane relative to the tip of the pipette, this will vary between patches and for these purposes is considered rate-limiting. The second factor contributing to the delay in channel activation is the multiple (2 or more) transitions the channel must pass through before entering the open state [204]. Assuming the number of conformational transitions along the activation pathway are equal between channels, this factor can be considered constant across all experiments. Therefore, these two factors summed together manifest as the delay in channel activation. However, we failed to notice a correlation between the duration of delay in channel activation verses $Ca^{2+}$-concentration and thus no further effort was made to analyze this component in the context of channel activation kinetics. Therefore, when fitting the current record to estimate activation kinetics the delay in channel activation was disregarded, which left the remaining portion of the current recording that is well described by a single exponential function [205].

*Modeling*. The 6-state kinetic model illustrated in Fig. 10 (A) was solved numerically to quantify how PCMBS perturbs the gating of KCa3.1 and to understand the overall contribution of S6 to the $Ca^{2+}$-dependent gating mechanism. Forward and reverse rate constants are labeled according to the channel state such that $k_{ij}$ is the rate of going from state i to state j. Thus, the model has 10 rate constants $k_{12}$, $k_{23}$, $k_{34}$, $k_{35}$, and $k_{46}$ are the forward rate constants and $k_{21}$, $k_{32}$, $k_{43}$, $k_{53}$, and $k_{64}$ are the reverse rate constants. The $Ca^{2+}$-dependent transitions are represented by the forward rate constants $k_{12}$, $k_{23}$, and $k_{34}$, and all other transitions are assumed to be $Ca^{2+}$-independent. We explored two version of the model with regard to the $Ca^{2+}$-dependence of these rate constants. First, we constructed a model in which the rate of $Ca^{2+}$ binding varied linearly with $Ca^{2+}$ concentration, $k=A\cdot[Ca]$, where A is a constant as proposed for KCa2.3 [206]. Second, we constructed a model in which the rate of $Ca^{2+}$ binding varied nonlinearly with $Ca^{2+}$

concentration, k=A·[Ca]/(B+[Ca]), where A and B are constants. The second rate takes the form of a Michaelis-Menten equation in which the rate of binding saturates at high $Ca^{2+}_i$ as further discussed in the results section. We used an 11$^{th}$ independent variable, N, to scale the single channel current resulting from the model to match macroscopic experimental currents. Thus, N represents the number of active channels in the patch. For a particular set of rate constants, we solved the system of equations corresponding to Fig. 10 (A) using a stiff solver routine in Matlab (7.6). We then calculated the root mean square difference (RMSD) between the simulated channel current and the experimentally recorded trace. Next, we used a Nelder-Mead search algorithm to search through parameter space in an attempt to minimize the RMSD [207]. A typical search involved solving the model 50,000 times for each $Ca^{2+}$ concentration. Furthermore, the search algorithm was rerun on each data set several times in an attempt to thoroughly explore parameter space for the best fit. This entire procedure was carried out for data sets recorded in the absence or presence of PCMBS in order to identify the transitions modulated by this compound.

The 6-state scheme was also used to predict the apparent $Ca^{2+}$ affinity and shift in apparent affinity observed with PCMBS. Channel $P_o$ was calculated from the model over the range of experimentally measured $Ca^{2+}$ concentrations, and the corresponding $EC_{50}$ was extracted from the resulting curve. We determined channel $P_o$ at each $Ca^{2+}_i$ concentration by running the model to steady state and dividing the probability of being in the open state (states 5 and 6) by the total probability (sum of states 1 through 6).

*Sensitivity analysis.* To determine which parameters were most critical for fitting the data, we varied each rate constant by ±10%, reran the model, and calculated the percent change in the

error. This analysis was only carried out on the final set of parameter values that produced the best fit for any given condition.

*Structural modeling*. We constructed a homology model of the pore domain of KCa3.1 with Modeller 9v7 [208] using Kv1.2 (PBD ID 2A79) and KcsA (PDB ID 1BL8) as a template structure.

*Hill equation.* $Ca^{2+}$ concentration response experiments were plotted as normalized current (I/Imax) against the corresponding $Ca^{2+}$ concentration p[$Ca^{2+}$],M and were fit with the following version of the Hill equation: $I=I_{min}+(I_{max}-I_{min})/(1+10^{((LogEC50-X)*HillSlope)})$. Fitting was performed using Prizm (GraphPad Software, Inc.).

*Chemicals.* All chemicals were obtained from Sigma-Aldrich (St. Louis, MO), unless otherwise stated. Adenosine-5'-triphosphate obtained from Roche Diagnostics and parachloromercuribenze sulfonate (PCMBS) purchased from Toronto Research Chemicals Inc., (ON, Canada) were freshly made on the day of the experiment and added directly to the bath solution prior to the experiment.

*Online Supplemental Material.* The results from the sensitivity analysis are included as an individual table for each data set.

## 2.4 RESULTS

### 2.4.1 PCMBS can be used as a Probe to Modulate KCa3.1 Gating

It was previously demonstrated that MTSET only transiently inhibits WT-KCa3.1 steady-state behavior [113]. Therefore, we wanted to determine whether PCMBS could alter steady-state current in excised membrane patches expressing KCa3.1. As shown in Fig. 12 (A-C), addition of PCMBS (500 μM) to the membrane patch increased channel activity at 0.3 μM (A), 0.6 μM (B), and 10 μM (defined as saturating) $Ca^{2+}_i$ concentrations. Furthermore, the effect of PCMBS could not be reversed upon washout, suggesting a covalent interaction between channel cysteine(s) and the sulfhydryl-reactive compound. To address whether PCMBS could activate KCa3.1 in the absence of $Ca^{2+}_i$, experiments were performed in which PCMBS (500 μM) was added following the addition of a $Ca^{2+}$ free bath solution. As shown in Fig. 12 (D), PCMBS is unable to activate KCa3.1 in the absence of $Ca^{2+}_i$, demonstrating that the compound potentiates channel current rather than directly activating the channel. Only after the addition of $Ca^{2+}_i$ can PCMBS increase steady-state current, suggesting the closed conformation prevents PCMBS from accessing the endogenous cysteine residue(s). Our results illustrate that PCMBS can covalently bind to endogenous cysteine residue(s), and these residue(s) must reside within a gating sensitive region of the channel.

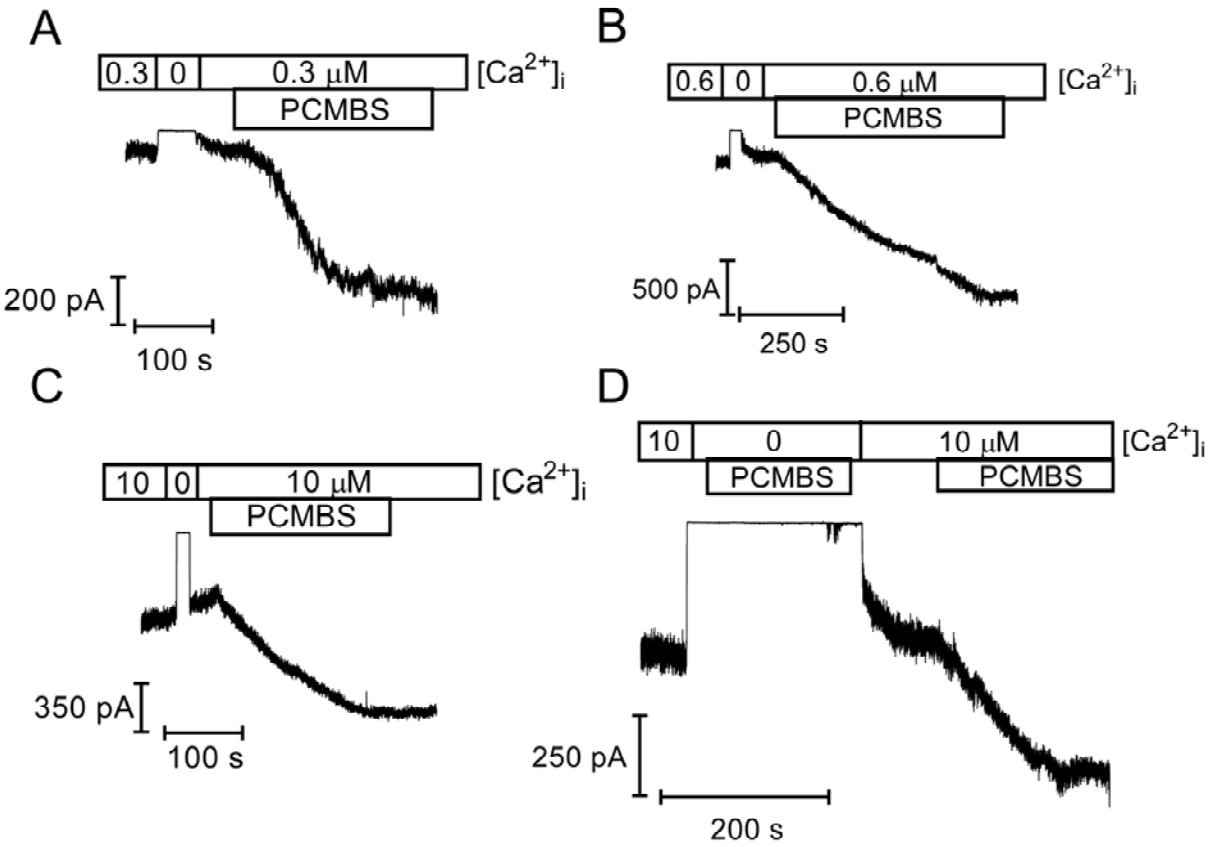


**Figure 12. PCMBS increases KCa3.1 steady-state current.** Macroscopic current records from KCa3.1 channels heterologously expressed in HEK cells to determine sensitivity to PCMBS. PCMBS (500 μM) was added to inside-out patches excised in 0.3 (A), 0.6 (B), and 10 μM (C) $Ca^{2+}_i$ following the establishment of steady-state current level. PCMBS washout lasted at least 1 minute to ensure channel activation was due to covalent binding, rather than an indirect interaction between channel and compound. (D) KCa3.1 current record demonstrating that PCMBS cannot activate the channel in the absence of $Ca^{2+}_i$. PCMBS can only increase current when the channel is in the open state. The patch was initially excised in 10 μM $Ca^{2+}_i$, followed by the addition of a $Ca^{2+}_i$-free solution, than a $Ca^{2+}_i$-free solution+PCMBS (500 μM) was added to the bath solution. PCMBS+$Ca^{2+}_i$-free solution was washed out with 10 μM $Ca^{2+}_i$ to reactivate the channel. After reaching a steady-state current level, PCMBS (500 μM) was reapplied to the patch resulting in channel activation.

### 2.4.2 Characterization of Potentiation by PCMBS

To gain insight into the mechanism by which PCMBS activates KCa3.1, we determined whether PCMBS increases steady-state current through an increase in N, $P_o$, or i using variance analysis, as described in the materials and methods section. Fig. 13 (A) depicts a representative current record in which a series of $Ca^{2+}_i$ concentrations were applied to the intracellular face of an inside-out patch expressing KCa3.1 channels, and following establishment of steady-state current in 10 μM $Ca^{2+}_i$, PCMBS (500 μM) was added to the bath. This current record was utilized to calculate $\sigma^2$ both in the absence (portion of the record excluding PCMBS) and presence (entire record) of PCMBS. Plotting $\sigma^2$ against <I> and fitting this relationship with Eq. 1 gave estimates of N, $P_o$, and i (Fig. 13 B-C). Analysis of these data indicate that potentiation results from a 50% increase in $P_{o(max)}$ (from 0.61 to 0.91 in PCMBS) rather than changes to N (1071 versus 1078 in PCMBS) or i (3.5 pA versus 3.4 pA in PCMBS). Analysis of multiple experiments (n=12) revealed that PCMBS increases $P_{o(max)}$ from 0.65±0.03 to 0.93±0.02 without an increase in N or i (3.3±0.03 pA versus 3.3±0.03 pA in PCMBS). Given the variability of N across patches, its average was not calculated. These data suggest that PCMBS acts through a $Ca^{2+}$-independent pathway to increase steady-state current through an increase in $P_{o(max)}$.

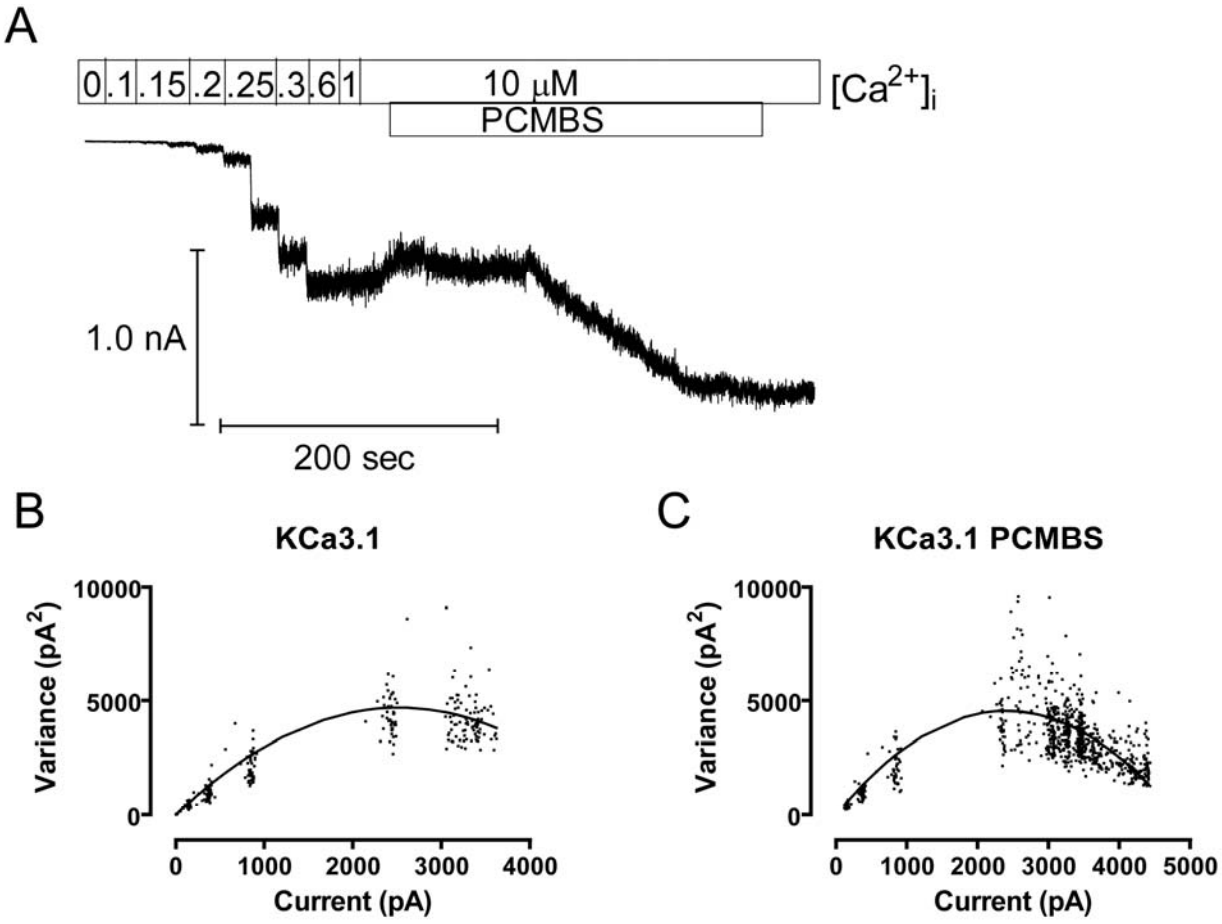


**Figure 13. P CMBS increases steady-state $P_{o(max)}$.** Variance analysis of KCa3.1 channel current was utilized to estimate $P_{o(max)}$, N, and i in the absence and presence of PCMBS. (A) Representative $Ca^{2+}$ concentration response experiment recorded from inside-out macropatches expressing KCa3.1 channels. Patches were initially excised in 10 μM $Ca^{2+}_i$, followed by a series of $Ca^{2+}_i$ concentrations (0, 0.1, 0.15, 0.2, 0.25, 0.3, 0.6, 1.0, and 10 μM) applied for 10 s intervals using a fast solution exchanger. After establishing steady-state current in 10 μM $Ca^{2+}_i$ PCMBS (500 μM) was added to the bath solution until reaching a second, steady-state, current level. (B) Variance analysis to determine $P_{o(max)}$, N, and i in the absence of PCMBS. Plot of variance ($\sigma^2$), which was calculated from the portion of the record excluding the time when PCMBS was added, against mean current <I> as fit with Eq. 1 (solid line) and $P_{o(max)}$ was calculated using Eq. 2: $P_{o(max)} = 0.61$, N=1071, and i=3.5 pA. (C) Variance analysis to determine $P_{o(max)}$, N, and i in the presence of PCMBS. Plot of $\sigma^2$, which was calculated from the entire record against <I> was fit with Eq. 1 (solid line) and $P_{o(max)}$ was calculated using Eq. 2: $P_{o(max)} = 0.91$, N=1078, and i=3.4 pA.

Importantly, the steady-state current increase observed in saturating $Ca^{2+}$ would mask any increase in channel activation occurring through a $Ca^{2+}$-dependent pathway. Therefore, to determine whether PCMBS also affects the $Ca^{2+}$-dependent pathway, we measured the apparent $Ca^{2+}$ affinity in the absence and presence of PCMBS as shown in Fig. 14 (A). This figure illustrates that PCMBS induced a significant current potentiation between 0.3 and 0.6 μM $Ca^{2+}_i$ compared to the equivalent current increase in the absence of the compound. These data were fit to a version of the Hill equation, Fig. 14 (B), demonstrating a PCMBS-dependent shift in the $EC_{50}$ from 508±13 nM (n=57) to 235±17 nM (n=6) without altering the Hill coefficient (2.0±0.2 and 2.5±0.2). These results indicate that PCMBS increases channel activation through both $Ca^{2+}$-independent and -dependent pathways, reflected by an increase in $P_{o(max)}$ and a shift in apparent $Ca^{2+}$ affinity, respectively.

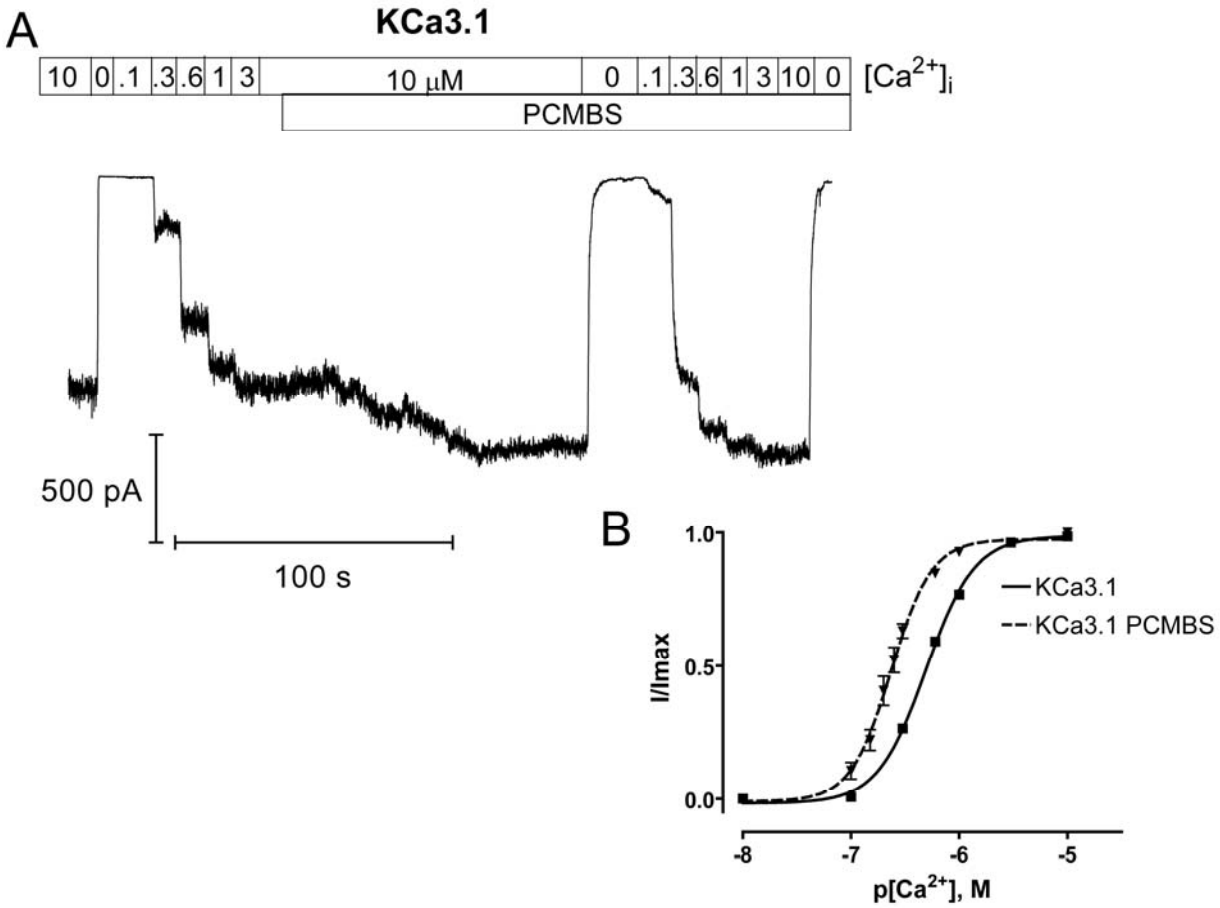


**Figure 14. PCMBS shifts apparent $Ca^{2+}$ affinity.** Complete $Ca^{2+}$ concentration response experiments were performed to estimate $EC_{50}$ and the Hill coefficient (h) in the absence and presence of PCMBS. (A) Representative macroscopic current record from an inside-out patch expressing KCa3.1 channels. The patch was excised in 10 μM $Ca^{2+}_i$ followed by a series of $Ca^{2+}_i$ concentrations beginning with 0, 0.1, 0.3, 0.6, 1.0, 3.0, and 10 μM $Ca^{2+}_i$, all applied in 10 s intervals using a rapid solution exchanger. After the current reached a steady-state level, PCMBS (500 μM) was added and a 2nd $Ca^{2+}_i$ concentration response experiment was performed using the above $Ca^{2+}_i$ concentrations in the presence of PCMBS. (B) Plot of normalized <I> current against the corresponding $Ca^{2+}_i$ for KCa3.1 (■) and KCa3.1+PCMBS (▲) fit with a variation of the Hill equation (see methods). This analysis gave estimates for KCa3.1 (solid line, n=57) $EC_{50}$=508±13 nM and h=2.0±0.2 and KCa3.1+PCMBS (dashed line, n=6) $EC_{50}$=235±17 nM and h=2.5±0.2. All experiments were done in pairs, but an alternate set of $Ca^{2+}_i$ concentrations (0.1, 0.15, 0.2, 0.25, 0.3, 0.6, 1.0 and 10 μM) were used when estimating $EC_{50}$ and h for KCa3.1+PCMBS. Error bars represent standard error of the mean (SEM). The error bars for KCa3.1 are smaller than the symbols (■).

Our results suggest that PCMBS shifts the gating equilibrium toward the open state, which we expect to be manifested as a change in the activation or deactivation kinetics of the channel. To determine which of these kinetic steps is being modified, we measured the kinetics of channel activation and deactivation in the absence and presence of PCMBS. The patch was excised in 10 μM $Ca^{2+}_i$, after which $Ca^{2+}_i$ was rapidly switched between a $Ca^{2+}$-free solution and a $Ca^{2+}_i$ solution, as depicted in the inset of Fig. 15. After 5-10 complete cycles (1 cycle consists of taking measurements using 0.5 (A), 0.7 (B), 1.0 (C), and 10 (D) μM $Ca^{2+}_i$), PCMBS was added to the bath solution and the protocol was repeated. Since PCMBS increases current at all $Ca^{2+}$-concentrations, current recordings were normalized to the maximum current level to compare channel kinetics in the absence and presence of PCMBS. Additionally, current records for each $Ca^{2+}_i$ -concentration were superimposed and averaged to produce the representative current records shown in Fig. 15 (A-D). Time constants (τ) for channel activation and deactivation were determined from fits of the data to a single-exponential and reported in Fig. 15 (E-F), see also Table (1). As shown, the data demonstrates that the activation kinetics are $Ca^{2+}$-dependent, becoming faster with increased $Ca^{2+}_i$-concentration, whereas the deactivation kinetics are $Ca^{2+}$-independent, being insensitive to changes in $Ca^{2+}_i$-concentration. The addition of PCMBS, Fig. 15 (A-D), results in a 6-fold increase in the time-constant for deactivation (Fig. 15 F) with only moderate effects on the time course for activation (Fig. 15 E, see also Table 1).

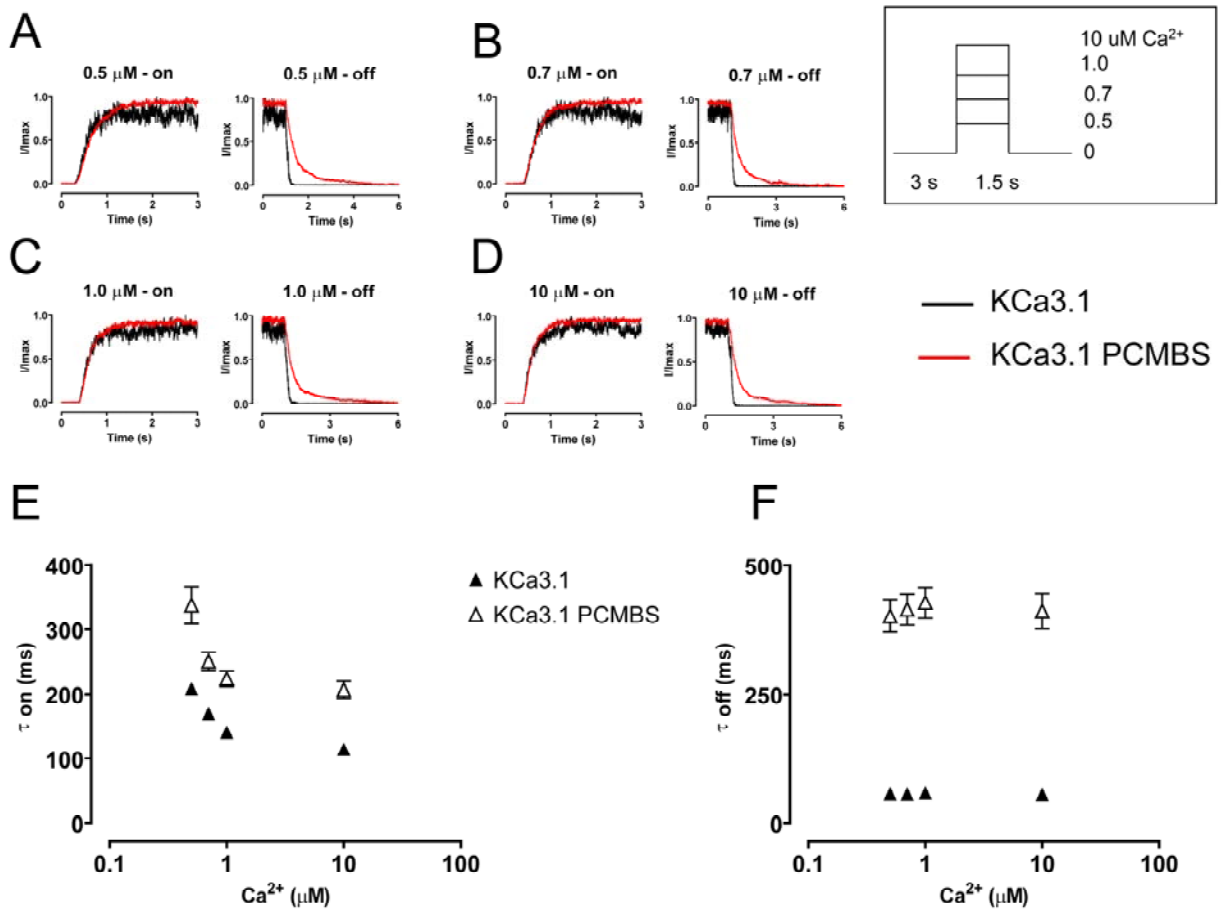


**Figure 15. PCMBS modulates channel kinetics.** Activation and deactivation kinetics were estimated with $Ca^{2+}$-jump experiments in the absence and presence of PCMBS. A rapid solution exchanger was utilized to quickly alternate between a $Ca^{2+}_i$-free solution and 1 of 4 $Ca^{2+}_i$ solutions: (A) 0.5, (B) 0.7, (C) 1.0, and (D) 10 μM $Ca^{2+}_i$ following the protocol illustrating one complete $Ca^{2+}$ cycle shown in the inset of this figure. 5-10 complete $Ca^{2+}$ cycles were recorded from a single patch in the absence and presence of PCMBS (500 μM). Activation and deactivation sweeps in the absence of PCMBS (black trace) were collected and averaged according to their respective $Ca^{2+}$-concentration, and superimposed against the corresponding PCMBS sweep (red trace). Current traces were normalized to the max current level, facilitating comparison of time courses between KCa3.1 and KCa3.1+PCMBS. Activation (E) and deactivation (F) rates were estimated by fitting activation and deactivation records with an exponential function and reported as a time constant (τ-on and τ-off) in the absence (▲) and presence (△) of PCMBS, see also Table (1).

**Table 1. Exponential fits comparing the activation and deactivation kinetics of KCa3.1.** Time constants (τ) from single exponential fits to channel activation or deactivation records from the four $[Ca^{2+}]_i$ concentrations examined.

| | | | | | PCMBS | | |
|---|---|---|---|---|---|---|---|
| Channel | $[Ca^{2+}]_i$ | on | off | n | on | off | n |
| | μM | (ms) | (ms) | | (ms) | (ms) | |
| KCa3.1 | 0.5 | 224±22 | 61±5 | 13 | 337±29 | 402±31 | 13 |
| (paired) | 0.7 | 185±11 | 60±5 | 13 | 250±14 | 414±30 | 13 |
| | 1.0 | 147±9 | 65±4 | 13 | 224±12 | 428±30 | 13 |
| | 10 | 123±11 | 59±4 | 13 | 206±13 | 411±34 | 13 |
| KCa3.1 | | | | | | | |
| C276A | 0.5 | 211±20 | 48±4 | 7 | 191±12 | 60±8 | 7 |
| | 0.7 | 186±15 | 46±4 | 7 | 154±13 | 57±6 | 7 |
| | 1.0 | 142±15 | 56±3 | 7 | 134±12 | 61±6 | 7 |
| | 10 | 120±11 | 43±3 | 7 | 103±6 | 59±6 | 7 |
| KCa3.1 | | | | | | | |
| C277A | 0.5 | 244±10 | 54±6 | 6 | 318±20 | 377±45 | 5 |
| | 0.7 | 186±9 | 59±6 | 6 | 262±18 | 336±46 | 5 |
| | 1.0 | 152±8 | 59±5 | 6 | 223±19 | 365±44 | 5 |
| | 10 | 129±12 | 59±7 | 6 | 194±14 | 332±39 | 5 |

| | | | | | | | |
|---|---|---|---|---|---|---|---|
| KCa3.1 | 0.5 | 209±9 | 57±2 | 51 | | | |
| | 0.7 | 170±5 | 57±2 | 51 | | | |
| | 1.0 | 141±5 | 59±2 | 51 | | | |
| | 10 | 114±5 | 56±2 | 51 | | | |
| KCa3.1 | | | | | | | |
| L281W | 0.5 | 149±12 | 186±11 | 23 | 175±20 | 267±20 | 8 |
| | 0.7 | 130±9 | 202±11 | 23 | 142±17 | 278±24 | 8 |
| | 1.0 | 119±10 | 198±9 | 23 | 119±13 | 293±27 | 8 |
| | 10 | 92±7 | 197±9 | 23 | 100±10 | 288±27 | 8 |
| KCa3.1 | | | | | | | |
| V282W | 0.5 | 161±11 | 59±3 | 13 | | | |
| | 0.7 | 131±8 | 59±2 | 13 | | | |
| | 1.0 | 113±8 | 59±3 | 13 | | | |
| | 10 | 84±5 | 58±3 | 13 | | | |

### 2.4.3 Cysteine 276 Confers PCMBS-sensitivity to KCa3.1 Potentiation

Potentiation by PCMBS is the result of cysteine modification, and KCa3.1 contains 9 endogenous cysteines residues. Fig. 16 (A) illustrates a model of the pore region for the open state of KCa3.1 obtained by homology modeling using the rKv1.2 channel structure [209]. This model shows that the four endogenous cysteine residues (267, 269, 276, and 277) are located along S6, making these residues likely candidates for conferring PCMBS-sensitivity. To isolate the residue(s) responsible for the PCMBS-mediated potentiation, each cysteine was mutated to an alanine and the effect of PCMBS determined. However, C267A and C269A failed to produce macroscopic currents, preventing their assessment in PCMBS-mediated channel potentiation. Therefore, we tested whether PCMBS (500 μM) could potentiate current in the C276A and C277A constructs. A representative $Ca^{2+}$ concentration response experiment for C277A is shown in Fig. 17 (A). PCMBS increases steady-state current in 10 μM $Ca^{2+}_i$ (left panel), in addition to causing a left shift in apparent $Ca^{2+}$ affinity (right panel). Furthermore, washout of PCMBS does not reverse the increase in current (unpublished data), demonstrating that PCMBS still covalently binds to the channel. We confirm through variance analysis (Fig. 17 B-C) that the steady-state current increase in saturating $Ca^{2+}_i$ is the result of an increase in $P_{o(max)}$ (see figure legend for details). Additionally, the C277A mutation did not alter the apparent $Ca^{2+}$ affinity or the $P_{o(max)}$ relative to the WT-channel, suggesting the increase in C277A activation is due to the binding of PCMBS and not to the mutation having an indirect effect on channel gating. In total, these results demonstrate the PCMBS-mediated channel activation does not require $Cys^{277}$.

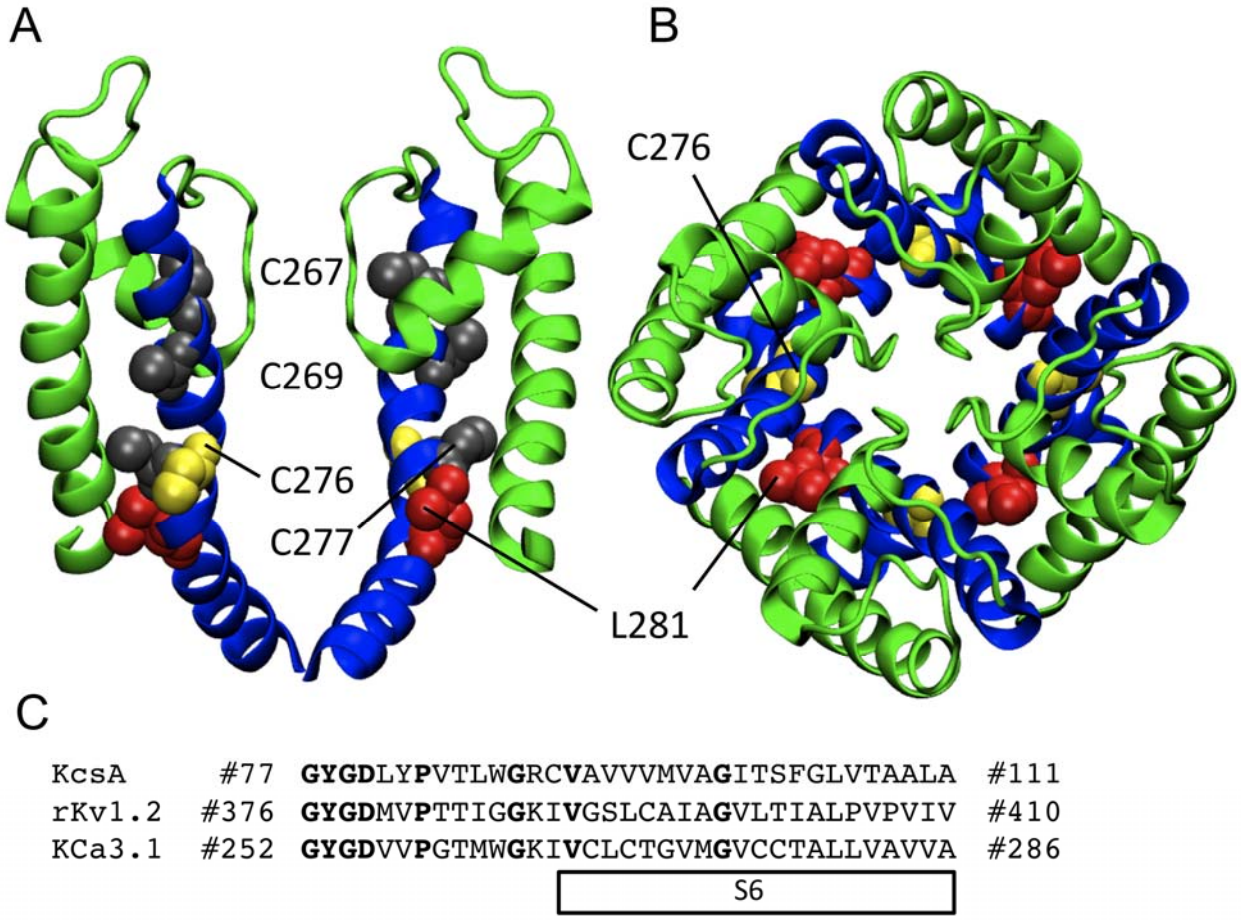


**Figure 16. Homology model of the pore region for the open state of KCa3.1 using the rKv1.2 structure .** (A) Representation of the S5- P-helix -S6 region viewed as a profile illustrating the predicted orientation of $Cys^{267}$, $Cys^{269}$, $Cys^{277}$ (all in gray) $Cys^{276}$ (yellow), and $Leu^{281}$ (red). Only two of the four subunits are shown for clarity. (B) Representation of the S5- P-helix -S6 region from the extracellular entrance showing the predicted non-luminal orientation of $Cys^{276}$ (yellow) and $Leu^{281}$ (red). The S5 and P-helix are colored green and the S6 helix is colored blue. All residues are illustrated in VDW format. (C) Sequence alignment used for the homology model of KCa3.1 in the open state (rKv1.2) and the closed state (KcsA model illustrated in Fig. 26). Bold font represents homologous amino acids used as a guide to align sequences.

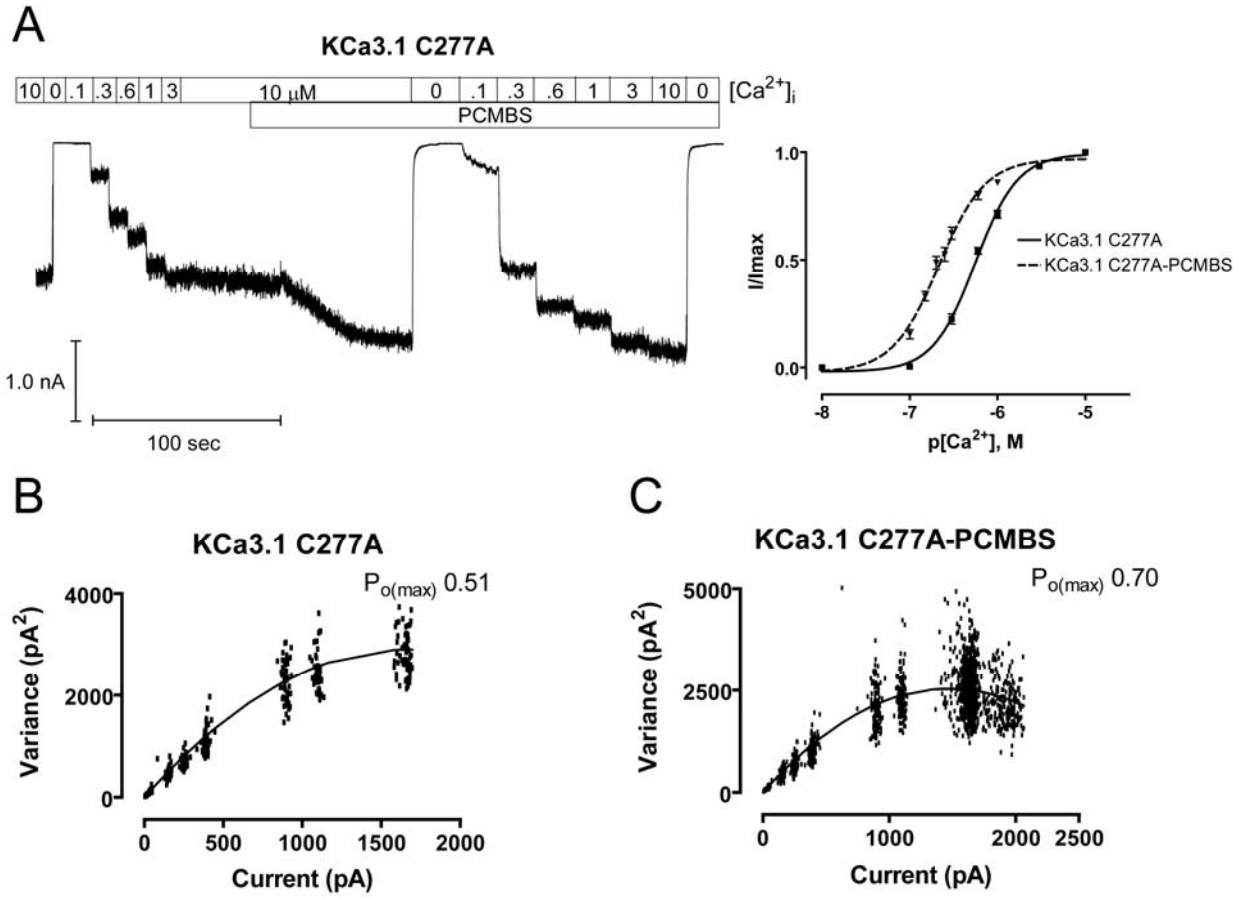


**Figure 17. PCMBS increases channel activation for KCa3.1 C277A.** $Ca^{2+}$-concentration response experiments and variance analysis were undertaken to determine whether PCMBS increases C277A channel activation in the same manner observed for the WT channel. (A, left panel) Representative macroscopic current record from an inside-out patch expressing KCa3.1 C277A channels. All experiments were performed utilizing the $Ca^{2+}$-concentraiton response protocol described in Fig. 14. (A, right panel) Plot of normalized <I> current against the corresponding $[Ca^{2+}]_i$ for KCa3.1 C277A (■) and KCa3.1 C277A+PCMBS (▼). All analysis was performed following the protocol described in Fig. 14 to give averages: KCa3.1 C277A (solid line, n=15) $EC_{50}$=566±24 nM and h=1.9±0.1 and KCa3.1 C277A+PCMBS (dashed line, n=7) $EC_{50}$=220±14 nM and h=1.7±0.2. Error bars represent standard error of the mean (SEM). (B) Variance analysis as described in Fig. 13 to determine $P_{o(max)}$, N, and i in the absence of PCMBS: $P_{o(max)}$ = 0.51, N=954, and i=3.5 pA. (C) Variance analysis as described in Fig. 13 to determine $P_{o(max)}$, N, and i in the presence of PCMBS $P_{o(max)}$ = 0.70, N=849, and i=3.5 pA. Analysis of multiple patches (n=6) indicates that PCMBS increase $P_{o(max)}$ from 0.55±0.02 to 0.84±0.03 without increasing N or i (3.8±0.1 pA versus 3.9±0.1 in PCMBS).

In contrast to the C277A mutation, C276A (Fig. 18 A) completely eliminated both the shift in apparent affinity (Fig. 18 B) and the increase of steady-state current in saturating $Ca^{2+}_i$ (Fig. 18 C, see figure legend for details). Additionally, the C276A mutation did not alter the apparent $Ca^{2+}$ affinity or the $P_{o(max)}$ relative to the WT-channel, suggesting the absence of channel potentiation is due to removing $Cys^{276}$, rather than the mutation having an indirect effect on channel gating. In total, these results indicate that channel potentiation is the result of PCMBS binding to $Cys^{276}$.

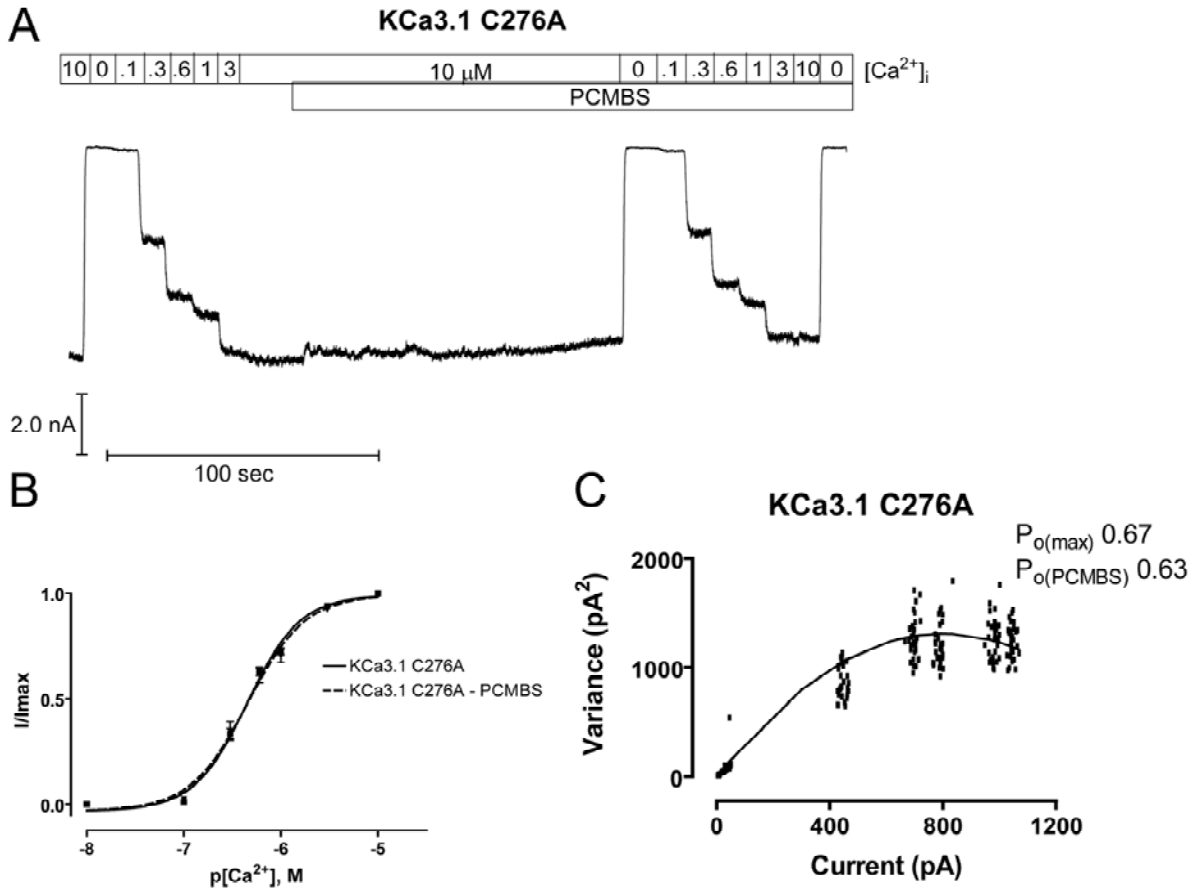


**Figure 18. C276A prevents the PCMBS-mediated increase in channel activation.** $Ca^{2+}$-concentration response experiments and variance analysis were undertaken to determine whether PCMBS increases C276A channel activation in the same manner observed for the WT channel. (A) Representative macroscopic current record from an inside-out patch expressing KCa3.1 C276A channels. All experiments were performed utilizing the $Ca^{2+}$-concentraiton response protocol described in Fig. 14. (B) Plot of normalized <I> current against the corresponding $Ca^{2+}_i$ for KCa3.1 C276A (■) and KCa3.1 C276A+PCMBS (▼). All analyses were performed following the protocol described in Fig. 14 to give averages: KCa3.1 C276A (solid line, n=18) $EC_{50}$=460±27 nM and h=1.7±0.04 and KCa3.1 C276A+PCMBS (dashed line, n=9) $EC_{50}$=485±68 nM and h=1.6±0.04. Error bars represent standard error of the mean (SEM). (C) Variance analysis as described in Fig. 13 to determine $P_{o(max)}$, N, and i in the absence of PCMBS: $P_{o(max)}$ = 0.67, N=488, and i=3.3 pA. PCMBS did not increase steady-state current in KCa3.1 C276A therefore, in order to obtain an estimate of $P_{o(PCMBS)}$, $P_o$ had to be extrapolated using the Eq. where $P_o=P_{o(max)}(I/I_{(max)})$ and $P_{o(PCMBS)}$=0.63. Analysis of multiple patches (n=6) indicates that PCMBS did not increase $P_{o(max)}$ (0.68±0.05 in the absence of PCMBS and 0.59±0.05 in PCMBS).

PCMBS modulated the kinetic as well as steady-state behavior of the WT-channel. Therefore, we also determined whether $Cys^{276}$ or $Cys^{277}$ played a role in PCMBS related changes to channel activation and deactivation. As depicted in Fig. 19 (A-D), C277A activation and deactivation records were similar to the WT-channel, both in the absence and presence of PCMBS. The average activation and deactivation time constants ($\tau$) are plotted in Fig. 19 E and F, respectively, as well as being reported in Table (1). These results further demonstrate that $Cys^{277}$ does not mediate the PCMBS-dependent potentiation of KCa3.1. However, as expected, $Cys^{276}$ eliminated the PCMBS-dependent changes in the kinetic behavior of the channel (Fig. 20 A-D). The elimination of the PCMBS effect on kinetic behavior cannot be explained through an indirect effect of the $Cys^{276}$ mutation, because the time course of activation and deactivation kinetics (in the absence of PCMBS) closely describe the values observed in the WT-channel (Table 1). Therefore, these results suggest that modification of the kinetic behavior is the result of PCMBS binding to $Cys^{276}$.

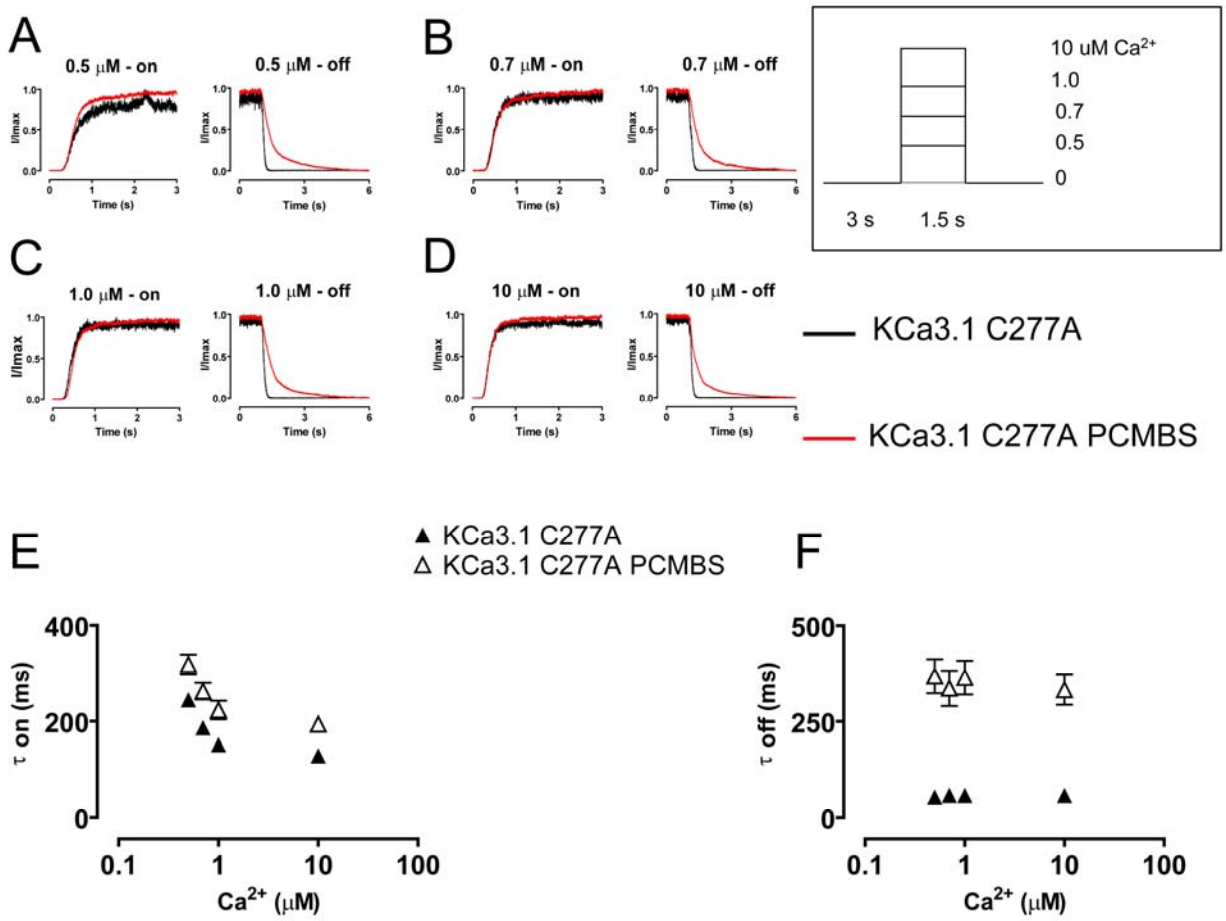


**Figure 19. PCMBS modulates C277A channel kinetics in a manner similar to the WT-channel.** Activation and deactivation kinetics were estimated with $Ca^{2+}$-jump experiments using $Ca^{2+}_i$ concentrations 0.5, (A) 0.7, (B) 1.0, (C) and 10 μM (D) in the absence (black trace) and presence (red trace) of PCMBS as described in Fig. 15. Activation (E) and deactivation (F) rates were estimated by fitting activation and deactivation records with an exponential function and reported as a time constant (τ-on and τ-off) in the absence (▲) and presence (△) of PCMBS, see also Table (1).

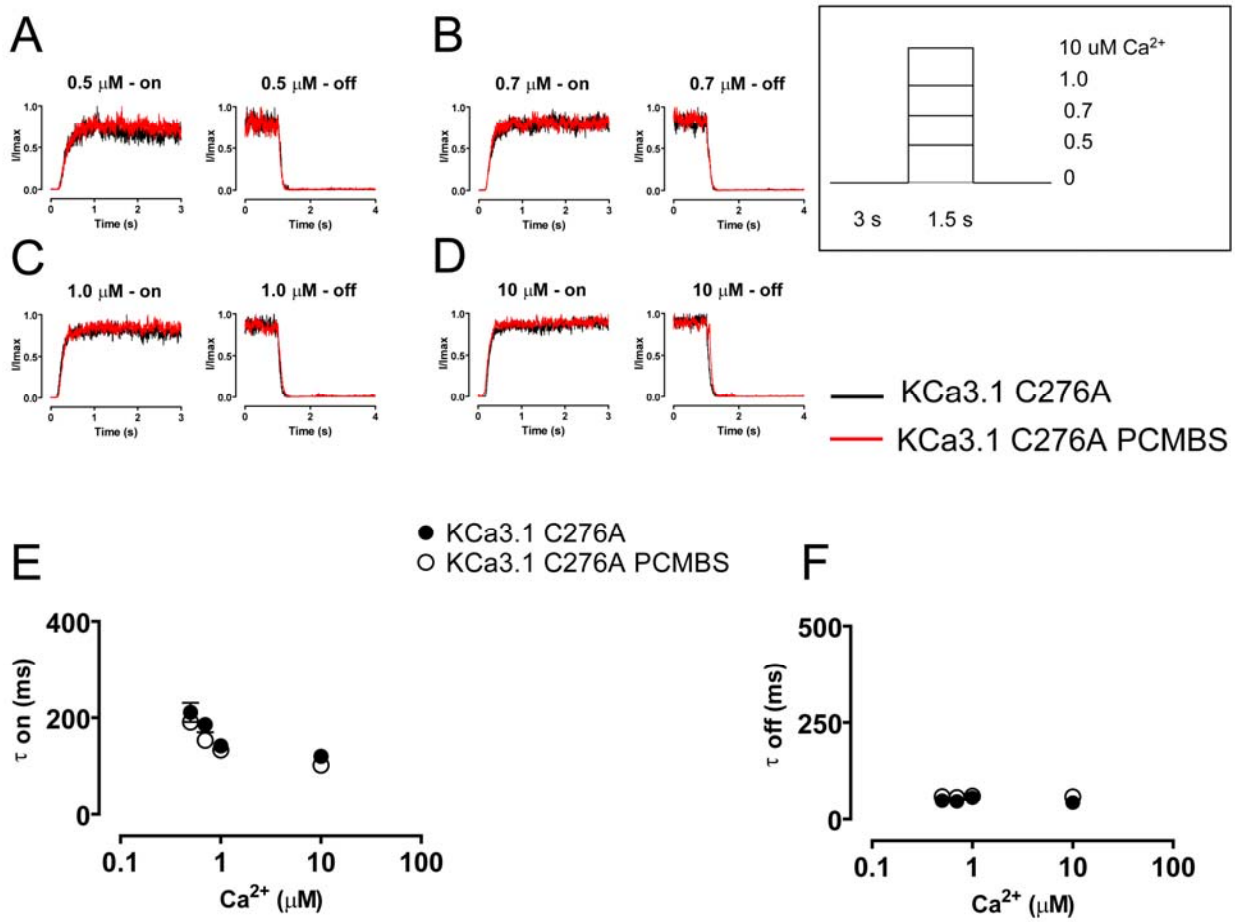


**Figure 20. C276A prevents the PCMBS-mediated modulation in channel kinetics.** Activation and deactivation kinetics were estimated with $Ca^{2+}$-jump experiments using $Ca^{2+}_i$ concentrations 0.5, (A) 0.7, (B) 1.0, (C) and 10 μM (D) in the absence (black trace) and presence (red trace) of PCMBS as described in Fig. 15. Activation (E) and deactivation (F) rates were estimated by fitting activation and deactivation records with an exponential function and reported as a time constant (τ-on and τ-off) in the absence (●) and presence (○) of PCMBS, see also Table (1).

### 2.4.4 Gating of KCa3.1 can be described with a 4-State Model

Our results demonstrate that PCMBS disrupts the steady-state and kinetic behavior of KCa3.1 by modifying $Cys^{276}$. Addressing the mechanism behind PCMBS modification is necessary for understanding how the molecular interactions surrounding position 276 contribute to the gating mechanism. To this end, we developed a kinetic model, which would enable us to identify the transitions along the activation or deactivation pathway altered by PCMBS. A previous investigation established that the gating of KCa2.2 (SK2) can be described by a 6-state gating scheme consisting of 4 closed states and 2 open states, with forward transitions between closed states being $Ca^{2+}$ dependent [206]. Therefore, we determined if this model (Fig. 21 A) could be used to describe the activation and deactivation kinetics of the closely related channel, KCa3.1. Activation and deactivation current records were fit with the 6-state model as described in the Materials and Methods section. The solid lines in Fig. 21 (B) represent the fit to the activation and deactivation records assuming the $Ca^{2+}$-dependent rate constants have a linear dependence on $Ca^{2+}$-concentration, as proposed for KCa2.2 [206]. This model gave an accurate description of all data sets, except for the activation rate in saturating $Ca^{2+}_i$, where the model predicted activation rates that were faster than those observed experimentally. To obtain a more accurate description of the activation rate in saturating $Ca^{2+}_i$, we assumed that the $Ca^{2+}$-dependent steps depended nonlinearly on the $Ca^{2+}$-concentration. This modification allowed for the $Ca^{2+}$-binding rate constants to saturate in high $Ca^{2+}_i$, giving a better description of the activation rates in 10 μM $Ca^{2+}_i$ (dashed lines Fig. 21 B), and therefore, was used for all further analysis. Sensitivity analysis was used to evaluate the importance of each parameter to the goodness of the fits for both variations of the model (Appendix Table A.7). This analysis showed that the final C-C and C-O transitions (box outline Fig. 21 A) were not required to fit the 4 sets of activation and

deactivation records (Table 2). Rather, these data were well described with a simpler 4-state model comprised of 3 closed states and 1 open state, and the best fit is achieved when the $Ca^{2+}$-dependent rate constants saturate in high $Ca^{2+}$.

We went on to further validate our kinetic scheme by predicting the apparent $Ca^{2+}$ affinity and the shift in apparent $Ca^{2+}$ affinity mediated by PCMBS. Fig. 21 (C) illustrates the simulated $Ca^{2+}$-concentration response curves in the absence (solid line) and presence (dashed line) of PCMBS plotted against the corresponding experimental data. The model accurately predicts the apparent $Ca^{2+}$ affinity as well as the shift induced by PCMBS. The success of the model is not entirely unexpected, since it was initially fit to the kinetic data, which encompasses the steady-state response. Nonetheless, the consistency between the model and the experimental data is reassuring.

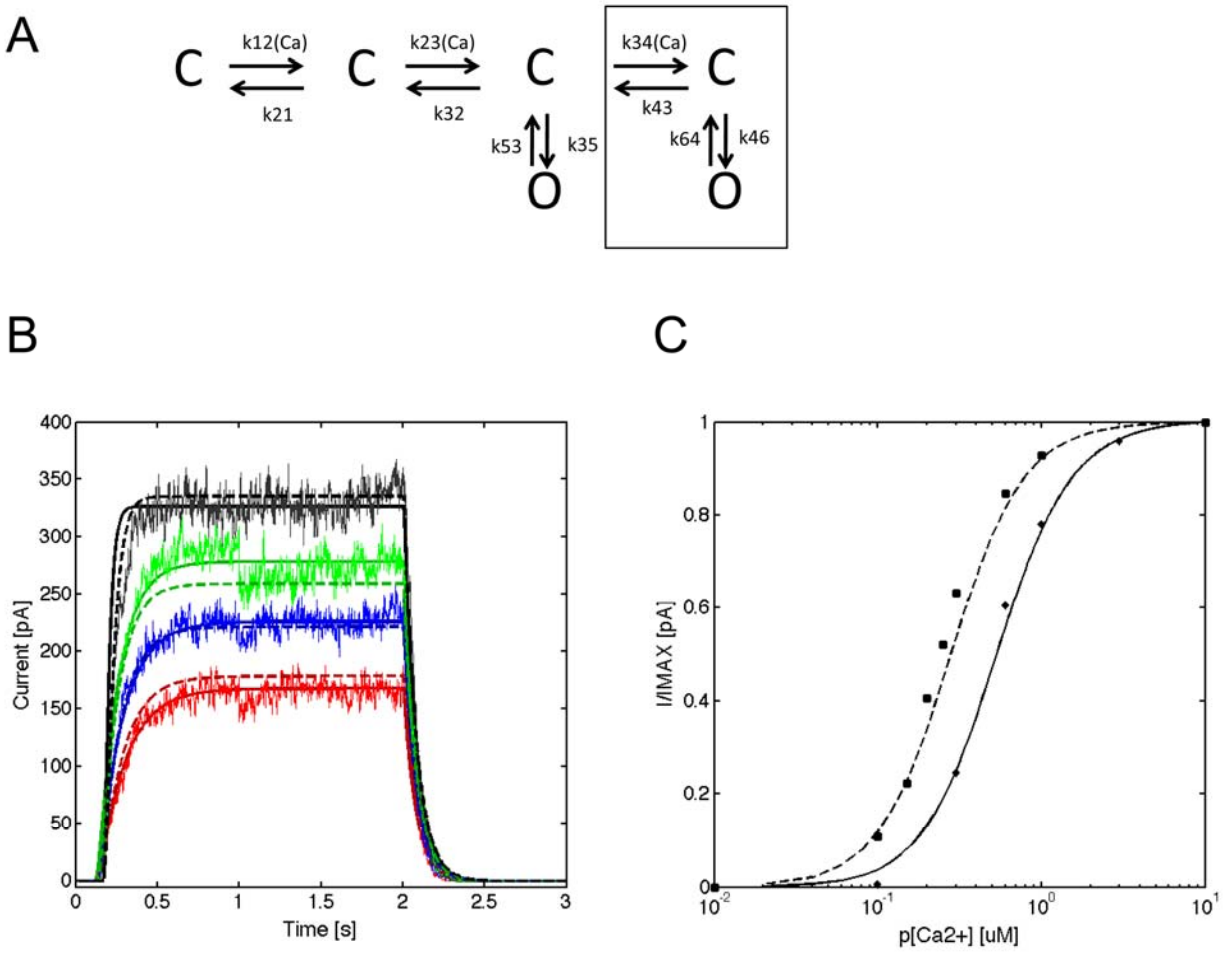


**Figure 21. A 4-state model can be used to fit the activation and deactivation kinetics for KCa3.1.** (A) Gating scheme used to describe the activation and deactivation kinetics of KCa3.1. The 6-state model is comprised of 4 closed states and 2 open states, with forward transitions between closed states being $Ca^{2+}$-dependent and all other transitions being $Ca^{2+}$-independent. The box outline represents the states that are not necessary to fit the activation and deactivation kinetics as determined through sensitivity analysis (appendix). (B) Representative activation and deactivation records fit with two variations of the model shown in (A). Activation and deactivation currents were recorded and fit following the protocol described in the methods sections. The colors refer to the different $Ca^{2+}$ concentrations, with red representing (0.5), blue (0.7), green (1.0), and black (10 μM) $Ca^{2+}$. The solid line represents the fit assuming $Ca^{2+}$-dependent rate constants have a linear dependence on $Ca^{2+}$-concentration, k= A·[Ca]. The dashed line represents the fit assuming $Ca^{2+}$-dependent rate constants have a non-linear dependence on $Ca^{2+}$-concentration, k= A·[Ca]/(B+[Ca]). Rate constants derived from the fit are summarized in Table (2) (C) The model can be used to predict the shift in apparent $Ca^{2+}$ affinity with PCMBS. Plot of normalized <I> current against the corresponding $Ca^{2+}_i$ for KCa3.1 and KCa3.1+PCMBS. The symbols represent the experimental data (KCa3.1 υ) and (KCa3.1+PCMBS ν)., which is plotted against the predicted apparent $Ca^{2+}$ affinity (KCa3.1 solid line) and (KCa3.1+PCMBS dashed line). Model prediction: KCa3.1 $EC_{50}$ 540 nM and KCa3.1+PCMBS $EC_{50}$ 280 nM. Experimental observation: KCa3.1 $EC_{50}$ 508 nM and KCa3.1+PCMBS $EC_{50}$ 235 nM.

**Table 2. Summary of the 6-State model used to describe the kinetic behavior of KCa3.1±PCMBS.**
Rate constants derived from fitting the model to KCa3.1 activation and deactivation records. (A) Rates constants derived using the model with all free parameters: KCa3.1, KCa3.1+PCMBS, and KCa3.1 L281W. (B) Rates constants derived using the $k_{53}$ model: KCa3.1+PCMBS and KCa3.1 L281W. (C) Rates constants derived using the $k_{12}$ $k_{23}$ and $k_{53}$ model: KCa3.1+PCMBS.

| | KCa3.1 | KCa3.1+PCMBS | | | Units |
|---|---|---|---|---|---|
| | (A) | (A) | (B) | (C) | |
| | n=2 | n=1 | n=1 | n=1 | |
| 12 | 27±3 | 10 | **27** | 20 | $\mu M^{-1}\ s^{-1}$ |
| 21 | 34±8 | 76 | **34** | **34** | $s^{-1}$ |
| 23 | 5425±2725 | 2911 | **5425** | 2820 | $\mu M^{-1}\ s^{-1}$ |
| 32 | 190±40 | 2978 | **190** | **190** | $s^{-1}$ |
| 34 | - | - | - | - | - |
| 43 | - | - | - | - | - |
| 35 | 34±7 | 291 | **34** | **34** | $s^{-1}$ |
| 53 | 20±5 | 3 | 3 | 3 | $s^{-1}$ |
| 46 | - | - | - | - | - |
| 64 | - | - | - | - | - |
| error | 38 | 45 | 42 | 43 | |

**bold**: fixed to $k_{KCa3.1(-PCMBS)}$

| | KCa3.1 L281W (A) n=1 | KCa3.1 L281W (B) n=1 | Units |
|---|---|---|---|
| 12 | 11 | **27** | $\mu M^{-1} s^{-1}$ |
| 21 | 76 | **34** | $s^{-1}$ |
| 23 | 12380 | **5425** | $\mu M^{-1} s^{-1}$ |
| 32 | 192 | **190** | $s^{-1}$ |
| 34 | - | - | - |
| 43 | - | - | - |
| 35 | 53 | **34** | $s^{-1}$ |
| 53 | 5 | 4 | $s^{-1}$ |
| 46 | - | - | - |
| 64 | - | - | - |
| error | 8 | 13 | |

bold face: fixed to $k_{KCa3.1(-PCMBS)}$

### 2.4.5 PCMBS slows the $k_{53}$ Transition

Previous studies on $K^+$ channels have shown that mutations along S6 perturb a concerted transition that occurs late in the activation pathway prior to opening [210]. Since our data suggests that PCMBS binds to a S6 residue ($Cys^{276}$) we determined whether the PCMBS-induced perturbation could also be traced to a late opening transition. To answer this, we analyzed activation and deactivation kinetics in the presence of 500 μM PCMBS, in terms of the scheme discussed above, and compared the rate constants with those obtained in the absence of the compound. Fig. 22 (A, dashed line) shows the fit of the model to a representative $Ca^{2+}$-jump experiment performed in the presence of PCMBS. As summarized in Table (2), initial modeling showed that PCMBS has complex effects on channel kinetics by altering multiple transitions along the activation and deactivation pathway. The largest changes occur for the $k_{32}$ (15-fold faster), $k_{35}$ (8-fold faster), and $k_{53}$ (7-fold slower) transitions, which made it difficult to interpret our results. However, due to the large parameter space in the kinetic model, it is impossible to prove that the fitted parameters are indeed the best fit. Additionally, it is impossible to know if there are different parameter sets with quantitatively similar goodness of fits. In an effort to account for this uncertainty, we started from the parameter values determined in the absence of PCMBS ($k_{-PCMBS}$), and we only allowed a few parameters to be fit at a time while holding all other values constant. In doing this, we isolated one parameter that is critical for describing the kinetic changes to the channel upon the application of PCMBS – $k_{53}$, the transition rate from the first open state back to the third closed state (Table 2). Simply modifying $k_{53}$ alone (solid line) results in a goodness of fit that is nearly identical to our first attempt (dashed line) indicating that an ~7-fold slowing of transition $k_{53}$ can account for our experimental observations (see Fig. 21 A and Table 2). After extensive parameter searches, we believe these results provide the most

parsimonious description of how PCMBS affects the channel; however, more complex interactions involving multiple rates cannot be ruled out. Our results demonstrate that PCMBS slows the first transition along the deactivation pathway, rather than altering a concerted transition late in the activation pathway.

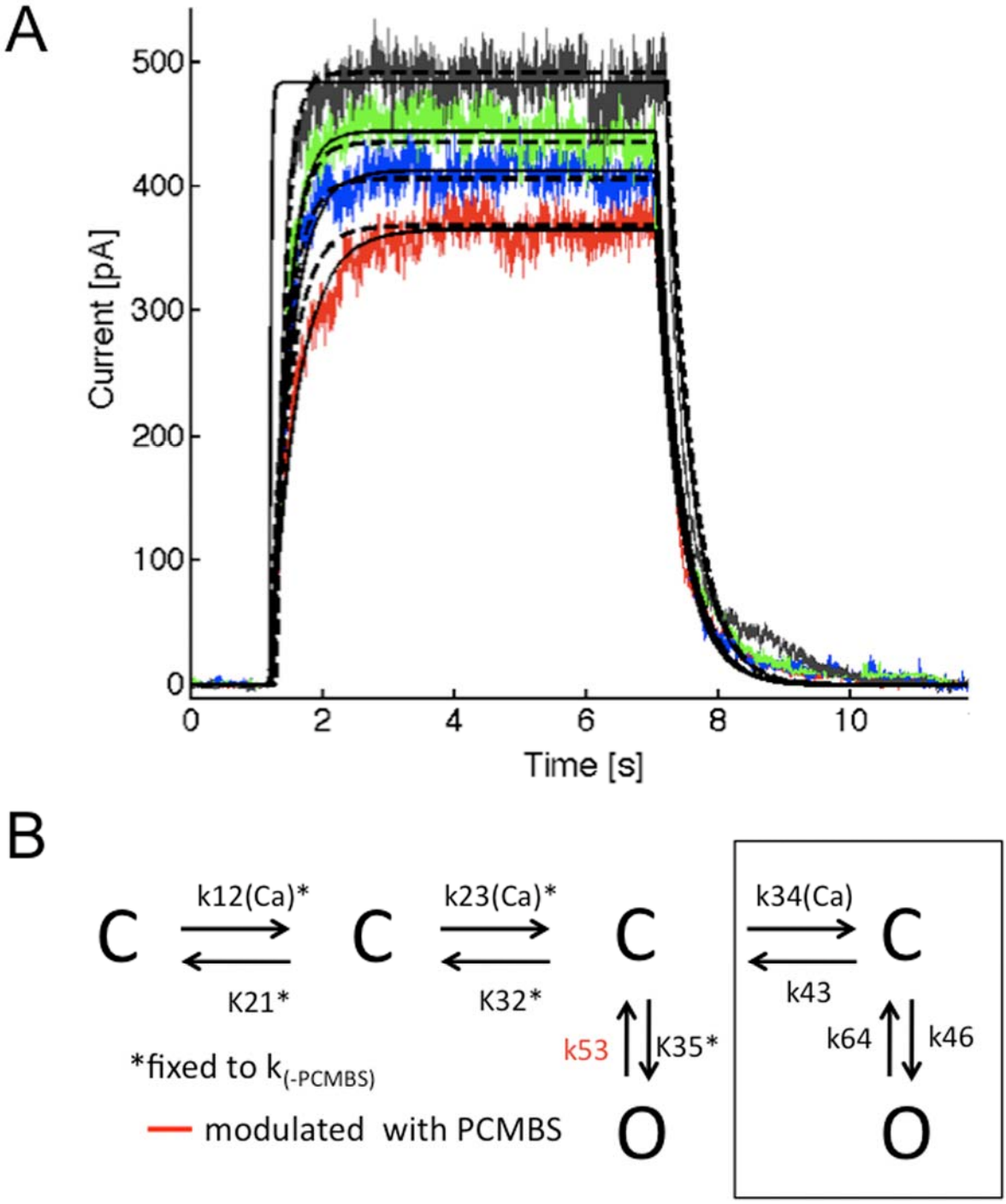
A
500
400
300
200
100
0
Current [pA]
0
2
4
6
8
10
Time [s]
B
C
k12(Ca)*
K21*
C
k23(Ca)*
K32*
C
k34(Ca)
k43
C
k53
K35*
k64
k46
O
O
*fixed to k(-PCMBS)
modulated with PCMBS

**Figure 22. PCMBS slows transition $k_{53}$, as determined through the constrained version of the model.** (A) Representative activation and deactivation records fit with two variations of the model. The dashed line represents the variation that allowed parameters $k_{12}$, $k_{21}$, $k_{23}$, $k_{32}$, $k_{35}$, and $k_{53}$ to be free, and the solid line represents the variation that held parameters $k_{12}$, $k_{21}$, $k_{23}$, $k_{32}$, and $k_{35}$ to $k_{(-PCMBS)}$ values, $k_{53}$ is the only free parameter, see results for details. As noted in the previous figure, the $Ca^{2+}$-dependent rate constants were assumed to have a non-linear dependence on $Ca^{2+}$-concentration, $k= A\cdot[Ca]/(B+[Ca])$. The colors refer to the different $Ca^{2+}$ concentrations, with red representing (0.5), blue (0.7), green (1.0), and black (10) μM $Ca^{2+}$. (B) Gating scheme detailing that parameter $k_{53}$ is modulated by PCMBS, as determined through the constrained version of the model.

### 2.4.6 L281W replicates the PCMBS phenotype

Our results suggest that $Cys^{276}$ is located within a gating sensitive region of the channel, since disrupting this site with PCMBS shifts the gating equilibrium toward the open state. Since PCMBS converts cysteine into a mercuriphenyl-sulphonate conjugate [200], we attempted to mimic the influence of PCMBS by placing a bulky tryptophan residue at position 276. However, as illustrated in Fig. 23 (A), the C276W mutation had no effect on apparent $Ca^{2+}$ affinity, $EC_{50}$ = 558±50 nM and h = 1.8±0.1 (n=7), when compared to the WT-channel $EC_{50}$ = 508±13 nM and h = 2.0±0.1 (n=57). This result demonstrates that $Trp^{276}$ does not reproduce the shift in apparent $Ca^{2+}$ affinity associated with the PCMBS-dependent channel potentiation. It should be noted that PCMBS is negatively charged at pH 7.2. However, experiments to determine whether PCMBS electrostatically disrupts channel structure could not be conducted because we were unable to record macroscopic current from the C276D mutation.

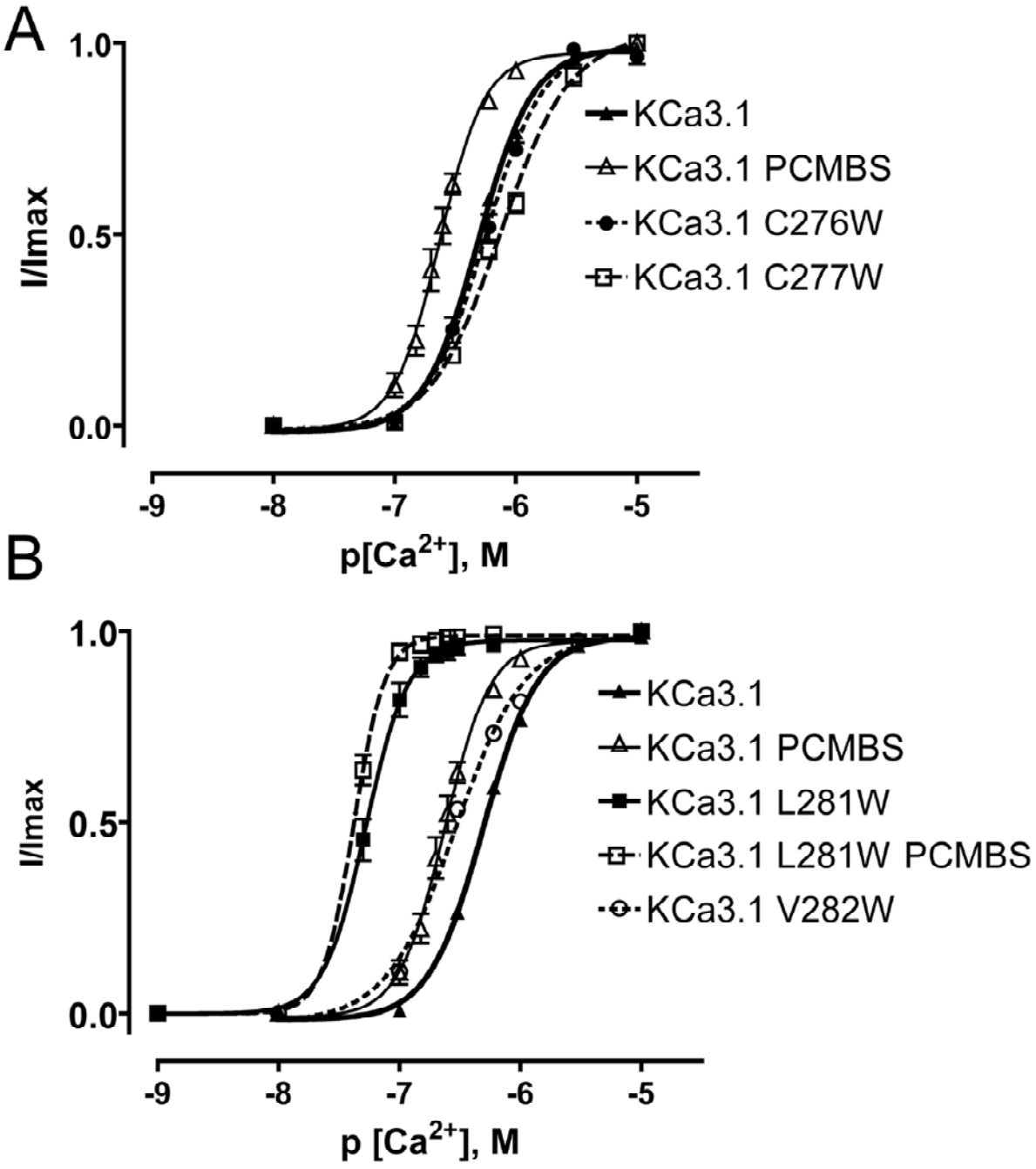
A
1.0
0.5
0.0
I/Imax
-9
-8
-7
-6
-5
p[Ca2+], M
KCa3.1
KCa3.1 PCMBS
KCa3.1 C276W
KCa3.1 C277W
B
1.0
0.5
0.0
I/Imax
-9
-8
-7
-6
-5
p [Ca2+], M
KCa3.1
KCa3.1 PCMBS
KCa3.1 L281W
KCa3.1 L281W PCMBS
KCa3.1 V282W

**Figure 23. $Trp^{281}$ and $Trp^{282}$ recapitulate the PCMBS-mediated shift in apparent $Ca^{2+}$ affinity.** Complete $Ca^{2+}$ concentration response experiments were performed to estimate $EC_{50}$ and Hill coefficients (h) for those constructs expressing macroscopic currents, as described in Fig. 14. (A) Plot of normalized <I> current against the corresponding $Ca^{2+}_i$ for KCa3.1 C276W (●) and C277W (□). KCa3.1 (▲) and KCa3.1+PCMBS (△) are included for comparison. KCa3.1 C276W (n=7) $EC_{50}$=558±50 nM and h=1.8±0.1, KCa3.1 C277W (n=6) $EC_{50}$=748±54 nM and h=1.5±0.1, KCa3.1 (n=57) $EC_{50}$=508±13 nM and h=2.0±0.2 and KCa3.1+PCMBS (n=6) $EC_{50}$=235±17 nM and h=2.5±0.2. (B) Plot of normalized <I> current against the corresponding $[Ca^{2+}]_i$ for KCa3.1 L281W (■), KCa3.1 L281W+PCMBS (□), and KCa3.1 V282W (○). KCa3.1 (▲) and KCa3.1+PCMBS (△) are included for comparison. KCa3.1 L281W (n=12) $EC_{50}$=54±6.4 nM and h=3.3±0.2, KCa3.1 L281W+PCMBS (n=3) $EC_{50}$=43±1.2 nM and h=3.6±0.5, KCa3.1 V282W (n=12) $EC_{50}$=296±14 nM and h=1.6±0.1, KCa3.1 (n=57) $EC_{50}$=508±13 nM and h=2.0±0.2, and KCa3.1+PCMBS (n=6) $EC_{50}$=235±17 nM and h=2.5±0.2. Error bars represent standard error of the mean (SEM). Error bars smaller than the symbols are not visible in the graph.

While $Trp^{276}$ does not manipulate apparent $Ca^{2+}$ affinity, PCMBS is a larger molecule, and it may exert its influence at a position distant from the $Cys^{276}$ anchoring point. To examine this possibility, we performed a partial tryptophan scan of S6, from $Gly^{274}$ to $Val^{282}$, and assessed whether these mutations recapitulated any characteristics of the PCMBS phenotype. Mutations G274W, V275W, T278W, A279W, and L280W all failed to produce macroscopic currents, thus preventing their assessment. As shown in Fig. 23 (A-B) C277W causes a right shift in apparent $Ca^{2+}$ affinity, while both L281W and V282W produced left shifts similar to PCMBS. Remarkably, $Trp^{281}$ mediates a large shift in apparent $Ca^{2+}$ affinity, an ~10-fold increase over the WT (-PCMBS) channel and an ~4-fold increase over the WT (+PCMBS) channel. To determine whether $Trp^{281}$ and $Trp^{282}$ also recapitulate the changes in kinetic behavior, $Ca^{2+}$-jump experiments were performed. As shown in Fig. 24, the $Trp^{281}$ mutation mimics the deactivation process, resulting in an ~3-fold slowing relative to the WT-channel. However, the mutation had no effect on the activation process. Furthermore, $Trp^{282}$ had no effect on channel activation or deactivation (Fig. 24 E-F). Since $Trp^{281}$ mimics the PCMBS phenotype, we wanted to assess whether the mutation prevented further modulation with PCMBS. PCMBS did not alter the apparent $Ca^{2+}$ affinity (Fig. 23 B) or activation kinetics of the $Trp^{281}$ mutation (Fig 24 E-F). However, the addition of PCMBS to the mutant channel further slowed channel deactivation by roughly 40% over the four $Ca^{2+}_i$ concentrations examined (Fig. 24 E-F), suggesting this compound can still bind $Cys^{276}$, but does not potentiate channel behavior.

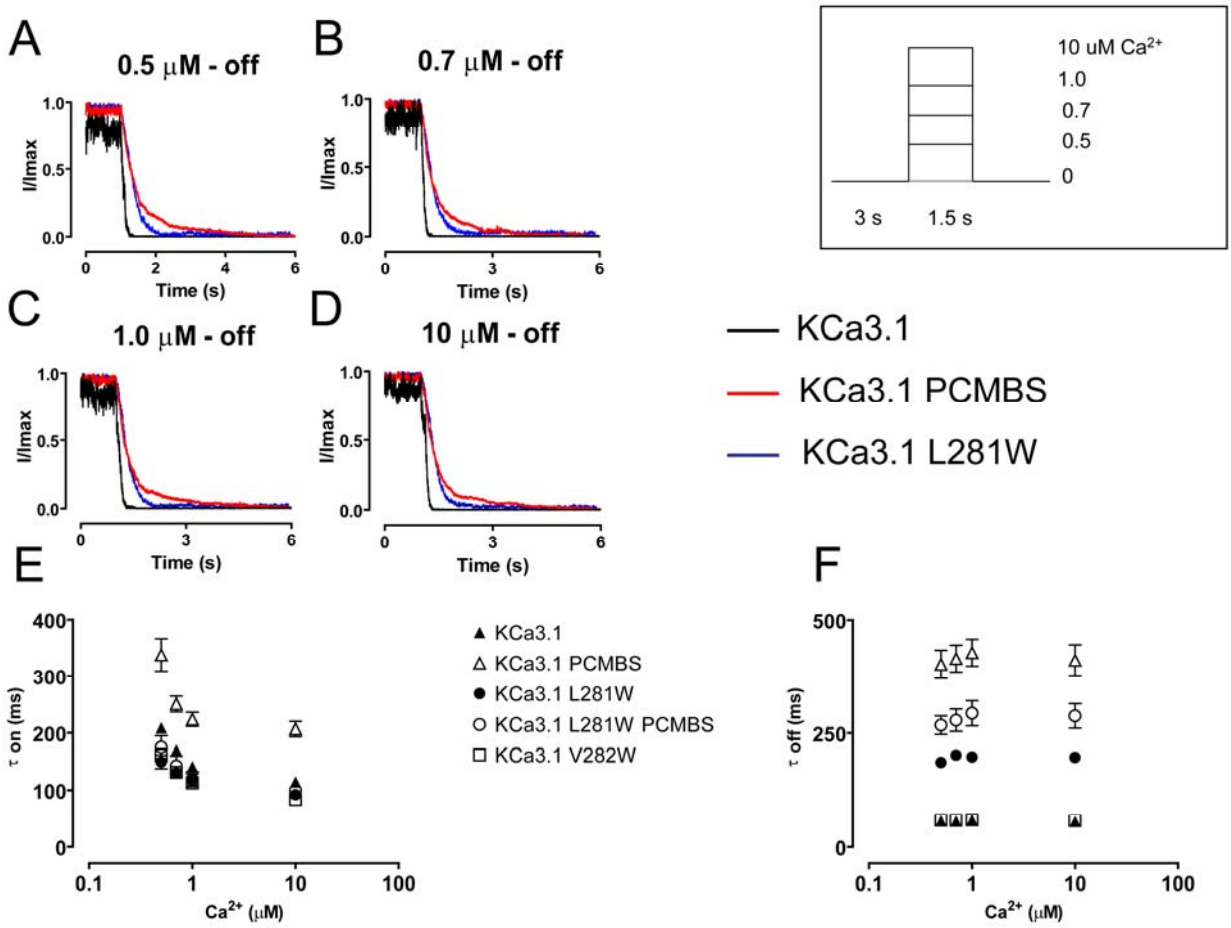


**Figure 24. Trp$^{281}$ recapitulates the PCMBS-mediated modulation in deactivation kinetics.** Activation and deactivation kinetics were estimated with $Ca^{2+}$-jump experiments as described in Fig. (4) using $Ca^{2+}_i$ concentrations 0.5, (A) 0.7, (B) 1.0, (C) and 10 μM (D) for L281W (blue trace) and KCa3.1 in the absence (black trace) and presence (red trace) of PCMBS were included for comparison. Activation (E) and deactivation (F) rates were estimated by fitting activation and deactivation records with an exponential function and reported as a time constant (τ-on and τ-off) for KCa3.1 (▲), KCa3.1 PCMBS (△), L281W (●), L281W PCMBS (○), and V282W (□), see also Table (1).

We also assessed whether the 4-state model can accurately describe L281W activation and deactivation records from the $Ca^{2+}$-jump experiments. As illustrated in Fig. 25 (A), the 4-state model accurately describes the 4-sets of activation and deactivation time courses. Fig. 25 (B) provides an enhanced depiction of the fit outlined by the dashed box in Fig. 25 (A). The rate constants derived from the fit are presented in Table 2. As shown in the table, the values for $k_{12}$, $k_{21}$, and $k_{53}$ are very similar to those values obtained from the initial analysis of KCa3.1+PCMBS. This surprising result suggests that L281W has many kinetic characteristics in common with the PCMBS modulated channel. Therefore, we asked whether the phenotype displayed by this construct could be explained by only modifying transition $k_{53}$. As shown in Table 2, the parameters from the KCa3.1 model ($k_{KCa3.1\text{-}PCMBS}$) were adequate to describe L281W activation and deactivation time courses. This result indicates that slowing of the deactivation process can be explained by slowing of transition $k_{53}$ for both the PCMBS modulated channel and the L281W construct. As discussed with PCMBS, we cannot rule out that the phenotype present in L281W is the result of complex interactions involving multiple rates. However, it is interesting that parameters from the KCa3.1 data can reproduce the fits for both PCMBS and the L281W $Ca^{2+}$-jump experiments. In total, these results indicate that sterically disrupting $Cys^{276}$ is not adequate to recapitulate the PCMBS phenotype. The results from the tryptophan scan suggest that $Leu^{281}$and $Val^{282}$ are located within a mechanically sensitive region of the channel. More importantly, L281W disrupts steady-state and kinetic behavior in a manner that is similar to PCMBS, suggesting that L281W and PCMBS may disrupt gating through a common mechanism.

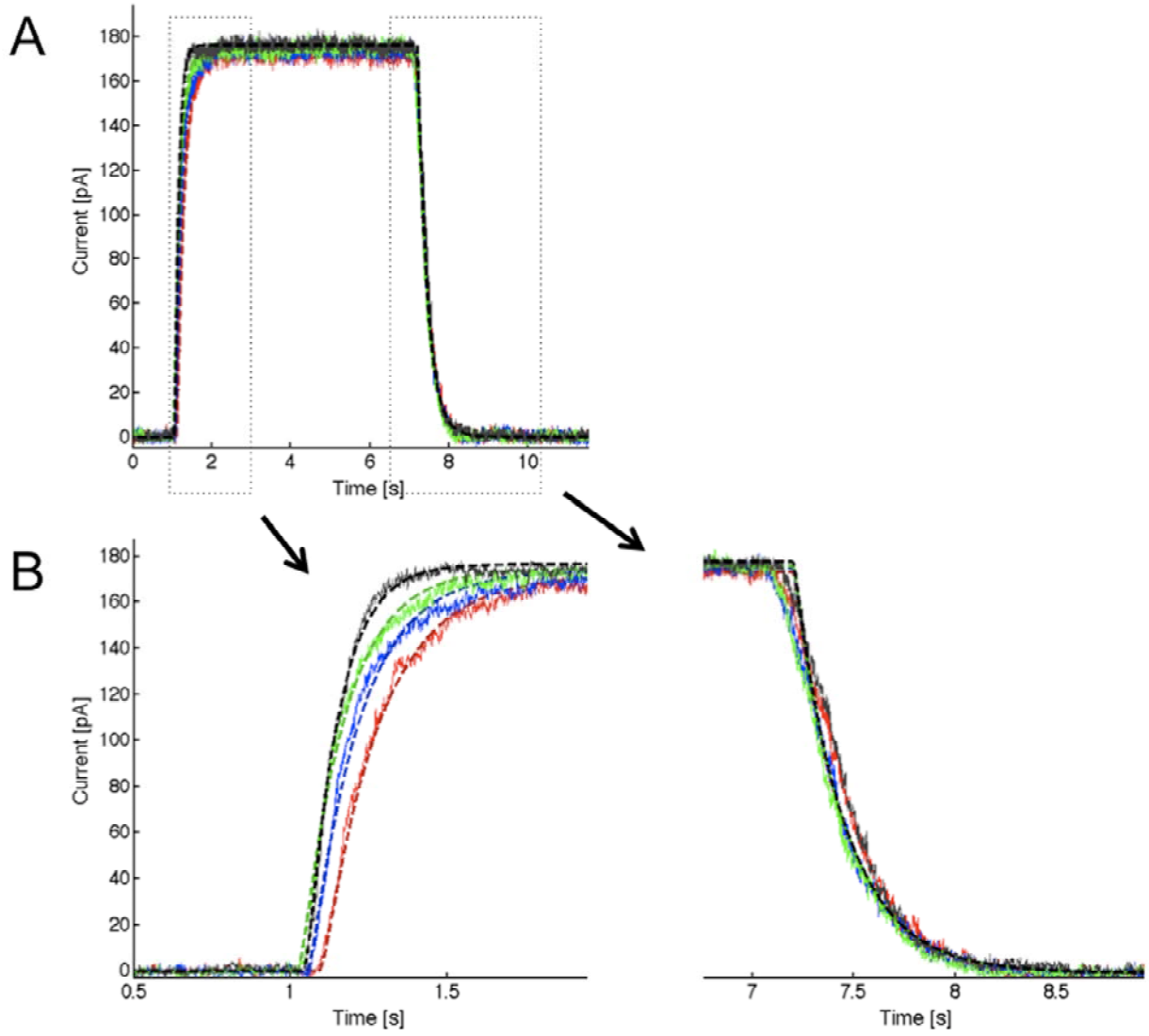


**Figure 25. A 4-state model can be used to fit the activation and deactivation kinetics for KCa3.1 L281W.** Representative activation and deactivation records fit with the model shown in Fig. 21 (A). Activation and deactivation currents were recorded and fit following the protocol described in the methods sections. The colors refer to the different $Ca^{2+}$ concentrations, with red representing (0.5), blue (0.7), green (1.0), and black (10 μM) $Ca^{2+}$. The dashed line represents the fit assuming $Ca^{2+}$-dependent rate constants have a non-linear dependence on $Ca^{2+}$-concentration, k= A·[Ca]/(B+[Ca]). Rate constants derived from the fit are summarized in Table (2). (B) Enhanced depiction of the fit outlined by the box in part (A).

## 2.5 DISCUSSION

Ligand-gated ion channels undergo a series of conformational changes in response to ligand binding, enabling the pore to transition from a non-conducting to a conducting configuration [5]. A chemo-mechanical gating model has been proposed to explain the $Ca^{2+}$-dependent gating mechanism of $K_{Ca}$ channels [192, 193]. This model states that the binding of $Ca^{2+}_i$ to CaM initiates a cascade of conformational changes within CaM/CaMBD. These conformational changes are then coupled, via the S6 transmembrane helix, to the pore enabling the channel to gate [188, 189, 192, 193]. Here we showed that PCMBS potentiates channel activation by manipulating steady-state and kinetic behavior through modification of $Cys^{276}$. A tryptophan scan of S6 revealed that L281W mimics modification by PCMBS suggesting that both may act through a common mechanism. Perturbations at each of these sites disrupt channel closing, supporting the notion that the non-luminal surface of this portion of S6 is allosterically coupled to the activation gate. Therefore, the $Ca^{2+}$-dependent activation mechanism utilizes the non-luminal surface along S6 to transition into the closed conformation.

### 2.5.1 Differences in Chemistries of the Compounds may explain discrepancy regarding the effect on the WT-Channel

It is interesting that MTSET fails to modulate WT-channel gating [111, 113], despite our results showing that PCMBS can modulate gating. There are several possible explanations for this difference, but the simplest is related to the chemical difference between PCMBS and MTSET. This conclusion is consistent with previous investigations showing that PCMBS, with a peripherally located cysteine reactive moiety, could access cysteines not accessible to MTSET's

more centrally located moiety [199-201]. Additionally, the larger size of PCMBS conjugated to cysteine was more likely to irreversibly modify behavior rather than transiently effect behavior as observed using MTSET [199-201]. Thus, the unique chemistry of PCMBS enables this compound to potentiate the WT-channel by modifying $Cys^{276}$.

Since $Cys^{276}$ is located within a region of the channel (V275-V282) inhibited by MTSET, why does PCMBS not inhibit the channel? The discrepancy in modulation can be explained by the orientation of $Cys^{276}$ relative to the lumen of the pore. $Val^{275}$ is known to line the pore from studies localizing the binding site of clotrimazole and arachidonic acid [211, 212]. Results from a SCAM analysis confirmed the orientation of this residue, and indicated a similar orientation for $Thr^{278}$ and $Val^{282}$ [113]. These results are in agreement with sequence alignments (Table A.1) that indicate $Val^{275}$, $Thr^{278}$, and $Val^{282}$ correspond to residues that are known to line the pore in KcsA [67, 213], and Shaker [214]. The luminal location of $Val^{275}$, $Thr^{278}$, and $Val^{282}$ indirectly argues for $Cys^{276}$ and $Leu^{281}$ to be oriented away from the pore. Thus, the non-luminal orientation of $Cys^{276}$ prevents PCMBS from modification induced channel block.

### 2.5.2 PCMBS potentiates Channel activation by shifting the Gating Equilibrium toward the Open Conformation

PCMBS cannot activate the channel in the absence of $Ca^{2+}_i$, (Fig. 12 D) suggesting the compound potentiates activation, rather than directly opening the gate. $Cys^{276}$ is only accessible in the open conformation (Fig. 12 D), suggesting that the closed conformation either blocks PCMBS from accessing $Cys^{276}$, or the orientation of $Cys^{276}$ may be inaccessible. A previous investigation indicated that once in the closed state, a constriction develops at the level of $Thr^{278}$-$Ala^{282}$ [111]. It is possible that this constriction blocks PCMBS from gaining access to $Cys^{276}$.

PCMBS influences both steady-state and kinetic behavior of the channel. The changes to the steady-state behavior occur in sub-saturating $Ca^{2+}_i$ as well as saturating $Ca^{2+}_i$ concentrations. These changes could occur independently through two separate pathways: a $Ca^{2+}$-dependent pathway that shifts the apparent $Ca^{2+}$ affinity and $Ca^{2+}$-independent pathway that increases $P_{o(max)}$. Thus, the shift in apparent affinity can be explained by either a change in the initial binding of $Ca^{2+}$ to CaM or modification of a conformational change subsequent to $Ca^{2+}$ binding. However, we observed that PCMBS increases $P_{o(max)}$, suggesting that modulation along the $Ca^{2+}$-dependent pathway cannot simply be explained by stabilizing the $Ca^{2+}$/CaM interaction. Rather, it suggests that PCMBS functions to shift the gating equilibrium toward the open conformation. Shifting the gating equilibrium toward the open conformation would explain both the increase in $P_{o(max)}$ and through a mass action effect the shift in apparent affinity. Therefore, the changes in steady-state behavior cannot occur through two independent pathways, but are related and a consequence of shifting the equilibrium toward the open conformation. These results are similar to a previous investigation, which characterized potentiation by $Ni^{2+}$ on cyclic nucleotide-activated channels (CNG) from rod photoreceptors [215].

We know from the change in steady-state behavior that PCMBS alters the energy difference between the closed and open conformations to favor channel opening. What we cannot infer from these experiments is whether the energetics of activation, deactivation, or a combination of the two are altered. Based on channel kinetics, PCMBS slows both channel activation and deactivation (Table 1). Although the slowing of channel activation is not congruent with our steady-state data, slowing of channel deactivation is the predominant effect and corresponds well with our steady-state results. Therefore, the primary manner in which

PCMBS shifts the gating equilibrium toward the open conformation is by disrupting the energetics of channel deactivation.

We demonstrated that a 4-state gating scheme describes the activation and deactivation records of KCa3.1. However, the rates describing the $Ca^{2+}$-dependent transitions must have a nonlinear rather than a linear dependence to fit the activation record in saturating $Ca^{2+}_i$. This need for nonlinear coefficients is not an artifact of the experimental system, since we were able to describe the full range of kinetic behavior for the closely related channel, KCa2.3 (unpublished data). The discrepancy may be related to channel behavior in saturating $Ca^{2+}_i$, as elevated $Ca^{2+}_i$ has been reported to block the channel [216].

As illustrated in Table (2), $k_{23}$ is substantially higher than the other rate constants, particularly $k_{12}$. Since the analysis from Hirschberg et al., reported $k_{12} \approx k_{23}$ we tested the model where $k_{12} = k_{23}$ to ensure that our results were not biased by $k_{23}$. However, forcing $k_{12} = k_{23}$ results in the model predicting faster activation time courses compared to the rates observed experimentally (unpublished data). Therefore, this analysis suggests $k_{23}$ must be higher than the other rates constants to accurately describe the activation time courses from the 4 sets of $Ca^{2+}$ concentrations. The discrepancy may exist because we simultaneously fit activation and deactivation records from 4 sets of $Ca^{2+}$ concentrations, where as the other investigation fit a single concentration.

### 2.5.3 Modeling the $Ca^{2+}$-dependent Gating of KCa3.1

The results from the initial kinetic analysis showed that good fits to the data can be obtained by modulating all transitions rates in the presence of PCMBS. However, more careful reanalysis revealed that only one rate constant, $k_{53}$, had to be changed to explain the influence of PCMBS

(Table 2). Reducing $k_{53}$ ~7-fold gives excellent fits to the activation and deactivation records, and further substantiates that PCMBS shifts the gating equilibrium toward the open conformation by disrupting channel closing. Assuming $k_{53}$ is the only transition effected by PCMBS may be an over simplification. As depicted in Table (2), PCMBS affects both channel activation and deactivation. Therefore, to address this question we reanalyzed the data allowing transitions $k_{12}$, $k_{23}$, and $k_{53}$ to change. Our subsequent analysis showed a slowing of the rate constants $k_{12}$ and $k_{23}$, which correlates well with the observed slowing of channel activation (Table 2). However, there was no improvement in the fit when compared to the $k_{53}$ model (Table 2). Therefore, the modest effect of PCMBS on channel activation does not require a substantial change in $k_{12}$ or $k_{23}$. The predominant effect on kinetic behavior is completely accounted for by the change in transition $k_{53}$, which accurately describes the slowing in channel deactivation.

In contrast to the WT-channel, the L281W mutation affects channel deactivation without affecting channel activation. Therefore, this made for an ideal model to confirm whether the change in the deactivation process can be completely explained by the change in transition $k_{53}$. The initial kinetic analysis showed that the change in channel deactivation can be explained by an ~4-fold slowing of transition $k_{53}$, which corresponds well with the observed change in $\tau$-off (Table 1). As predicted, we were able to reproduce the fit from the initial kinetic analysis by modifying only transition $k_{53}$ (Table 2). This result argues that the slowing of channel deactivation observed with PCMBS and L281W can be explained by slowing of transition $k_{53}$. The results from the kinetic analysis correspond well with the observed phenotype for both the PCMBS modulated channel and the L281W mutation. This correspondence would suggest that PCMBS and the L281W mutation disrupt channel behavior through a common mechanism, which will be discussed further in the following section. Although our data are consistent with

PCMBS and L281W stabilizing the open conformation, based upon our analysis of macroscopic currents we cannot eliminate the possibility that the observed effects are the result of destabilizing the closed conformation [210]. Therefore, a physical interpretation of the manipulation by PCMBS and L281W are that both perturbations disrupt channel closing, suggesting that $Cys^{276}$ and $Leu^{281}$ are located in a region of S6 that is allosterically coupled to the activation gate.

### 2.5.4 Potential Mechanism of PCMBS

Our results are consistent with PCMBS binding to $Cys^{276}$; however, we cannot recreate this effect by sterically perturbing position 276 with a tryptophan substitution. Furthermore, mutation to $Gly^{276}$, $Phe^{276}$, $Tyr^{276}$, and the aforementioned $Ala^{276}$ and $Asp^{276}$ (no expression) also failed to alter the apparent $Ca^{2+}$ affinity (unpublished data). Although many scenarios may account for this result, the simplest explanation is that $Cys^{276}$ is not coupled to the activation gate. Furthermore, mutation of the adjacent amino acid, C277W had only modest effects on apparent $Ca^{2+}$ affinity, also suggesting that $Cys^{277}$ is not coupled to the activation gate. These results are in agreement with a previous investigation, which predicted that the channel cavity extends from $Val^{272}$ to $Thr^{278}$ [111, 113]. Modeling of the open (computer derived structure) and closed state using the KcsA structure, indicates that the major conformational change occurs along S6 between $Thr^{278}$ and $Val^{282}$ [113]. Gating sensitive residues are found in regions of the channel where amino acid packing rearranges as the channel transitions from one conformational state to another [210]. Therefore, interpreting our results in the context of previous investigations suggest that mutations at $Cys^{276}$ and $Cys^{277}$ do not modulate gating because this region is predicted to

undergo little movement, whereas $Leu^{281}$ and $Val^{282}$ are thought to modulate gating because these positions are predicted to undergo major conformational change [113].

Mutating $Leu^{281}$ or $Val^{282}$ to tryptophan shifts the gating equilibrium toward the open state, demonstrating this region rearranges as the channel transitions between conformational states. More importantly, the $Trp^{281}$ mutation has the additional effect of slowing the deactivation process. The similarity between modification by PCMBS and L281W supports the notion that these two perturbations are disrupting the channel through a common mechanism. Thus, PCMBS and L281W may function to shift the gating equilibrium toward the open conformation by either stabilizing the open state or destabilizing the closed state [210]. Our data cannot eliminate either of these possibilities. Therefore, we propose two hypotheses to describe how PCMBS and the L281W mutation disrupt the gating of KCa3.1. To attempt to visualize rearrangements that occur in this region during gating, we constructed a closed state model of KCa3.1 based on the KcsA x-ray structure and an open state model based on Kv1.2 (Fig. 26). The open state model predicts that $Leu^{281}$ is oriented toward S5 (inset Fig. 26). Our kinetic modeling predicts that PCMBS and L281W slow transition $k_{53}$. Therefore, our first hypothesis is that these perturbations hinder the possible rotational movement of S6 that was shown to accompany the closed to open transition in the KcsA $K^+$ channel [217]. The increase in side-chain volume with the L281W mutation could sterically hinder the rotation of S6 by disrupting a potential S5-S6 interaction. Additionally, Ackerman et al., characterized the binding mechanism of PCMBS to Charcot-Leyden crystal protein, and determined that PCMBS binds to $Cys^{57}$, but results in downstream perturbation at the $Arg^{60}$ side-chain [218]. Therefore, PCMBS may interact with neighboring residues in the open state to disrupt the conformational change in S6. This model supports our data well because these interactions could energetically stabilize the open conformation.

However, we cannot rule out the possibility that PCMBS and L281W shift the gating equilibrium toward the open conformation by destabilizing the closed conformation of the channel. Along these lines, the open and closed state models of KCa3.1 predict that $Cys^{276}$ and $Leu^{281}$ sterically clash in the closed state but not in the open state. Therefore, an alternate hypothesis is that when PCMBS is conjugated to $Cys^{276}$ it disrupts the closing transition by sterically clashing with $Leu^{281}$. The L281W mutation would work through a similar mechanism, except this mutation would disrupt the closing transition by sterically clashing with $Cys^{276}$. Although there is an agreement between the length of PCMBS and the distance between the β-carbons of the corresponding residues from KcsA and KirBac1.1 (Fig. 26), the steric clash predicted by this model could lead to an energetic destabilization of the closed state. This conclusion is inconsistent with our kinetic modeling. Furthermore, the KcsA structure cannot account for the closed conformation of KCa3.1, as the region in KCa3.1, corresponding to the bundle crossing in KcsA, does not function as an activation gate [110, 111]. Thus, while this is an interesting model that predicts an intersubunit interaction, it is an unlikely representation for the molecular function of PCMBS.

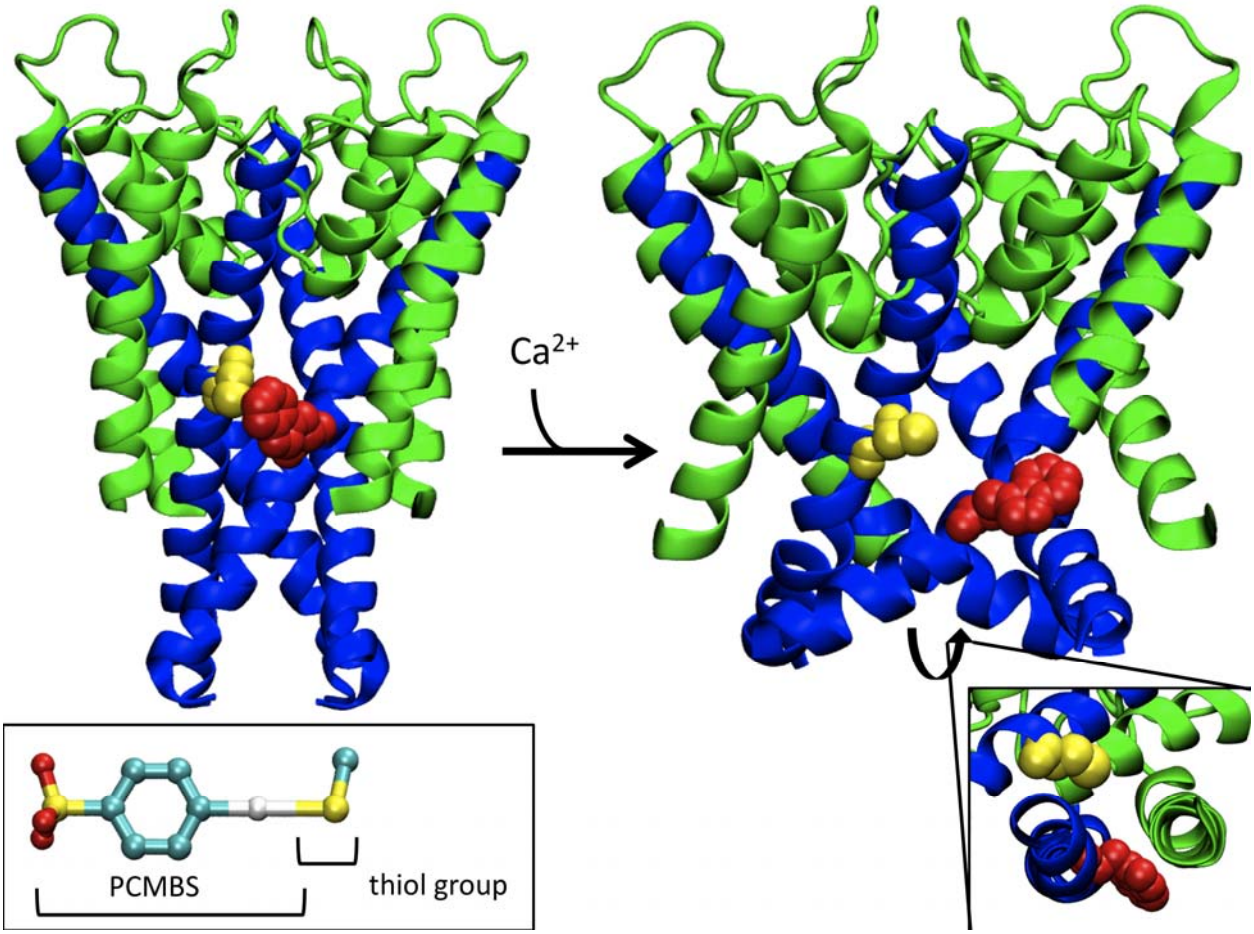


**Figure 26. Homology model of the pore region for the open and closed state of KCa3.1.** (left panel) Representation of the S5- P-helix -S6 region viewed as a profile illustrating the predicted orientation of $Cys^{276}$ (yellow), and the L281W mutation (red) in the closed state using the KcsA structure. (Inset) Structure of PCMBS adapted from the crystal structure of PCMBS in complex with the Charcot-Leyden crystal protein (Ackermen et al., 2002). PCMBS is 6.5 Å in length and 9.0 Å in length when the thiol group is included. The color red represents oxygen molecules, yellow (sulfur), cyan (carbon), and white (mercury). (right panel) Representation of the S5- P-helix -S6 region viewed as a profile illustrating the predicted orientation of $Cys^{276}$ (yellow), and the L281W mutation (red) in the open state based upon the structure of rKv1.2. Sequence alignments used for homology modeling can be found in Fig. 5 (C). (Inset) Representation of S5 and S6 viewed from the intercellular aspect of the pore to illustrate that $Leu^{281}$ (L281W) is oriented toward S5. $Cys^{276}$ and L281W from the adjacent subunit are the only residues illustrated to compare the predicted orientation in the closed and open state. The S5 and P-helix are colored green and the S6 helix is colored blue. All residues are illustrated in VDW format. The C-terminal portion of the S5 helix was removed to prevent obscuring the view of L281W.

## 2.6 ACKNOWLEDGEMENTS

We thank Dr. Peter Drain for many stimulating discussions and Dr. Gordon MacGregor for the initial help with variance analysis.

This work was supported by National Institute of Health grants HL083060 and HL092157 to D.C.D., and by a grant to M.G. from the Myrtle Forsha Memorial Trust and the Lloyd Foundation through the PNC Charitable Trust Grant Review Committee.

# 3.0 DISCUSSION AND FUTURE DIRECTIONS

One of the most fundamental questions in the field of ion channel biophysics concerns the conformational changes that are required to transition from the closed to the open conformation. In answering this question, it is convenient to think of ligand-gated ion channels, in this case KCa3.1, as having three separate domains: 1) the pore-forming domain, 2) the ligand-binding domain, and 3) the coupling domain. The pore domain, as introduced previously, contains the ion permeation pathway, the selectivity filter, and the activation gate. The ligand-binding domain contains the ligand binding sites; the coupling domain is the machinery that links the ligand-binding domain to the activation gate. The coupling domain is critical for the functioning of the channel as it enables the chemical energy of $Ca^{2+}$ binding to be transduced into a mechanical force to open the pore. Although much progress has been made toward understanding how channels gate, large gaps still exist in our knowledge. Specifically, these gaps are related to the coupling mechanism and the regions of the channel that actively participate in this process. During the past 12 years, ion channel crystal structures have provided direct structural evidence for the regions associated with the gating mechanism. These atomic structures have provided great insight into the mechanism of the pore-forming and ligand-binding domains. For example, the crystal structures of CaM/CaMBD and apoCaM/CaMBD of KCa2.2 have provided a potential mechanism for $Ca^{2+}$ binding and the subsequent conformational changes occurring in the CaMBD [192, 193]. However, little progress has been made toward understanding what

movements are critical in the coupling of $Ca^{2+}$ binding to gate opening. The difficulty lies in the fact that the coupling mechanism might not rely on a direct physical linkage between domains. As discussed previously, the linkage may be indirect making it difficult to resolve the mechanism by simply examining static structures. Although results from site-directed mutagenesis can at times be difficult to interpret, it is a powerful tool for locating gating sensitive residues. The sensitivity of gating to mutations provides valuable information about the energetics and mechanism of pore opening. Transitioning between different conformational states causes amino acids to pack differently. If the conformation of a particular amino acid is critical for the pore to transition from one conformational state to another, altering that amino acid through site-directed mutagenesis will change the energetics of channel gating. Therefore, characterizing how mutations alter gating energetics is a valuable method to gain insight into the gating mechanism.

The significance of S6 in the gating mechanism is demonstrated from observations that mutations along the pore affect a late concerted non-voltage-dependent opening step in Kv channels [210]. This is not surprising since S6 forms part of the pore, and it is widely accepted that this transmembrane domain contributes significantly to the activation process in all $K^+$ channels. The contribution of S6 to the gating of KCa3.1 has been investigated using SCAM [113]. In this series of investigations, it was concluded that the C-terminal region of S6 participates in the activation mechanism. Furthermore, based upon the state-dependent modification of positions $Val^{284}$ and $Val^{285}$, it is predicted that the $Ala^{283}$-$Ala^{286}$ region undergoes significant conformational change [111, 113]. However, the hydrophilic MTS reagents (MTSET and MTSEA) used in their investigation cannot access residues orientated opposite to the lumen. Therefore, this approach could not assess whether the non-luminal residues are involved in the

gating mechanism. Since this region of the channel is predicted to participate in the activation mechanism, it would be informative to determine whether the non-luminal residues are also incorporated into this process. The goal of this dissertation was to investigate the role of S6 in the activation mechanism of KCa3.1, particularly whether the non-luminal residues in the C-terminal portion of S6 are required for the closed to open transition.

KCa3.1 contains nine endogenous cysteines residues, and four of these residues are located in S6. Three out of the four residues are predicted to have a non-luminal orientation ($Cys^{269}$, $Cys^{276}$ and $Cys^{277}$), based on homology modeling with KcsA and Kv1.2. The arrangement of these cysteines served as a convenient tool to assess whether the non-luminal face of S6 participates in the activation mechanism. The mercurial based sulfhydryl reagent PCMBS has been shown in previous investigations to have the ability to access residues not accessible using any of the various MTS reagents [199-201]. Utilizing this compound, we made the observation that PCMBS irreversibly increases current when added to the intracellular side of an excised membrane patch expressing KCa3.1 (Fig. 12). We proposed that PCMBS increases channel activation through modification of an endogenous cysteine residue(s) in S6. Therefore, characterizing the mechanism of PCMBS activation enabled us to test the hypothesis that the non-luminal residues in the C-terminal portion of S6 are important in the activation mechanism of KCa3.1.

## 3.1 MERCURIAL BASED SULFHYDRYL REAGENTS AS PROBES FOR NON-LUMINAL CYSTEINE RESIDUES

As discussed previously, PCMBS binds to $Cys^{276}$ thereby influencing both the steady-state and the kinetic behavior of the channel (Figs. 20, 12, 14-15). The difference in accessibility between PCMBS and MTSET or MTSEA is most likely due to the difference in the location of the cysteine reactive moiety, and/or the probability that the PCMBS/cysteine conjugate is more likely to disrupt the local environment. However, an investigation examining the helix packing of EmrE suggests mercurial based compounds may be better probes for cysteines predicted to be located in low dielectric environments. EmrE is a small multidrug transporter in *Escherichia coli*, and cysteines substituted in the transmembrane domains were only accessible to organic mercurials and not sulfhydryl reagents such as maleimides and methanethiosulfonates [219]. Additionally, we observed that thimerosal, a mercurial based sulfhydryl reagent, added to the intracellular side of the membrane resulted in a left-shift in apparent $Ca^{2+}$ affinity (Fig. A.1A and A.1B); like PCMBS, thimerosal-sensitivity was traced to modification of $Cys^{276}$ (Fig. A.2). Therefore our results using PCMBS and thimerosal, would also indicate that mercurial compounds can access cysteines predicted to be in low dielectric environments. However, none of the endogenous cysteines in KCa3.1 were accessible with Et-$Hg^{+}$ [111], suggesting the effect on the WT-channel is not related to the presence of mercury, but the unique size and chemistry of PCMBS and thimerosal. MTS reagents do not affect gating of the closely related channel KCa2.3 [197, 198], suggesting these compounds cannot bind to the endogenous cysteine(s). KCa2.3 has two endogenous cysteine residues in S6, $Cys^{525}$ and $Cys^{535}$, which are equivalent to $Cys^{267}$ and $Cys^{277}$ in KCa3.1. Therefore, I wanted to ask whether PCMBS could access and modify the endogenous cysteines in KCa2.3 as a way to determine whether mercurial

compounds are better at accessing cysteines in low dielectric environments. However, unlike KCa3.1, the addition of PCMBS to KCa2.3 had no effect on steady-state behavior (Fig. A.3A). KCa2.3 has a glycine ($Gly^{534}$) at the position corresponding to $Cys^{276}$ in KCa3.1. Therefore, we tested whether the mutation G534C could confer PCMBS sensitivity to KCa2.3. As we observed in the WT-channel, the addition of PCMBS did not affect steady-state behavior of the channel (A.3B). The inability of PCMBS to modify G534C can be explained by the inability of PCMBS to access G534C, or the mutation could mimic the phenotype from KCa3.1, masking any potential effect by the compound. As illustrated in Figs. (A.5A and A.5D) and (A.7A and A.7D), the mutation G534C influenced channel behavior in a manner similar to the effect of PCMBS on KCa3.1. That is, the mutation causes a left-shift in apparent $Ca^{2+}$ affinity and a slight slowing in the deactivation process (see Table A.3 and A.5). Therefore, PCMBS may be able to access G534C, but the mutation affects channel gating; masking any potential effect the compound may have on the channel. In total, the results from experiments with thimerosal and PCMBS interpreted in context with the EmrE investigation argue for mercurial based compounds as better probes for cysteines in low dielectric environments. The discrepancy with the Et-$Hg^{+}$ result may be due to the inability of this compound to act as a perturbing molecule rather than an accessibility problem. Et-$Hg^{+}$ is smaller than MTSEA, with dimensions closer to the size of a dehydrated $K^{+}$ ion [111]. Therefore, Et-$Hg^{+}$ may access the endogenous cysteine(s) in S6, but because of the compound's small size, it cannot disrupt channel gating.

## 3.2 S6 IS A DYNAMIC COMPONENT OF THE GATING MECHANISM

The idea that S6 is critical for the gating mechanism is intrinsic to the chemomechanical gating model proposed for the activation of KCa3.1. In this model, the chemical energy of $Ca^{2+}$-binding is transformed into a mechanical force enabling the channel to transition into the open state. S6, due to its relative location between the CaM/CaMBD and the pore, is a logical choice to couple the conformational change occurring in the CaMBD to the pore. Thus, S6, in addition to forming part of the pore, is also a dynamic component in the gating machinery. Considering this, it was no surprise that perturbation to this region modulated the gating of KCa3.1. However, it was interesting to note that while only a small number of the mutations from the tryptophan scan resulted in functional channels, the ones that did tended to shift the gating equilibrium toward the open conformation (see Table A.2). Furthermore, the addition of PCMBS and the V275A mutation also shifted the gating equilibrium toward the open conformation (see Table 1 and A.2). It is difficult to draw any generalizations about the nature of perturbations to S6 from such a small sample size, but these results are consistent with a previous investigation on the Kv channel [210]. Yifrach et al., made the observation that the majority of mutations along S6 shifted the gating equilibrium toward the open conformation. This can occur in one of two ways: the mutations can stabilize the open or destabilize the closed conformation. Based solely upon theoretical reasoning, they proposed that the mutations destabilize the closed conformation for the following reasons. 1) Mutations are more likely to disrupt protein structure then to stabilize it. 2) The closed state is more stable compared to the open state due to a higher number of favorable protein interactions. Since there are more ways to disrupt an optimally packed protein, they suspect that the closed state is more susceptible to perturbations. Although we cannot determine if the shift in gating equilibrium is the result of stabilizing the open conformation or

destabilizing the closed conformation, interpreting our data in context with the Yifrach et al., investigation may provide insight into the nature of S6 in KCa3.1. By drawing an analogy to this investigation, we can infer that perturbation to S6 causes the gating equilibrium to shift toward the open conformation because the closed conformation of KCa3.1 is intrinsically more stable, thus the lowest energy state of the protein. Therefore, any perturbation to this region will destabilize the structure causing the gating equilibrium to shift toward the open conformation.

Does this line of reasoning follow for S6 in all ion channels? Not all perturbations to S6 shift the gating equilibrium toward the open conformation. There are many examples where mutations along this domain shift the gating equilibrium toward the closed state. For example, in KCa2.3 mutations along S6 tended to shift the gating equilibrium in both directions (see Table A.3). Following the line of reasoning discussed above, the tendency for perturbation to shift the gating equilibrium in both directions could be explained because the closed conformation of S6 is not the most stable conformation, and therefore not the lowest energy conformation. Therefore, mutations in S6 may destabilize the closed conformation, pushing the gating equilibrium toward the open conformation; mutations may also stabilize the closed conformation, pushing the gating equilibrium toward the closed state. How mutations in S6 disrupt the energetics of gating suggests a functional difference in this transmembrane domain that is at odds with the sequence similarity between these channels. Although this discrepancy may be explained by the four amino acid difference in S6 (Table A.1), it suggests that the coupling between CaM and the activation gate may account for the mutational phenotype. If the coupling pathway is different between these channels, it can be expected that mutations in S6 will have a different effect on the energetics of channel gating. As discussed below, functional

differences between these channels can be used as a tool to isolate the regions of the channel responsible for this behavior.

## 3.3 KCa3.1 VERSUS KCa2.3

KCa3.1 and KCa2.3 have a high degree of homology along the CaM/CaMBD, which is reflected by their apparent $Ca^{2+}$ affinities being similar (Table A.2 and A.3). However, the activation rate for KCa2.3 is about 10-fold faster compared to KCa3.1 (Table A.4 and A.5). Additionally, the $P_{o(max)}$ values derived from variance analysis are 0.6 and 0.9 for KCa3.1 and KCa2.3, respectively (Fig. 13 and A.8). Since the apparent $Ca^{2+}$ affinities are equivalent, the differences between $P_{o(max)}$ and the activation rates are quite interesting. The most logical explanation would be the differences in the gating machinery: S5, S6, and the CaMBD. However, S6 and the CaMBD, are highly homologous (Table A.1), which would argue for the discrepancy in behavior possibly originating from S5. A chimeric approach would be effective for determining whether S5 or specific regions of S5 are responsible for the difference in behavior. However, KCa2.2 with the S5 from KCa3.1 does not express (Devor lab unpublished data). Therefore, a less invasive approach where only a few amino acids are swapped between channels at a time to avoid non-functional channels will be necessary. Furthermore, determining whether the chimeric channel adopts the behavior of the donor channel based on effects on binding or conformation change would be critical for understanding the coupling mechanism. However, one of the most fundamental problems in ligand-gated ion channels is making the distinction between effects on binding and effects on conformational change. Robert Stephenson first noted that the action of an agonist could not be described by just an affinity constant; there must be another quantity he

termed efficacy that describes the ability of the agonist to activate the receptor [220]. Therefore, two terms are used to describe the action of an agonist. Affinity is defined as the initial binding reaction and efficacy describes everything that occurs after the initial binding of the agonist. For ion channels, the equivalent terminology is binding and gating [221]. Therefore, all behavioral characteristics of ligand-gated ion channels can be reduced to differences in binding or gating. However, obtaining useful and accurate measurements of these quantities have been difficult. This is due in part to the fact that these terms are not independent of one another [221]. Binding affects gating, which means that gating must affect binding. This concept is a reflection of the basic physical principle of reciprocity, if A affects B then B must affect A [222, 223]. Therefore, for any ligand that produces a conformational change, the total amount of binding as measured in a ligand binding experiment depends not only on the affinity of the initial binding, but also on the extent to which the conformational change takes place once ligand had become bound [221]. In the case of KCa3.1 and KCa2.2, it would be nearly impossible to measure affinity and efficacy of $Ca^{2+}$ without a detailed activation mechanism such as that described for the muscle nicotinic acetylcholine receptor [224, 225]. However, as explained in the next section, Li et al., [196] show that the trivalent lanthanide ion, terbium ($Tb^{3+}$), can act as a substitute for $Ca^{2+}$; binding to the same sites on KCa2.2 CaM but with a higher affinity. Characterizing the functional effects of $Tb^{3+}$ on the activation of KCa3.1 and KCa2.2 will be a useful tool for understanding the coupling between CaM and the channel, which may provide insight into a mechanism for separately measuring affinity and efficacy.

## 3.4 CYSTEINE 276 AS AN IMPORTANT SITE FOR THE COUPLING OF $Ca^{2+}$ BINDING TO CHANNEL GATING

One of the more interesting effects of using PCMBS is its ability to increase $P_{o(max)}$ in saturating $[Ca^{2+}]_i$, suggesting that 10 μM $Ca^{2+}$ is insufficient to saturate the activation of KCa3.1. However, increasing $[Ca^{2+}]_i$ above 10 μM does not increase residual current (unrecorded observation). Compounds that potentiate the closely related channel, KCa2.2 are thought to stabilize the CaM/channel interaction. EBIO and NS309 increase the apparent $Ca^{2+}$ affinity; EBIO slows the deactivation process; and NS309 increases current in saturating $Ca^{2+}$. Stabilizing the CaM/channel interaction as a means to potentiate channel activation was confirmed by characterizing the effect of $Tb^{3+}$ on the activation of KCa2.2. $Tb^{3+}$ has been shown biochemically to bind to the same $Ca^{2+}$ binding sites, activating the purified CaM protein, thus acting as a substitute for $Ca^{2+}$. Investigating the effect of $Tb^{3+}$ on a CaM-dependent ion channel, Li et al., [196] showed $Tb^{3+}$ binds to the same sites as $Ca^{2+}$, but with a higher affinity. The higher affinity causes a dramatic left-shift in the apparent $Ca^{2+}$ affinity, in addition to a dramatic slowing in the deactivation process [196]. PCMBS binds to an amino acid ($Cys^{276}$) in S6, but influences channel behavior in a manner similar to compounds that stabilize the CaM/channel interaction. This result can be explained if $Cys^{276}$ is in a region of the channel associated with the coupling machinery. If coupling is a direct or indirect transfer of the energy from the CaM/CaMBD to the activation gate, than any perturbation to this pathway should mimic the effect of stabilizing the CaM/channel interaction. Therefore, $Cys^{276}$ (or the neighboring residues; see section regarding the potential mechanism of PCMBS) functions to allosterically couple the energy of $Ca^{2+}$ binding to the activation gate. The same conclusion also applies for $Leu^{281}$, on account of the

L281W mutation mimicking the effects EBIO, NS309, and $Tb^{3+}$. These results are not surprising considering the C-terminal linker between the CaMBD and S6 is the most likely pathway for the transfer of activation energy. This has been confirmed in the BK channel. Modifying the linker length inversely influences channel $P_o$ [129]. However, what is not obvious is how these domains function to transduce the chemical energy of $Ca^{2+}$ binding into a mechanical force to open the channel. In the next section I will present two potential mechanisms based upon PCMBS and the L281W mutation that attempt to partially describe the coupling between CaM and KCa3.1.

## 3.5 POTENTIAL COUPLING MECHANISM

As previously explained in the review of the chemomechanical gating model, the binding of $Ca^{2+}$ to CaM results in a conformational change in the CaMBD, which leads to a rotational movement of this domain that is transmitted to the activation gate through S6 [189, 192, 193]. However, what is not understood is how the conformational change in CaM/CaMBD is allosterically coupled to the activation gate. In this dissertation, I am proposing that the non-luminal face of the C-terminal portion of S6 forms an interaction surface that functions to allosterically couple conformational changes to the activation gate. Therefore, understanding the functional effects of PCMBS and the L281W mutation may provide insight into the coupling between CaM and the channel. I will propose two potential coupling pathways based upon these perturbations, and in the conclusion/future directions section I will propose how to go about testing for each of these models.

My first hypothesis states that shifting the gating energetics toward the open conformation is due to a potential interaction between S6 transmembrane domains from adjacent

subunits. This idea flows from the homology model of the closed and open states of KCa3.1 using the x-ray structures of KcsA and Kv1.2, respectively. The closed state model predicts a steric clash between $Cys^{276}$ and $Leu^{281}$ from the adjacent transmembrane domain (Fig. 26). From this model we can estimate that the distance between the β-carbon of $Cys^{276}$ and the β-carbon of $Leu^{281}$ is 7.0 Å, which is comparable to the distance between the corresponding β-carbons in KcsA (7 Å) and KirBac1.1 (9 Å). PCMBS is 6.5 Å from the mercury atom to the sulfur atom (inset Fig. 26), and this length increases to 9.0 Å when measured from the sulfur atom to the thiol group of the conjugated cysteine (inset Fig. 26). Therefore, I hypothesize that when PCMBS is conjugated to $Cys^{276}$ it disrupts the closing transition by sterically clashing with $Leu^{281}$. This mechanism would suggest that S6 would have to undergo a combined rotation and inward lateral movement to transition from the predicted orientation in the open state model to the orientation depicted in the closed state model (Fig. 26). This type of conformational change would suggest that the coupling mechanism occurs along the linkers between transmembrane domains, suggesting the C-terminal linker and the bottom end of S6 as a likely pathway for the transfer of energy to the activation gate. Therefore, the conformational change originating in the CaMBD would travel along the C-terminal linker to the bottom end of S6. If KCa3.1 has a similar gating mechanism as MthK, the presence of a glycine in S6 would enable the helix to bend in an outward lateral direction. Removing $Ca^{2+}$ would reverse this process, causing the helix to move in an inward lateral direction, which would orient $Cys^{276}$ and $Leu^{281}$ from the adjacent helix into close approximation.

My second hypothesis states that the shift in gating energetics toward the open conformation is due to a potential S5-S6 interaction. $Leu^{281}$ is oriented toward S5 (inset Fig. 26). Increasing side-chain volume with the L281W mutation is expected to disrupt this interaction,

preventing the transition into the closed conformation. Mutations in transmembrane domains S5 and S6 indicate this interaction is important for the opening and closing of $K^+$ channels [128]. Therefore, based upon the L281W mutation, the coupling mechanism is expected to be dependent upon the interacting surfaces between transmembrane domains. In the spHCN1 pace maker channel, the S4-S5 linker and the C-terminal linker come in close approximation during gating. Utilizing this model in context with my hypothesis suggests a possible coupling pathway between CaM and the activation gate. The energy from $Ca^{2+}$ binding could travel from the CaMBD to the activation gate via the C-terminal linker, which in the spHCN1 channel, interacts with the S4-S5 linker. From the S4-S5 linker the activation energy would be predicted to follow S5 and through a S5-S6 coupling finally end at the activation gate. Therefore, based upon the functional effects of PCMBS and the L281W mutation, I presented two possible coupling pathways that are mediated through either: 1) an intersubunit interaction or 2) an S5-S6 interaction. In the next section I will propose a series of experiments to distinguish between these potential interactions.

## 3.6 CONCLUSION/FUTURE DIRECTIONS

The goal of this dissertation was to investigate the role of S6 in the activation mechanism of KCa3.1. In doing so, we learned that not only is S6 a structural component of the pore, but also a dynamic element participating in the activation mechanism. Previous investigations noted that the luminal surface of the C-terminal end of S6 participates in the activation mechanism [110, 111, 113]. We furthered this model by showing that the non-luminal surface of this segment is important for allosterically coupling the conformational change in CaM to the activation gate.

Disrupting this region with PCMBS or the L281W mutation shifts the gating equilibrium toward the open state by disrupting the closing transition. Therefore, the updated chemomechanical model states that the activation energy from $Ca^{2+}$ causes a conformational change in CaMBD, which through the luminal and non-luminal surfaces of the C-terminal end of S6 is allosterically coupled to the activation gate. Furthermore, the activation energy is potentially transmitted to the activation gate through either the linkers connecting transmembrane domains, or through the interacting surfaces between transmembrane domains.

The overall importance of S6 to the activation mechanism was confirmed by investigating this domain in the closely related channel, KCa2.2. Similar to KCa3.1, mutations in S6 altered the energetics of channel gating. Although the functional effect of the mutations was quite similar (Tables A.2-A.5), important functional differences exist between these channels. Exploring these functional differences would be an effective strategy for furthering our understanding of the activation mechanism. To that end, I proposed two potential mechanisms for coupling between CaM and KCa3.1 based upon the functional effects of PCMBS and the L281W mutation. Although these mechanisms propose two different pathways for the transfer of energy to the activation gate, these mechanisms are not meant to be mutually exclusive. It is possible that the coupling mechanism incorporates a S5-S6 interaction in combination with an intersubuit interaction. Therefore, the next objective in this dissertation would be to investigate whether either of these mechanisms is associated with the activation of KCa3.1.

The first hypothesis states that $Cys^{276}$ and $Leu^{281}$ come into close approximation in the closed conformation. We would attempt to cross-link these residues using cysteine cross-linkers as a means to test this hypothesis. Additionally, using variable length cross-linkers we could gauge the distance between these positions in the closed conformation. Since we are attempting

to crosslink residues on adjacent subunits, we would use tandem dimers to control subunit stoichiometry. This approach has been employed numerous times beginning in the early 90's to look at subunit stoichiometry [226] and more recently to examine possible interacting sites within the channel [227, 228]. Following this approach would ensure that the channel assembles as ABAB rather than ABBA. This is a critical part of the experiment, as my objective is to crosslink residues from adjacent subunits rather then from diagonal subunits. Before attempting the cross-linking experiment, I would confirm that the WT and mutant tandem constructs are functional, and display gating behavior that is similar to the WT-monomer. The first subunit in the tandem construct used in the cross-linking experiments would be cysteine-less except for a cysteine at position 276. The second subunit would also be cysteine-less, but in this case, a cysteine would be engineered in position 281. The channels would be expressed in a heterologous expression system and crosslinking reagents would be applied to the intercellular surface of an excised membrane patch. Our model indicates the potential for steric clash between $Cys^{276}$ and $Leu^{281}$ from the adjacent subunit in the closed conformation. Therefore, to obtain an accurate estimate of the distance between these residues, the cross-linking reagent would be added after the channel entered the closed conformation. Since I am using a series of cross-linking reagents with variable lengths, I would expect the majority of the reagents to cross-link the channel. However, the linker length that best describes the distance between these positions in the closed conformation would prevent the channel from transitioning into the open conformation upon the addition of $Ca^{2+}$. For instance, there may be enough slack using the longest linkers that the channel may be able to fully transition into the open conformation. Medium length linkers may only allow for a partial opening; the just right length linker would lock the channel in the closed conformation. Recovery from the closed state would only occur

with the addition of a reducing agent. Since PCMBS is open-state dependent, the cross-linking reagents may not have access to $Cys^{276}$ and $Cys^{281}$ in the closed conformation. Therefore, I would like to add the caveat that cross-linking may not occur in the closed state. If this is the case, I would add the reagents to the open state in order to increase the probability of cross-linking the channel. In an actively gating channel, I would expect the linker length that best describes the closed-state distance between these two positions to lock the channel in this state, even in the presence of $Ca^{2+}$. Linkers that are longer than the closed-state distance may allow for full or even partial gating transitions. However, even in the open-state, MTS reagents did not have access to the non-luminal face of S6 [113]. Again, I would add the caveat that cross-linking may not occur in the open state. In which case, I would follow the protocol from Soskin et al., for cross-linking cysteines in low dielectric environments [219].

The second hypothesis states that a S5-S6 interaction is important for the activation mechanism. Increasing the volume at position 281 may prevent the rotation of S6 that is thought to accompany the open to closed transition in KcsA [217]. To test this hypothesis, I would first determine whether substitution of large volume side-chain amino acids such as tyrosine and phenylalanine could reproduce the effect of the L281W mutation. If the phenotype is the result of an increase in side-chain volume at that position then substitution of amino acids with similar sized side-chains would be expected to reproduce the functional effect of the mutation. The endogenous amino acid is a leucine, therefore, substitution of amino acids with smaller or similar sized side-chains would not be expected to disrupt channel gating. Therefore, as an additional test of this hypothesis, I would locate the potential interacting amino acid in S5. To do this I would perform a tryptophan scan in this helix. Mutations that are expected to interact with S6 would have a similar phenotype as the L281W mutation. To determine whether the two positions

interact, one would have to assess the independence of the two mutations; the mutation in S5 and the L281W mutation in S6. Two mutations can separately effect channel gating; when these positions are coupled, the combination of the two mutations will have an additive effect on gating energetics [210]. In a S5-S6 interaction, I expect the mutations to be close enough to directly interact. Therefore, as an assessment of this interaction, I would expect the mutation in S5 that interacts with S6 to have an additive effect on the energetics of gating. If the mutation in S5 does not interact with the mutation in S6, I would expect the effects of both mutations to cancel out.

In conclusion, the work presented in this dissertation refines the current chemomechanical gating model to include the non-luminal surface of the C-terminal portion of S6 as a potential interacting site. This site functions to allosterically couple the conformational changes in the CaMBD to the pore, enabling the channel to transition from a non-conducting to a conducting configuration. Furthermore, from this work I developed two hypotheses that describe a potential coupling pathway between CaM and the activation gate. As an additional component of my dissertation, I investigated S6 in the activation mechanism of KCa2.3. Although the conclusions were not as definitive when compared to the KCa3.1 investigation, the results confirm the important of S6 in the activation mechanism. Furthermore, the important functional differences I outlined between these channels can be exploited to better understand the coupling mechanism and the specific regions that participate in this process.

# 4.0 APPENDIX

## 4.1 INTRODUCTION: STRUCTURE-FUNCTION INVESTIGATION OF S6 IN KCa3.1 AND KCa2.3

As previously described, PCMBS influences the steady-state and kinetic behavior of KCa3.1 by binding to $Cys^{276}$. The closely related channel, KCa2.3 has a glycine residue at the equivalent position ($Gly^{534}$), see Table (A.1). Therefore, we proposed that KCa2.3 would be insensitive to PCMBS. As illustrated in Fig. (A.3A), and consistent with our hypothesis, PCMBS had no effect on the steady-state current of this channel. Since $Cys^{276}$ in KCa3.1 is required for PCMBS-sensitivity, we proposed that the equivalent mutation (G534C) would confer PCMBS sensitivity to KCa2.3. However, and much to our surprise, PCMBS had no effect on the steady-state current of this channel (Fig. A.3B). The inability of PCMBS to modulate the gating of this channel may occur because PCMBS cannot bind to $Cys^{534}$, or the G534C mutation modulated channel gating in a manner that may mask any potential effect by PCMBS. As shown in Figs. (A.5 and A.7) along with Tables (A.3 and A.5), the mutation influenced steady-state and kinetic behavior in manner similar to the observed effect of PCMBS on KCa3.1. This modulation in channel gating would mask any potential effects this compound may have on the gating of KCa2.3. This was a rather surprising result. The high degree of homology in S6 between KCa3.1 and KCa2.3 would suggest functional homogeneity for the corresponding residues located along this transmembrane

domain, see Table (A.1). Since our investigation into the molecular mechanism of PCMBS required a series of mutations along S6 in KCa3.1, we decided to make the corresponding mutations in KCa2.3 as a means to determine whether any other distinct functional domains exist between these channels. The segment of S6 we investigated begins at the proposed glycine-gating hinge ($Gly^{274}$ in KCa3.1 and $Gly^{532}$ in KCa2.3) and extends C-terminally, five amino acids before the end of S6 ($Val^{282}$ in KCa3.1 and $Val^{540}$ in KCa2.3). We performed a tryptophan scan of this region, looking for mutations that disrupt the steady-state and/or kinetic behavior of the channel. Furthermore, we focused on the predicted binding site of PCMBS ($Cys^{276}$) and the corresponding residue ($Gly^{534}$) in KCa2.3, in addition to the residues neighboring these positions as they are conserved in both channels $Cys^{277}$ and $Cys^{535}$ in KCa3.1 and KCa2.3, respectively. Our results indicate that the segment of S6 we investigated is functionally equivalent between KCa3.1 and KCa2.3. However, KCa2.3 has more mutations that influence both the steady-state and kinetic behavior of the channel, suggesting this region of S6 may undergo a more complicated conformational change as the channel transitions from the closed to the open conformation.

## 4.2 RESULTS

### 4.2.1 Results Table 1

**The mutations made along S6 in KCa3.1 and KCa2.3.** The mutations are aligned according to the position along S6 and grouped based on the substituted amino acid or the corresponding amino acid present in the other channel.

| KC3.1 | KCa2.3 |
|---|---|
| Position | Position |
| G274W | G532W |
| V275A | A533V |
| V275W | A533W |
| C276A | |
| C276D | G534D |
| C276F | G534F |
| C276G | G534C |
| C276W | G534W |
| C276Y | G534Y |
| C277A | |
| C277D | C535D |
| C277F | C535F |
| C277G | C535G |
| C277W | C535W |
| C277Y | C535Y |
| T278W | T536W |
| A279W | A537W |
| L280W | L538W |
| L281W | V539W |
| V282W | V540W |

### 4.2.2 Results Table 2

**The mutations that expressed macroscopic currents in KCa3.1 and KCa2.3.** Constructs that expressed highly enough to produce macroscopic currents are demarcate from the constructs that do not express by a yes. It is interesting, with the exceptions of V275A and C277Y in KCa3.1 and C535F in KCa2.3, that all of the mutations in KCa3.1 with little to no channel expression corresponded to the mutations KCa2.3 having little to no channel expression. This result would suggest that the residues required for packing are equivalent in both channels.

| | KC3.1 | | KCa2.3 |
|---|---|---|---|
| Position | macroscopic current | Position | macroscopic current |
| G274W | | G532W | |
| V275A | Yes | A533V | |
| V275W | | A533W | |
| C276A | Yes | | |
| C276D | | G534D | |
| C276F | Yes | G534F | Yes |
| C276G | Yes | G534C | Yes |
| C276W | Yes | G534W | Yes |
| C276Y | | G534Y | |
| C277A | Yes | | |
| C277D | | C535D | |
| C277F | | C535F | Yes |
| C277G | Yes | C535G | Yes |
| C277W | Yes | C535W | Yes |
| C277Y | Yes | C535Y | |
| T278W | | T536W | |
| A279W | | A537W | |
| L280W | | L538W | |
| L281W | Yes | V539W | Yes |
| V282W | Yes | V540W | Yes |

### 4.2.3 Results Table 3

**The mutations that mediated a left-shift in apparent $Ca^{2+}$ affinity in KCa3.1 and KCa2.3.** The strike-through represents the mutations with little to no channel expression. Mutations resulting in a left-shift in apparent affinity are grouped at the bottom two positions, $Leu^{281}$ and $Val^{282}$ in KCa3.1 and $Val^{539}$ and $Val^{540}$ in KCa2.3. This result is not surprising since a previous investigation showed that significant conformational change is expected to occur in the C-terminal segment of S6. Furthermore, our results would also suggest that gating sensitive residues are located one ($Val^{275}$) and two ($Gly^{534}$) amino acids down from the predicted gating hinge ($Gly^{274}$) and ($Gly^{532}$) in KCa3.1 and KCa2.3, respectively. Assuming KCa3.1 and KCa2.3 incorporate a glycine gating hinge in the mechanism for transitioning from the closed to the open conformation, it would follow that residues neighboring the gating hinge would also undergo a significant conformation change.

| KC3.1 | | KCa2.3 | |
|---|---|---|---|
| Position | Phenotype | Position | Phenotype |
| ~~G274W~~ | | ~~G532W~~ | |
| V275A | left-shift | ~~A533V~~ | |
| ~~V275W~~ | | ~~A533W~~ | |
| C276A | | | |
| ~~C276D~~ | | ~~G534D~~ | |
| C276F | | G534F | |
| C276G | | G534C | left shift |
| C276W | | G534W | |
| ~~C276Y~~ | | ~~G534Y~~ | |
| C277A | | | |
| ~~C277D~~ | | ~~C535D~~ | |
| ~~C277F~~ | | C535F | |
| C277G | | C535G | |
| C277W | | C535W | |
| C277Y | | ~~C535Y~~ | |
| ~~T278W~~ | | ~~T536W~~ | |
| ~~A279W~~ | | ~~A537W~~ | |
| ~~L280W~~ | | ~~L538W~~ | |
| L281W | left-shift | V539W | left-shift |
| V282W | left-shift | V540W | left-shift |

### 4.2.4 Results Table 4

**The mutations that mediated a right-shift in apparent $Ca^{2+}$ affinity in KCa3.1 and KCa2.3.** As observed in the previous Table, the mutations causing a right-shift in apparent $Ca^{2+}$ affinity are grouped around the same residue, $Cys^{277}$ and $Cys^{535}$ in KCa3.1 and KCa2.3, respectively.

| KC3.1 | | KCa2.3 | |
|---|---|---|---|
| Position | Phenotype | Position | Phenotype |
| ~~G274W~~ | | ~~G532W~~ | |
| V275A | left-shift | ~~A533V~~ | |
| ~~V275W~~ | | ~~A533W~~ | |
| C276A | | | |
| ~~C276D~~ | | ~~G534D~~ | |
| C276F | | G534F | |
| C276G | | G534C | left-shift |
| C276W | | G534W | right-shift |
| ~~C276Y~~ | | ~~G534Y~~ | |
| C277A | | | |
| ~~C277D~~ | | ~~C535D~~ | |
| ~~C277F~~ | | C535F | right-shift |
| C277G | | C535G | |
| C277W | slight right-shift | C535W | right-shift |
| C277Y | slight right-shift | ~~C535Y~~ | |
| ~~T278W~~ | | ~~T536W~~ | |
| ~~A279W~~ | | ~~A537W~~ | |
| ~~L280W~~ | | ~~L538W~~ | |
| L281W | left-shift | V539W | left-shift |
| V282W | left-shift | V540W | left-shift |

### 4.2.5 Results Table 5

**The mutations that alter activation or deactivation kinetics in KCa3.1 and KCa2.3.** Unlike the previous results, the mutations that disrupt deactivation kinetics are randomly distributed along S6. The exception would be the mutation in KCa3.1 (C277F) and the corresponding position in KCa2.3 (G534C). It is interesting to note that none of the mutations disrupt activation kinetics. KCa2.3 has 3 mutations (to 1 mutation in KCa3.1) that disrupt both the steady-state and kinetic behavior of the channel, suggesting the channel may undergo a more complicated conformational change as it transitions from the closed to open conformation.

| KC3.1 | | KCa2.3 | |
|---|---|---|---|
| Position | Phenotype | Position | Phenotype |
| ~~G274W~~ | | ~~G532W~~ | |
| V275A | left-shift | ~~A533V~~ | |
| ~~V275W~~ | | ~~A533W~~ | |
| C276A | | | |
| ~~C276D~~ | | ~~G534D~~ | |
| C276F | deactivation is SLOWER | G534F | |
| C276G | | G534C | left-shift/deactivation is SLOWER |
| C276W | | G534W | right-shift |
| ~~C276Y~~ | | ~~G534Y~~ | |
| C277A | | | |
| ~~C277D~~ | | ~~C535D~~ | |
| ~~C277F~~ | | C535F | right-shift/deactivation is FASTER |
| C277G | | C535G | |
| C277W | slight right-shift | C535W | right shift |
| C277Y | slight right-shift | ~~C535Y~~ | |
| ~~T278W~~ | | ~~T536W~~ | |
| ~~A279W~~ | | ~~A537W~~ | |
| ~~L280W~~ | | ~~L538W~~ | |
| L281W | left-shift/deactivation is SLOWER | V539W | left-shift |
| V282W | left-shift | V540W | left-shift/deactivation is SLOWER |

### 4.2.6 Results Table 6

**Summary of the effects that the mutations had on S6 residues in KCa3.1 and KCa2.3.** Mutations that had no effect on channel behavior are in italics. In summary, these results indicate that the residues required for channel expression are equivalent between KCa3.1 and KCa2.3. The mutations that cause a right-shift in apparent $Ca^{2+}$ affinity are grouped in the middle of the search region, whereas the mutations that cause a left-shift in apparent $Ca^{2+}$ affinity are grouped toward the C-terminal end of the search region. This result would indicate the basic architecture of the search region is equivalent between both channels. The only discrepancy from this investigation is that KCa2.3 has more mutations that disrupt both steady-state and kinetic behavior of the channel, suggesting this channel may undergo a more complicated conformational change(s) as it transitions from the closed to the open conformation.

| KC3.1 | | KCa2.3 | |
|---|---|---|---|
| Position | Phenotype | Position | Phenotype |
| ~~G274W~~ | | ~~G532W~~ | |
| V275A | left-shift | ~~A533V~~ | |
| ~~V275W~~ | | ~~A533W~~ | |
| *C276A* | | | |
| ~~C276D~~ | | ~~G534D~~ | |
| C276F | deactivation is SLOWER | *G534F* | |
| *C276G* | | G534C | left-shift/deactivation is SLOWER |
| *C276W* | | G534W | right-shift |
| ~~C276Y~~ | | ~~G534Y~~ | |
| *C277A* | | | |
| ~~C277D~~ | | ~~C535D~~ | |
| ~~C277F~~ | | C535F | right-shift/deactivation is FASTER |
| *C277G* | | *C535G* | |
| C277W | slight right-shift | C535W | right shift |
| C277Y | slight right-shift | ~~C535Y~~ | |
| ~~T278W~~ | | ~~T536W~~ | |
| ~~A279W~~ | | ~~A537W~~ | |
| ~~L280W~~ | | ~~L538W~~ | |
| L281W | left-shift/deactivation is SLOWER | V539W | left-shift |
| V282W | left-shift | V540W | left-shift/deactivation is SLOWER |

## 4.3 DISCUSSION/CONCLUSIONS

KCa3.1 and KCa2.3 are closely related channels with a high degree of homology, especially in S6 and the CaM/CaMBD region in the C-terminal domain. This homology is reflected by the similarity in the apparent $Ca^{2+}$ affinity between these channels, see Table (A.2) and (A.3). However, this is where the similarity between channel function ends. KCa2.3 has a higher $P_{o(max)}$ (Fig. A.8) compared to KCa3.1 (Fig. 13). Although, both channels have a similar deactivation rate, the activation rate for KCa2.3 is 10-fold faster when compared to KCa3.1. Therefore, we asked whether any of these differences could be attributed to any potential functional differences existing along S6. Our results would indicate that the segment of S6 we investigated is similar between both channels, with the lone discrepancy being that there are more mutations that influence both the steady-state and kinetic behavior of KCa2.3, suggesting this region of the channel may undergo a more complex conformational change as the channel transitions from the closed to the open conformation. The functional similarity we reported between these channels is not surprising, since the region we investigated only differs by a couple of amino acids. Therefore, the observed differences in channel function must be explained by differences in other regions of the channel. Since we only investigated the region of S6 surrounding the PCMBS binding site, it is possible that functional differences exist either above or below this segment. Therefore, one possible avenue for investigation would be to complete the tryptophan scan of S6 as a means to determine whether functionally different regions exist outside of the previously examined region. Another approach, and one more likely to find functional differences in the channel is to investigate how S5 contributes to the activation mechanism in both of these channels. Unlike S6, which is highly homologous between these channels, the S5 sequence is quite different (15 out of 23 amino acids). Therefore, another avenue of investigation would be

to swap S5 domains between these channels. However, the chimera does not express when the full S5 is switched between channels (DC Devor, unpublished observations). Therefore, an alternative approach would be to switch the non-conserved amino acids between channels. If S5 significantly contributes to the activation mechanism, then the chimeric channel would display the functional properties of the donor channel.

Although our investigation did not report any significant functional differences between these channels, we can conclude that S6 actively participates in the $Ca^{2+}$-dependent activation mechanism. The wide disparity between $P_o$ and activation kinetics indicates these channels are functionally much different than their sequence suggests. These discrepancies cannot be explained by the existence of functionally different domains present along the S6 segment we investigated. However, the potential exists for these disparate channel properties to be explained by differences in the S5 transmembrane domain or the regions of S6 that were outside our area of investigation.

## 4.4 APPENDIX FIGURES

**Figure A.1A**

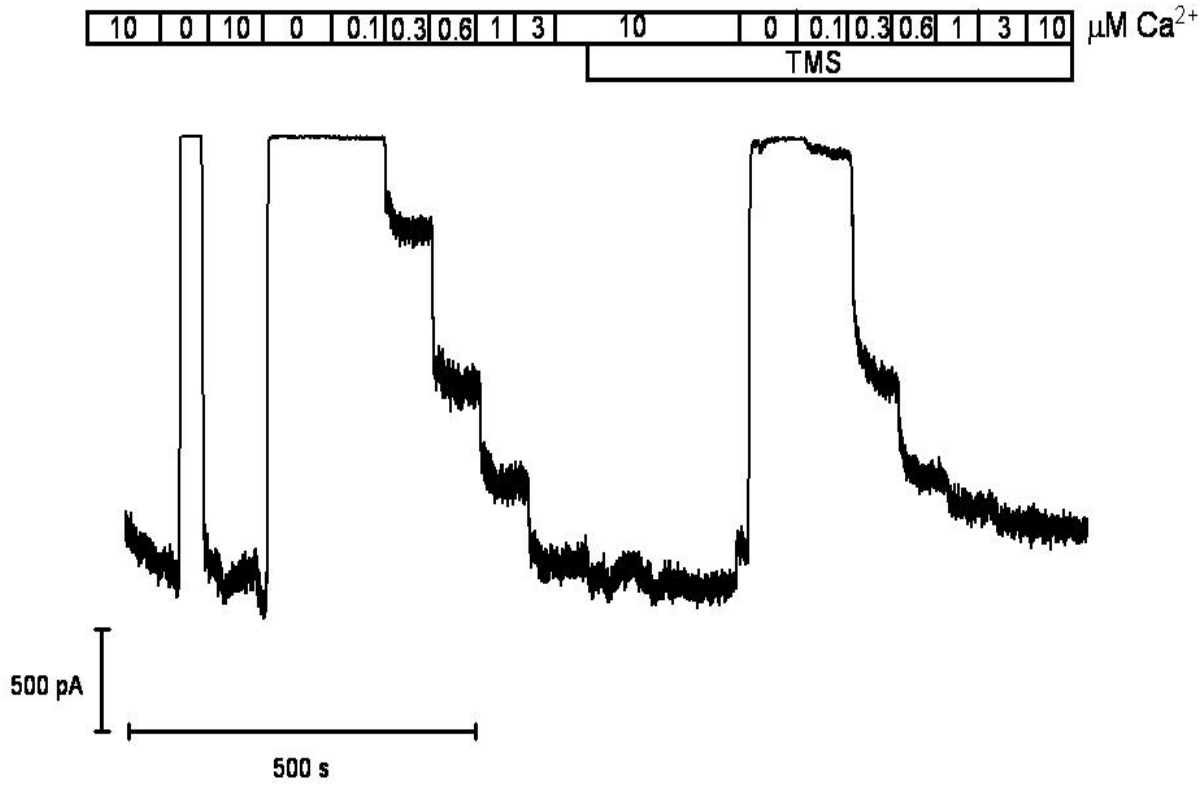

**Figure A.1B**

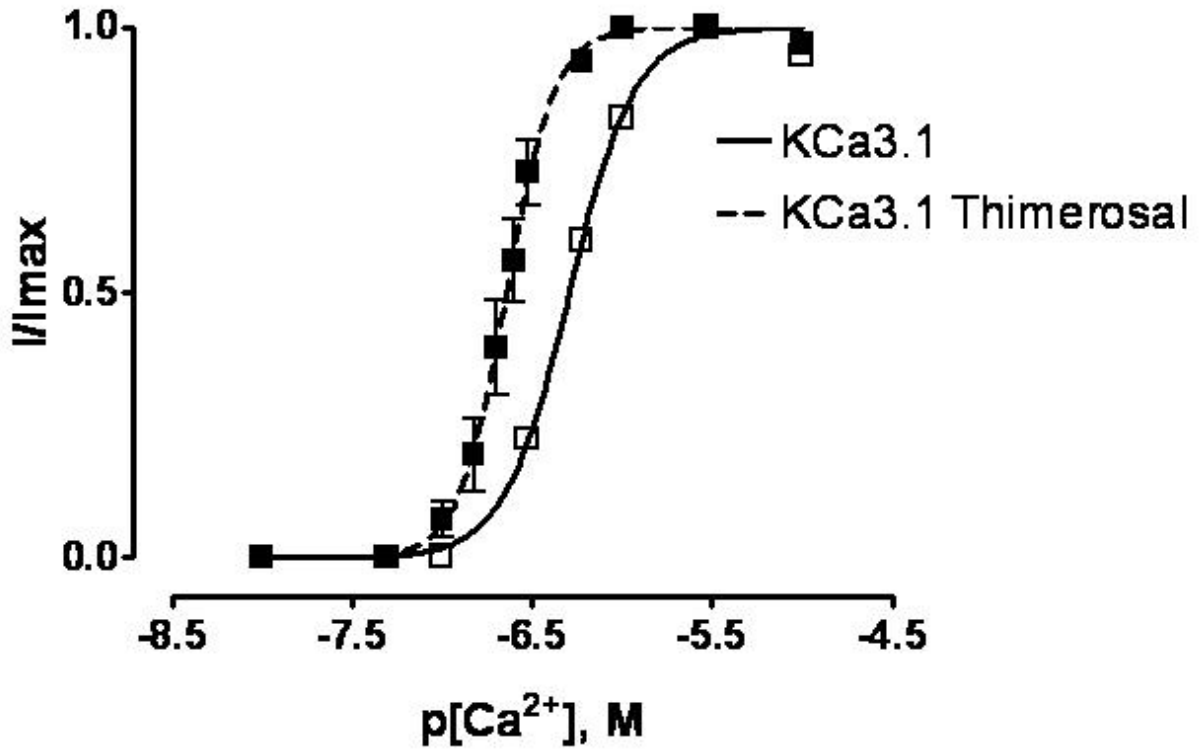


**Figure A.1. Thimerosal shifts the apparent $Ca^{2+}$ affinity in KCa3.1.** Complete $Ca^{2+}$ concentration response experiments were performed to estimate $EC_{50}$ and the Hill coefficient (h) in the absence and presence of thimerosal. (A) Representative macroscopic current record from an inside-out patch expressing KCa3.1 channels. The patch was excised in 10 μM $Ca^{2+}_i$ followed by a series of $Ca^{2+}_i$ concentrations beginning with 0, 0.1, 0.3, 0.6, 1.0, 3.0, and 10 μM $Ca^{2+}_i$, all applied in 10 s intervals using a rapid solution exchanger. After the current reached a steady-state level, thimerosal (500 μM) was added and a 2nd $Ca^{2+}_i$ concentration response experiment was performed using the above $Ca^{2+}_i$ concentrations in the presence of thimerosal. (B) Plot of normalized <I> current against the corresponding $Ca^{2+}_i$ for KCa3.1 (□) and KCa3.1+thimerosal (■) fit with a variation of the Hill equation (see methods). This analysis gave estimates for KCa3.1 (solid line, n=15) $EC_{50}$=498±14 nM and h=2.4±0.04 and KCa3.1+thimerosal (dashed line, n=10) $EC_{50}$=229±22 nM and h=3.3±0.04. All experiments were done in pairs, but an alternate set of $Ca^{2+}_i$ concentrations (0.1, 0.15, 0.2, 0.25, 0.3, 0.6, 1.0 and 10 μM) were used when estimating $EC_{50}$ and h for KCa3.1+thimerosal. Error bars represent standard error of the mean (SEM). The error bars for KCa3.1 are smaller than the symbols (□).

Figure A.2

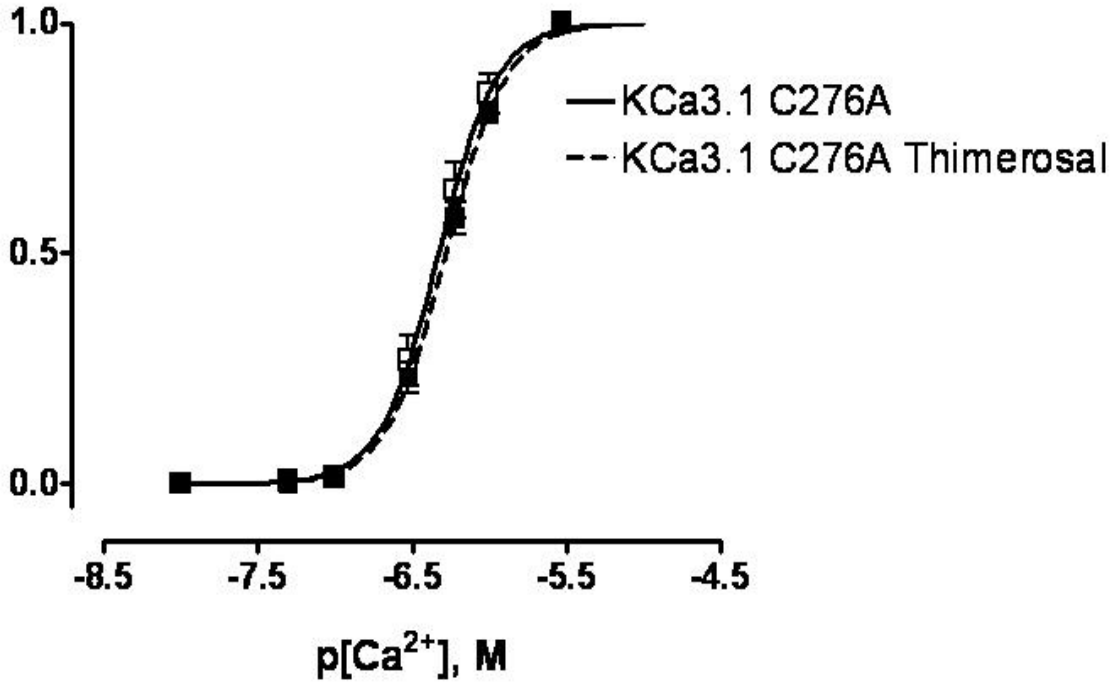


**Figure A.2. C276A prevents the thimerosal-dependent increase in apparent $Ca^{2+}$ affinity.** Plot of normalized <I> current against the corresponding $Ca^{2+}_i$ for KCa3.1 C276A (□) and KCa3.1 C276A+thimerosal (■). All analyses were performed following the protocol described in Fig. A.1 to give averages: KCa3.1 C276A (solid line, n=7) $EC_{50}$=506±76 nM and h=2.5±0.2 and KCa3.1 C276A+thimerosal (dashed line, n=7) $EC_{50}$=557±47 nM and h=2.1±0.1. Error bars represent standard error of the mean (SEM).

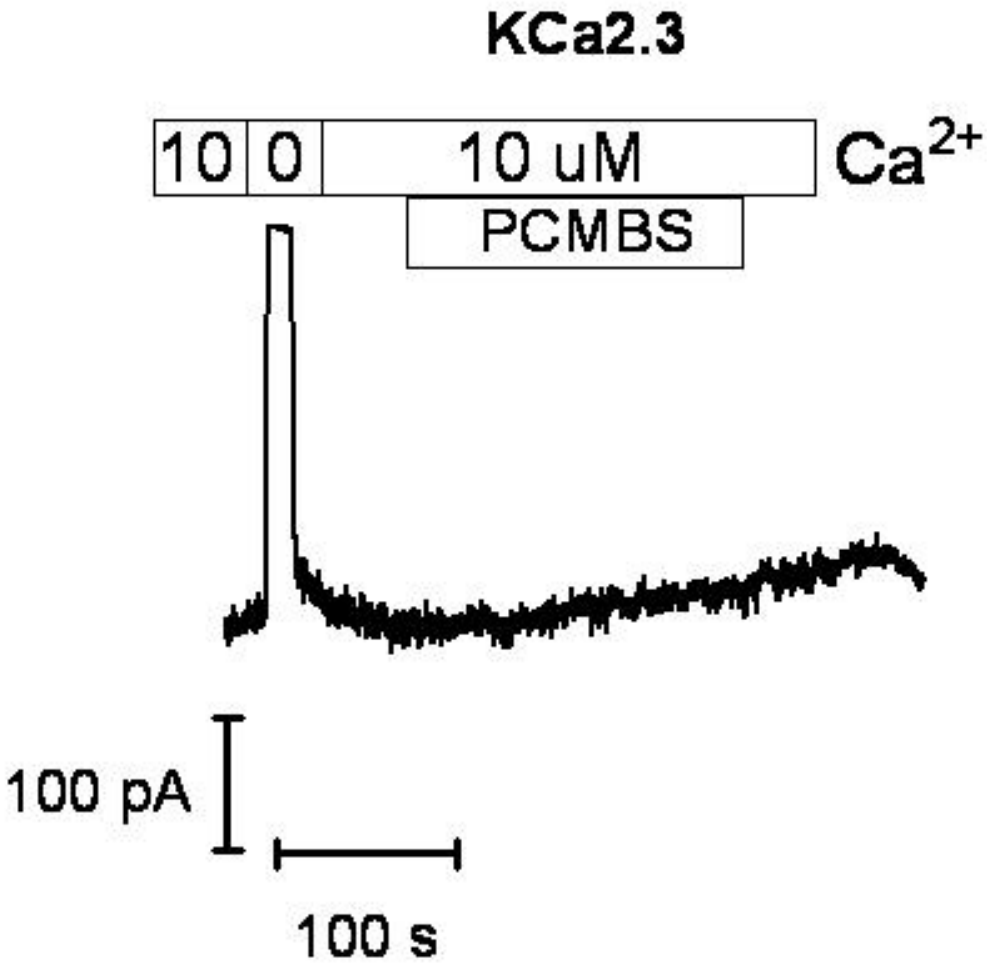


Figure A.3A

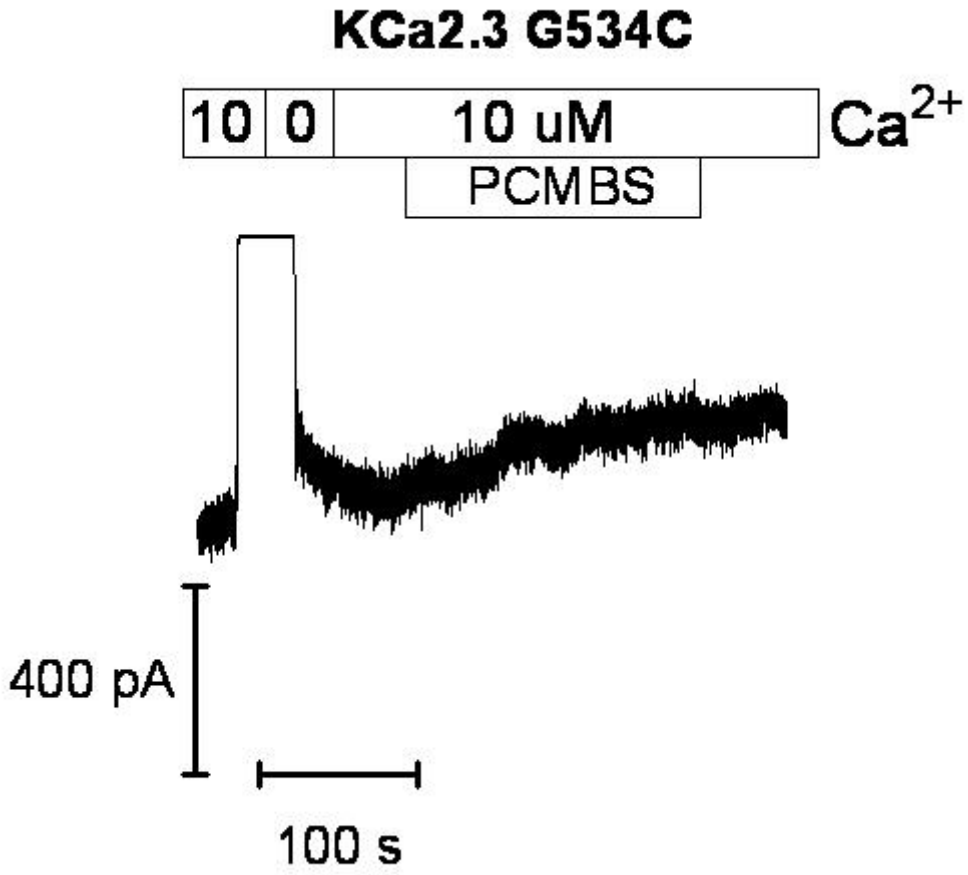


Figure A.3B

**Figure A.3. PCMBS does not increase the steady-state current in (A) KCa2.3 or (B) KCa2.3 G534C.** Macroscopic current records from KCa2.3 channels heterologously expressed in HEK cells to determine sensitivity to PCMBS. PCMBS (500 μM) was added to inside-out patches excised in 10 μM $Ca^{2+}_i$ following the establishment of steady-state current level. PCMBS washout lasted at least 1 minute to ensure there were not any experimental artifacts associated with the addition of the compound.

Figure A.4A

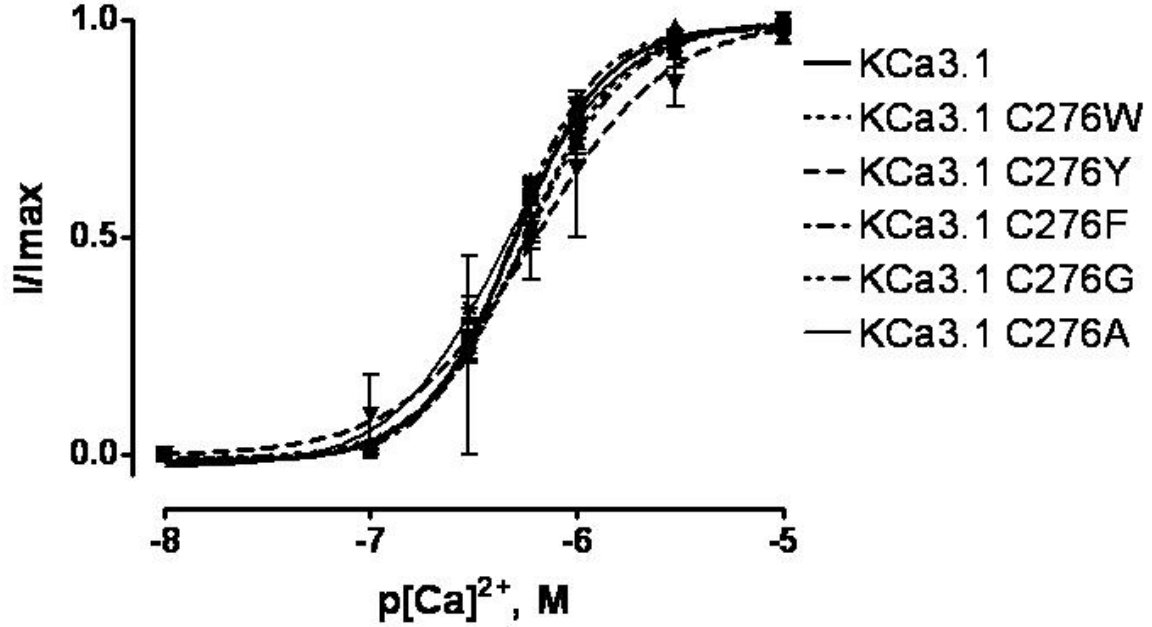


Figure A.4B

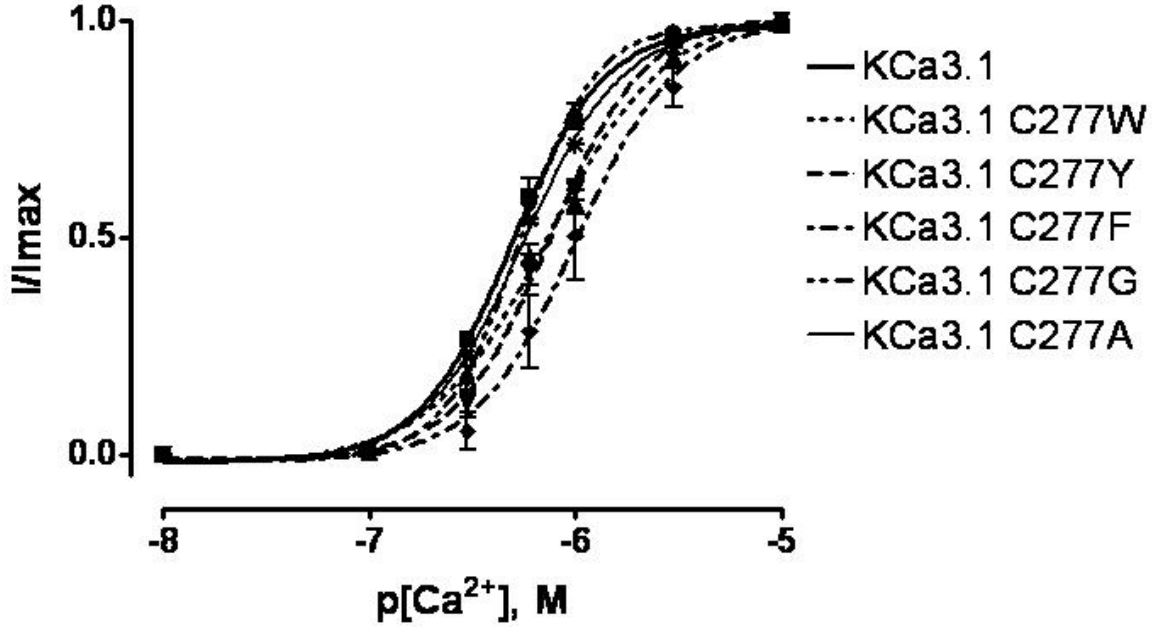

Figure A.4C

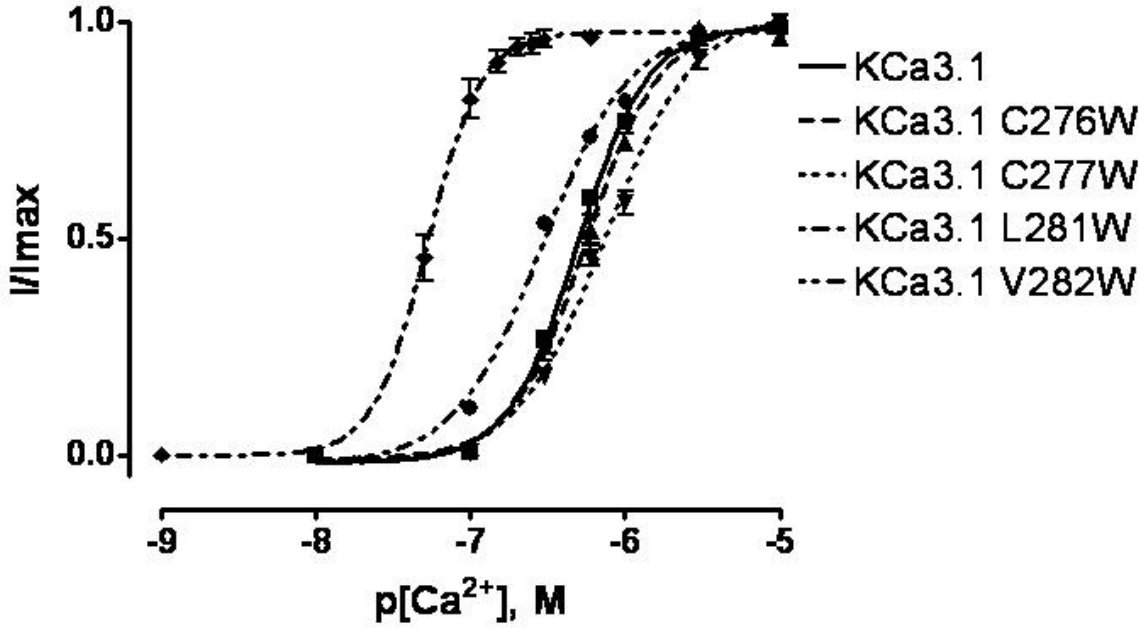


Figure A.4D

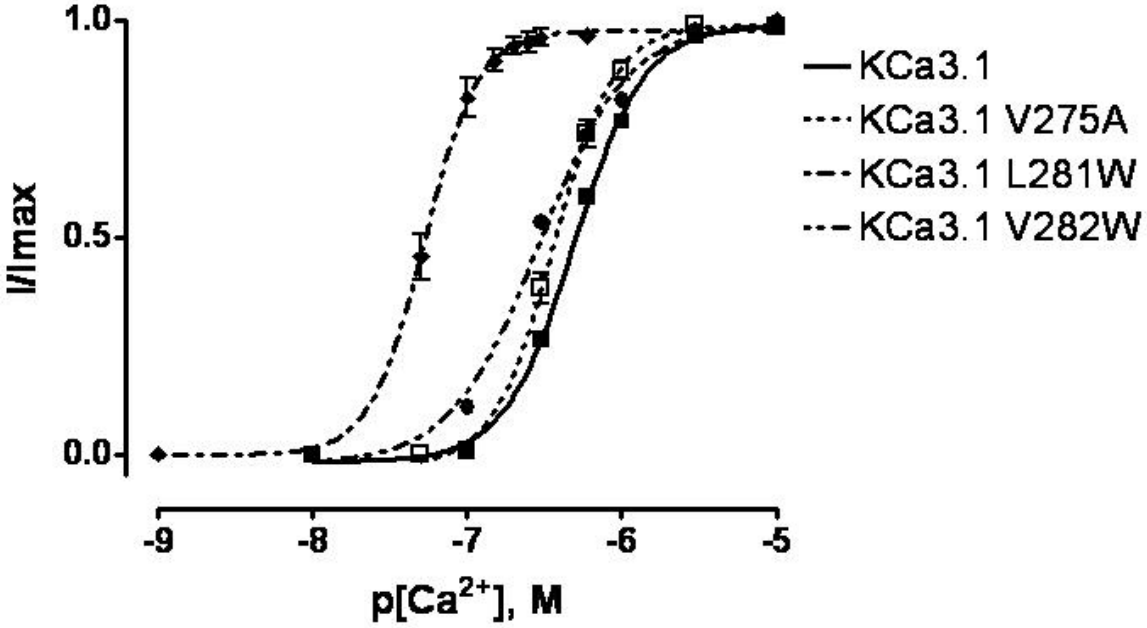

Figure A.4E

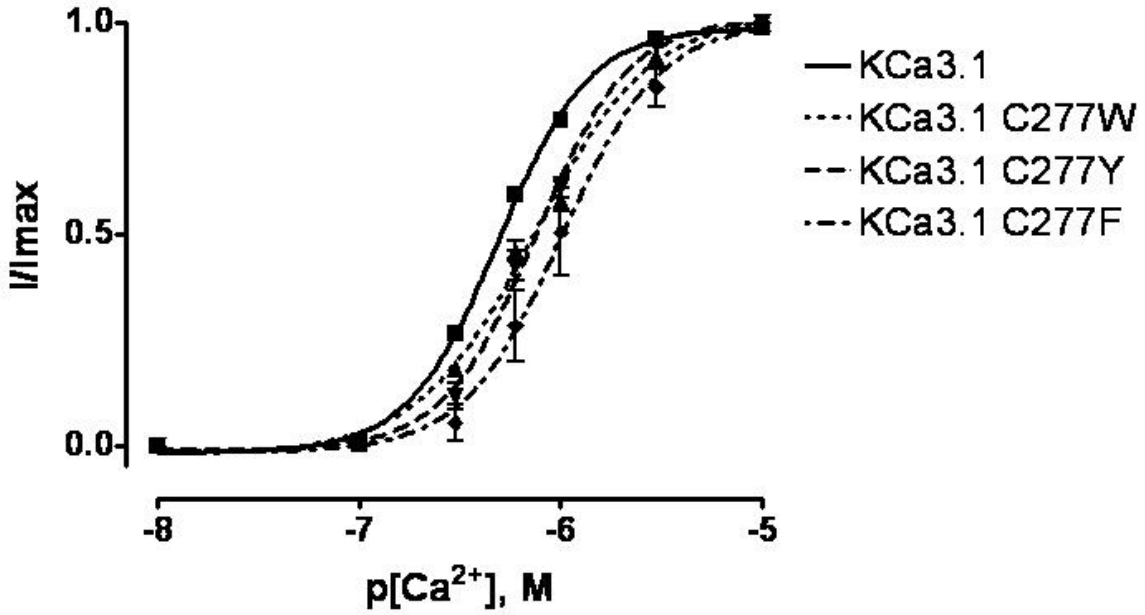


Figure A.4F

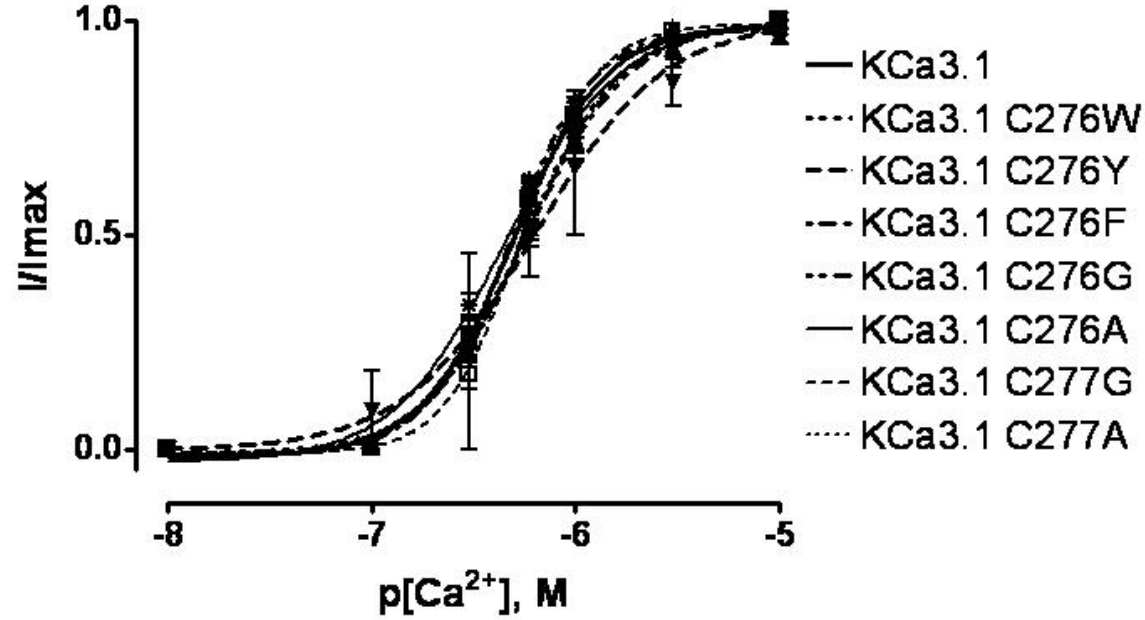

**Figure A.4 KCa3.1 $Ca^{2+}$ concentration response experiments.** Complete $Ca^{2+}$ concentration response experiments were performed to estimate the $EC_{50}$ and the Hill coefficients (h) for KCa3.1 and the corresponding mutations along S6. The patch was excised in 10 μM $Ca^{2+}_i$ followed by a series of $Ca^{2+}_i$ concentrations beginning with 0, 0.1, 0.3, 0.6, 1.0, 3.0, and 10 μM $Ca^{2+}_i$, all applied in 10 sec intervals using a rapid solution exchanger. Plot of normalized <I> current against the corresponding $Ca^{2+}_i$ for KCa3.1 S6 mutations fit with a variation of the Hill equation (see methods). The plots of KCa3.1 $Ca^{2+}$ response curves are organized in two ways: the first is according to the position and type of mutation and the second is according to the effect of the mutation. (A) Mutations at position C276 - C276W, C276Y, C276F, C276G, and C276A. (B) Mutations at position C277 - C277W, C277Y, C277F, C277G, and C277A. (C) Tryptophan mutations – C276W, C277W, L281W, and V282W. (D) Left shift in apparent $Ca^{2+}$ affinity - V275A, L281W, and V282W (E) Right shift in apparent $Ca^{2+}$ affinity - C277W, C277Y, and C277F and (F) No effect on apparent $Ca^{2+}$ affinity - C276W, C276Y, C276F, C276G, C276A, C277G, and C277A. The WT $Ca^{2+}$ response curve is included in every figure as a means for comparing the mutations. Refer to table A.2 for estimates of $EC_{50}$ and h. Error bars represent standard error of the mean (SEM).

Figure A.5A

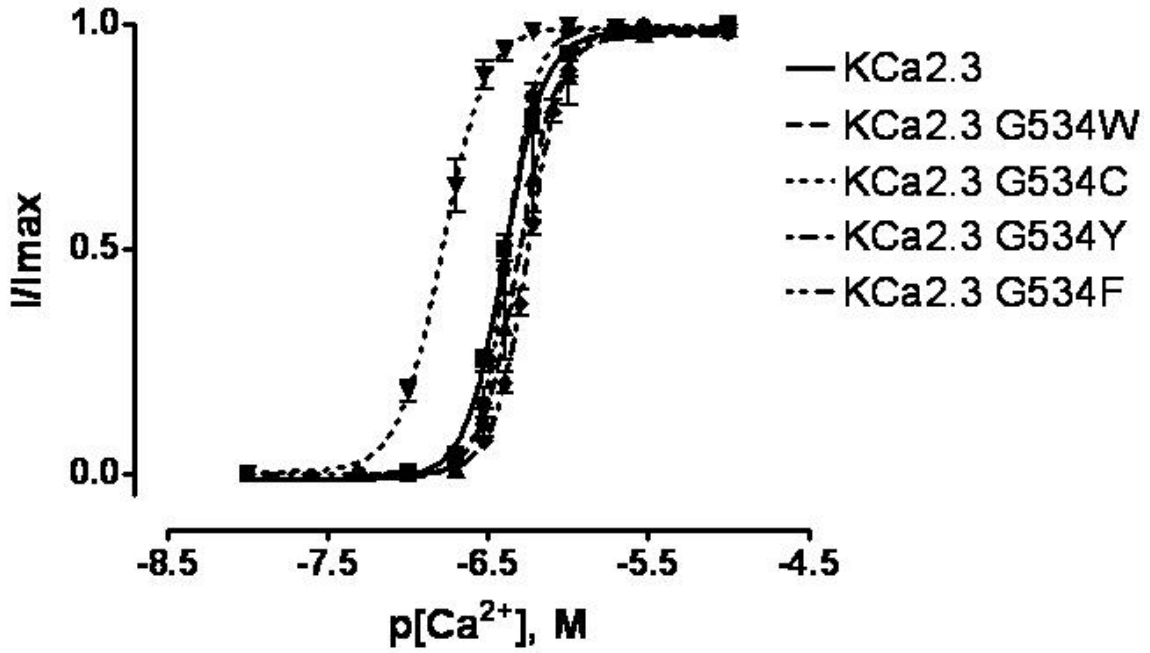


Figure A.5B

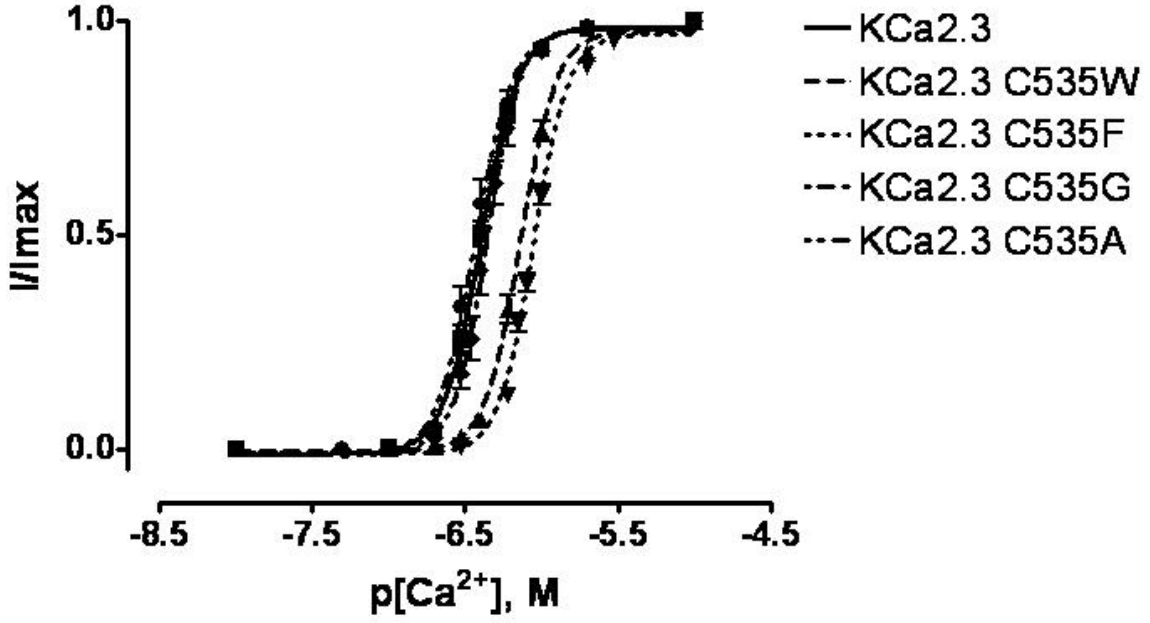

Figure A.5C

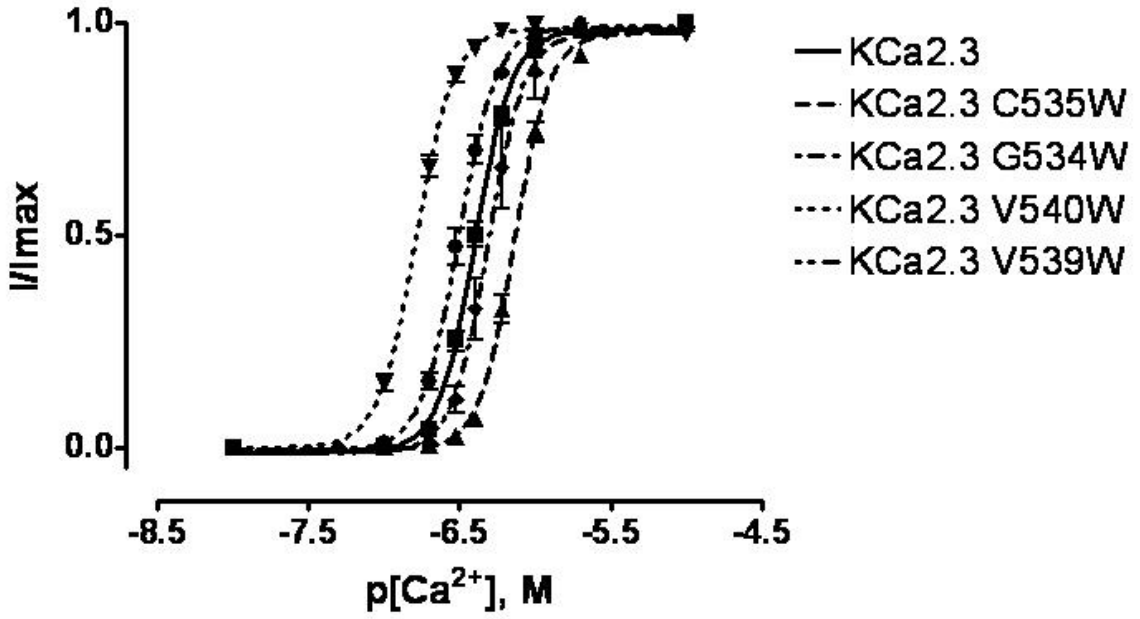


Figure A.5D

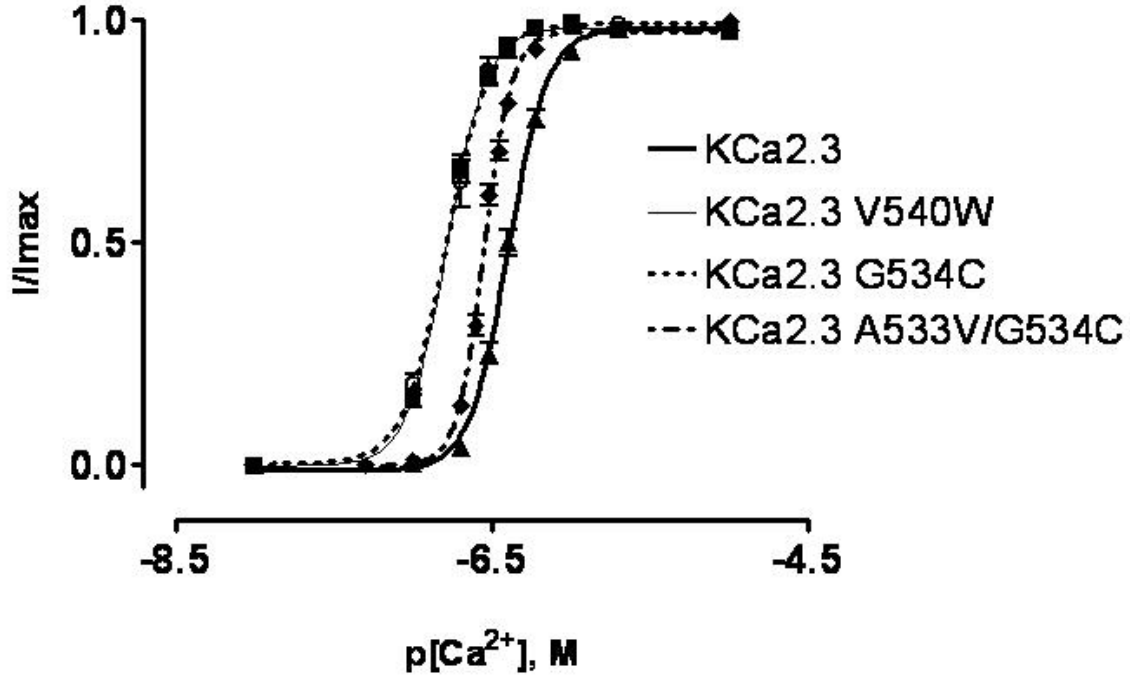

Figure A.5E

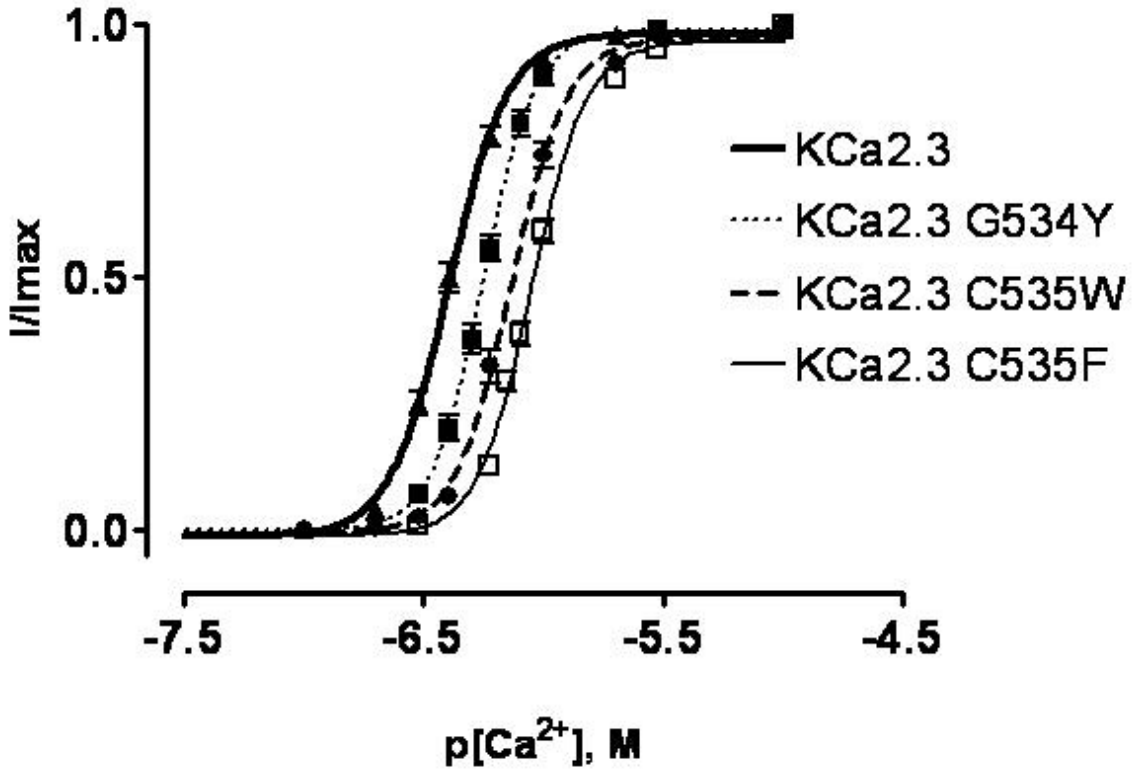


Figure A.5F

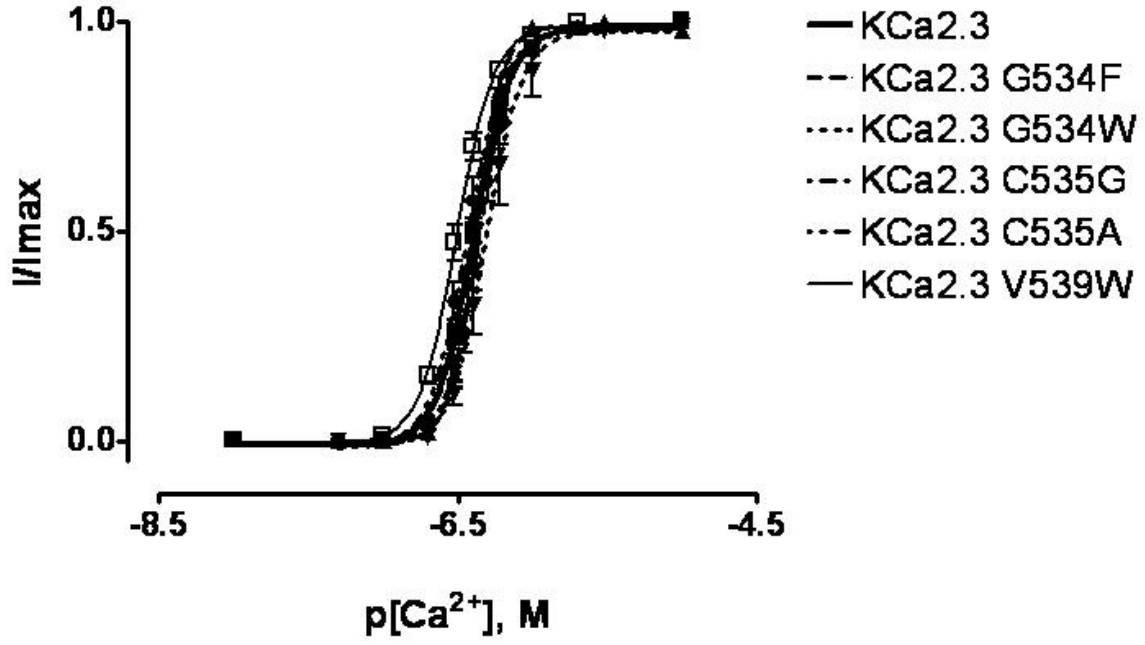

**Figure A.5. KCa2.3 $Ca^{2+}$ concentration response experiments.** Complete $Ca^{2+}$ concentration response experiments were performed to estimate the $EC_{50}$ and the Hill coefficients (h) for KCa2.3 and the corresponding mutations along S6. The patch was excised in 10 μM $Ca^{2+}_i$ followed by a series of $Ca^{2+}_i$ concentrations beginning with 0, 0.1, 0.3, 0.6, 1.0, 3.0, and 10 μM $Ca^{2+}_i$, all applied in 10 sec intervals using a rapid solution exchanger. Plot of normalized <I> current against the corresponding $Ca^{2+}_i$ for KCa2.3 S6 mutations fit with a variation of the Hill equation (see methods). The plots of KCa2.3 $Ca^{2+}$ response curves are organized in two ways: the first is according to the position and type of mutation and the second is according to the effect of the mutation. (A) Mutations at position G534 – G534W, G534C, G534Y, and G534F. (B) Mutations at position C535 – C535W, C535F, C535G, and C535A. (C) Tryptophan mutations – G534W, C535W, V539W, and V540W. (D) Left shift in apparent $Ca^{2+}$ affinity – V540W, G534C, and A533V/G534CV275A. (E) Right shift in apparent $Ca^{2+}$ affinity – G534Y, C535W, and C535F. (F) No effect on apparent $Ca^{2+}$ affinity – G534F, G534W, C535G, C535A, and V539W. The WT $Ca^{2+}$ response curve is included in every figure as a means for comparing the mutations. Refer to table A.3 for estimates of $EC_{50}$ and h. Error bars represent standard error of the mean (SEM).

Figure A.6A

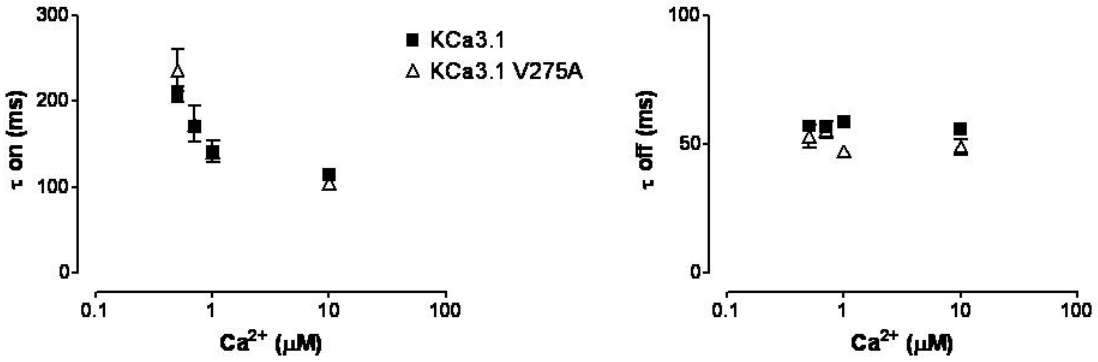


Figure A.6B

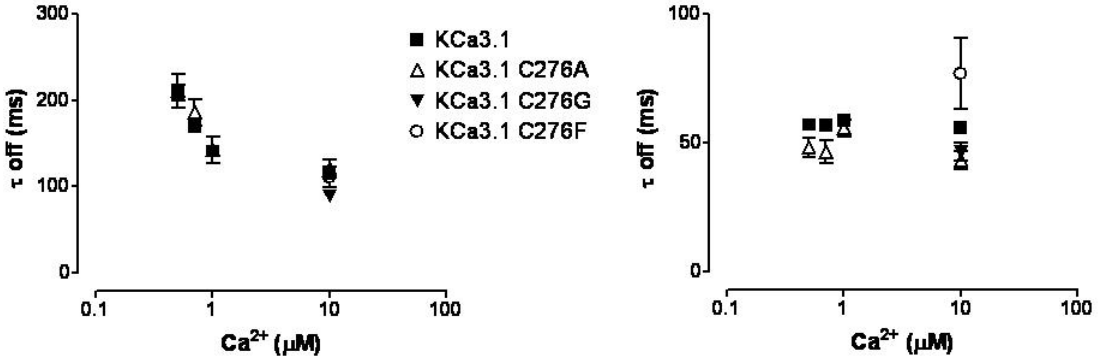


Figure A.6C

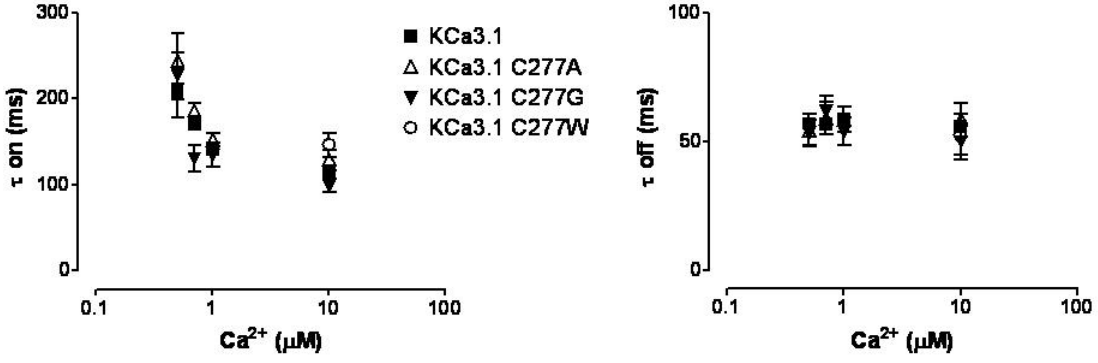

Figure A.6D

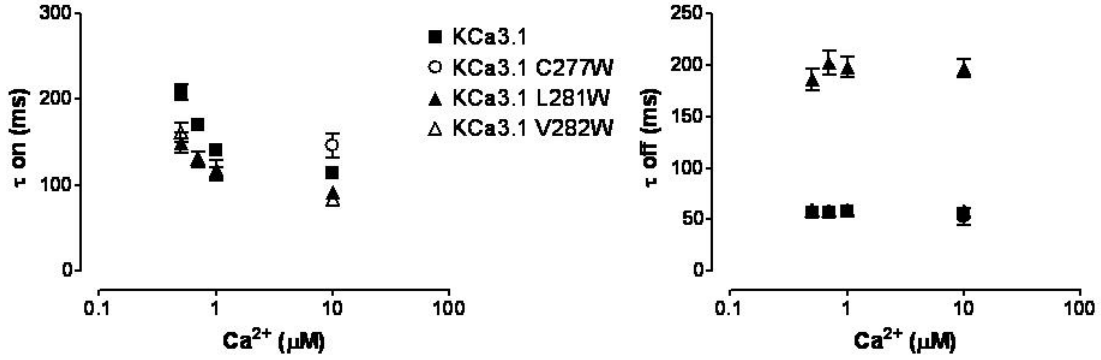


Figure A.6E

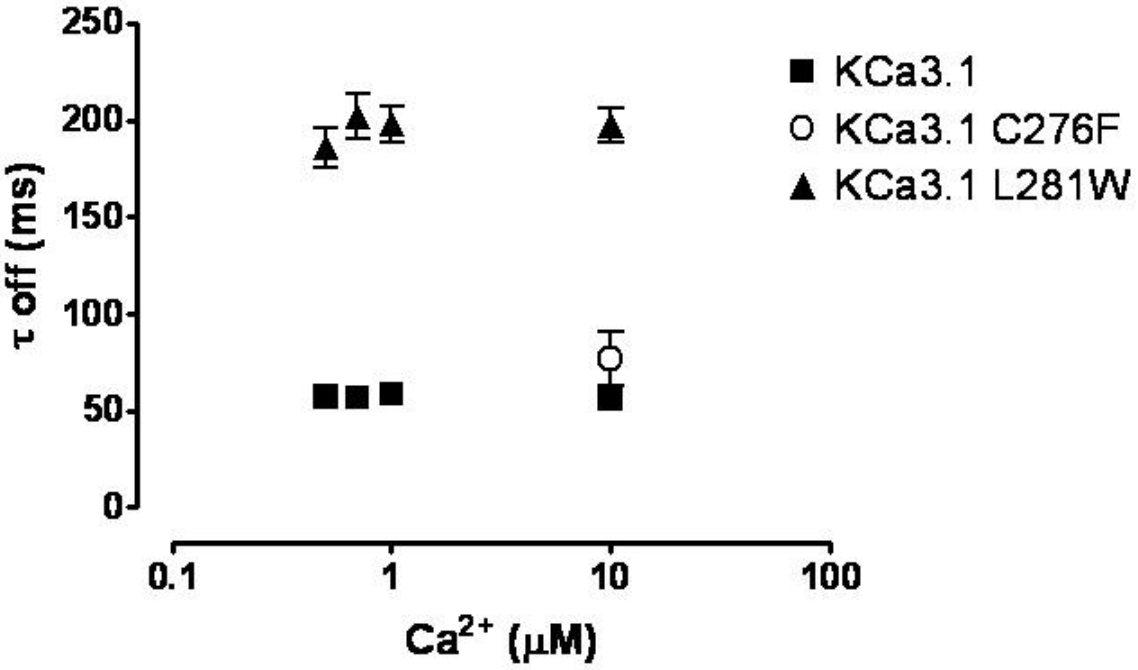

Figure A.6F

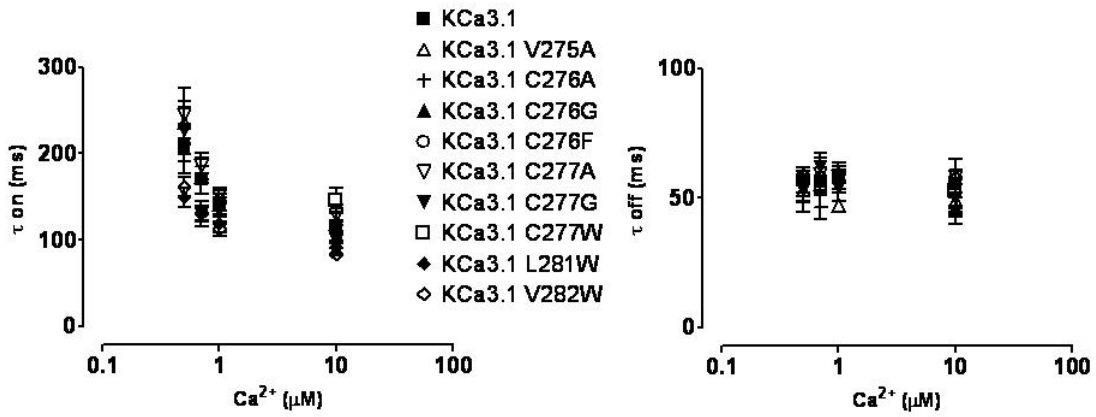


**Figure A.6. KCa3.1 activation and deactivation rates.** Activation and deactivation kinetics were estimated with $Ca^{2+}$-jump experiments for KCa3.1 and the corresponding mutations along S6. A rapid solution exchanger was utilized to quickly alternate between a $Ca^{2+}{}_i$-free solution and 1 of 4 $Ca^{2+}{}_i$ solutions: 0.5, 0.7, 1.0, and 10 μM $Ca^{2+}{}_i$ following the protocol illustrating one complete $Ca^{2+}$ cycle shown in the inset of figure (5). 5-10 complete $Ca^{2+}$ cycles were recorded from a single patch. Activation and deactivation sweeps were collected and averaged according to their respective $Ca^{2+}$-concentration. The graphs illustrating the activation (left panel) and deactivation rates (right panel) were estimated by fitting activation and deactivation records with an exponential function and reported as a time constant (τ-on and τ-off), see also Table (A.4). (A) Activation and deactivation rates between WT and the mutation at position V275 - V275A. (B) Activation and deactivation rates between WT and the mutations at position C276 - C276A, C276G, and C276F. (C) Activation and deactivation rates between WT and the mutations at position C277 - C277A, C277G, and C277W. (D) Activation and deactivation rates between WT and the tryptophan mutations - C277W, L281W, and V282W. (E) Mutations that slowed the deactivation process - C276F and L281W. (F) Mutations that had no effect on the activation and/or deactivation process – V275A, C276A, C276G, C276F, C277A, C277G, C277W, L281W, V282W.

Figure A.7A

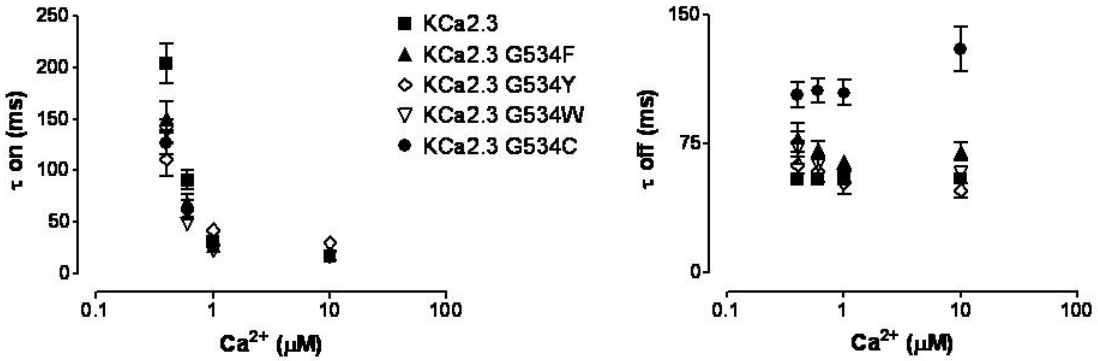


Figure A.7B

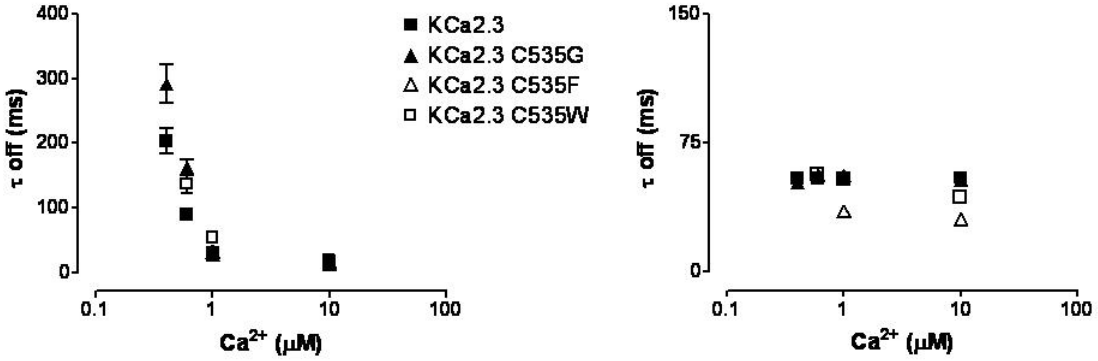


Figure A.7C

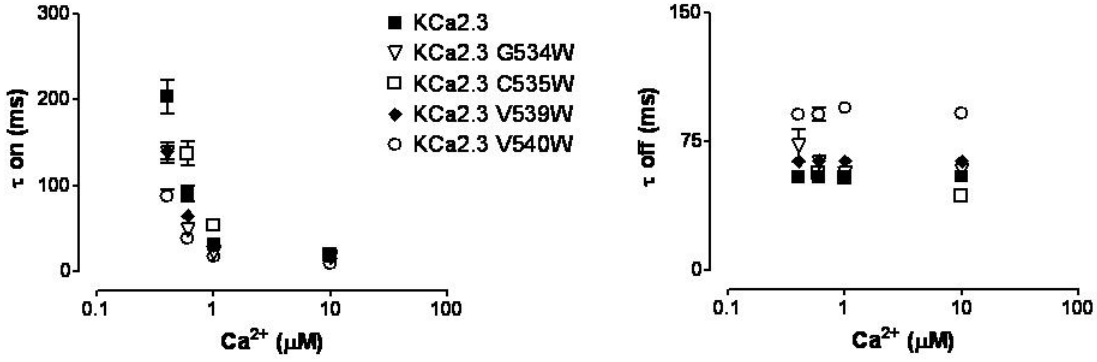

Figure A.7D

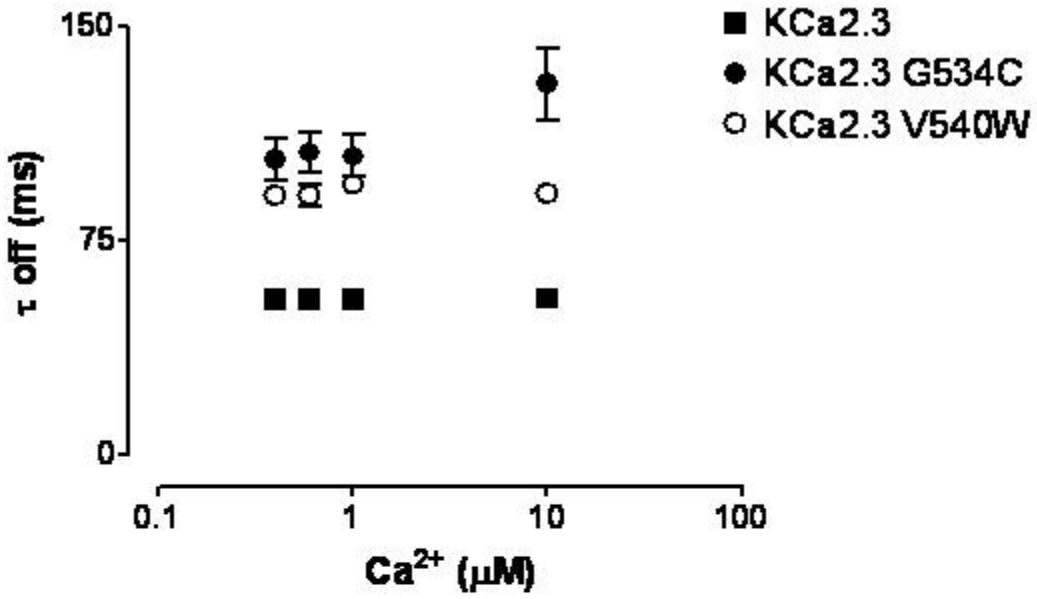
150
75
0
τ off (ms)
0.1
1
10
100
Ca2+ (μM)
KCa2.3
KCa2.3 G534C
KCa2.3 V540W

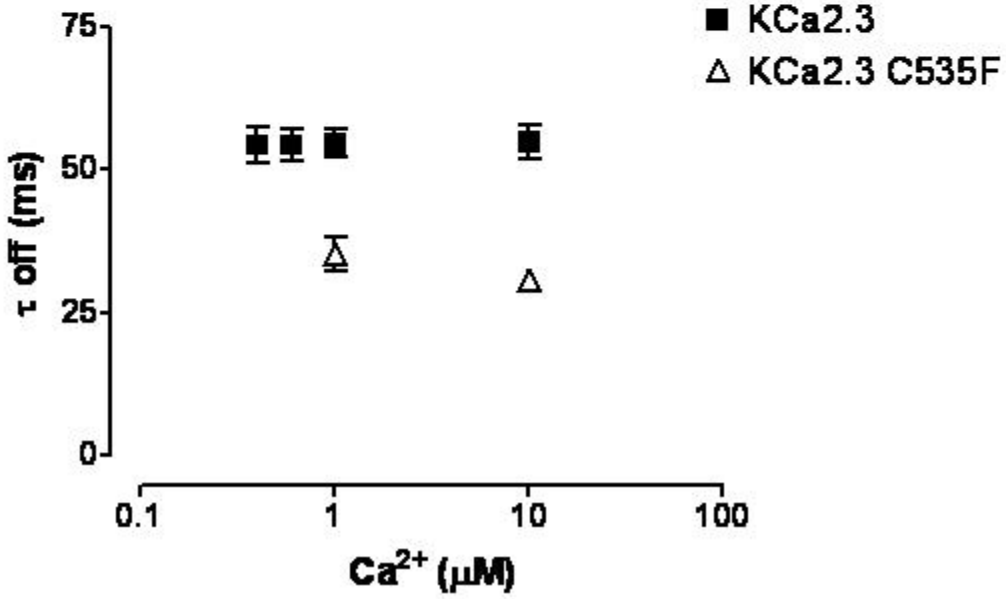
75
50
25
0
τ off (ms)
0.1
1
10
100
Ca2+ (μM)
KCa2.3
KCa2.3 C535F

Figure A.7E

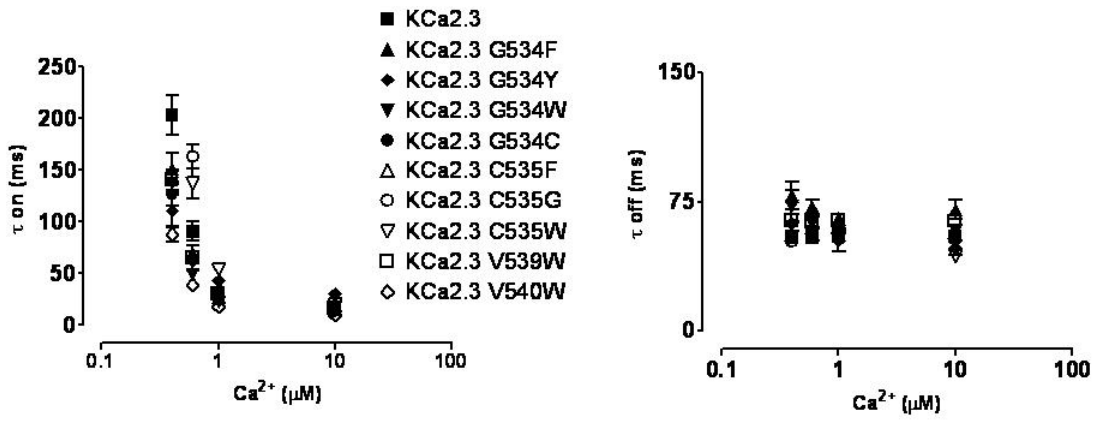


**Figure A.7. KCa2.3 activation and deactivation rates.** Activation and deactivation rates Activation and deactivation kinetics were estimated with $Ca^{2+}$-jump experiments for KCa2.3 and the corresponding mutations along S6. A rapid solution exchanger was utilized to quickly alternate between a $Ca^{2+}_i$-free solution and 1 of 4 $Ca^{2+}_i$ solutions: 0.5, 0.7, 1.0, and 10 μM $Ca^{2+}_i$ following the protocol illustrating one complete $Ca^{2+}$ cycle shown in the inset of figure (5). 5-10 complete $Ca^{2+}$ cycles were recorded from a single patch. Activation and deactivation sweeps were collected and averaged according to their respective $Ca^{2+}$-concentration. The graphs illustrating the activation (left panel) and deactivation rates (right panel) were estimated by fitting activation and deactivation records with an exponential function and reported as a time constant (τ-on and τ-off), see also Table (A.5). (A) Activation and deactivation rates between WT and the mutations at position G534 - G534F, G534Y, G534W, and G534C. (B) Activation and deactivation rates between WT and the mutations at position C535 - C535G, C535F, and C535W. (C) Activation and deactivation rates between WT and the tryptophan mutations - G534W, C535W, V539W, and V540W. (D) Top panel – mutations that slowed the deactivation process - G534C and V540W. Bottom panel – mutation that increase the rate of deactivation - C535F. (E) Mutations that had no effect on the activation and/or deactivation process – G534F, G534Y, G534W, G534C, C535F, C535G, C535W, V539W, and V540W.

Figure A.8

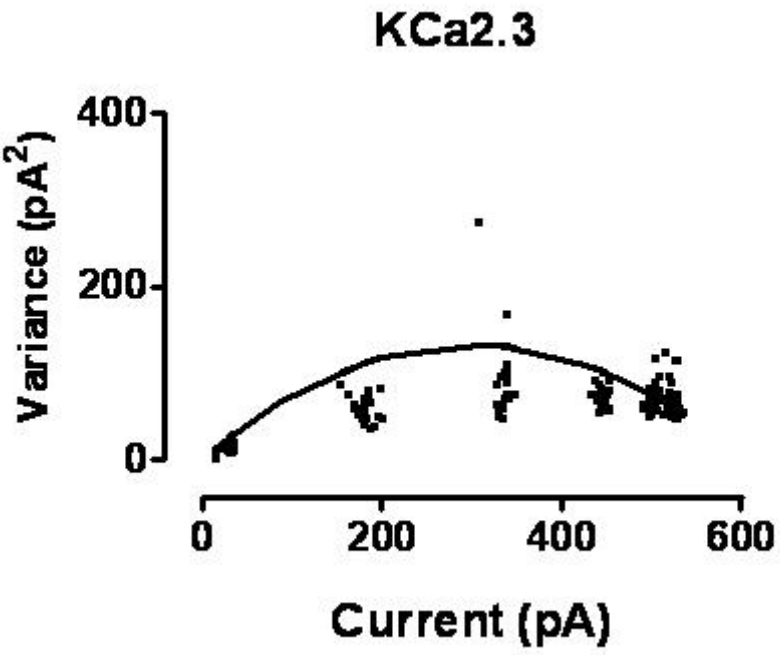


**Figure A.8. Estimate of KCa2.3 $P_{o(max)}$.** Variance analysis of KCa2.3 channel current was utilized to estimate $P_{o(max)}$. Plot of variance ($\sigma^2$), against mean current <I> as fit with Eq. 1 (solid line) and $P_{o(max)}$ was calculated using Eq. 2: $P_{o(max)} = 0.89$, N=680, and i=0.9 pA, n=1.

## 4.5 APPENDIX TABLES

**Table A.1. Sequence alignment between KCa3.1 and KCa2.3.** The clustal program was used to align the full-length sequences for KCa3.1 and KCa2.3. The highlighted area in S6 represents the region in KCa3.1 and KCa2.3 examined by site-directed mutagenesis. The regions of the channel comprising transmembrane domains 1-6 are underlined, in addition to the segment of the C-terminus representing the CaMBD.

Sequence Alignment

```
KCa3.1    ------------------------------------------------------------
KCa2.3    MSSCRYNGGVMRPLSNLSSSRRNLHEMDSEAQPLQPPASVVGGGGGASSPSAAAAASSSA 60


KCa3.1    --------------------MGGDLVLGLG------------------------------ 10
KCa2.3    PEIVVSKPEHNNSNNLALYGTGGGGSTGGGGGGGGGGGGSGHGSSSGTKSSKKKNQNIGY 120
                                      **.   * *

                             ______S1___________                _________
KCa3.1    ALRRRKRLLEQEKSLAGWALVLAGTGIGLMVLHAEMLWFGGCSWALYLFLVKCTISISTF 70
KCa2.3    KLGHRRALFEKRKRLSDYALIFGMFGIVVMVIETELSWGAYDKASLYSLALKCLISLSTI 180
           * :*: *:*:.* *:.:**::.  ** :**:.:*: * .  . :** : :** **:**:

          ___S2____                                 __________S3________
KCa3.1    LLLCLIVAFHAKEVQLFMTDNGLRDWRVALTGRQAAQIVLELVVCGLHPAPVRGPPCVQD 130
KCa2.3    ILLGLIIVYHAREIQLFMVDNGADDWRIAMTYERIFFICLEILVCAIHPIPGN---YTFT 237
          :** **:.:**:*:****.***  ***:*:* .:   * **::**.:** * .    .

                                              _________S4_________
KCa3.1    LGAPLTSPQPWPGFLGQGEALLSLAMLLRLYLVPRAVLLRSGVLLNASYRSIGALNQVRF 190
KCa2.3    WTARLAFSYAPSTTTADVDIILSIPMFLRLYLIARVMLLHSKLFTDASSRSIGALNKINF 297
            * *: . . .   .: : :**:.*:*****:.*.:**:* :: :** *******::.*

                      __________S5_____________                 ________
KCa3.1    RHWFVAKLYMNTHPGRLLLGLTLGLWLTTAWVLSVAER--QAVNATGHLSDTLWLIPITF 248
KCa2.3    NTRFVMKTLMTICPGTVLLVFSISLWIIAAWTVRACERYHDQQDVTSNFLGAMWLISITF 357
          .  ** *  *.  ** :** :::.**: :**.: ..**  :  :.*.:: .::***.***

          ____P-Loop_____  ________S6_________ ____________________________
KCa3.1    LTIGYGDVVPGTMWGKIVCLCTGVMGVCCTALLVAVVARKLEFNKAEKHVHNFMMDIQYT 308
KCa2.3    LSIGYGDMVPNTYCGKGVCLLTGIMGAGCTALVVAVVARKLELTKAEKHVHNFMMDTQLT 417
          *:*****:**.*  ** *** **:**. ****:*********:.************ * *

                          _____CaMBD_____________________________________
KCa3.1    KEMKESAARVLQEAWMFYKHTR--RKESHA-ARRHQRKLLAAINAFRQVRLKHRKLREQV 365
KCa2.3    KRVKNAAANVLRETWLIYKNTKLVKKIDHAKVRKHQRKFLQAIHQLRSVKMEQRKLNDQA 477
          *.:*::**.**:*:*::**:*:  :* .** .*:****:* **: :*.*:::***.:*.

          _______________
KCa3.1    NSMVDISKMHMILYDLQQNLSSSHR-------ALEKQIDTLAGKLDALTELLSTALGPRQ 418
KCa2.3    NTLVDLAKTQNIMYDMISDLNERSEDFEKRIVTLETKLETLIGSIHALPGLISQTIRQQQ 537
          *::**::* : *:**: .:*..  .       :**.:::** *.:.**. *:* ::  :*


KCa3.1    ---------------------------------LPEPSQQSK 427
KCa2.3    RDFIETQMENYDKHVTYNAERSRSSSRRRRSSSTAPPTSSESS 580
                                           * .*.:*.
```

Table A.2

**Table A.2. KCa3.1 $Ca^{2+}$ concentration experiments.** Results from $Ca^{2+}$ concentration response experiments on KCa3.1 and all of the corresponding mutations that were capable of expressing macroscopic currents. $EC_{50}$ and Hill coefficients (h) were calculated by fitting the plot of the normalized <I> current against the corresponding $Ca^{2+}{}_i$ with a variation of the Hill equation as described in the Materials and Methods section. The number of times the experiment was performed is represented by (n).

| Construct | $EC_{50}$ | h | n |
|---|---|---|---|
| WT | 508±13 nM | 2.0±0.1 | 57 |
| V275A | 377±28 nM | 2.4±0.1 | 11 |
| C276A | 460±27 nM | 1.7±0.04 | 18 |
| C276F | 482±31 nM | 2.3±0.2 | 10 |
| C276G | 570±51 nM | 1.7±0.1 | 5 |
| C276W | 565±48 nM | 1.9±0.05 | 7 |
| C276Y | 631±286 nM | 1.4±0.2 | 2 |
| C277A | 566±24 nM | 1.9±0.1 | 15 |
| C277F | 1048±258 nM | 1.9±0.1 | 2 |
| C277G | 542±44 nM | 2.5±0.1 | 4 |
| C277W | 761±53 nM | 1.5±0.1 | 6 |
| C277Y | 753±51 nM | 2.0±0.1 | 8 |
| L281W | 54±6 nM | 3.2±0.2 | 12 |
| V282W | 296±14 nM | 1.6±0.1 | 12 |

Table A.3

**Table A.3. KCa2.3 $Ca^{2+}$ concentration experiments.** Results from $Ca^{2+}$ concentration response experiments on KCa2.3 and all of the corresponding mutations capable of expressing macroscopic currents. $EC_{50}$ and Hill coefficients (h) were calculated by fitting the plot of the normalized <I> current against the corresponding $Ca^{2+}{}_i$ with a variation of the Hill equation as described in the Materials and Methods section. The number of times the experiment was performed is represented by (n).

| Construct | $EC_{50}$ | h | n |
|---|---|---|---|
| KCa2.3 | 411±14 nM | 4.0±0.1 | 30 |
| A533V/G534C | 284±6 nM | 5.2±0.3 | 9 |
| G534C | 165±14 nM | 3.6±0.1 | 12 |
| G534F | 418±17 nM | 5.1±0.2 | 6 |
| G534W | 530±77 nM | 4.2±0.3 | 6 |
| C535A | 375±24 nM | 3.8±0.2 | 7 |
| C535F | 891±19 nM | 4.0±0.2 | 13 |
| C535G | 450±27 nM | 4.5±0.2 | 12 |
| C535W | 737±28 nM | 4.0±0.1 | 16 |
| V539W | 318±15 nM | 3.8±0.1 | 14 |
| V540W | 164±6 nM | 3.6±0.2 | 10 |

Table A.4

**Table A.4 KCa3.1 activation and deactivation rates.** Activation and deactivation time constants from $Ca^{2+}$ jump experiments on KCa3.1 and all of the corresponding mutations capable of expressing macroscopic currents. Activation (tau (τ) on) and deactivation (tau (τ) off) time constants were estimated by fitting activation and deactivation records with an exponential function as reported in the Materials and Methods section. The number of times the experiment was performed is represented by (n).

| Construct | $Ca^{2+}$ (μM) | τ on (ms) | τ off (ms) | n |
|---|---|---|---|---|
| KCa3.1 | 0.5 | 209±9 | 57±2 | 51 |
| | 0.7 | 170±5 | 57±2 | 51 |
| | 1.0 | 141±5 | 59±2 | 51 |
| | 10 | 114±5 | 56±2 | 51 |
| V275A | 0.5 | 236±24 | 53±4 | 9 |
| | 0.7 | 173±21 | 55±3 | 9 |
| | 1.0 | 141±12 | 47±2 | 9 |
| | 10 | 104±5 | 49±3 | 9 |
| C276A | 0.5 | 211±20 | 48±4 | 7 |
| | 0.7 | 186±15 | 46±4 | 7 |
| | 1.0 | 142±15 | 56±3 | 7 |
| | 10 | 120±11 | 43±3 | 7 |
| C276F | 10 | 111±12 | 77±14 | 5 |
| C276G | 10 | 89±6 | 47±4 | 2 |

| | | | | |
|---|---|---|---|---|
| C277A | 0.5 | 244±10 | 54±6 | 6 |
| | 0.7 | 186±9 | 59±6 | 6 |
| | 1.0 | 152±8 | 59±5 | 6 |
| | 10 | 129±12 | 59±7 | 6 |
| C277G | 0.5 | 227±49 | 53±5 | 3 |
| | 0.7 | 130±15 | 62±6 | 3 |
| | 1.0 | 135±14 | 54±5 | 3 |
| | 10 | 99±8 | 50±7 | 3 |
| C277W | 10 | 146±14 | 53±8 | 7 |
| L281W | 0.5 | 149±12 | 186±11 | 23 |
| | 0.7 | 130±9 | 202±11 | 23 |
| | 1.0 | 119±10 | 198±9 | 23 |
| | 10 | 92±7 | 197±8 | 23 |
| V282W | 0.5 | 161±11 | 59±3 | 13 |
| | 0.7 | 131±8 | 59±2 | 13 |
| | 1.0 | 113±8 | 59±3 | 13 |
| | 10 | 84±5 | 58±3 | 13 |

Table A.5

**Table A.5 KCa2.3 activation and deactivation rates.** Activation and deactivation time constants from $Ca^{2+}$ jump experiments on KCa2.3 and all of the corresponding mutation capable of expressing macroscopic currents. Activation (tau (τ) on) and deactivation (tau (τ) off) time constants were estimated by fitting activation and deactivation records with an exponential function as reported in the Materials and Methods section. The number of times the experiment was performed is represented by (n). In a couple of constructs the apparent $Ca^{2+}$ affinity was right shifted and as a result macroscopic currents could only be observed and recorded in high [$Ca^{2+}$].

| Construct | $Ca^{2+}$ (μM) | τ on (ms) | τ off (ms) | n |
|---|---|---|---|---|
| KCa2.3 | 0.4 | 204±19 | 54±3 | 8 |
| | 0.6 | 91±9 | 54±3 | 8 |
| | 1.0 | 32±2 | 55±2 | 8 |
| | 10 | 17±1 | 55±3 | 8 |
| G534C | 0.4 | 127±12 | 103±7 | 13 |
| | 0.6 | 64±6 | 106±7 | 13 |
| | 1.0 | 28±3 | 104±7 | 13 |
| | 10 | 18±2 | 130±3 | 13 |
| G534F | 0.4 | 152±15 | 78±8 | 5 |
| | 0.6 | 70±8 | 72±4 | 5 |
| | 1.0 | 28±1 | 65±3 | 5 |
| | 10 | 20±3 | 70±5 | 5 |

| | | | | |
|---|---|---|---|---|
| G534W | 0.4 | 138±12 | 73±9 | 4 |
| | 0.6 | 49±2 | 63±4 | 4 |
| | 1.0 | 22±2 | 57±1 | 4 |
| | 10 | 17±2 | 58±3 | 4 |
| G534Y | 0.4 | 111±17 | 63±5 | 6 |
| | 0.6 | 62±9 | 59±7 | 6 |
| | 1.0 | 43±5 | 52±7 | 6 |
| | 10 | 30±5 | 48±4 | 6 |
| C277G | 0.5 | 227±49 | 53±5 | 3 |
| | 0.7 | 130±15 | 62±6 | 3 |
| | 1.0 | 135±14 | 54±5 | 3 |
| | 10 | 99±8 | 50±7 | 3 |
| C535F | 0.4 | - | - | - |
| | 0.6 | - | - | - |
| | 1.0 | 33±3 | 35±3 | 8 |
| | 10 | 15±2 | 30±2 | 8 |
| C535G | 0.4 | 292±30 | 52±2 | 8 |
| | 0.6 | 163±12 | 56±1 | 8 |
| | 1.0 | 29±5 | 56±1 | 8 |
| | 10 | 13±1 | 54±2 | 8 |

| | | | | |
|---|---|---|---|---|
| C535W | 0.4 | - | - | - |
| | 0.6 | 137±14 | 56±3 | 12 |
| | 1.0 | 53±4 | 54±2 | 12 |
| | 10 | 19±2 | 43±2 | 12 |
| V539W | 0.4 | 140±10 | 64±3 | 9 |
| | 0.6 | 65±4 | 64±4 | 9 |
| | 1.0 | 30±3 | 64±3 | 9 |
| | 10 | 16±2 | 64±3 | 9 |
| V540W | 0.4 | 88±7 | 91±3 | 7 |
| | 0.6 | 39±3 | 91±4 | 7 |
| | 1.0 | 18±1 | 95±3 | 7 |
| | 10 | 10±1 | 92±3 | 7 |

Table A.6A **Table A.6. Primers.** Primers used for site directed mutagenesis in KCa3.1 (6A) and KCa2.3 (6B). Bold indicates the amino acid mutation and the corresponding nucleotide change.

KCa3.1

| | | |
|---|---|---|
| V275**W** | F | 5′ ACTGGAGTCATGGGT**TGG**TGCTGCACAGCCCTGCTG 3′ |
| | R | 5′ CAGGGCTGTGCAGCA**CCA**ACCCATGACTCCAGTGCA 3′ |
| C276**A** | F | 5′ GGAGTCATGGGTGTC**GCC**TGCACAGCCCTGCTG 3′ |
| | R | 5′ CAGCAGGGCTGTGCA**GGC**GACACCCATGACTCC 3′ |
| C276**D** | F | 5′ GGAGTCATGGGTGTC**GAC**TGCACAGCCCTGCTG 3′ |
| | R | 5′ CAGCAGGGCTGTGCA**GTC**GACACCCATGACTCC 3′ |
| C276**F** | F | 5′ GGAGTCATGGGTGTC**TTC**TGCACAGCCCTGCTG 3′ |
| | R | 5′ CAGCAGGGCTGTGCA**GAA**GACACCCATGACTCC 3′ |
| C276**G** | F | 5′ GGAGTCATGGGTGTC**GGC**TGCACAGCCCTGCTG 3′ |
| | R | 5′ CAGCAGGGCTGTGCA**GCC**GACACCCATGACTCC 3′ |
| C276**W** | F | 5′ GGAGTCATGGGTGTC**TGG**TGCACAGCCCTGCTG 3′ |
| | R | 5′ CAGCAGGGCTGTGCA**CCA**GACACCCATGACTCC 3′ |
| C276**Y** | F | 5′ GGAGTCATGGGTGTC**TAC**TGCACAGCCCTGCTG 3′ |
| | R | 5′ CAGCAGGGCTGTGCA**GTA**GACACCCATGACTCC 3′ |
| C277**A** | F | 5′ GTCATGGGTGTCTGC**GCC**ACAGCCCTGCTGGTG 3′ |
| | F | 5′ CACCAGCAGGGCTGT**GGC**GCAGACACCCATGAC 3′ |
| C277**D** | F | 5′ GTCATGGGTGTCTGC**GAC**ACAGCCCTGCTGGTG 3′ |
| | R | 5′ CACCAGCAGGGCTGT**GTC**GCAGACACCCATGAC 3′ |
| C277**F** | F | 5′ GTCATGGGTGTCTGC**TTC**ACAGCCCTGCTGGTG 3′ |
| | R | 5′ CACCAGCAGGGCTGT**GAA**GCAGACACCCATGAC 3′ |
| C277**G** | F | 5′ GTCATGGGTGTCTGC**GGC**ACAGCCCTGCTGGTG 3′ |
| | R | 5′ CACCAGCAGGGCTGT**GCC**GCAGACACCCATGAC 3′ |
| C277**W** | F | 5′ GTCATGGGTGTCTGC**TGG**ACAGCCCTGCTGGTG 3′ |
| | R | 5′ CACCAGCAGGGCTGT**CCA**GCAGACACCCATGAC 3′ |
| C277**Y** | F | 5′ GTCATGGGTGTCTGC**TAC**ACAGCCCTGCTGGTG 3′ |
| | R | 5′ CACCAGCAGGGCTGT**GTA**GCAGACACCCATGAC 3′ |
| T278**W** | F | 5′ ATGGGTGTCTGCTGC**TGG**GCCCTGCTGGTGGCC 3′ |
| | R | 5′ GGCCACCAGCAGGGC**CCA**GCAGCAGACACCCAT 3′ |
| A279**W** | F | 5′ GGTGTCTGCTGCACA**TGG**CTGCTGGTGGCCGTG 3′ |
| | R | 5′ CACGCCCACCAGCAG**CCA**TGTGCAGCAGACACC 3′ |

| | | |
|---|---|---|
| L280**W** | F 5′ | GTCTGCTGCACAGCC**TGG**CTGGTGGCCGTGGTG 3′ |
| | R 5′ | CACCACGCCCACCAG**CCA**GGCTGTGCAGCAGAC 3′ |
| L281**W** | F 5′ | TGCTGCACAGCCCTG**TGG**GTGGCCGTGGTGGCC 3′ |
| | R 5′ | GGCCACCACGGCCAC**CCA**CAGGGCTGTGCAGCA 3′ |
| V282**W** | F 5′ | TGCACAGCCCTGCTG**TGG**GCCGTGGTGGCCCGG 3′ |
| | R 5′ | CCGGGCCACCACGCC**CCA**CAGCAGGGCTGTGCA 3′ |
| V275**A**/C276**G** | F 5′ | ACTGGAGTCATGGGT**GCCGGC**TGCACAGCCCTG 3′ |
| | F 5′ | CAGGGCTGTGCAGCC**GGCACC**CATGACTCCAGT 3′ |

Table A.6B

KCa2.3

| | | |
|---|---|---|
| G532**W** | F 5′ | CTCACTGGCATCATG**TGG**GCAGGCTGCACTGCC 3′ |
| | R 5′ | GGCAGTGCAGCCTGC**CCA**CATGATGCCAGTGAG 3′ |
| A533**V** | F 5′ | ACTGGCATCATGGGT**GTA**GGCTGCACTGCCCTC 3′ |
| | R 5′ | GAGGGCAGTGCAGCC**TAC**ACCCATGATGCCAGT 3′ |
| A533**W** | F 5′ | CTCACTGGCATCATGGGT**TGG**GGCTGCACTGCCCTC 3′ |
| | R 5′ | GAGGGCAGTGCAGCC**CCA**ACCCATGATGCCAGTGAG 3′ |
| G534**C** | F 5′ | GGCATCATGGGTGCA**TGC**TGCACTGCCCTCGTG 3′ |
| | R 5′ | CACGAGGGCAGTGCA**GCA**TGCACCCATGATGCC 3′ |
| G534**D** | F 5′ | GGCATCATGGGTGCA**GAC**TGCACTGCCCTCGTG 3′ |
| | R 5′ | CACGAGGGCAGTGCA**GTC**TGCACCCATGATGCC 3′ |
| G534**F** | F 5′ | GGCATCATGGGTGCA**TTC**TGCACTGCCCTCGTG 3′ |
| | R 5′ | CACGAGGCCAGTGCA**GAA**TGCACCCATGATGCC 3′ |
| G534**W** | F 5′ | GGCATCATGGGTGCA**TGG**TGCACTGCCCTCGTG 3′ |
| | R 5′ | CACGAGGGCAGTGCA**CCA**TGCACCCATGATGCC 3′ |
| G534**Y** | F 5′ | GGCATCATGGGTGCA**TAC**TGCACTGCCCTCGTG 3′ |
| | R 5′ | CACGAGGGCAGTGCA**GTA**TGCACCCATGATGCC 3′ |
| C535D | F 5′ | GGCATCATGGGTGCAGGC**GAC**ACTGCCCTCGTGGTAGCT 3′ |
| | R 5′ | AGCTACCACGAGGGCAGT**GTC**GCCTGCACCCATGATGCC 3′ |
| C535F | F 5′ | GGCATCATGGGTGCAGGC**TTC**ACTGCCCTCGTGGTAGCT 3′ |
| | R 5′ | AGCTACCACGAGGGCAGT**GAA**GCCTGCACCACTGATGCC 3′ |
| C535G | F 5′ | GGCATCATGGGTGCAGGC**GGC**ACTGCCCTCGTGGTAGCT 3′ |
| | R 5′ | AGCTACCACGAGGGCAGT**GCC**GCCTGCACCCATGATGCC 3′ |
| C535W | F 5′ | GGCATCATGGGTGCAGGC**TGG**ACTGCCCTCGTGGTAGCT 3′ |
| | R 5′ | AGCTACCACGAGGGCAGT**CCA**GCCTGCACCCATGATGCC 3′ |
| C535Y | F 5′ | GGCATCATGGGTGCAGGC**TAC**ACTGCCCTCGTGGTAGCT 3′ |
| | R 5′ | AGCTACCACGAGGGCAGT**GTA**GCCTGCACCCATGATGCC 3′ |
| T536W | F 5′ | ATGGGTGCAGGCTGC**TGG**GCCCTCGTGGTAGCT 3′ |
| | R 5′ | AGCTACCACGAGGGC**CCA**GCAGCCTGCACCCAT 3′ |
| A537W | F 5′ | GGTGCAGGCTGCACT**TGG**CTCGTGGTAGCTGTGGTTGCC 3′ |
| | R 5′ | GGCAACCACAGCTACCACGAG**CCA**AGTGCAACCTGCACC 3′ |
| L538W | F 5′ | GCAGGCTGCACTGCC**TGG**GTGGTAGCTGTGGTTGCC 3′ |
| | R 5′ | GGCAACCACAGCTACCAC**CCA**GGCAGTGCAGCCTGC 3′ |
| V539W | F 5′ | GGCTGCACTGCCCTC**TGG**GTAGCTGTGGTTGCC 3′ |
| | R 5′ | GGCAACCACAGCTAC**CCA**GAGGGCAGTGCAGCC 3′ |

| | | |
|---|---|---|
| V540W | F | 5′ TGCACTGCCCTCGTG**TGG**GCTGTGGTTGCCCGG 3′ |
| | R | 5′ CCGGGCAACCACAGC**CCA**CACGAGGGCAGTGCA 3′ |
| A533V/G534C | F | 5′ GGCATCATGGGT**GTATGC**TGCACTGCCCTCGTGGTAGCT 3′ |
| | R | 5′ AGCTACCACGAGGGCAGTGCA**GCATAC**ACCCATGATGCC 3′ |

Table A.7A

Sensitivity Analysis

| Sensitivity Analysis KCa3.1: linear dependence on $Ca^{2+}$ concentration, k=A·[Ca]. Data set #1 | | | |
|---|---|---|---|
| Kinetic Transition | Rate Constant | Change in Error +10% rate constant | Change in Error -10% rate constant |
| 12 | 7 $\mu M^{-1}$ $s^{-1}$ | 14% | 17% |
| 21 | 36 $s^{-1}$ | 10% | 12% |
| 23 | 1200 $\mu M^{-1}$ $s^{-1}$ | 13% | 16% |
| 32 | 230 $s^{-1}$ | 13% | 16% |
| 34 | * | * | * |
| 43 | * | * | * |
| 35 | 35 $s^{-1}$ | 51% | 58% |
| 53 | 16 $s^{-1}$ | 50% | 61% |
| 46 | * | * | * |
| 64 | * | * | * |

total error = 31

Table A.7B

Sensitivity Analysis KCa3.1: non-linear dependence on $Ca^{2+}$ concentration, k=A·[Ca]/(B+[Ca]).

Data set #1

| Kinetic Transition | Rate Constant | Change in Error +10% rate constant | Change in Error -10% rate constant |
|---|---|---|---|
| 12 | 30 $\mu M^{-1} s^{-1}$ | 10% | 5% |
| 21 | 26 $s^{-1}$ | 4% | 7% |
| 23 | 2700 $\mu M^{-1} s^{-1}$ | 10% | 9% |
| 32 | 230 $s^{-1}$ | 8% | 12% |
| 34 | * | * | * |
| 43 | * | * | * |
| 35 | 27 $s^{-1}$ | 37% | 35% |
| 53 | 15 $s^{-1}$ | 30% | 45% |
| 46 | * | * | * |
| 64 | * | * | * |

total error = 38

Table A.7C

Sensitivity Analysis KCa3.1: linear-dependence on $Ca^{2+}$ concentration, k=A·[Ca]. Data set #2 (paired)

| Kinetic Transition | Rate Constant | Change in Error +10% rate constant | Change in Error -10% rate constant |
|---|---|---|---|
| 12 | 5 $\mu M^{-1}$ $s^{-1}$ | 8% | 10% |
| 21 | 21 $s^{-1}$ | 4% | 6% |
| 23 | 1740 $\mu M^{-1}$ $s^{-1}$ | 6% | 8% |
| 32 | 280 $s^{-1}$ | 7% | 8% |
| 34 | * | * | * |
| 43 | * | * | * |
| 35 | 32 $s^{-1}$ | 37% | 44% |
| 53 | 21 $s^{-1}$ | 38% | 43% |
| 46 | * | * | * |
| 64 | * | * | * |

total error = 38

Table A.7D

Sensitivity Analysis KCa3.1: non-linear dependence on $Ca^{2+}$ concentration, k=A·[Ca]/(B+[Ca]).

Data set #2 (paired)

| Kinetic Transition | Rate Constant | Change in Error +10% rate constant | Change in Error -10% rate constant |
|---|---|---|---|
| 12 | 24 $\mu M^{-1} s^{-1}$ | 8% | 11% |
| 21 | 42 $s^{-1}$ | 6% | 6% |
| 23 | 8150 $\mu M^{-1} s^{-1}$ | 6% | 9% |
| 32 | 150 $s^{-1}$ | 7% | 7% |
| 34 | * | * | * |
| 43 | * | * | * |
| 35 | 39 $s^{-1}$ | 34% | 42% |
| 53 | 24 $s^{-1}$ | 36% | 40% |
| 46 | * | * | * |
| 64 | * | * | * |

total error = 38

Table A.7E

Sensitivity Analysis KCa3.1+PCMBS: linear dependence on $Ca^{2+}$ concentration, k=A·[Ca]. Data set #2 (paired)

| Kinetic Transition | Rate Constant | Change in Error +10% rate constant | Change in Error -10% rate constant |
|---|---|---|---|
| 12 | 5 $\mu M^{-1}$ $s^{-1}$ | 1% | 2% |
| 21 | 23 $s^{-1}$ | 1% | 1% |
| 23 | 550 $\mu M^{-1}$ $s^{-1}$ | 1% | 2% |
| 32 | 660 $s^{-1}$ | 1% | 1% |
| 34 | * | * | * |
| 43 | * | * | * |
| 35 | 290 $s^{-1}$ | 1% | 2% |
| 53 | 4 $s^{-1}$ | 2% | 2% |
| 46 | * | * | * |
| 64 | * | * | * |

total error = 64

Table A.7F

Sensitivity Analysis KCa3.1+PCMBS: non-linear dependence on $Ca^{2+}$ concentration, $k=A\cdot[Ca]/(B+[Ca])$.

Data set #2 (paired)

| Kinetic Transition | Rate Constant | Change in Error +10% rate constant | Change in Error -10% rate constant |
|---|---|---|---|
| 12 | 10 $\mu M^{-1}$ $s^{-1}$ | 4% | 3% |
| 21 | 76 $s^{-1}$ | 3% | 3% |
| 23 | 2900 $\mu M^{-1}$ $s^{-1}$ | 3% | 4% |
| 32 | 2980 $s^{-1}$ | 3% | 4% |
| 34 | * | * | * |
| 43 | * | * | * |
| 35 | 290 $s^{-1}$ | 3% | 4% |
| 53 | 3 $s^{-1}$ | 5% | 4% |
| 46 | * | * | * |
| 64 | * | * | * |

total error = 45

Table A.7G

Sensitivity Analysis KCa3.1+PCMBS constrained: non-linear dependence on $Ca^{+}$ concentration, $k=A\cdot[Ca]/(B+[Ca])$.

| Kinetic Transition | Rate Constant | Change in Error +10% rate constant | Change in Error -10% rate constant |
|---|---|---|---|
| 12 | *27 $\mu M^{-1}$ $s^{-1}$ | 2% | 2% |
| 21 | *34 $s^{-1}$ | 1% | 1% |
| 23 | *5425 $\mu M^{-1}$ $s^{-1}$ | 1% | 2% |
| 32 | *190 $s^{-1}$ | 2% | 2% |
| 34 | * | * | * |
| 43 | * | * | * |
| 35 | *34 $s^{-1}$ | 3% | 5% |
| 53 | 3 $s^{-1}$ | 5% | 4% |
| 46 | * | * | * |
| 64 | * | * | * |

total error = 43

Table A.7H

Sensitivity Analysis KCa3.1 L281W: non-linear dependence on $Ca^{+}$ concentration, $k=A\cdot[Ca]/(B+[Ca])$.

| Kinetic Transition | Rate Constant | Change in Error +10% rate constant | Change in Error -10% rate constant |
|---|---|---|---|
| 12 | 11 $\mu M^{-1}$ $s^{-1}$ | 0.3% | 0.3% |
| 21 | 76 $s^{-1}$ | 0.2% | 0.2% |
| 23 | 12380 $\mu M^{-1}$ $s^{-1}$ | 0.2% | 0.2% |
| 32 | 192 $s^{-1}$ | 0.2% | 0.2% |
| 34 | * | * | * |
| 43 | * | * | * |
| 35 | 53 $s^{-1}$ | 2% | 3% |
| 53 | 5 $s^{-1}$ | 3% | 3% |
| 46 | * | * | * |
| 64 | * | * | * |

total error = 8

Table A.7I

Sensitivity Analysis KCa3.1 L281W constrained: non-linear dependence on $Ca^{+}$ concentration, k=A·[Ca]/(B+[Ca]).

| Kinetic Transition | Rate Constant | Change in Error +10% rate constant | Change in Error -10% rate constant |
|---|---|---|---|
| 12 | *27 $\mu M^{-1}$ $s^{-1}$ | 0.2% | 0.2% |
| 21 | *34 $s^{-1}$ | 0.2% | 0.1% |
| 23 | *5425 $\mu M^{-1}$ $s^{-1}$ | 0.2% | 0.3% |
| 32 | *190 $s^{-1}$ | 0.0% | 0.2% |
| 34 | * | * | * |
| 43 | * | * | * |
| 35 | *34 $s^{-1}$ | 2% | 2% |
| 53 | 4 $s^{-1}$ | 1% | 3% |
| 46 | * | * | * |
| 64 | * | * | * |

total error = 13

**Table A.7. Sensitivity analysis.** Rate constants and values from the sensitivity analysis. Sensitivity analysis was performed to determine whether the rate constants obtained from the kinetic modeling were the best estimates for the corresponding parameter. (A) Rate constants and sensitivity analysis values derived from the kinetic modeling of KCa3.1 assuming a linear dependence on $Ca^{2+}$ concentration. Current recordings were taken from data set #1. (B) KCa3.1 assuming a non-linear dependence on $Ca^{2+}$ concentration, recording were taken from data set #1. (C) KCa3.1 assuming a linear dependence on $Ca^{2+}$ concentration, recordings were taken from data set #2. (D) KCa3.1 assuming a non-linear dependence on $Ca^{2+}$ concentration, recordings were taken from data set #2. (E) KCa3.1+PCMBS assuming a linear dependence on $Ca^{2+}$ concentration, recordings were taken from data set #2. (F) KCa3.1+PCMBS assuming a non-linear dependence on $Ca^{2+}$ concentration, recordings were taken from data set #2. (G) KCa3.1+PCMBS constrained model, assuming a non-linear dependence on $Ca^{2+}$ concentration. Transitions 12, 21, 23, 32, 35 are fixed to the average value from KCa3.1 (without PCMBS) data sets #1 and #2. (H) KCa3.1 L281W assuming a non-linear dependence on $Ca^{2+}$ concentration. (I) KCa3.1 L281W constrained model assuming a non-linear dependence on $Ca^{2+}$ concentration. Transitions 12, 21, 23, 32, 35 are fixed to the average value from KCa3.1 (without PCMBS) data sets #1 and #2.

Table A.8

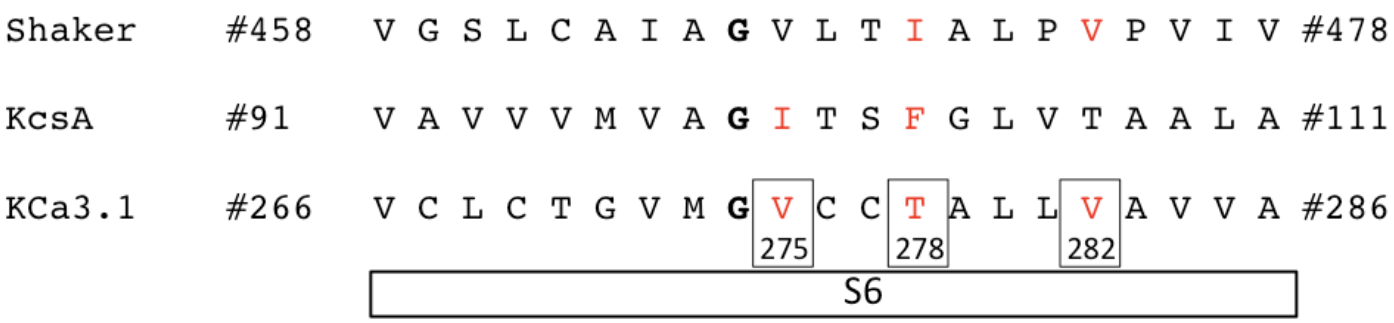


**Table A.8. Sequence alignment.** Sequence alignment of S6 between KCa3.1, KcsA, and Shaker illustrating a correspondence between residues Val$^{275}$ and Thr$^{278}$ to the known pore lining residues Ile$^{100}$ and Phe$^{103}$ in KcsA, and residues Thr$^{278}$ and Val$^{282}$ to the known pore lining residues Ile$^{402}$ and Val$^{406}$ in Shaker.

## BIBLIOGRAPHY


1. Nelson, D.L., *Lehninger Principles of Biochemistry*. Third ed. 2000, New York: Worth Publishers. 1152.

2. Creighton, T.E., *Proteins: Structures and Molecular Properties*. Second ed. 1993, New York: W.H. Freeman and Company. 473.

3. Koshland, D.E., Jr., G. Nemethy, and D. Filmer, *Comparison of experimental binding data and theoretical models in proteins containing subunits.* Biochemistry, 1966. 5(1): p. 365-85.

4. Monod, J., J. Wyman, and J.P. Changeux, *ON THE NATURE OF ALLOSTERIC TRANSITIONS: A PLAUSIBLE MODEL.* J Mol Biol, 1965. 12: p. 88-118.

5. Hille, B., *Ion channels of excitable membranes*. 3rd ed. 2001, Sunderland, Mass.: Sinauer. xviii, 814 p., [8] p. of plates.

6. Boron, W.F., *Medical Physiology*. 2003, Philadelphia: Saunders. 1319.

7. Hodgkin, A.L. and A.F. Huxley, *A quantitative description of membrane current and its application to conduction and excitation in nerve.* J Physiol, 1952. 117(4): p. 500-44.

8. Hodgkin, A.L. and A.F. Huxley, *The dual effect of membrane potential on sodium conductance in the giant axon of Loligo.* J Physiol, 1952. 116(4): p. 497-506.

9. Hodgkin, A.L. and A.F. Huxley, *The components of membrane conductance in the giant axon of Loligo.* J Physiol, 1952. 116(4): p. 473-96.

10. Hodgkin, A.L. and A.F. Huxley, *Currents carried by sodium and potassium ions through the membrane of the giant axon of Loligo.* J Physiol, 1952. 116(4): p. 449-72.

11. Hodgkin, A.L., A.F. Huxley, and B. Katz, *Measurement of current-voltage relations in the membrane of the giant axon of Loligo.* J Physiol, 1952. 116(4): p. 424-48.

12. Cole, K.S., *Some physical aspects of bioelectric phenomena.* Proc Natl Acad Sci U S A, 1949. 35(10): p. 558-66.

13. Mullins, L.J., *A single channel or a dual channel mechanism for nerve excitation.* J Gen Physiol, 1968. 52(3): p. 550-6.

14. Mullins, L.J., *Single or Dual Channel Mechanisms.* J Gen Physiol, 1968. 52(3): p. 555-556.

15. Hille, B., *Ionic channels in nerve membranes.* Prog Biophys Mol Biol, 1970. 21: p. 1-32.

16. Armstrong, C.M., *Ionic pores, gates, and gating currents.* Q Rev Biophys, 1974. 7(2): p. 179-210.

17. Narahashi, T., J.W. Moore, and W.R. Scott, *TETRODOTOXIN BLOCKAGE OF SODIUM CONDUCTANCE INCREASE IN LOBSTER GIANT AXONS.* J Gen Physiol, 1964. 47: p. 965-74.

18. Armstrong, C.M. and L. Binstock, *ANOMALOUS RECTIFICATION IN THE SQUID GIANT AXON INJECTED WITH TETRAETHYLAMMONIUM CHLORIDE.* J Gen Physiol, 1965. 48: p. 859-72.

19. Hagiwara, S. and N. Saito, *Voltage-current relations in nerve cell membrane of Onchidium verruculatum.* J Physiol, 1959. 148: p. 161-79.

20. Tasaki, I. and A.S. Hagiwar, *Demonstration of two stable potential states in the squid giant axon under tetraethylammonium chloride.* J Gen Physiol, 1957. 40(6): p. 859-85.

21. Mullins, L.J., *An analysis of conductance changes in squid axon.* J Gen Physiol, 1959. 42(5): p. 1013-35.

22. Armstrong, C.M., *Evidence for ionic pores in excitable membranes.* Biophys J, 1975. 15(9): p. 932-3.

23. Armstrong, C.M., F. Bezanilla, and E. Rojas, *Destruction of sodium conductance inactivation in squid axons perfused with pronase.* J Gen Physiol, 1973. 62(4): p. 375-91.

24. Armstrong, C.M., *Inactivation of the potassium conductance and related phenomena caused by quaternary ammonium ion injection in squid axons.* J Gen Physiol, 1969. 54(5): p. 553-75.

25. Armstrong, C.M., *Interaction of tetraethylammonium ion derivatives with the potassium channels of giant axons.* J Gen Physiol, 1971. 58(4): p. 413-37.

26. Hille, B., *Gating in sodium channels of nerve.* Annu Rev Physiol, 1976. 38: p. 139-52.

27. Gordon, H.T. and J.H. Welsh, *The role of ions in axon surface reactions to toxic organic compounds.* J Cell Physiol, 1948. 31(3): p. 395-419.

28. Brink, F., *The role of calcium ions in neural processes.* Pharmacol Rev, 1954. 6(3): p. 243-98.

29. Armstrong, C.M., F.M. Bezanilla, and P. Horowicz, *Twitches in the presence of ethylene glycol bis( -aminoethyl ether)-N,N'-tetracetic acid.* Biochim Biophys Acta, 1972. 267(3): p. 605-8.

30. Baker, P.F., A.L. Hodgkin, and E.B. Ridgway, *Depolarization and calcium entry in squid giant axons.* J Physiol, 1971. 218(3): p. 709-55.

31. Hille, B., A.M. Woodhull, and B.I. Shapiro, *Negative surface charge near sodium channels of nerve: divalent ions, monovalent ions, and pH.* Philos Trans R Soc Lond B Biol Sci, 1975. 270(908): p. 301-18.

32. Meves, H. and W. Vogel, *Calcium inward currents in internally perfused giant axons.* J Physiol, 1973. 235(1): p. 225-65.

33. Chandler, W.K. and H. Meves, *Voltage clamp experiments on internally perfused giant axons.* J Physiol, 1965. 180(4): p. 788-820.

34. Hille, B., *The permeability of the sodium channel to organic cations in myelinated nerve.* J Gen Physiol, 1971. 58(6): p. 599-619.

35. Hille, B., *The permeability of the sodium channel to metal cations in myelinated nerve.* J Gen Physiol, 1972. 59(6): p. 637-58.

36. Armstrong, C.M. and F. Bezanilla, *Currents related to movement of the gating particles of the sodium channels.* Nature, 1973. 242(5398): p. 459-61.

37. Armstrong, C.M., *Sodium channels and gating currents.* Physiol Rev, 1981. 61(3): p. 644-83.

38. Bezanilla, F. and C.M. Armstrong, *Gating currents of the sodium channels: three ways to block them.* Science, 1974. 183(126): p. 753-4.

39. Nachmansohn, D., *Proteins of excitable membranes.* J Gen Physiol, 1969. 54(1): p. 187-224.

40. Changeux, J.P., A. Devillers-Thiery, and P. Chemouilli, *Acetylcholine receptor: an allosteric protein.* Science, 1984. 225(4668): p. 1335-45.

41. Conti-Tronconi, B.M. and M.A. Raftery, *The nicotinic cholinergic receptor: correlation of molecular structure with functional properties.* Annu Rev Biochem, 1982. 51: p. 491-530.

42. Corringer, P.J., N. Le Novere, and J.P. Changeux, *Nicotinic receptors at the amino acid level.* Annu Rev Pharmacol Toxicol, 2000. 40: p. 431-58.

43. Lindstrom, J., *Neuronal nicotinic acetylcholine receptors.* Ion Channels, 1996. 4: p. 377-450.

44. Karlin, A., *Explorations of the nicotinic acetylcholine receptor.* Harvey Lect, 1989. 85: p. 71-107.

45. Karlin, A., *Structure of nicotinic acetylcholine receptors.* Curr Opin Neurobiol, 1993. 3(3): p. 299-309.

46. Noda, M., et al., *Structural homology of Torpedo californica acetylcholine receptor subunits.* Nature, 1983. 302(5908): p. 528-32.

47. Raftery, M.A., et al., *Acetylcholine receptor: complex of homologous subunits.* Science, 1980. 208(4451): p. 1454-6.

48. Numa, S., *A molecular view of neurotransmitter receptors and ionic channels.* Harvey Lect, 1987. 83: p. 121-65.

49. Barnard, E.A., R. Miledi, and K. Sumikawa, *Translation of exogenous messenger RNA coding for nicotinic acetylcholine receptors produces functional receptors in Xenopus oocytes.* Proc R Soc Lond B Biol Sci, 1982. 215(1199): p. 241-6.

50. Sumikawa, K., et al., *Active multi-subunit ACh receptor assembled by translation of heterologous mRNA in Xenopus oocytes.* Nature, 1981. 292(5826): p. 862-4.

51. Mishina, M., et al., *Expression of functional acetylcholine receptor from cloned cDNAs.* Nature, 1984. 307(5952): p. 604-8.

52. Jan, L.Y. and Y.N. Jan, *Structural elements involved in specific K+ channel functions.* Annu Rev Physiol, 1992. 54: p. 537-55.

53. Pongs, O., *Molecular biology of voltage-dependent potassium channels.* Physiol Rev, 1992. 72(4 Suppl): p. S69-88.

54. Pongs, O., *Structural basis of voltage-gated K+ channel pharmacology.* Trends Pharmacol Sci, 1992. 13(9): p. 359-65.

55. Tanouye, M.A. and A. Ferrus, *Action potentials in normal and Shaker mutant Drosophila.* J Neurogenet, 1985. 2(4): p. 253-71.

56. Tanouye, M.A., A. Ferrus, and S.C. Fujita, *Abnormal action potentials associated with the Shaker complex locus of Drosophila.* Proc Natl Acad Sci U S A, 1981. 78(10): p. 6548-52.

57. Kamb, A., J. Tseng-Crank, and M.A. Tanouye, *Multiple products of the Drosophila Shaker gene may contribute to potassium channel diversity.* Neuron, 1988. 1(5): p. 421-30.

58. Papazian, D.M., et al., *Cloning of genomic and complementary DNA from Shaker, a putative potassium channel gene from Drosophila.* Science, 1987. 237(4816): p. 749-53.

59. Pongs, O., et al., *Shaker encodes a family of putative potassium channel proteins in the nervous system of Drosophila.* EMBO J, 1988. 7(4): p. 1087-96.

60. Schwarz, T.L., et al., *Multiple potassium-channel components are produced by alternative splicing at the Shaker locus in Drosophila.* Nature, 1988. 331(6152): p. 137-42.

61. Tempel, B.L., et al., *Sequence of a probable potassium channel component encoded at Shaker locus of Drosophila.* Science, 1987. 237(4816): p. 770-5.

62. Anderson, P.A. and R.M. Greenberg, *Phylogeny of ion channels: clues to structure and function.* Comp Biochem Physiol B Biochem Mol Biol, 2001. 129(1): p. 17-28.

63. MacKinnon, R., *Determination of the subunit stoichiometry of a voltage-activated potassium channel.* Nature, 1991. 350(6315): p. 232-5.

64. Ishii, K., *[Molecular structure, function and regulation of K+ channels].* Nippon Rinsho, 1993. 51(6): p. 1477-82.

65. Jan, L.Y. and Y.N. Jan, *A superfamily of ion channels.* Nature, 1990. 345(6277): p. 672.

66. Jan, L.Y. and Y.N. Jan, *How might the diversity of potassium channels be generated?* Trends Neurosci, 1990. 13(10): p. 415-9.

67. Doyle, D.A., et al., *The structure of the potassium channel: molecular basis of K+ conduction and selectivity.* Science, 1998. 280(5360): p. 69-77.

68. Falke, J.J., et al., *Structure of a bacterial sensory receptor. A site-directed sulfhydryl study.* J Biol Chem, 1988. 263(29): p. 14850-8.

69. Karlin, A. and M.H. Akabas, *Substituted-cysteine accessibility method.* Methods Enzymol, 1998. 293: p. 123-45.

70. Roberts, D.D., et al., *Reactivity of small thiolate anions and cysteine-25 in papain toward methyl methanethiosulfonate.* Biochemistry, 1986. 25(19): p. 5595-601.

71. Hartmann, H.A., et al., *Exchange of conduction pathways between two related K+ channels.* Science, 1991. 251(4996): p. 942-4.

72. Kirsch, G.E., et al., *A single nonpolar residue in the deep pore of related K+ channels acts as a K+:Rb+ conductance switch.* Biophys J, 1992. 62(1): p. 136-43; discussion 143-4.

73. Yool, A.J. and T.L. Schwarz, *Alteration of ionic selectivity of a K+ channel by mutation of the H5 region.* Nature, 1991. 349(6311): p. 700-4.

74. Lopez, G.A., Y.N. Jan, and L.Y. Jan, *Evidence that the S6 segment of the Shaker voltage-gated K+ channel comprises part of the pore.* Nature, 1994. 367(6459): p. 179-82.

75. MacKinnon, R., *New insights into the structure and function of potassium channels.* Curr Opin Neurobiol, 1991. 1(1): p. 14-9.

76. MacKinnon, R., L. Heginbotham, and T. Abramson, *Mapping the receptor site for charybdotoxin, a pore-blocking potassium channel inhibitor.* Neuron, 1990. 5(6): p. 767-71.

77. MacKinnon, R. and C. Miller, *Mechanism of charybdotoxin block of the high-conductance, Ca2+-activated K+ channel.* J Gen Physiol, 1988. 91(3): p. 335-49.

78. MacKinnon, R. and C. Miller, *Mutant potassium channels with altered binding of charybdotoxin, a pore-blocking peptide inhibitor.* Science, 1989. 245(4924): p. 1382-5.

79. MacKinnon, R., P.H. Reinhart, and M.M. White, *Charybdotoxin block of Shaker K+ channels suggests that different types of K+ channels share common structural features.* Neuron, 1988. 1(10): p. 997-1001.

80. MacKinnon, R. and G. Yellen, *Mutations affecting TEA blockade and ion permeation in voltage-activated K+ channels.* Science, 1990. 250(4978): p. 276-9.

81. Miller, C., *Competition for block of a Ca2(+)-activated K+ channel by charybdotoxin and tetraethylammonium.* Neuron, 1988. 1(10): p. 1003-6.

82. Anderson, C.S., et al., *Charybdotoxin block of single Ca2+-activated K+ channels. Effects of channel gating, voltage, and ionic strength.* J Gen Physiol, 1988. 91(3): p. 317-33.

83. Isacoff, E.Y., Y.N. Jan, and L.Y. Jan, *Putative receptor for the cytoplasmic inactivation gate in the Shaker K+ channel.* Nature, 1991. 353(6339): p. 86-90.

84. Armstrong, C.M. and F. Bezanilla, *Inactivation of the sodium channel. II. Gating current experiments.* J Gen Physiol, 1977. 70(5): p. 567-90.

85. Baukrowitz, T. and G. Yellen, *Modulation of K+ current by frequency and external [K+]: a tale of two inactivation mechanisms.* Neuron, 1995. 15(4): p. 951-60.

86. Hoshi, T., W.N. Zagotta, and R.W. Aldrich, *Two types of inactivation in Shaker K+ channels: effects of alterations in the carboxy-terminal region.* Neuron, 1991. 7(4): p. 547-56.

87. Kiss, L., J. LoTurco, and S.J. Korn, *Contribution of the selectivity filter to inactivation in potassium channels.* Biophys J, 1999. 76(1 Pt 1): p. 253-63.

88. Liu, Y., M.E. Jurman, and G. Yellen, *Dynamic rearrangement of the outer mouth of a K+ channel during gating.* Neuron, 1996. 16(4): p. 859-67.

89. Lopez-Barneo, J., et al., *Effects of external cations and mutations in the pore region on C-type inactivation of Shaker potassium channels.* Receptors Channels, 1993. 1(1): p. 61-71.

90. Yellen, G., et al., *An engineered cysteine in the external mouth of a K+ channel allows inactivation to be modulated by metal binding.* Biophys J, 1994. 66(4): p. 1068-75.

91. Choi, K.L., R.W. Aldrich, and G. Yellen, *Tetraethylammonium blockade distinguishes two inactivation mechanisms in voltage-activated K+ channels.* Proc Natl Acad Sci U S A, 1991. 88(12): p. 5092-5.

92. Demo, S.D. and G. Yellen, *The inactivation gate of the Shaker K+ channel behaves like an open-channel blocker.* Neuron, 1991. 7(5): p. 743-53.

93. Hoshi, T., W.N. Zagotta, and R.W. Aldrich, *Biophysical and molecular mechanisms of Shaker potassium channel inactivation.* Science, 1990. 250(4980): p. 533-8.

94. Murrell-Lagnado, R.D. and R.W. Aldrich, *Interactions of amino terminal domains of Shaker K channels with a pore blocking site studied with synthetic peptides.* J Gen Physiol, 1993. 102(6): p. 949-75.

95. Murrell-Lagnado, R.D. and R.W. Aldrich, *Energetics of Shaker K channels block by inactivation peptides.* J Gen Physiol, 1993. 102(6): p. 977-1003.

96. Zagotta, W.N., T. Hoshi, and R.W. Aldrich, *Restoration of inactivation in mutants of Shaker potassium channels by a peptide derived from ShB.* Science, 1990. 250(4980): p. 568-71.

97. Bezanilla, F. and C.M. Armstrong, *Inactivation of the sodium channel. I. Sodium current experiments.* J Gen Physiol, 1977. 70(5): p. 549-66.

98. Holmgren, M., M.E. Jurman, and G. Yellen, *N-type inactivation and the S4-S5 region of the Shaker K+ channel.* J Gen Physiol, 1996. 108(3): p. 195-206.

99. McCormack, K., et al., *A role for hydrophobic residues in the voltage-dependent gating of Shaker K+ channels.* Proc Natl Acad Sci U S A, 1991. 88(7): p. 2931-5.

100. Choi, K.L., et al., *The internal quaternary ammonium receptor site of Shaker potassium channels.* Neuron, 1993. 10(3): p. 533-41.

101. Gomez-Lagunas, F. and C.M. Armstrong, *Inactivation in ShakerB K+ channels: a test for the number of inactivating particles on each channel.* Biophys J, 1995. 68(1): p. 89-95.

102. MacKinnon, R., R.W. Aldrich, and A.W. Lee, *Functional stoichiometry of Shaker potassium channel inactivation.* Science, 1993. 262(5134): p. 757-9.

103. Zhou, M., et al., *Potassium channel receptor site for the inactivation gate and quaternary amine inhibitors.* Nature, 2001. 411(6838): p. 657-61.

104. Holmgren, M., et al., *On the use of thiol-modifying agents to determine channel topology.* Neuropharmacology, 1996. 35(7): p. 797-804.

105. Akabas, M.H., et al., *Identification of acetylcholine receptor channel-lining residues in the entire M2 segment of the alpha subunit.* Neuron, 1994. 13(4): p. 919-27.

106. Akabas, M.H., et al., *Acetylcholine receptor channel structure probed in cysteine-substitution mutants.* Science, 1992. 258(5080): p. 307-10.

107. Stauffer, D.A. and A. Karlin, *Electrostatic potential of the acetylcholine binding sites in the nicotinic receptor probed by reactions of binding-site cysteines with charged methanethiosulfonates.* Biochemistry, 1994. 33(22): p. 6840-9.

108. Smith, D.J., E.T. Maggio, and G.L. Kenyon, *Simple alkanethiol groups for temporary blocking of sulfhydryl groups of enzymes.* Biochemistry, 1975. 14(4): p. 766-71.

109. Kuner, T., et al., *Structure of the NMDA receptor channel M2 segment inferred from the accessibility of substituted cysteines.* Neuron, 1996. 17(2): p. 343-52.

110. Garneau, L., et al., *Hydrophobic interactions as key determinants to the KCa3.1 channel closed configuration. An analysis of KCa3.1 mutants constitutively active in zero Ca2+.* J Biol Chem, 2009. 284(1): p. 389-403.

111. Klein, H., et al., *Structural determinants of the closed KCa3.1 channel pore in relation to channel gating: results from a substituted cysteine accessibility analysis.* J Gen Physiol, 2007. 129(4): p. 299-315.

112. Pascual, J.M., et al., *K+ pore structure revealed by reporter cysteines at inner and outer surfaces.* Neuron, 1995. 14(5): p. 1055-63.

113. Simoes, M., et al., *Cysteine mutagenesis and computer modeling of the S6 region of an intermediate conductance IKCa channel.* J Gen Physiol, 2002. 120(1): p. 99-116.

114. Jiang, Y., et al., *The open pore conformation of potassium channels.* Nature, 2002. 417(6888): p. 523-6.

115. Ye, S., et al., *Crystal structures of a ligand-free MthK gating ring: insights into the ligand gating mechanism of K+ channels.* Cell, 2006. 126(6): p. 1161-73.

116. Horrigan, F.T. and R.W. Aldrich, *Coupling between voltage sensor activation, Ca2+ binding and channel opening in large conductance (BK) potassium channels.* J Gen Physiol, 2002. 120(3): p. 267-305.

117. Perozo, E., *New structural perspectives on K(+) channel gating.* Structure, 2002. 10(8): p. 1027-9.

118. Kuo, A., et al., *Crystal structure of the potassium channel KirBac1.1 in the closed state.* Science, 2003. 300(5627): p. 1922-6.

119. Doyle, D.A., *Structural themes in ion channels.* Eur Biophys J, 2004. 33(3): p. 175-9.

120. Guy, H.R. and F. Conti, *Pursuing the structure and function of voltage-gated channels.* Trends Neurosci, 1990. 13(6): p. 201-6.

121. Hackos, D.H., T.H. Chang, and K.J. Swartz, *Scanning the intracellular S6 activation gate in the shaker K+ channel.* J Gen Physiol, 2002. 119(6): p. 521-32.

122. Unwin, N., *Nicotinic acetylcholine receptor at 9 A resolution.* J Mol Biol, 1993. 229(4): p. 1101-24.

123. Unwin, N., *Acetylcholine receptor channel imaged in the open state.* Nature, 1995. 373(6509): p. 37-43.

124. Sansom, M.S., et al., *Water in ion channels and pores--simulation studies.* Novartis Found Symp, 2002. 245: p. 66-78; discussion 79-83, 165-8.

125. Beckstein, O., et al., *Ion channel gating: insights via molecular simulations.* FEBS Lett, 2003. 555(1): p. 85-90.

126. Jiang, Y., et al., *Crystal structure and mechanism of a calcium-gated potassium channel.* Nature, 2002. 417(6888): p. 515-22.

127. Horn, R., *Conversation between voltage sensors and gates of ion channels.* Biochemistry, 2000. 39(51): p. 15653-8.

128. Larsson, H.P., *The search is on for the voltage sensor-to-gate coupling.* J Gen Physiol, 2002. 120(4): p. 475-81.

129. Niu, X., X. Qian, and K.L. Magleby, *Linker-gating ring complex as passive spring and Ca(2+)-dependent machine for a voltage- and Ca(2+)-activated potassium channel.* Neuron, 2004. 42(5): p. 745-56.

130. Craven, K.B. and W.N. Zagotta, *Salt bridges and gating in the COOH-terminal region of HCN2 and CNGA1 channels.* J Gen Physiol, 2004. 124(6): p. 663-77.

131. Flynn, G.E., et al., *Structure and rearrangements in the carboxy-terminal region of SpIH channels.* Structure, 2007. 15(6): p. 671-82.

132. Islas, L.D. and W.N. Zagotta, *Short-range molecular rearrangements in ion channels detected by tryptophan quenching of bimane fluorescence.* J Gen Physiol, 2006. 128(3): p. 337-46.

133. Taraska, J.W. and W.N. Zagotta, *Structural dynamics in the gating ring of cyclic nucleotide-gated ion channels.* Nat Struct Mol Biol, 2007. 14(9): p. 854-60.

134. Kanevsky, M. and R.W. Aldrich, *Determinants of voltage-dependent gating and open-state stability in the S5 segment of Shaker potassium channels.* J Gen Physiol, 1999. 114(2): p. 215-42.

135. Espinosa, F., et al., *Dynamic interaction of S5 and S6 during voltage-controlled gating in a potassium channel.* J Gen Physiol, 2001. 118(2): p. 157-70.

136. Horn, R., S. Ding, and H.J. Gruber, *Immobilizing the moving parts of voltage-gated ion channels.* J Gen Physiol, 2000. 116(3): p. 461-76.

137. del Camino, D., et al., *Blocker protection in the pore of a voltage-gated K+ channel and its structural implications.* Nature, 2000. 403(6767): p. 321-5.

138. Ishii, T.M., et al., *A human intermediate conductance calcium-activated potassium channel.* Proc Natl Acad Sci U S A, 1997. 94(21): p. 11651-6.

139. Joiner, W.J., et al., *hSK4, a member of a novel subfamily of calcium-activated potassium channels.* Proc Natl Acad Sci U S A, 1997. 94(20): p. 11013-8.

140. Devor, D.C., et al., *Modulation of Cl- secretion by benzimidazolones. I. Direct activation of a Ca(2+)-dependent K+ channel.* Am J Physiol, 1996. 271(5 Pt 1): p. L775-84.

141. Syme, C.A., et al., *Pharmacological activation of cloned intermediate- and small-conductance Ca(2+)-activated K(+) channels.* Am J Physiol Cell Physiol, 2000. 278(3): p. C570-81.

142. Begenisich, T., et al., *Physiological roles of the intermediate conductance, Ca2+-activated potassium channel Kcnn4.* J Biol Chem, 2004. 279(46): p. 47681-7.

143. Vandorpe, D.H., et al., *cDNA cloning and functional characterization of the mouse Ca2+-gated K+ channel, mIK1. Roles in regulatory volume decrease and erythroid differentiation.* J Biol Chem, 1998. 273(34): p. 21542-53.

144. Warth, R., et al., *Molecular and functional characterization of the small Ca(2+)-regulated K+ channel (rSK4) of colonic crypts.* Pflugers Arch, 1999. 438(4): p. 437-44.

145. Ghanshani, S., et al., *Up-regulation of the IKCa1 potassium channel during T-cell activation. Molecular mechanism and functional consequences.* J Biol Chem, 2000. 275(47): p. 37137-49.

146. Fanger, C.M., et al., *Calcium-activated potassium channels sustain calcium signaling in T lymphocytes. Selective blockers and manipulated channel expression levels.* J Biol Chem, 2001. 276(15): p. 12249-56.

147. Wulff, H., et al., *The voltage-gated Kv1.3 K(+) channel in effector memory T cells as new target for MS.* J Clin Invest, 2003. 111(11): p. 1703-13.

148. Logsdon, N.J., et al., *A novel gene, hKCa4, encodes the calcium-activated potassium channel in human T lymphocytes.* J Biol Chem, 1997. 272(52): p. 32723-6.

149. Dharmsathaphorn, K. and S.J. Pandol, *Mechanism of chloride secretion induced by carbachol in a colonic epithelial cell line.* J Clin Invest, 1986. 77(2): p. 348-54.

150. Bohme, M., M. Diener, and W. Rummel, *Calcium- and cyclic-AMP-mediated secretory responses in isolated colonic crypts.* Pflugers Arch, 1991. 419(2): p. 144-51.

151. Devor, D.C. and M.E. Duffey, *Carbachol induces K+, Cl-, and nonselective cation conductances in T84 cells: a perforated patch-clamp study.* Am J Physiol, 1992. 263(4 Pt 1): p. C780-7.

152. Reenstra, W.W., *Inhibition of cAMP- and Ca-dependent Cl- secretion by phorbol esters: inhibition of basolateral K+ channels.* Am J Physiol, 1993. 264(1 Pt 1): p. C161-8.

153. Valverde, M.A., G.M. Mintenig, and F.V. Sepulveda, *Cl- currents of unstimulated T84 intestinal epithelial cells studied by intracellular recording.* J Membr Biol, 1994. 137(3): p. 237-47.

154. Walters, R.J. and F.V. Sepulveda, *A basolateral K+ conductance modulated by carbachol dominates the membrane potential of small intestinal crypts.* Pflugers Arch, 1991. 419(5): p. 537-9.

155. Devor, D.C. and R.A. Frizzell, *Calcium-mediated agonists activate an inwardly rectified K+ channel in colonic secretory cells.* Am J Physiol, 1993. 265(5 Pt 1): p. C1271-80.

156. Mieyal, P., et al., *NO-independent vasodilation to acetylcholine in the rat isolated kidney utilizes a charybdotoxin-sensitive, intermediate-conductance Ca(++)-activated K+ channel.* J Pharmacol Exp Ther, 1998. 285(2): p. 659-64.

157. Rapacon, M., et al., *Contribution of calcium-activated potassium channels to the vasodilator effect of bradykinin in the isolated, perfused kidney of the rat.* Br J Pharmacol, 1996. 118(6): p. 1504-8.

158. Nilius, B. and G. Droogmans, *Ion channels and their functional role in vascular endothelium.* Physiol Rev, 2001. 81(4): p. 1415-59.

159. Vanhoutte, P.M., et al., *Endothelial dysfunction and vascular disease.* Acta Physiol (Oxf), 2009. 196(2): p. 193-222.

160. Bellien, J., C. Thuillez, and R. Joannides, *Contribution of endothelium-derived hyperpolarizing factors to the regulation of vascular tone in humans.* Fundam Clin Pharmacol, 2008. 22(4): p. 363-77.

161. Coleman, H.A., M. Tare, and H.C. Parkington, *Endothelial potassium channels, endothelium-dependent hyperpolarization and the regulation of vascular tone in health and disease.* Clin Exp Pharmacol Physiol, 2004. 31(9): p. 641-9.

162. Feletou, M. and P.M. Vanhoutte, *Endothelium-dependent hyperpolarizations: past beliefs and present facts.* Ann Med, 2007. 39(7): p. 495-516.

163. Ledoux, J., et al., *Calcium-activated potassium channels and the regulation of vascular tone.* Physiology (Bethesda), 2006. 21: p. 69-78.

164. Luksha, L., S. Agewall, and K. Kublickiene, *Endothelium-derived hyperpolarizing factor in vascular physiology and cardiovascular disease.* Atherosclerosis, 2009. 202(2): p. 330-44.

165. Brahler, S., et al., *Genetic deficit of SK3 and IK1 channels disrupts the endothelium-derived hyperpolarizing factor vasodilator pathway and causes hypertension.* Circulation, 2009. 119(17): p. 2323-32.

166. Si, H., et al., *Impaired endothelium-derived hyperpolarizing factor-mediated dilations and increased blood pressure in mice deficient of the intermediate-conductance Ca2+-activated K+ channel.* Circ Res, 2006. 99(5): p. 537-44.

167. Taylor, M.S., et al., *Altered expression of small-conductance Ca2+-activated K+ (SK3) channels modulates arterial tone and blood pressure.* Circ Res, 2003. 93(2): p. 124-31.

168. Feletou, M., *Calcium-activated potassium channels and endothelial dysfunction: therapeutic options?* Br J Pharmacol, 2009. 156(4): p. 545-62.

169. Feletou, M. and P.M. Vanhoutte, *EDHF: an update.* Clin Sci (Lond), 2009. 117(4): p. 139-55.

170. Feletou, M. and P.M. Vanhoutte, *Endothelium-dependent hyperpolarization of canine coronary smooth muscle.* Br J Pharmacol, 1988. 93(3): p. 515-24.

171. Feletou, M. and P.M. Vanhoutte, *Endothelium-derived hyperpolarizing factor: where are we now?* Arterioscler Thromb Vasc Biol, 2006. 26(6): p. 1215-25.

172. Fleming, I., *Realizing its potential: the intermediate conductance Ca2+-activated K+ channel (KCa3.1) and the regulation of blood pressure.* Circ Res, 2006. 99(5): p. 462-4.

173. Shimokawa, H., et al., *The importance of the hyperpolarizing mechanism increases as the vessel size decreases in endothelium-dependent relaxations in rat mesenteric circulation.* J Cardiovasc Pharmacol, 1996. 28(5): p. 703-11.

174. Eichler, I., et al., *Selective blockade of endothelial Ca2+-activated small- and intermediate-conductance K+-channels suppresses EDHF-mediated vasodilation.* Br J Pharmacol, 2003. 138(4): p. 594-601.

175. Marchenko, S.M. and S.O. Sage, *Calcium-activated potassium channels in the endothelium of intact rat aorta.* J Physiol, 1996. 492 ( Pt 1): p. 53-60.

176. Burnham, M.P., et al., *Characterization of an apamin-sensitive small-conductance Ca(2+)-activated K(+) channel in porcine coronary artery endothelium: relevance to EDHF.* Br J Pharmacol, 2002. 135(5): p. 1133-43.

177. Bychkov, R., et al., *Characterization of a charybdotoxin-sensitive intermediate conductance Ca2+-activated K+ channel in porcine coronary endothelium: relevance to EDHF.* Br J Pharmacol, 2002. 137(8): p. 1346-54.

178. Kohler, R., et al., *Impaired hyperpolarization in regenerated endothelium after balloon catheter injury.* Circ Res, 2001. 89(2): p. 174-9.

179. Neylon, C.B., et al., *Molecular cloning and characterization of the intermediate-conductance Ca(2+)-activated K(+) channel in vascular smooth muscle: relationship between K(Ca) channel diversity and smooth muscle cell function.* Circ Res, 1999. 85(9): p. e33-43.

180. Quignard, J.F., et al., *Role of endothelial cell hyperpolarization in EDHF-mediated responses in the guinea-pig carotid artery.* Br J Pharmacol, 2000. 129(6): p. 1103-12.

181. Sandow, S.L. and C.E. Hill, *Incidence of myoendothelial gap junctions in the proximal and distal mesenteric arteries of the rat is suggestive of a role in endothelium-derived hyperpolarizing factor-mediated responses.* Circ Res, 2000. 86(3): p. 341-6.

182. Griffith, T.M., *Endothelium-dependent smooth muscle hyperpolarization: do gap junctions provide a unifying hypothesis?* Br J Pharmacol, 2004. 141(6): p. 881-903.

183. Lang, N.N., et al., *Connexin 43 mediates endothelium-derived hyperpolarizing factor-induced vasodilatation in subcutaneous resistance arteries from healthy pregnant women.* Am J Physiol Heart Circ Physiol, 2007. 292(2): p. H1026-32.

184. Nelson, M.T. and J.M. Quayle, *Physiological roles and properties of potassium channels in arterial smooth muscle.* Am J Physiol, 1995. 268(4 Pt 1): p. C799-822.

185. Prior, H.M., et al., *K(+)-induced dilation of a small renal artery: no role for inward rectifier K+ channels.* Cardiovasc Res, 1998. 37(3): p. 780-90.

186. Edwards, G., et al., *K+ is an endothelium-derived hyperpolarizing factor in rat arteries.* Nature, 1998. 396(6708): p. 269-72.

187. Bond, C.T., et al., *Respiration and parturition affected by conditional overexpression of the Ca2+-activated K+ channel subunit, SK3.* Science, 2000. 289(5486): p. 1942-6.

188. Keen, J.E., et al., *Domains responsible for constitutive and Ca(2+)-dependent interactions between calmodulin and small conductance Ca(2+)-activated potassium channels.* J Neurosci, 1999. 19(20): p. 8830-8.

189. Xia, X.M., et al., *Mechanism of calcium gating in small-conductance calcium-activated potassium channels.* Nature, 1998. 395(6701): p. 503-7.

190. Li, W., et al., *EF hands at the N-lobe of calmodulin are required for both SK channel gating and stable SK-calmodulin interaction.* J Gen Physiol, 2009. 134(4): p. 281-93.

191. Lee, W.S., et al., *Small conductance Ca2+-activated K+ channels and calmodulin: cell surface expression and gating.* J Biol Chem, 2003. 278(28): p. 25940-6.

192. Schumacher, M.A., et al., *Structure of the gating domain of a Ca2+-activated K+ channel complexed with Ca2+/calmodulin.* Nature, 2001. 410(6832): p. 1120-4.

193. Schumacher, M.A., M. Crum, and M.C. Miller, *Crystal structures of apocalmodulin and an apocalmodulin/SK potassium channel gating domain complex.* Structure, 2004. 12(5): p. 849-60.

194. Babu, Y.S., et al., *Three-dimensional structure of calmodulin.* Nature, 1985. 315(6014): p. 37-40.

195. Maylie, J., et al., *Small conductance Ca2+-activated K+ channels and calmodulin.* J Physiol, 2004. 554(Pt 2): p. 255-61.

196. Li, W. and R.W. Aldrich, *Activation of the SK potassium channel-calmodulin complex by nanomolar concentrations of terbium.* Proc Natl Acad Sci U S A, 2009. 106(4): p. 1075-80.

197. Bruening-Wright, A., et al., *Evidence for a deep pore activation gate in small conductance Ca2+-activated K+ channels.* J Gen Physiol, 2007. 130(6): p. 601-10.

198. Bruening-Wright, A., et al., *Localization of the activation gate for small conductance Ca2+-activated K+ channels.* J Neurosci, 2002. 22(15): p. 6499-506.

199. Milligan, C.J. and D. Wray, *Local movement in the S2 region of the voltage-gated potassium channel hKv2.1 studied using cysteine mutagenesis.* Biophys J, 2000. 78(4): p. 1852-61.

200. Wang, M.H., et al., *Effect of cysteine substitutions on the topology of the S4 segment of the Shaker potassium channel: implications for molecular models of gating.* J Physiol, 1999. 521 Pt 2: p. 315-26.

201. Yusaf, S.P., D. Wray, and A. Sivaprasadarao, *Measurement of the movement of the S4 segment during the activation of a voltage-gated potassium channel.* Pflugers Arch, 1996. 433(1-2): p. 91-7.

202. Bolton, T.B., R.J. Lang, and T. Takewaki, *Mechanisms of action of noradrenaline and carbachol on smooth muscle of guinea-pig anterior mesenteric artery.* J Physiol, 1984. 351: p. 549-72.

203. Sigworth, F.J., *The variance of sodium current fluctuations at the node of Ranvier.* J Physiol, 1980. 307: p. 97-129.

204. Zagotta, W.N., et al., *Shaker potassium channel gating. II: Transitions in the activation pathway.* J Gen Physiol, 1994. 103(2): p. 279-319.

205. Smith-Maxwell, C.J., J.L. Ledwell, and R.W. Aldrich, *Role of the S4 in cooperativity of voltage-dependent potassium channel activation.* J Gen Physiol, 1998. 111(3): p. 399-420.

206. Hirschberg, B., et al., *Gating of recombinant small-conductance Ca-activated K+ channels by calcium.* J Gen Physiol, 1998. 111(4): p. 565-81.

207. Press, W.H., *Numerical recipes : the art of scientific computing*. 3rd ed. 2007, Cambridge, UK ; New York: Cambridge University Press. xxi, 1235 p.

208. Sali, A. and T.L. Blundell, *Comparative protein modelling by satisfaction of spatial restraints.* J Mol Biol, 1993. 234(3): p. 779-815.

209. Long, S.B., E.B. Campbell, and R. Mackinnon, *Crystal structure of a mammalian voltage-dependent Shaker family K+ channel.* Science, 2005. 309(5736): p. 897-903.

210. Yifrach, O. and R. MacKinnon, *Energetics of pore opening in a voltage-gated K(+) channel.* Cell, 2002. 111(2): p. 231-9.

211. Hamilton, K.L., C.A. Syme, and D.C. Devor, *Molecular localization of the inhibitory arachidonic acid binding site to the pore of hIK1.* J Biol Chem, 2003. 278(19): p. 16690-7.

212. Wulff, H., et al., *Delineation of the clotrimazole/TRAM-34 binding site on the intermediate conductance calcium-activated potassium channel, IKCa1.* J Biol Chem, 2001. 276(34): p. 32040-5.

213. Gross, A., et al., *Structure of the KcsA potassium channel from Streptomyces lividans: a site-directed spin labeling study of the second transmembrane segment.* Biochemistry, 1999. 38(32): p. 10324-35.

214. Liu, Y., et al., *Gated access to the pore of a voltage-dependent K+ channel.* Neuron, 1997. 19(1): p. 175-84.

215. Gordon, S.E. and W.N. Zagotta, *A histidine residue associated with the gate of the cyclic nucleotide-activated channels in rod photoreceptors.* Neuron, 1995. 14(1): p. 177-83.

216. Ledoux, J., A.D. Bonev, and M.T. Nelson, *Ca2+-activated K+ channels in murine endothelial cells: block by intracellular calcium and magnesium.* J Gen Physiol, 2008. 131(2): p. 125-35.

217. Perozo, E., D.M. Cortes, and L.G. Cuello, *Structural rearrangements underlying K+-channel activation gating.* Science, 1999. 285(5424): p. 73-8.

218. Ackerman, S.J., et al., *Charcot-Leyden crystal protein (galectin-10) is not a dual function galectin with lysophospholipase activity but binds a lysophospholipase inhibitor in a novel structural fashion.* J Biol Chem, 2002. 277(17): p. 14859-68.

219. Soskine, M., S. Steiner-Mordoch, and S. Schuldiner, *Crosslinking of membrane-embedded cysteines reveals contact points in the EmrE oligomer.* Proc Natl Acad Sci U S A, 2002. 99(19): p. 12043-8.

220. Stephenson, R.P., *A modification of receptor theory.* Br J Pharmacol Chemother, 1956. 11(4): p. 379-93.

221. Colquhoun, D., *Binding, gating, affinity and efficacy: the interpretation of structure-activity relationships for agonists and of the effects of mutating receptors.* Br J Pharmacol, 1998. 125(5): p. 924-47.

222. Edsall, J.T., Wyman, J., *Biophysical Chemistry*. 1958, New York: Academic Press.

223. Wyman, J., Gill, S.J., *Binding and Linkage Functional chemistry of biological macromolecules*. 1990, Mill Valley, CA.: University Science Books.

224. Colquhoun, D. and B. Sakmann, *Fluctuations in the microsecond time range of the current through single acetylcholine receptor ion channels.* Nature, 1981. 294(5840): p. 464-6.

225. Colquhoun, D. and B. Sakmann, *Fast events in single-channel currents activated by acetylcholine and its analogues at the frog muscle end-plate.* J Physiol, 1985. 369: p. 501-57.

226. Liman, E.R., J. Tytgat, and P. Hess, *Subunit stoichiometry of a mammalian K+ channel determined by construction of multimeric cDNAs.* Neuron, 1992. 9(5): p. 861-71.

227. Labro, A.J., A.L. Raes, and D.J. Snyders, *Coupling of voltage sensing to channel opening reflects intrasubunit interactions in kv channels.* J Gen Physiol, 2005. 125(1): p. 71-80.

228. Prole, D.L. and G. Yellen, *Reversal of HCN channel voltage dependence via bridging of the S4-S5 linker and Post-S6.* J Gen Physiol, 2006. 128(3): p. 273-82.